

Numerical Modeling Investigations on Waste Disposal Salt Caverns

by

Meng Li

A thesis submitted in partial fulfillment of the requirements for the degree of

Master of Science

in

Geotechnical Engineering

Department of Civil and Environmental Engineering

University of Alberta

© Meng Li, 2015

## ABSTRACT

Over the past decades, the increased volume of oil-field waste disposal and the recognition of the environment and health impacts from conventional and traditional disposal approaches have led to an increased demand for solution-mined salt caverns as an effective method for permanent abandonment of oil field solid waste. The favourable geomechanical properties of the rock salt including very low permeability and high ductility behavior ensure the underground solution mined salt caverns provide secure containment facilities for petroleum industry products, with much higher storage volumes and decreased surface land requirements and correspondingly lower costs. The post-closure geomechanical behavior during long-term abandonment are of primary importance in the assessing the feasibility of disposal salt caverns for oil field waste, as well as the multiple-cavern configurations around the same site.

This thesis focuses on significant numerical modeling investigations of the structural stability and integrity of the salt caverns, the likelihood of nonsalt caprock failure, the induced surface subsidence and theoretical casing behavior, the closure behavior of the salt caverns, and the interactions between adjacent caverns during operation and permanent abandonment under various cavern configurations and internal pressure conditions. The analysis of field core logging results and laboratory testing studies assisted the above-mentioned numerical studies. It was shown that for all simulated cavern configurations, the disposal of oil field solid waste into the salt caverns would significantly increase the stability and structural integrity of the caverns and mitigate the induced deformations and cavern storage volume loss remarkably. Multiple-cavern configurations at a site could be considered if they are designed well and operated and abandoned appropriately with injected dense waste.

## ACKNOWLEDGEMENT

This thesis and the work upon it, have debts to many people and institutions.

Foremost, I am most grateful to my supervisor, Dr. Rick Chalaturnyk, for his many valuable suggestions and guidance during my research, and my study at the University of Alberta. Dr. Chalaturnyk is also acknowledged for providing much encouragement and insight toward my master study and research. He spent lots of time reviewing and helping improve this thesis.

I also want to express my thanks to Dr. Xiaolan Huang, who was full of great ideas on the numerical simulation, and thanks to her assistance in the programming and implementation.

Special thanks to other team members involved in this salt project: Tanya Schulz and Sander Osinga. Thanks to their diligent efforts on the laboratory program providing the base for my research. As well, thanks to Tanya who considered her time to review my thesis and provided valuable comments.

The development of this dissertation would not have been possible without the continuous love and unconditional support of my parents in China. Their encouragement, patience and understanding are the most motivation for me to do the right thing.

Finally, I would like to thank all my friends and colleagues, particularly Nathan Deisman, Lang Liu, Jingyu Wu, Yazhao Wang, etc. Thank Nathan for his valuable advice in FLAC<sup>3D</sup> programming, and thank Lang, Jingyu and Yazhao for many discussions helped better understanding geomechanics.

## Table of Contents

Chapter	Page
<b>1 INTRODUCTION.....</b>	<b>1</b>
1.1 Problem Statement .....	1
1.2 Objective of Thesis .....	2
1.3 Scope of Thesis .....	3
<b>2 LITERATURE REVIEW.....</b>	<b>5</b>
2.1 Introductions .....	5
2.2 Solution-mined Salt Caverns and Its Storage Use .....	5
2.2.1 Solution Mining Operation .....	5
2.2.2 Solution Mined Salt Cavern Use.....	8
2.3 Site Geological Settings for Disposal Salt Caverns .....	13
2.3.1 Geological Considerations .....	13
2.3.2 Hydrogeological Considerations.....	14
2.4 Cavern Waste Disposal Characterization.....	14
2.4.1 Waste Disposal in Salt Caverns .....	14
2.4.2 Post-Closure Behavior of Disposal Salt Caverns.....	16
2.5 Mechanical Properties of Rock Salt.....	17
2.5.1 Time-dependent Deformation Mechanism of Rock Salt.....	17
2.5.2 Norton Creep Law.....	20

<b>3</b>	<b>NUMERICAL ANALYTICAL METHODOLOGY FOR DISPOSAL SALT CAVERNS .....</b>	<b>22</b>
3.1	Introduction.....	22
3.2	Geological Overview of Disposal Salt Cavern Site .....	22
3.3	Disposal Salt Cavern Description .....	26
3.4	Geomechanical Properties.....	29
3.4.1	Geomechanical Properties of Salt Formations .....	29
3.4.2	Geomechanical Properties of Nonsalt Formations.....	36
3.5	In Situ Conditions .....	40
3.5.1	In Situ Lithostatic Stress Distribution .....	40
3.5.2	Cavern Waste Disposal Stress Distribution .....	42
3.6	Numerical Modeling Solutions .....	46
3.6.1	Finite-Difference Program .....	46
3.6.2	Three-Dimensional Finite Differential Model .....	47
<b>4</b>	<b>SENSITIVITY ANALYSIS OF NUMERICAL MODELING SOLUTIONS IN FLAC<sup>3D</sup> .....</b>	<b>52</b>
4.1	Introduction.....	52
4.2	Reference Models in Sensitivity Analysis .....	53
4.2.1	Geometrical description of the Reference Model .....	53
4.2.2	Rock Mechanical Material Parameters .....	54
4.2.3	Internal Algorithm Parameters.....	54
4.3	Sensitivity Analysis of Geometrical Parameters in FLAC <sup>3D</sup> Models.....	54

4.3.1	Sensitivity Analysis of Gridding Generation Method.....	55
4.3.2	Sensitivity Analysis of Boundary Size.....	61
4.4	Sensitivity Analysis of Creep Timestep Parameter.....	63
4.4.1	Methodology .....	63
4.4.2	Results and Conclusions .....	66
4.5	Sensitivity Analysis of Mechanical Parameters .....	67
4.5.1	Elastic Properties.....	67
4.5.2	Power Law Parameters.....	69
4.6	Summary and Conclusions.....	73
<b>5</b>	<b>LONG-TERM ABANDONMENT BEHAVIOR SIMULATION OF WASTE DISPOSAL SALT CAVERNS.....</b>	<b>75</b>
5.1	Introduction.....	75
5.2	Long-term Abandonment Behavior Simulation of Single Cavern.....	77
5.2.1	Long-term Abandonment Behavior Considering Instantaneous Excavation .....	77
5.2.2	Long-term Abandonment Behavior Considering Sequential Excavations	77
5.2.3	Results and Conclusions .....	79
5.3	Long-term Abandonment Behavior Simulation of Lotsberg Caverns .....	92
5.3.1	Long-term Abandonment Behavior Considering Instantaneous Excavation .....	92
5.3.2	Long-term Abandonment Behavior Considering Sequential Excavations .....	92

5.3.3	Results and Conclusions .....	94
5.4	Long-term Abandonment Behavior Simulation of Vertical Adjacent Caverns .....	107
5.4.1	Long-term Abandonment Behavior Considering Sequential Excavations .....	107
5.4.2	Results and Conclusions .....	109
5.5	Long-term Abandonment Behavior Simulation of Full Development of Lotsberg and Prairie Evaporite Caverns .....	120
5.5.1	Long-term Abandonment Behavior Considering Sequential Excavations .....	120
5.5.2	Results and Conclusions .....	122
5.6	Summary and Conclusions.....	136
<b>6</b>	<b>CONCLUSIONS AND RECOMMENDATIONS.....</b>	<b>141</b>
6.1	Generals .....	141
6.2	Conclusions.....	142
6.3	Recommendations for Future Research .....	145
	<b>REFERENCES.....</b>	<b>147</b>
	<b>APPENDIX A Geological Review.....</b>	<b>149</b>
	<b>APPENDIX B Numerical Analytical Methodology .....</b>	<b>156</b>
	<b>APPENDIX C Numerical Modeling Results.....</b>	<b>160</b>

## LIST OF TABLES

Table 3.1 Stratigraphy Modeled in the Numerical Simulations.....	27
Table 3.2 Two-component power Law Creep Parameters used in Numerical Simulations .....	34
Table 3.3 Elastic Properties and Densities of the Geological Units in FLAC <sup>3D</sup> .....	37
Table 3.4 Mohr-Coulomb Strength Parameters of Non-Salt Formations .....	40
Table 3.5 Anisotropic Stress Ratio of Geological Units used for Numerical Modeling..	41
Table 3.6 Internal Stress Calculation Ranges with internal material status in cavern .....	46
Table 3.7 Varied Cases Analyzed in FLAC <sup>3D</sup> Numerical Modeling.....	51
Table 4.1 Algorithm Parameters Setting in the Reference Models.....	54
Table 4.2 Comparison of 50-year Abandonment Behavior Results Simulated in Rad- Cylindrical and Rad-Tunnel Models.....	57
Table 4.3 Summarized 50-year Measurements for Varied Boundary Sizes .....	63
Table 4.4 Maximum Creep Timestep Estimation .....	65
Table 4.5 Maximum Timestep for Variation Comparison Cases.....	66
Table 4.6 Results of Creep Timestep Sensitivity Analysis .....	67
Table 4.7 Sensitivity Analysis Results of Young’s Modulus, Time = 5 years .....	68
Table 4.8 Sensitivity Analysis Results of A parameter for Power Law, Time = 5 years..	70
Table 4.9 Sensitivity Analysis Results of n parameter for Power Law, Time = 5 years..	71
Table 4.10 Sensitivity Analysis Results of A & n parameter for Power Law, Time = 5 years.....	71
Table 5.1 Comparison of Simulation Results for Instantaneous Excavations and Sequential Excavations ( <i>1-13 LTBG brine</i> ).....	82
Table 5.2 Summarized Simulation Results for <i>Cavern 1-13 LTBG</i> .....	91

Table 5.3 Comparison of Simulation Results for Instantaneous Excavations and Sequential Excavations ( <i>1-13&amp;8-13 LTBG dense-brine</i> ) .....	97
---	----

## LIST OF FIGURES

Figure 2.1 Direct and Reverse Circulation Method in Solution Mining Salt.....	8
Figure 2.2 Idealized Creep Curve as a Function of Time .....	19
Figure 3.1 Stratigraphical View from GR, $V_p$ and Rho log from 8-13 Well Logging.....	25
Figure 3.2 Schematic Cross-Sectional View of the Formation and Caverns at the site....	28
Figure 3.3 Comparison between Creep Strain Rate Measured and Predicted based on the Power Law of Prairie Evaporite Formation (RG2, 2013) .....	33
Figure 3.4 Comparison between Creep Strain Rate Observed and Predicted based on the Power Law of Lotsberg Formation (RG2, 2013) .....	33
Figure 3.5 Predicted Salt Dilatation Criterion Fitting on the Laboratory Results (RG2, 2013) .....	36
Figure 3.6 Three Different Stages for Interpretation of Cavern Internal Boundary Stresses .....	44
Figure 3.7 Cavern Internal Boundary Stress Analysis for Development Stage .....	44
Figure 3.8 Cavern Internal Boundary Stress Analysis for Abandonment Stage .....	45
Figure 4.1 Detailed Gridding View of Rad-Tunnel Model (Reference Model).....	58
Figure 4.2 Detailed Gridding View of Rad-Cylindrical Model .....	59
Figure 4.3 Predicted <i>DSR</i> Value in the Salt Strata Surrounding Cavern 1-13 LTBG.....	60
Figure 4.5 Edge Subsidence Varied with Boundary Size .....	63
Figure 4.6 Sensitivity Plot of Young's Modulus .....	69
Figure 4.7 Sensitivity Plot of A parameter for Power Law, Time = 5 years.....	71
Figure 4.8 Sensitivity Plot of n parameter for Power Law, Time = 5 years .....	72
Figure 4.9 Contour of A and n representing same results as Reference Model .....	72
Figure 5.1 Three-Dimensional Finite Difference Model of <i>Cavern 1-13 LTBG</i> .....	78

Figure 5.2 Predicted <i>DSR</i> and <i>SSR</i> Value Evolution over Abandonment Time ( <i>1-13 LTBG brine</i> ).....	83
Figure 5.3 Contour of Deviatoric Stresses Surrounding <i>Cavern 1-13 LTBG</i> .....	84
Figure 5.4 <i>DSR</i> Value Distributions Surrounding <i>Cavern 1-13 LTBG</i> .....	85
Figure 5.5 <i>SSR</i> Value Distributions Surrounding <i>Cavern 1-13 LTBG</i> .....	86
Figure 5.6 <i>DSR</i> and <i>SSR</i> Value Change with Simulation Time for <i>Cavern 1-13 LTBG</i> ..	87
Figure 5.7 Predicted Cavern Closure as a Function of Time for <i>Cavern 1-13 LTBG</i> .....	87
Figure 5.8 Accumulated Vertical Strains along the Axis of Symmetry during Abandonment Simulation of <i>Cavern 1-13 LTBG</i> .....	88
Figure 5.9 Surface Subsidence Plot under <i>1-13 LTBG brine</i> case .....	89
Figure 5.10 Surface Subsidence Plot under <i>1-13 LTBG dense</i> case .....	90
Figure 5.11 Predicted Maximum Surface Subsidence over Time ( <i>1-13 LTBG</i> ) .....	91
Figure 5.12 Three-Dimensional Finite Difference Model of <i>Cavern 1-13&amp;8-13 LTBG</i>	93
Figure 5.13 Predicted <i>DSR</i> and <i>SSR</i> Value Evolution over Abandonment Time ( <i>1-13&amp;8-13 LTBG dense-brine</i> ).....	97
Figure 5.14 Contour of Deviatoric Stresses Surrounding <i>Cavern 1-13&amp;8-13 LTBG</i> .....	98
Figure 5.15 <i>DSR</i> Value Distributions Surrounding <i>Cavern 1-13&amp;8-13 LTBG</i> .....	99
Figure 5.16 <i>SSR</i> Value Distributions Surrounding <i>Cavern 1-13&amp;8-13 LTBG</i> .....	100
Figure 5.17 <i>DSR</i> and <i>SSR</i> Value Varied with Simulation Time for <i>Cavern 1-13&amp;8-13 LTBG</i> .....	101
Figure 5.18 Predicted Caverns Closure as a Function of Time for <i>Cavern 1-13&amp;8-13 LTBG</i> .....	102
Figure 5.19 Accumulated Vertical Strains along the Axis of Symmetry during Abandonment Simulation ( <i>1-13&amp;8-13 LTBG dense-brine</i> ) .....	103
Figure 5.20 Accumulated Casing Strains at the End of Simulation for <i>Cavern 1-13 LTBG (1-13&amp;8-13 LTBG)</i> .....	104

Figure 5.21 Accumulated Casing Strains at the End of Simulation for Cavern 8-13 LTBG ( <i>1-13&amp;8-13 LTBG</i> ).....	105
Figure 5.22 Predicted Maximum Surface Subsidence over Time ( <i>1-13&amp;8-13 LTBG</i> ) .	106
Figure 5.23 Three-Dimensional Finite Difference Model of <i>Cavern 1-13 LTBG &amp; PRVP</i> .....	108
Figure 5.24 Contour of Deviatoric Stresses Surrounding <i>Cavern 1-13 LTBG &amp; PRVP</i>	112
Figure 5.25 <i>DSR</i> Value Distributions Surrounding <i>Cavern 1-13 LTBG &amp; PRVP</i> .....	113
Figure 5.26 <i>SSR</i> Value Distributions Surrounding <i>Cavern 1-13 LTBG &amp; PRVP</i> .....	114
Figure 5.27 <i>DSR</i> and <i>SSR</i> Value Varied with Simulation Time ( <i>Cavern 1-13 LTBG &amp;</i> <i>PRVP</i> ).....	115
Figure 5.28 Predicted Caverns Closure as a Function of Time ( <i>1-13 LTBG &amp; PRVP</i> ) .	116
Figure 5.29 Accumulated Casing Strains during Simulation for Cavern 1-13 LTBG and Cavern 1-13 PRVP ( <i>1-13 LTBG &amp; PRVP dense-brine</i> ).....	117
Figure 5.30 Accumulated Casing Strains during Simulation for Cavern 1-13 LTBG and Cavern 1-13 PRVP ( <i>1-13 LTBG &amp; PRVP</i> ).....	118
Figure 5.31 Predicted Maximum Surface Subsidence over Time ( <i>1-13 LTBG &amp; PRVP</i> ) .....	119
Figure 5.32 Three-Dimensional Finite Difference Model of <i>Cavern 1-13&amp;8-13</i> <i>LTBG&amp;PRVP</i> .....	121
Figure 5.33 Contour of Deviatoric Stresses Surrounding <i>Cavern 1-13&amp;8-13</i> <i>LTBG&amp;PRVP</i> .....	125
Figure 5.34 <i>DSR</i> Value Distributions Surrounding <i>Cavern 1-13&amp;8-13 LTBG&amp;PRVP</i>	126
Figure 5.35 <i>SSR</i> Value Distributions Surrounding <i>Cavern 1-13&amp;8-13 LTBG&amp;PRVP</i> .	127
Figure 5.36 Minimum <i>DSR</i> and <i>SSR</i> Value Varied with Simulation Time ( <i>Cavern 1-</i> <i>13&amp;8-13 LTBG&amp;PRVP</i> ).....	128

Figure 5.37 <i>DSR Value Evolution of Each Cavern during Simulation (1-13&amp;8-13 LTBG&amp;PRVP)</i> .....	129
Figure 5.38 <i>Predicted Caverns Closure as a Function of Time (1-13&amp;8-13 LTBG&amp;PRVP)</i> .....	130
Figure 5.39 <i>Accumulated Casing Strains during Simulation for Cavern 1-13 LTBG and Cavern 1-13 PRVP (1-13 LTBG&amp;PRVP dense-brine-brine-dense)</i> .....	131
Figure 5.40 <i>Accumulated Casing Strains during Simulation for Cavern 8-13 LTBG and Cavern 8-13 PRVP (1-13 LTBG&amp;PRVP dense- brine-brine-dense)</i> .....	132
Figure 5.41 <i>Accumulated Casing Strains during Simulation for 1-13 Well Caverns (1-13&amp;8-13 LTBG&amp;PRVP)</i> .....	133
Figure 5.42 <i>Accumulated Casing Strains during Simulation for 8-13 Well Caverns (1-13&amp;8-13 LTBG&amp;PRVP)</i> .....	134
Figure 5.43 <i>Predicted Maximum Surface Subsidence over Time (1-13&amp;8-13 LTBG&amp;PRVP)</i> .....	135

# 1 INTRODUCTION

## 1.1 Problem Statement

Due to the favourable geomechanical properties of rock salt, including very low permeability and high ductility behavior, underground salt caverns have increasingly attracted the attention of petroleum industry as secure storage facilities for gas and liquid storage and for the disposal of waste. Underground storage of petroleum products is more economical than surface storage tanks as they can provide much greater volumes and pressures to be achieved. This becomes more evident when taking into account the small surface footprint and decreased security against external influences. The other advantage of the underground storage in salt deposits is that salt caverns may be created by solution mining techniques instead of the more costly conventional excavation techniques. These advantages make salt formation one of the prime alternatives for the development of underground cavities for storage of petroleum products, non-hazardous oil field wastes, or radioactive wastes and hazardous chemical wastes.

In 1996, the Argonne National Laboratory conducted a preliminary technical and legal evaluation of the disposal of non-hazardous oil field wastes into salt caverns at the request of the U.S. Department of Energy. Since then, the disposal of oil field wastes into salt caverns became feasible and legal. If the salt caverns are sited and designed well, operated carefully, abandoned properly, and monitored routinely, they can be a suitable means for oil field waste disposal. Due to the increasing interest in using salt caverns for nonhazardous oil field waste disposal, additional investigations of the geomechanical response and the accompanying risks associated with such disposal were conducted in recent years.

This thesis focuses on the numerical assessment of the geomechanical response and performance of solution-mined salt caverns during their development, operation (both dissolution and waste disposal) and long-term abandonment intervals. The geomechanical investigation assigns emphasis on the structural stability and the integrity of the salt caverns, the likelihood of nonsalt overlying caprock failure and casing failure, stress development surrounding the caverns, and the maximum surface subsidence induced both during operation and permanent abandonment. Additionally, the numerical investigations are performed on multiple salt caverns, with up to four salt caverns (two downhole caverns in one salt formation and two vertically aligned uphole caverns in a second salt formation), to assess the interactions between adjacent caverns. The constitutive model to characterize the mechanical behavior of rock salt uses a Lagrangian three-dimensional finite-difference program to simulate the geomechanical behavior of the disposal salt caverns during cavern development, operation and abandonment.

## **1.2 Objective of Thesis**

The accuracy of numerical performance predictions and analysis of the geomechanical behavior of the disposal salt caverns will depend on how well the applied simulators match the physical properties of the geological units.

The overall objective of the research documented in this thesis is the analysis of the numerical modeling results to identify the geomechanical performance of the salt caverns used to contain oil field solid waste disposal, during the development, operation and abandonment. Related analysis of the field core logging, laboratory testing geological studies, and parametric sensitivity studies were performed to contribute to the numerical investigations.

The objective of the geological framework, core logging interpretation and laboratory testing program is the determination of the stratigraphic settings, geomechanical properties of the reservoir materials, including both salt and nonsalt strata. The constitutive models used to characterize the mechanical behavior of the materials are determined based on the above work, benefiting the numerical modeling studies.

The objective of the parametric sensitivity analysis for the three-dimensional finite difference programs is the degree of verification and applicability of the suggested simulators used for assessing the geomechanical response of the proposed disposal caverns for permanent abandonment.

The objective of the numerical investigations of the long-term geomechanical behavior of the disposal salt caverns is to identify the structural stability and integrity, the deformation and closure behavior of the salt caverns, and the interactions between adjacent solution-mined salt caverns under various configurations and cavern disposal conditions.

### **1.3 Scope of Thesis**

The rapid increase in the development of salt caverns for oil field waste disposal has led to increased researches and literature. Chapter 2 introduces and discusses selected concepts specific to the area dealing with waste disposal salt caverns, including associated geological considerations and the characterization of disposed waste and cavern post-closure behavior.

Chapter 3 presents all the primary work performed related to the northeast Alberta disposal cavern site, in support of the subsequent numerical modeling investigations. The parameters used to characterize the geomechanical behavior of the salt and nonsalt strata

were evaluated from laboratory testing results, generated in a parallel study to this research, and geophysical logging interpretation.

In Chapter 4, the sensitivity analyses focused on various model conditions and mechanical parameters were performed and analyzed using the three-dimensional finite difference programs, to provide a degree of verification that the numerical approach can reasonably represent the geomechanical response of the waste-filled salt caverns during operation and after abandonment.

Chapter 5 illustrates and analyzes the numerical analytical geomechanical response of disposal salt caverns under different cavern injection conditions and various configurations of multiple caverns, in terms of comparing specific cavern structural stability and integrity assessment criterions. Chapter 6 provides the conclusions derived from the research and recommendations for further research.

## **2 LITERATURE REVIEW**

### **2.1 Introductions**

Due to the favourable geomechanical properties of rock salt (halite), which includes low permeability and creep behavior, underground salt caverns have been used increasingly for gas and liquid storage and the disposal of waste. Underground depositories in salt are safer from an environmental point of view than conventional depositories in shallow ground. The purpose of this chapter is to present a summary of published literature pertaining to the underground solution mined salt caverns used for storage of oilfield waste disposal. A brief introduction of the solution mining operational scenario for salt caverns and their use as storage facilities in engineering practise are described in Section 2.2. The special and featured site geological settings of salt caverns for disposing solid waste are considered in Section 2.3. Section 2.4 emphasizes the characterization of the waste disposal and the post-closure behavior of salt caverns after sealing and permanent abandonment. The time-dependent deformation mechanism of the rock salt is demonstrated in Section 2.5, as well as the Norton power law and its limitations in characterizing the geomechanical response for underground salt caverns.

### **2.2 Solution-mined Salt Caverns and Its Storage Use**

#### **2.2.1 Solution Mining Operation**

Salt solution mining is the process of mining various amount of salts by dissolving them using fresh water or unsaturated brine and is based on the high solubility of the rock salt formation. Fluids are injected through a specifically designed well drilled into a salt bed to form a void or cavern. Typically every 7 to 8 m<sup>3</sup> of freshwater could dissolve 1 m<sup>3</sup> of halite. Once the cavern reaches its maximum permitted size or cannot be operated

efficiently, brine production stops and the cavern is either filled with brine or used for other purposes such as hydrocarbon storage or waste disposal.

The advantage of the solution mining method compared with conventional mining is that the product quality and the extraction operation are not significantly influenced by climate conditions or rock strength. When complex situations such as folded or disturbed beds and deep lying strata are encountered, solution mining can still be used while conventional mining techniques cannot be efficiently applied. Moreover, unlike the large amount of aboveground waste piles and tailing impoundments generated by conventional mining operations, insoluble waste components remain in the cavern to settle down to the bottom of the salt caverns during the solution mining process when the brine production is being pumped to the surface facilities.

Salt caverns are usually located at depths greater than 400 to 500 m and may be as deep as 2000 m. To date, the deepest salt cavity is in the northern Netherlands in Zechstein salts at a depth of 2900 m. The cavern volume is likely significantly reduced due to the higher salt creep rate of the rock salt formation under large overburden pressures.

The first step in solution mining is to drill a borehole to the target depth within the salt strata. The diameter of the borehole needs to be large enough to accommodate all the required casings, including surface casing (outer casing), final casing and middle casing (tubing), which are all concentrically layered. The surface casing is positioned outermost and is cemented in place to prevent any leakage and contamination onto the groundwater, thus the surface casing does not typically extend all the way down to the depth of the cavern roof. Internal to the surface casing is the cemented in-place final casing, which is dropped down to some depth below the top of the aimed salt strata for the purpose of maintaining a minimum required thickness of salt formation over the dissolved salt cavity.

roof, increasing the structural stability and integrity of salt cavern. Inside the final casing there are two or more non-cemented casing strings also called annular tubing and middle tubing. The tubing strings firstly extend to designed depth of the cavern bottom and then as the cavern is expanded by solution mining, they are rotated and raised to fulfill the planned size and shape of the cavity.

Since freshwater has a lower density than brine, it will float in the upper part of the cavity. The vertical rate of dissolution of speed rock salt is 1.5 to 2.0 times faster than in horizontal direction. To control the upward leaching velocity and prevent possible cavern roof collapse, a fluid blanket with inert properties and a lower density than feed solvents is usually utilized and injected through the annular space between the outer casing and middle tubing. Currently, compressed nitrogen and/or air are the preferred fluid blanket as it is relatively free of environmental and safety issues.

Direct circulation and indirect circulation (reverse circulation) are the most commonly used methods of salt cavern development, as shown in Figure 2.1. For direct circulation method, the feed solvent (freshwater or unsaturated brine) is injected through the middle tubing string and the resulting brine is withdrawn via the annular space between the final casing and middle tubing. For reverse circulation, feed solvent enters the cavern through the annular tubing and brine is pumped out via the middle tubing string. The cavity dissolved by reverse circulation method usually has a wider top and narrow bottom part, while direct circulation solutioning tends to generate a more cylindrical shaped void.

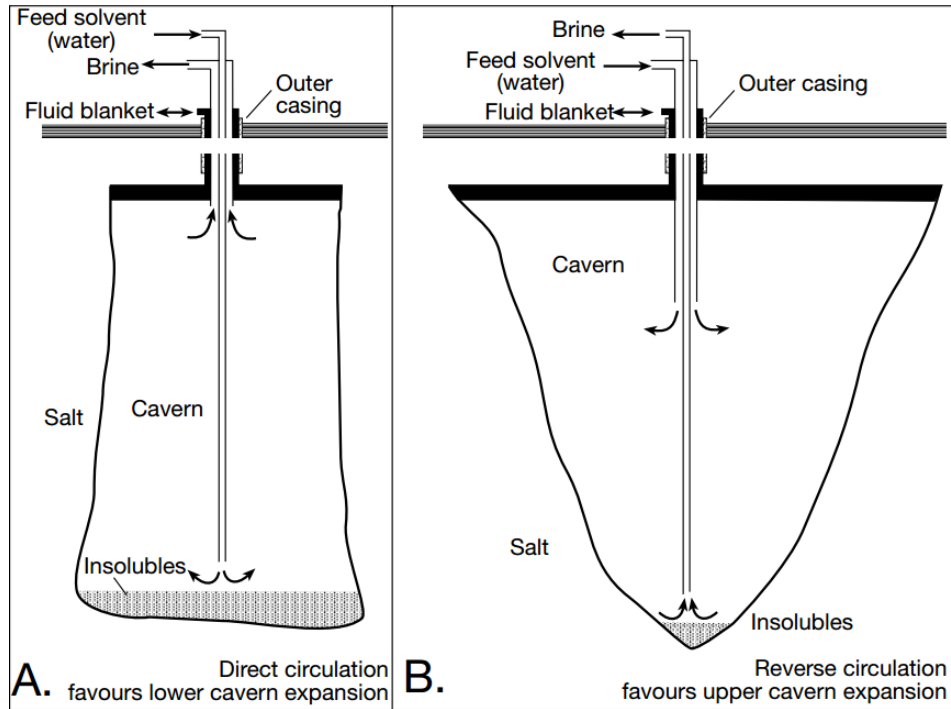


Figure 2.1 Direct and Reverse Circulation Method in Solution Mining Salt

## 2.2.2 Solution Mined Salt Cavern Use

In the past decades, there has been a rapid increase in the number of salt caverns solution mined specifically for the purpose as the storage vessels for hydrocarbons and wastes, as compared to those only for brine production or other chemical feedstock. Storage of liquid and gaseous hydrocarbons was successful early on and remains the primary use of salt caverns today. Disposal of wastes constitutes the second most important application for salt caverns.

### 2.2.2.1 Hydrocarbon Storage

Initially, salt caverns were only dissolved for brine production. The brine could be dried and used for salt; other inorganic chemicals could be extracted, or be sold for use in drilling fluids for drilling oil and gas wells.

Various types of hydrocarbons had been stored in solution-mined caverns since the 1940s in North America and then spread rapidly throughout the world. The types of the stored hydrocarbon products within salt caverns include liquefied petroleum gas (LPG), light hydrocarbon (propane, butane, ethane, ethylene, fuel oil, and gasoline), natural gas and crude oil.

Storage of light hydrocarbon via the brine compensation method represents the first and most widespread use of salt caverns worldwide (Thoms and Gehle, 2000). The first reportedly conceived storage of liquids and gases in solution mined salt caverns was in Canada early during World War II (Bays, 1963), followed by the storage of Liquefied petroleum gas (LPG) within caverns in bedded Permian salts near Kermit, Texas in United States a few years later in 1949 (Warren, 2006).

The event of crude oil storage into salt caverns first occurred in England in the early 1950s (Joachim, 1994). The Strategic Petroleum Reserve (SPR) maintained by US department of Energy (DOE), which was founded in 1975, aimed to store the first 250 million barrels of crude oil in previously solution-mined salt caverns to apply a rapid way for securing an emergency supply of crude oil following the oil shocks of the 1970s. Additional caverns were created to stockpile more in later years. SPR now owns the largest underground storage operations in the United States and currently stores up to more than 700 million barrels (83.47 million cubic meters) of crude oil in 62 underground caverns along the coastline of the Gulf of Mexico located in Louisiana and Texas. The total crude oil storage in salt caverns of USA had reached approximately  $102.1 \times 10^6 \text{ m}^3$  in 2000 (after R.L. Thoms and R.M. Gehle).

Storage of natural gas in salt caverns was introduced at Unity, Saskatchewan in Canada early in 1959 (Warren, 2006). In 1963, the first engineered purposely designed solution

mined gas storage salt caverns were constructed at a depth of 1100 m in bedded Devonian salt in Saskatchewan, Canada. Due to the relatively higher internal storage pressures required for gas, as opposed to liquid hydrocarbons, and correspondingly, increased concerns on the cavern integrity related to bedded salt, the first designed gas cavern in a salt dome was solution mined in Eminence, Mississippi in US, at the depth of 1740 to 2040 meters. The total natural gas storage in salt caverns targeted to be 552.7 million cubic meters in Canada and to 3423 million cubic meters in USA respectively in 2000 (Thoms and Gehle, 2000). In recent years, the natural gas storage volume is still increasing rapidly, and is attributed to its distinct advantages compared to conventional ground-level gas storage and other underground facilities (e.g. depleted oil and gas fields or suitable aquifers). A gas storage salt cavern can offer very high deliverability and rapid product cycling that operators can change from injection to withdrawal in 15 minutes and back to injection within 30 minutes (Warren, 2006). Moreover, the purposely developed natural gas storage caverns are consistently safer and cleaner than other alternative storage facilities, however, there are significantly higher initial construction costs. Maintenance costs are higher for the ground level facilities due to much lower cycling rates, limited storage capacity and higher potential for damage and failure during an incident, and a greater demand for cushion gas (permanent gas inventory in a storage reservoir to maintain adequate pressure and deliverability rates throughout the withdrawal season). In conclusion, deep caverns in thicker salt domes or homogeneous salt strata are considered to be the safest storage facilities for hydrocarbon products.

#### **2.2.2.2 Waste Disposal**

Various types of wastes are generated during the process of drilling oil and gas wells and pumping or producing oil and gas to the surface, and these oil field wastes must be addressed in an environmentally secure manner. Solution mined salt caverns of distinct

geomechanical properties can represent secure repositories to dispose large volumes of petroleum industry wastes, and have been recognized by companies world-wide.

Solution-mined salt cavern for the disposal of wastes, likely residues from local salt-based industries was first introduced in 1959 at south Manchester, England (Warren, 2006). Aside from brine wastes, salt caverns are now used as environmentally secure containment for disposal of various types of oil field waste. The state of Texas in the USA have legislated six salt caverns for nonhazardous oilfield waste (NOW) disposal and one salt cavern for naturally occurring radioactive material (NORM). Canada has also authorized the disposal of oilfield wastes into salt caverns near Edmonton, Alberta and Unity, Saskatchewan. In the oil industry, the wastes suitable for salt cavern disposal include (1) produced sand and solids from heavy oil operations; (2) contaminated soils from produced oil and water spills; (3) tank bottoms (solids or semisolids that settle in the bottoms of storage tanks) from treaters and other facilities; (4) ecology pit solids and sludge with heavy metals; (5) NORMS from pipe scale and other sources; (6) Refinery catalysts and noxious solids streams; (7) site remediation solids (i.e, refinery site cleanup) (Davidson and Dusseault, 1997). In Alberta and Saskatchewan, salt caverns located between the depth of 1200 and 1500 m are mainly being used for non-hazardous oilfield wastes disposal and the storage for natural gas and liquids (propane, glycol, etc.).

Naturally occurring radioactive wastes disposed of in salt caverns are of more concern due to their toxicity and potential migration and contamination of the surrounding environment as a result of potential cavern failure during the life of the cavern. Germany requires all waste that cannot be stored for extensive periods at ground level without posing a serious threat to the biosphere even after treatment should be stored in proper underground geological formations. Early in 1990s, the German government engineered and operated the first radioactive waste repositories in the Gorleben and Asse salt domes

and on the Konrad iron ore mine. Until 1979, this facility was still used as the final repository of low level radioactive waste disposal. Experimental studies supported the movement of this waste into the Gorleben salt disposal caverns over the next two decades.

In March 1999, the Department of Energy (DOE) in the USA opened its Waste Isolation Pilot Plant (WIPP) for the purpose of placing nuclear waste in a bedded salt formation in New Mexico after years of careful studies. This provided support for the secure protection offered by salt formations. Although the caverns were constructed by conventional mining in bedded salt bodies, the caverns are subjected to the same creep, closure, temperature and pressure considerations as pressurized solution mined caverns. However, the experimental studies still remained focused on relatively shallow sites (about 500 m below the ground) but not on the development of deep engineered disposal caverns at that stage. Several planned natural gas explosions in the salt cavities demonstrated that the salt caverns could tolerate all the purposely designed blasts and were only enlarged by 17 metres (55 feet) and no leakage of radioactivity has been observed on the salt site to date. This illustrated the secure containment and continued integrity of the salt cavern, even when subjected to the rigorous nuclear explosions within the caverns (Warren, 2006).

The high costs associated with the disposal of non-toxic wastes in salt caverns likely limits their use, but permanent abandonment of toxic materials (including low toxicity wastes such as foundry sands, contaminated soil and other granular solid wastes) in salt caverns is economically competitive as compared to other alternative disposal or storage approaches (Duyvestyn and Davidson, 1998). Disposal of high level toxic wastes in small volume purposely designed and developed caverns is justified on the basis of waste isolation and environmental security. Typically, caverns with a volume no more than 200,000 m<sup>3</sup> are more suitable for medium and high toxicity wastes, while relatively large

caverns of up to 500,000 m<sup>3</sup> can be utilized to store non-toxic or low toxicity wastes without any sacrifice in security and stability (Davison and Dusseault, 1997).

## **2.3 Site Geological Settings for Disposal Salt Caverns**

The search for potential new salt caverns development areas or use of existing solution mined caverns for the permanent disposal of oilfield solid waste of low-risk requires a comprehensive site investigation of the geological setting that must address the evaluation of geological features and hydrogeological conditions which are of primary importance, as well as exploitation technical approaches and regulatory issues, which are not the focus in this thesis and will not be discussed in the following section.

### **2.3.1 Geological Considerations**

The ideal geological settings for disposal caverns will be composed of either thick extensive flat-lying or gently sloping salt strata at depths greater than 350 m with overburden and under-burden beds of alternating low and high permeability strata (Davison and Dusseault, 1997).

Specifically whether the bedded salt strata or salt domes can be utilized for encapsulation of industrial solid wastes depends on the following geological factors. Firstly, the site topography should be of low relief. Irregular topography may indicate complex geological and hydrogeological conditions and high relief topography may imply differential stress conditions on the salt that could impair the long-term integrity of the salt caverns. Secondly, it is desirable that the lithostratigraphy be comprised of continuous thick sediment sequences with alternating low and high permeability horizontal beds above and below the salt. Lastly, significant faults and joint zones in the overlying and underlying formations which may provide pathways for formation fluids as well as the fluids expelled from caverns during long-term abandonment are less preferred.

### **2.3.2 Hydrogeological Considerations**

The assessment of hydrogeological characteristics is mainly focused on the state of isolation of the disposal salt caverns from shallow potable waters and deep aquifer formation water flux. Once contaminated fluids leave a cavern, they would be expected to migrate laterally and vertically through different formations and aquifers, potential contaminating biosphere. The local water resource conditions and formation water distributions and embedment features need to be well understood and identified. Typically the volumes of the feed solvent for dissolving salt caverns will be seven to ten time of the cavern capacity. Regional and local flow regimes are required to analyze the disposal caverns integrity during long-term abandonment. The groundwater flow mechanism will be established from the information of fractures network in over-burden and under-burden layers, and the pressure distributions as well as hydraulic conductivity of rock units.

## **2.4 Cavern Waste Disposal Characterization**

### **2.4.1 Waste Disposal in Salt Caverns**

Various types of wastes could be generated during the process of drilling oil and gas wells and pumping or producing oil and gas to the surface, and those oil filed waste must be buried and abandoned in an environmentally secure manner.

In the oil industry, the wastes suitable for salt cavern disposal include (1) produced sand and solids from heavy oil operations; (2) contaminated soils from produced oil and water spills; (3) tank bottoms (solids or semisolids that settle in the bottoms of storage tanks) from treaters and other facilities; (4) ecology pit solids and sludge with heavy metals; (5) NORMS from pipe scale and other sources; (6) Refinery catalysts and noxious solids

streams; (7) site remediation solids (i.e., refinery site cleanup). The majority of material disposed into the salt caverns would be tank bottom wastes, and this solid or sludge-like waste consists of accumulated heavy hydrocarbons, paraffin, inorganic solids and heavy emulsions. The waste consists of approximately 50% water, 15% clay, 10% shale, 10% corrosion products, 10% oil, and 5% sands (Tomasko, 1997).

The underground solution-mined salt caverns would be filled with brine fluid initially, and then the waste would be introduced into the cavern as slurry of waste and brine or fresh water as the fluid carrier. The disposal waste can be pumped down the middle tubing to the cavern bottom and the displaced brine can be withdrawn through the annulus similar to the direct solution mining scenario, or the reversed injection scenario could be used. Another way of waste injection is that the waste can be injected through one well and the displaced brine will be pumped out through another well. Once the waste slurry is injected, the cavern will act as an oil-water-solids separator such that the solids, oils, and other liquids will separate into distinct layers. The heavier solids fall to the bottom and form a pile, the less dense oily materials float to the top where they form a protective pad, preventing unwanted dissolution of the cavern roof. The brine and other watery fluids remain in a middle layer, forming a suspension above the brine-waste interface. The brine displaced during waste disposal operation becomes dirtier than brine from other hydrocarbon storage salt cavern, and it will have a higher clay and oil content. The dirty brine can present operational difficulties such as clogging of the pumps and additional costs. Once the cavern is fully filled with disposal waste it will be sealed and the borehole will be plugged with cement. Bridge plugs will be placed above and below the water bearing intervals in the wellbore to isolate these intervals permanently (Tomasko, 1997), which is often used in oil and gas industry to abandon wells.

#### **2.4.2 Post-Closure Behavior of Disposal Salt Caverns**

Various complex physical processes take place in the waste-filled salt caverns after abandonment. The salt units surrounding the disposal caverns will flow into the cavern due to creep behavior, causing the volumetric reduction of the storage caverns. Moreover, the convective mixing in the upper brine-filled portion of the caverns, differential settling and compaction of the solids, chemical reaction and compaction of the waste material, and an increased pressure produced by the combined effects of the salt creep and the addition of sensible heat derived from the geothermal gradient vertically across the cavern, would occur within the plugged and abandoned waste storage caverns.

The metal components of the waste material could corrode and generate hydrogen gas, especially in an acidic environment. The presence of small quantity of gas in the seal caverns can mitigate the influence of the pressure buildup because the gas could increase the cavern compressibility dramatically or reduce the cavern stiffness (Berest et al, 1997a). However, the produced gas quantity controlled and limited for several reasons to prevent the equipment failure in the production systems. In a waste cavern, the pH is controlled by the partial pressure of the carbon dioxide. The carbon dioxide levels in the surrounding units of the cavern would not support a significant corrosion rate and thus the induced hydrogen gas would be negligible. Additionally, the gas production in caverns will also be controlled by the pressure effects. The rate of the gas generation would fall correspondingly with the built-up cavern pressures.

The permeability of the ambient material of the caverns can influence the pressure buildup as well (Wallner and Paar, 1997). The cavern pressure can exceed the lithostatic values after a long time period due to the salt creep and thermal expansion of the brine. When the brine pressure is balanced with the average lithostatic pressure, a slight excess of brine pressure at the top of the cavern will be generated because the brine pressure is

isotropic within the cavern while the lithostatic pressure increases linearly with the depth (Langer et al, 1984). When the fluid pressure exceeds the salt stresses, stress-induced microfractures may be produced on the top of the cavern and the rock salt units become permeable. Then small leakage rates will be predicted, which could compensate for the over-pressurization at the top of the cavern and return the system to an equilibrium condition.

## **2.5 Mechanical Properties of Rock Salt**

The mechanical behaviour of rock salt shows very distinctive features in comparison with other common rock types such as hard rocks found in the Canadian Shield. The behaviour of rock salt is more ductile, and its increased deformability is accompanied by a strong time dependency. This non-linear rate-dependent behaviour must be taken into account in the analysis of underground openings in rock salt. However, modeling such response is a challenging task, especially when dealing with the different inelastic phases, which typically include quasi-instantaneous (elastic and/or plastic), transient and steady-state responses.

### **2.5.1 Time-dependent Deformation Mechanism of Rock Salt**

Time-dependent deformation is recognized as one of the most important properties of rock salt. Idealized phenomenological creep response under a constant state of external loading was suggested to depict the non-linear time-dependent deformation behavior of salt rock. The typical creep curve as shown in Figure 2.2 has up to four stages, namely the pseudo-instantaneous strain stage (Phase I), primary creep (Phase II), the secondary creep (Phase III), and the tertiary creep (Phase IV). At the very beginning of phase I, instantaneous elastic strains are produced as a result of the applied stress, including elastic  $\varepsilon^e$  and plastic  $\varepsilon^p$  strains. Then the subsequent concave-downwards strain-time

curve represents the primary or transient creep. If the applied stress were released during the transient phase, all deformations would be recovered. If there is no stress release, then the secondary or steady-state creep will be characterized by a constant strain rate. It is suggested that if the differential stress is suddenly reduced to zero after the secondary stage has initialized, part of the total deformation will be permanent strain and will not be recoverable. Kaiser and Morgenstern (1981) suggested that the steady-state creep might only exist under very special rare conditions. The tertiary or accelerating creep presented by a concave-upwards curve with strain rate ascending with time, leads to rapid failure. The dependence between the creep rate and the applied differential stress is also shown in the figure. The creep deformation will increase with the higher applied differential stresses, at the same confining stress level.

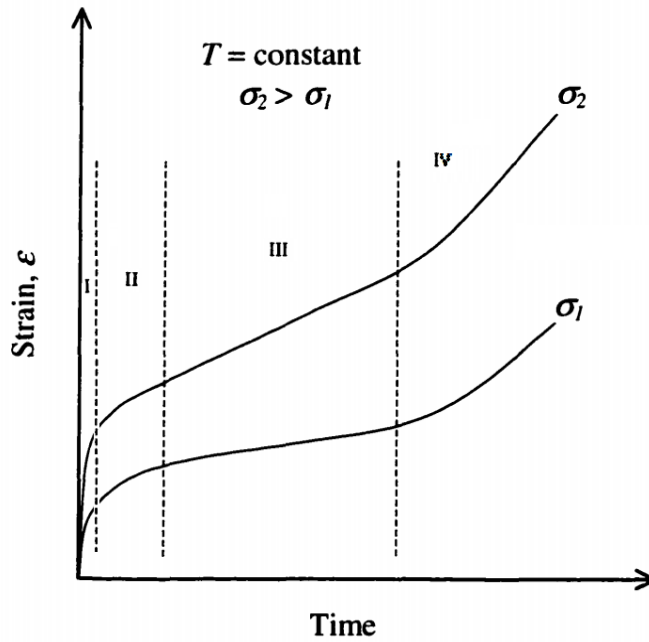


Figure 2.2 Idealized Creep Curve as a Function of Time

The last three phases of time-dependent creep strains  $\epsilon^c$  includes the transient strain  $\epsilon_t$ , steady-state or stationary strain  $\epsilon_s$ , and accelerating or tertiary strain  $\epsilon_a$ . Tertiary strain is frequently omitted in usual applications, and the total strain rate can be expressed by the following equations:

$$\dot{\epsilon} = \dot{\epsilon}^e + \dot{\epsilon}^p + \dot{\epsilon}^c \quad \text{Equation 2-1}$$

with

$$\dot{\epsilon}^c = \dot{\epsilon}_t + \dot{\epsilon}_s + \dot{\epsilon}_a \quad \text{Equation 2-2}$$

Each component in the equations can be described by distinct functions or laws. In this thesis, the constitutive model of Norton creep law associated with a steady-state flow law is used to characterize the rock salt inelastic responses.

## 2.5.2 Norton Creep Law

The Norton creep law (1929) is a classical power law used to describe the stationary creep, written as equations:

$$\dot{\varepsilon}_{cr} = A\bar{\sigma}^n \quad \text{Equation 2-3}$$

$$\Delta\sigma_{ij}^d = 2G(\dot{\varepsilon}_{ij}^d - \dot{\varepsilon}_{ij}^c)\Delta t \quad \text{Equation 2-4}$$

$$\dot{\varepsilon}_{ij}^c = \left(\frac{3}{2}\right)\dot{\varepsilon}_{cr} \left(\frac{\sigma_{ij}^d}{\bar{\sigma}}\right) \quad \text{Equation 2-5}$$

where:

$\dot{\varepsilon}_{cr}$ : Steady-state creep rate

A and n: Material properties

$\bar{\sigma}$ : Von Mises stress, by definition  $\bar{\sigma} = \sqrt{3J_2}$

$J_2$ : Second invariant of the effective deviatoric-stress tensor,  $J_2 = \frac{1}{2}\sigma_{ij}^d\sigma_{ij}^d$

G: Shear modulus

$\dot{\varepsilon}_{ij}^c$ : Creep strain tensor

$\dot{\varepsilon}_{ij}^d$ : Deviatoric part of the strain-rate tensor

Equation 2-3 indicates that the creep of the salt is activated by the Von Mises stress based on the power law. As shown in Equation 2-4, the deviatoric stress increments are

viscoelastic. The microphysical mechanism involved in the power law is the dislocation climb. It is the most common mechanism investigated by salt researchers. The dislocation mechanism is controlled by a thermal activated equilibrium process and occurs at moderate to high temperature when blocked dislocations move out of their glide planes.

It is important to note that the Norton creep law is only an approximation of the actual creep behavior of salt. It neglects the strain occurring in the transient phase, and it idealises the stress-strain rate relationship, which has been shown to be better described by the hyperbolic sine law (Julien 1999, Yahya et al. 2000). This model is nevertheless largely used because of its simplicity of application. However, the fundamental limitations of the Norton power law may induce some significant deviation from the actual rock salt behavior, especially under the complex loading conditions encountered in natural geomechanical settings (Aubertin et al. 1993, 1999a).

Several numerical investigations of the implementation of the Norton power law in characterizing the rock salt mechanical response, in contrast with other constitutive models were performed on pressurized thick wall cylinders and mind pillars (Boulianne, 2004). It is suggested that the Norton power law could predict appreciable stress variations inside along the cylinder radius of the thick-wall cavities. However, the Norton model will largely underestimate the strain and deformation behavior because it only considers the steady-state creep phase inherently. This limitation can be even more pronounced when it comes to describe the actual underground cylindrical openings under more complex geometry and/or loading conditions. Moreover, the stresses obtained with Norton creep law are smaller in the pillar but larger in the roof of the excavations.

### **3 NUMERICAL ANALYTICAL METHODOLOGY FOR DISPOSAL SALT CAVERNS**

#### **3.1 Introduction**

A geological overview of the potential disposal cavern site, interpretations of the wireline logging data, and numerous laboratory testing studies of the core specimens recovered from the field were performed prior to the numerical investigations of the geomechanical performance of the solution-mined disposal caverns in northeast Alberta. The geological framework of Elk Point Group, in which the cavern site is located, is detailed in Section 3.2. Then the stratigraphic setting and the descriptions of the northeast Alberta disposal salt caverns were built based on the previous work are described in Section 3.3. Section 3.4 specifies the geomechanical properties used for both salt and non-salt strata as evaluated from the various laboratory testing performed on core specimens to characterize the mechanical behavior and response during numerical simulation analysis. The in-situ stress conditions as well as the representation of the waste disposal for numerical studies are interpreted in Section 3.5. A brief introduction of the three-dimensional finite-difference program, which will be the numerical analytical tool in this thesis is given in Section 3.6, including the modeling solutions.

#### **3.2 Geological Overview of Disposal Salt Cavern Site**

Several extensive regionally distributed salt deposits are located in the Western Canada Sedimentary Basin, especially within the Devonian Elk Point Group. The term Elk Point Formation was first introduced by McGehee (1994) and then was raised to a group unit by Belyea (1952) to describe the thick succession of evaporitic deposits in the subsurface

of the east-central Alberta between pre-Devonian rocks and the upper Devonian. The Elk Point Group contains almost 60,000 km<sup>3</sup> rock salt in total (Zharkov, 1988).

The salt caverns designed for oilfield solid waste disposal of research interests in this thesis are placed in the Elk Point Group, within northeast Alberta. The field well logging data used to interpret the formation mechanical properties for geomechanical assessment studies are all taken from the 8B WD LIND 8-13 well. It is about 5.25 km from the Anglo-Canadian Elk Point No. 11 well, which is the type section for the Elk Point Group.

Drees (1986) depicted and modified the detailed schematic picture of the formations of the Devonian Elk Point Group (Appendix Figure A.1) and the Albert Energy and Utilities Board (AEUB) and Alberta Geological Survey (AGS) conducted more project data checking and processing and updated the geological settings of the Elk Point Group in 2000. As shown in Figure A.1, the Elk point Group was divided into upper and lower Elk Point subgroups. In central Alberta, the lower Elk Point consists of the Basal Red Beds unit, the Lotsberg salt, the Ernestina Lake, the Cold Lake and Contact Rapids formation in ascending order. Due to the history of repeated solution and redistribution, the Lotsberg and Cold Lake formations contain extraordinarily pure salt. An unnamed red shale interval separates the upper Lotsberg and lower Lotsberg formation in the lower Elk Point Group, which has a thickness of 28 to 67 m by Grobe (2000). Grobe also mapped all the distribution and thickness of each salt formation within the Elk Point Group. According to values given from the depth and isopach maps of salt strata, it can be estimated that the proposed disposal salt caverns are sited in the region of about 125 m - thick of upper Lotsberg salt and around 40 m - thick of Cold Lake salt. The thickness of lower Lotsberg salt is not shown within the isopach map, which may indicate that no lower Lotsberg formation locally exist under the salt caverns. The upper Elk Point Group is comprised of Winnipegosis, which is stratigraphically equivalent to Keg River in Northern Alberta, and

Prairie Evaporite salt, Dawson Bay Formation and Watt Mountain Formation. Within the salt caverns region, the Prairie Evaporite salt is interbedded with anhydrite, and overlain by red beds and carbonates. It contains more than 40% of halite, with a thickness of approximately 150 m evaluated from the provided isopach map. The upper most unit of the Elk Point Group in central Alberta is the Watt Mountain Formation.

The local geological description and exact formation depths were determined from the gamma ray (GR) log, density (Rho) log and compressive velocity ( $V_p$ ) log extracted from the 8-13 wireline logging data for the disposal salt caverns at site, using RokDoc™. Figure 3.1 shows that the well reaches the subsurface of the Watt Mountain Formation from the surface ground, and then penetrates into the Prairie Evaporite salt and Cold Lake salt strata completely and extends to the depth of 1244.2 m, only 30 m into the Lotsberg salt, leaving the thickness of the Lotsberg formation undetermined. Another logging well located about 340 m away named 8B WD LIND 2-13, reaching downward to more than 1600 m, indicates that the Lotsberg salt has the thickness of approximately 115 m at this location. A group of another 10 vertical well logs in the surrounding area confirms the thickness of other salt and non-salt formations and the geological consistency of all the interest formations, which includes the Lotsberg, Ernestina Lake, Cold Lake, Keg River, Prairie Evaporite, and Watt Mountain Formation in ascending elevation order.

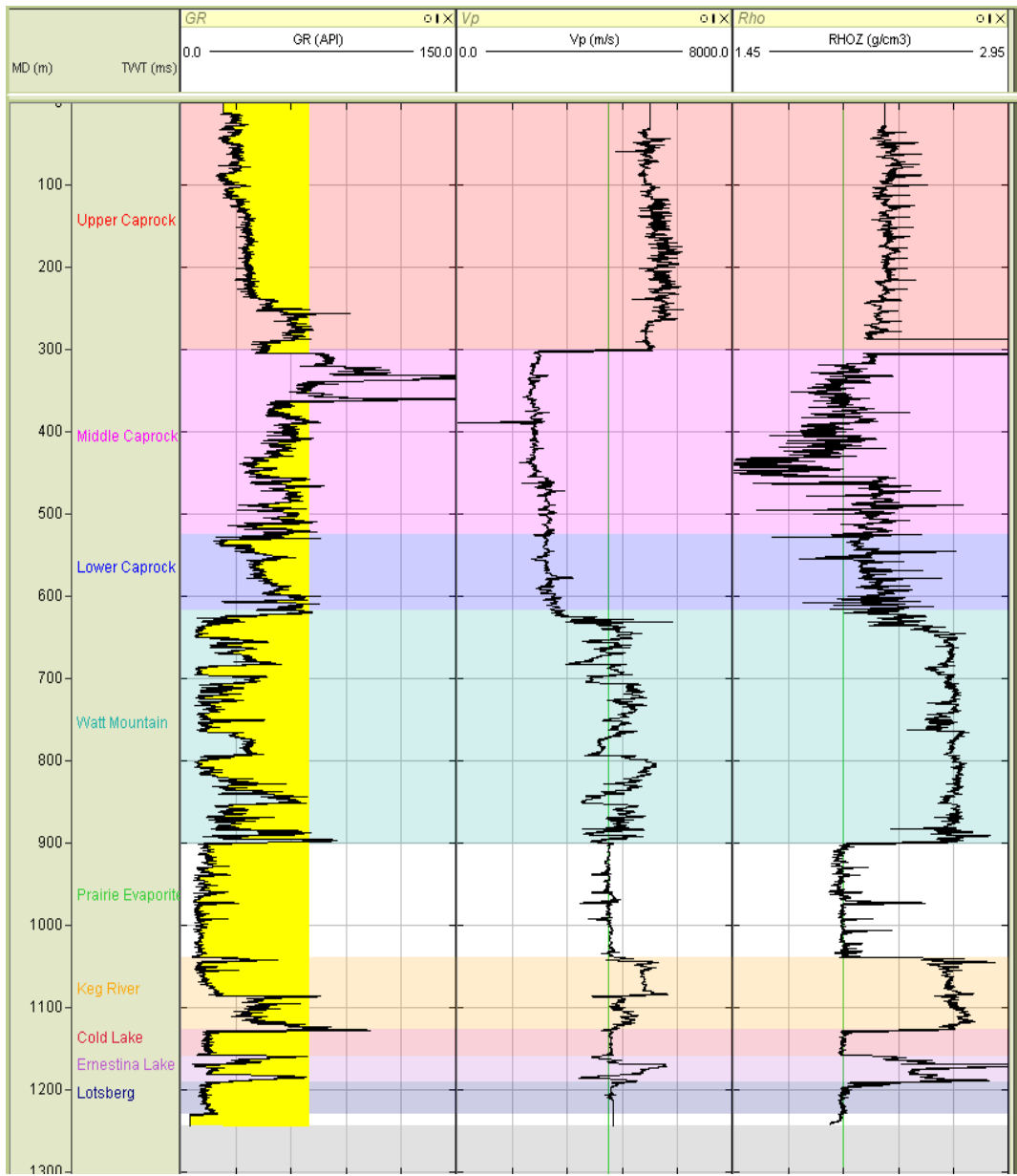


Figure 3.1 Stratigraphical View from GR,  $V_p$  and Rho log from 8-13 Well Logging

### **3.3 Disposal Salt Cavern Description**

Initially four waste disposal caverns were planned to be solution mined in the field domain, including two upper caverns in the Prairie Evaporite Formation and two lower caverns in the Lotsberg Formation. Figure 3.2 illustrates the schematic cross-sectional view of the site formations and disposal caverns. Each cavern is notated by its formation name and well location, thus these four caverns are named by Cavern 1-13 LTBG, Cavern 8-13 LTBG, Cavern 1-13 PRVP, and Cavern 8-13 PRVP respectively, as indicated in Figure 3.2.

Solution mining of the 1-13 LTBG cavern started in 2004 followed with the development of the 8-13 LTBG cavern in 2012. Both 1-13 LTBG and 8-13 LTBG caverns are located between the depth of about 1206 m and 1305 m in Lotsberg Formation, having a proposed volume of approximately 750,000 m<sup>3</sup>. The spacing from cavern top or bottom to the surrounding formation interface is about 10 m, which may benefit the cavern stability and integrity from engineering experience. Cavern 1-13 LTBG is almost reaching the target size now and has an irregular shape with a maximum diameter of approximately 145 m. Cavern 8-13 LTBG was mined to be more regular and cylindrical based on the solutioning experience gained from Cavern 1-13 LTBG. Two uphole Prairie Evaporite caverns, i.e. cavern 1-13 PRVP and 8-13 PRVP, are expected to be developed following the abandonment of two Lotsberg caverns, and then injected with disposal waste, plugged and abandoned subsequently. The centre to centre spacing of 1-13 and 8-13 well caverns is about 300 m.

The geological description and formation was analysed and determined in Petrel (Version 2010.2.2) and RokDoc<sup>TM</sup> (Version 5.6.3) based on the downhole wireline logs performed in the site cavern wells. Ten strata were developed for the numerical modelling solutions,

which include: overburden formation (three subsections by different bulk density), Watt Mountain Formation, Prairie Evaporite Formation, Keg River Formation, Cold Lake Formation, Ernestina Lake Formation, Lotsberg Formation and underburden Formation. The stratigraphic information modeled in the numerical simulations is detailed in Table 3.1.

Table 3.1 Stratigraphy Modeled in the Numerical Simulations

Formation	Top depth (m)	Bottom Depth (m)	thickness (m)
Upper Caprock	0	300	300
Middle Caprock	300	450	150
Lower Caprock	450	630	180
Watt Mountain	630	907	277
Prairie Evaporite	907	1046	139
Keg River	1046	1133	87
Cold Lake	1133	1175	42
Ernestina Lake	1175	1196	21
Lotsberg	1196	1315	119
Underburden	1315	1715	400

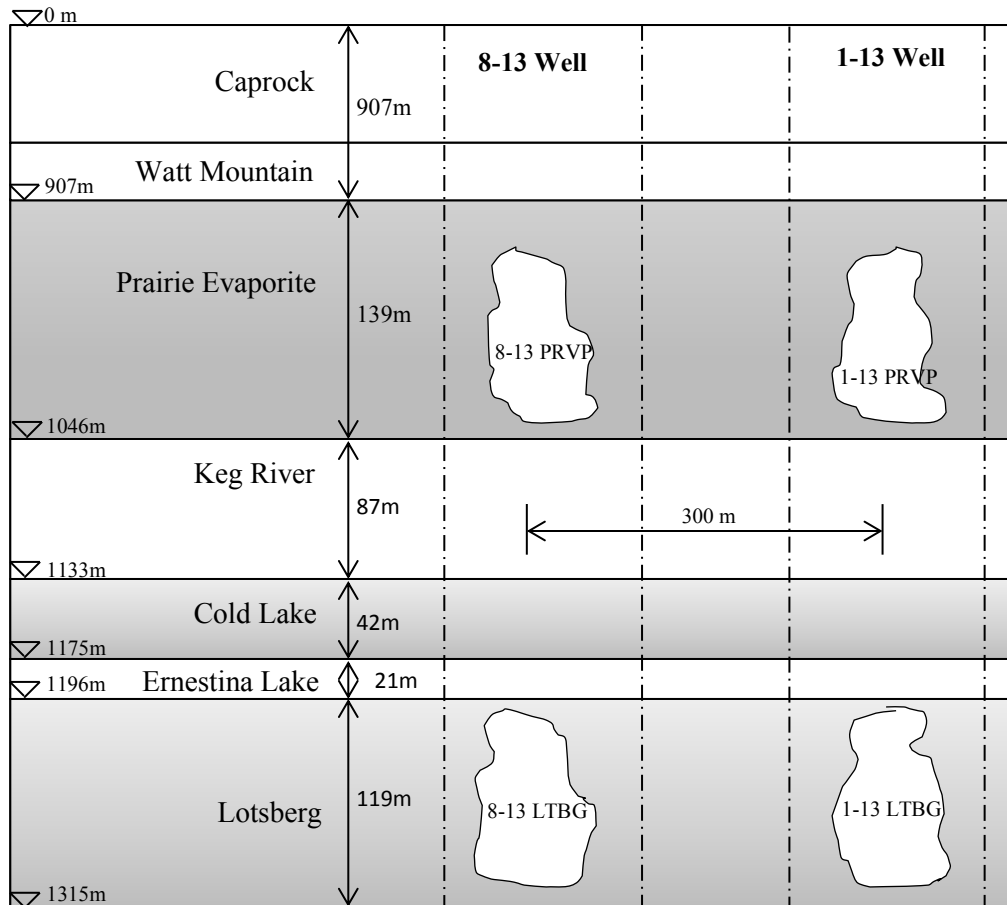


Figure 3.2 Schematic Cross-Sectional View of the Formation and Caverns at the site

### **3.4 Geomechanical Properties**

Site-specific formation rock properties and strength criteria characterizing the mechanical behavior of the salt and non-salt strata are essential to accurately analyze the geomechanical response of the disposal salt caverns during sump development operation and abandonment. A series of laboratory experiments were carried out on the core recovered from LIND 8B-WD-13 well in the Geomechanical Reservoir Experimental Facility of University of Alberta, to determine the material properties of the salt and overlying and underlying non-salt formations. In addition, the wireline logs from the cavern site that can demonstrate the continuous properties from ground surface down toward the bottom, aided to confirm the material density and mechanical properties by analyzing in RokDoc™ (Ikon Science).

#### **3.4.1 Geomechanical Properties of Salt Formations**

##### **3.4.1.1 Elastic Properties and Densities**

The properties used to evaluate the elastic deformation of the salt strata are Young's Modulus and Poisson's ratio. For the simulation under the condition of salt cavern excavation, the static values of the elastic properties are more applicable and preferable to the range of elastic strain and are typically smaller than the dynamic values.

Available test matrix conducted in the GeOREF laboratory on core samples composed of salt units includes 8 unconfined compressive (UCS) tests and 8 constant mean stress compressive (CMC) tests. The CMC tests were conducted under the mean stress of 5, 10, 15 MPa. The static Young's modulus and Poisson's ratio for the Prairie Evaporite, Cold Lake and Lotsberg formations can all be obtained from these laboratory tests. In

RokDoc™ estimation, the dynamic Young's modulus and Poisson's can be calculated from the density log, compressive velocity and shear velocity logs, using the equation:

$$E_d = \frac{\rho V_s^2 (3V_p^2 - 4V_s^2)}{(V_p^2 - V_s^2)} \quad \text{Equation 3-1}$$

$$\nu_d = \frac{V_p^2 - 2V_s^2}{2(V_p^2 - V_s^2)} \quad \text{Equation 3-2}$$

Where:

$E_d$  : Dynamic Young's modulus (GPa)

$\rho$  : Bulk density (g/cm<sup>3</sup>)

$V_p$  : Compressional velocity (m/s)

$V_s$  : Shear velocity (m/s)

$\nu_d$  : Dynamic Poisson's ratio

A literature review was conducted on the relationship between the dynamic and static Young's moduli. Based on laboratory testing of ten different rock types with a wide range of static Young's moduli (7 GPa to 150 GPa), Heerden (1987) proposed the following empirical relation between the static and dynamic Young's modulus:

$$E_s = a(E_d)^b \quad \text{Equation 3-3}$$

Where:

$E_s$  : Static Young's modulus (GPa)

$a, b$  : Stress dependent parameters

Savich (1984) proposed the value of  $a = 0.16$  and  $b = 1.227$  for the empirical equation, which could provide a better prediction of the salt rock type. Appendix Table B.1 lists the static and dynamic Young's modulus along with the predicted static value using Savich's method.

### 3.4.1.2 Salt Creep Model and Parameters

The deformation rate of the salt can consist of elastic deformation rate, viscoplastic deformation rate and thermal deformation rate. The viscoplastic deformation rate is stress and temperature dependent, and it usually dominates the strain rate of the salt within the range of the stress and temperature representing the surrounding conditions of the disposal caverns. The viscoplastic parameters used to describe the creep behavior of the salt formations are derived from four creep tests on the Prairie Evaporite salt units, and one creep test on Lotsberg salt core specimen. All the creep tests were performed as multi stage creep under the constant room temperature (20°C for all salt samples). The differential stresses at every stage were increased by decreasing the confining stress instantaneously, and the values of the differential stresses vary from 5 MPa to 20 MPa, which were designed to characterize the stress change conditions around the disposal salt caverns by solution mining operations.

FLAC<sup>3D</sup>, which was used for the numerical modeling studies, has several built-in creep constitutive models to simulate the abandonment behavior of the waste disposal salt caverns. Since no consideration of temperature in the laboratory creep tests for estimating creep parameters of the salt formations, the Norton power law (Norton 1929) will be used in the three-dimensional finite differential simulations to predict the geomechanical response and performance of underground waste disposal sands during long-term

abandonment. As discussed earlier, the Norton creep law has been found to underestimate the salt creep deformation largely because it only takes the stationary creep rate into account, which may not be adequate for the modeling of underground structures in rock salt. However, as the time intervals considered in this thesis are in a range such that the steady-state creep is dominant, the Norton power law has been assumed to be applicable and is a valuable modeling tool due to its simplicity and convenience.

The power law parameters  $A$  and  $n$  could be determined from the exponential plot of Von Mises and creep strain rate based on laboratory multi-stage creep experiments, using the relationship  $\ln \dot{\varepsilon}_{cr} = \ln A + n \ln \bar{\sigma}$  derived from Equation (2-3). Figure 3.3 illustrates the laboratory observed creep strain rate and the predicted using the power law for the Prairie Evaporite formation. A series of laboratory data from the creep test on Core 27 were not used for the fitting process but are also shown in Figure 3.3. Core 27 is recovered from the interface of the Prairie Evaporite and Keg Rive formation, presenting significantly lower creep strain rate than specimens from other locations. The power law predicted strain rate fits the observed data fairly well for the Prairie Evaporite specimens. The creep strain rate predicted by Power Law well matches the observed strain for Lotsberg salt specimens as shown in Figure 3.4. The introduced material parameters of the one-component power law for salt strata FLAC<sup>3D</sup> numerical simulation model are listed in Table 3.2. The power law parameters used to model the Cold Lake salt are the same as those determined for Lotsberg salt.

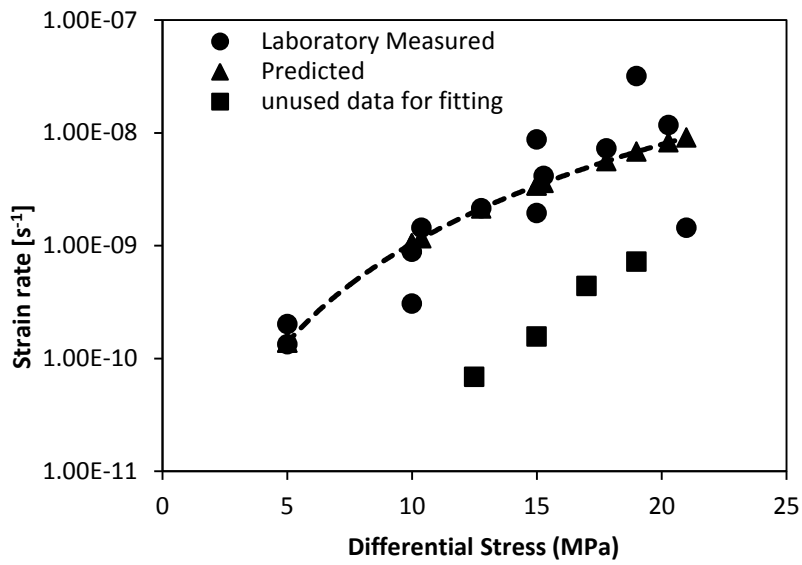


Figure 3.3 Comparison between Creep Strain Rate Measured and Predicted based on the Power Law of Prairie Evaporite Formation (RG2, 2013)

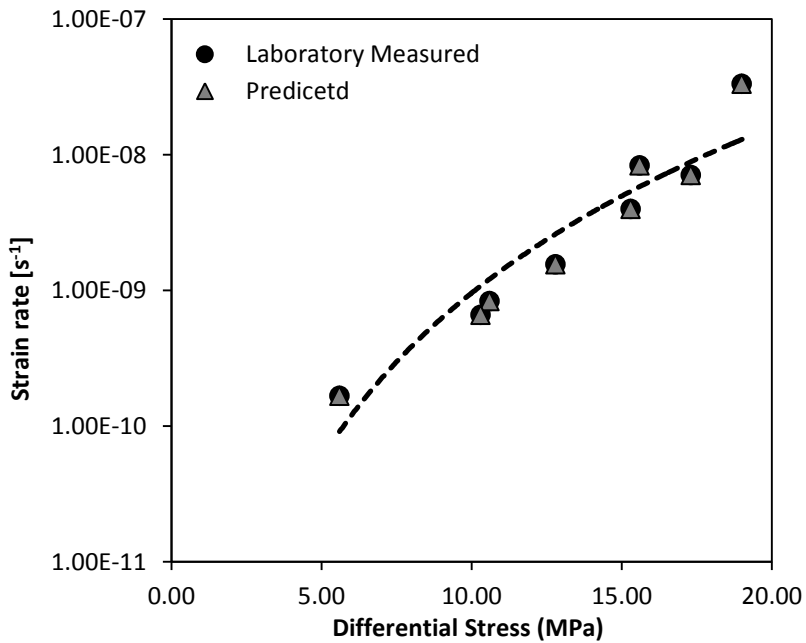


Figure 3.4 Comparison between Creep Strain Rate Observed and Predicted based on the Power Law of Lotsberg Formation (RG2, 2013)

Table 3.2 Two-component power Law Creep Parameters used in Numerical Simulations

Parameter	Unit	Prairie Evaporite	Lotsberg
A	s <sup>-1</sup>	1.35 x 10 <sup>-27</sup>	2.0 x 10 <sup>-50</sup>
n	---	2.52	5.75

Notes: Creep parameters are calculated for room temperature of 20°C.

### 3.4.1.3 Salt Dilation Criterion and Parameters

Salt cavern are favourable for the storage of hydrocarbon and oilfield waste disposal mainly due to the visco-plastic behavior of the rock salt that makes it difficult to fail under moderate confining stress. Only microfractures will be produced when the rock salt is carrying an induced shear stress greater than the salt shear strength at which point, salt dilation is initialized with increased porosity and volume.

The dilation criterion to define the onset of the salt dilation for Lotsberg and Prairie Evaporite formation was also determined by fitting the tests results from the entire laboratory constant mean stress tests. Constant mean stress test is considered to be the most appropriate method for estimating the dilation limit for rock salt, as compared with standard triaxial tests (Mellegard and Pfeifle, 1999). The constant mean stress tests are conducted at mean stresses of 5, 15 and 30 MPa, which reflects the expected stress state in the salt surrounding the disposal caverns. Figure 3.5 illustrate two empirical rock salt dilatancy boundary laws fitting in the stress invariant space based on all the constant mean compression tests measured data, where  $I_1$  is the first invariant of the stress tensor and  $J_2$  is the second invariant of the deviatoric stress tensor. The dilatancy boundary is defined as the point where the derivative of the volumetric strain curve reaches zero and a further increase in deviatoric stress will cause micro-fracturing and a volume-increase in the samples. The specimens used in the constant mean stress extension tests present much weaker behavior and tend to dilate at very low differential stress values, mainly resulting

from the pre-existing microcracks. The derived dilation criterion by Ratigan (1991) shows reasonable agreement with the measured data of Lotsberg formation, and it will be used for both Prairie Evaporite and Lotsberg salt units in the numerical simulations.

In FLAC<sup>3D</sup> simulation of the potential for salt dilation is identified with the ratio between the dilation strength evaluated by assumed dilation criterion and the potential of dilation (*DSR*). The *DSR* value is defined in the equation below:

$$DSR = \frac{0.162I_1}{\sqrt{J_2}} \quad \text{Equation 3-4}$$

where:

$$I_1 = \sigma_1 + \sigma_2 + \sigma_3 \quad \text{Equation 3-5}$$

$$J_2 = \frac{1}{6} [(\sigma_1 - \sigma_2)^2 + (\sigma_2 - \sigma_3)^2 + (\sigma_3 - \sigma_1)^2] \quad \text{Equation 3-6}$$

and:

$\sigma_1, \sigma_2, \sigma_3$ : Principal stresses

The *DSR* value is used to quantify the salt dilation intensity. The salt dilation is expected to occur if the *DSR* value is lower than 1, and more dilation and increased volume will be generated with a decreasing *DSR* value. When *DSR* is greater than 1, no dilation of the salt units is expected to be induced and the safety of the salt caverns expelled from dilation will increase with the ascending *DSR* value.

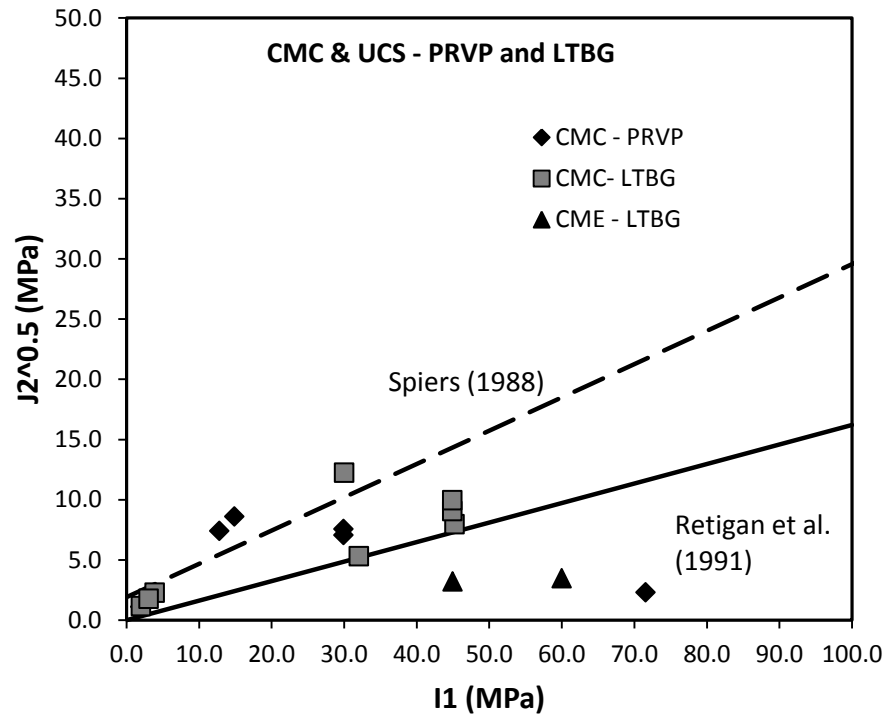


Figure 3.5 Predicted Salt Dilation Criterion Fitting on the Laboratory Results (RG2, 2013)

### 3.4.2 Geomechanical Properties of Non-Salt Formations

#### 3.4.2.1 Elastic Properties and Densities

The non-salt formations were assumed to behave elastically and no yield or failure occurs during the solution mining process and the injection of oilfield solid waste of the caverns. The static elastic property parameters for estimating the elastic deformation of the non-salt strata were determined from 10 unconfined compressive (UCS) tests and 12 standard triaxial compression (STC) tests. The STC tests were performed at the confining stress of 5, 10, 15 and 20 MPa. These tests conditions were selected to represent the lithostatic stress of the overlying and underlying non-salt caprock formations. The dynamic elastic parameters can also be extracted from the available field wireline loggings using equation 3.1 and 3.2 respectively in RokDoc™. Savich's method (1984) was used again to predict

the static elastic parameters of the non-salt formations. The static and dynamic Young's modulus along with the predicted static value using Savich's method for all the geological salt and non-salt units are included in Table B.2 in Appendix B. The elastic parameters and densities of the salt and nonsalt units used for FLAC<sup>3D</sup> numerical modeling are summarized in Table 3.3. The bulk modulus and shear modulus of the geological strata as the input number for FLAC<sup>3D</sup> models were calculated using the following equations:

$$K = \frac{E}{3(1-2\nu)} \quad \text{Equation 3-6}$$

$$G = \frac{E}{2(1+\nu)} \quad \text{Equation 3-7}$$

Where:

$E$  : static value of Young's modulus (GPa)

$\nu$  : Poisson's ratio

Table 3.3 Elastic Properties and Densities of the Geological Units in FLAC<sup>3D</sup>

Geological Unit	Density (g/cm <sup>3</sup> )	Young's Modulus (GPa)	Poisson's Ratio	Bulk Modulus (GPa)	Shear Modulus (GPa)
Upper Caprock	2.25	4	0.32	3.70	1.52
Middle Caprock	1.90	4	0.32	3.70	1.52
Lower Caprock	2.10	4	0.32	3.70	1.52
Watt Mountain	2.65	5	0.32	4.63	1.89
Prairie Evaporite	2.15	7	0.25	4.67	2.80
Keg River	2.65	15	0.28	11.36	5.86
Cold Lake	2.10	7	0.25	2.00	1.20
Ernestina Lake	2.50	8	0.3	6.67	3.08
Lotsberg	2.15	7	0.26	4.86	2.78
Underburden	2.50	8	0.3	6.67	3.08

### 3.4.2.2 Non-Salt Strength Criterion and Parameters

The shear strength and behavior of nonsalt formations can be predicted with Mohr-Coulomb failure criterion adequately. Cohesion and internal friction angles are needed to specify the Mohr-coulomb strength of each geological unit. The strength criterion of the Watt Mountain Formation and Keg River Formation are obtained based on 8 laboratory standard triaxial compression tests. For the overburden and underburden formations no laboratory tests were performed to determine the strength parameters. Thus strength properties based on a literature review of engineering practice are assigned in FLAC<sup>3D</sup> numerical modelling.

The strength determined from the laboratory tests on rock core are typically greater than the strength of the same rock in the field, resulting from the fact that small sized specimens tend to have limited number of weaker defects and pre-existing micro-cracks with critical orientations. Goodman (1980) proposed that in weak rock such as coal and shales the ratio of the lab-to-field strengths sometimes attains the value of 10 or more, while for strong rock the value of the ratio varies with the range of 2 to 5. For the purpose of conservative simulation in FLAC<sup>3D</sup>, the cohesion values modeled will be the laboratory-measured values reduced by a ratio of 3 for the nonsalt strata. The internal friction angle measured in laboratory will be reduced by a ratio of 3 using the strength reduction technique in the equation given below:

$$\varphi_m = \arctan\left(\frac{1}{F} \tan \varphi_{lab}\right) \quad \text{Equation 3-8}$$

where:

$\varphi_m$  : friction angle used inFLAC<sup>3D</sup> modeling (°)

$F$  : reduction ratio

$\varphi_{lab}$  : friction angle measured from laboratory tests (°)

The internal friction angle of other nonsalt formations with no laboratory tests conducted will be the same the value of the Keg River formation, conservatively. The Mohr-Coulomb strength parameters for the nonsalt strata are listed in Table 3.4.

To analyze and quantify the potential of no shear for nonsalt formations, the strength over stress ratio is introduced and is defined as the ratio between the Mohr-Coulomb strength of the material and the applied stress:

$$SSR = \frac{c \cos \varphi - \frac{\sigma_1 + \sigma_3}{2} \sin \varphi}{\sqrt{J_2} \cos \psi} \quad \text{Equation 3-9}$$

Where:

$$\psi = \tan^{-1} \frac{1}{\sqrt{3}} \left( \frac{2\sigma_2 - \sigma_1 - \sigma_3}{\sigma_1 - \sigma_3} \right) \quad \text{Equation 3-10}$$

And:

$c$  : Mohr-Coulomb cohesion (°)

$\varphi$  : Mohr-Coulomb friction angle (°)

Table 3.4 Mohr-Coulomb Strength Parameters of Non-Salt Formations

Nonsalt Unit	Laboratory Friction Angle (°)	Modeled Friction Angle (°)	Laboratory Cohesion (MPa)	Modeled Cohesion (MPa)
Upper Caprock		39.5		4
Middle Caprock		39.5		4
Lower Caprock		39.5		4
Watt Mountain	60	49	0.5	0.33
Keg River	51	39.5	6	4
Ernestina Lake		39.5		4
Underburden		39.5		4

Note: (lab) indicates the parameter value is determined on laboratory results, otherwise the value is assumed from engineering experience.

### 3.5 In Situ Conditions

#### 3.5.1 In Situ Lithostatic Stress Distribution

The initial in-situ lithostatic stress conditions are of importance to reasonably establish the three dimensional finite difference models. The thickness of the geological units listed in Table 3.1 and the bulk densities given in Table 3.3 were used to evaluate the initial undisturbed lithostatic stress distributions of the salt site before solution mining of the disposal caverns. The in situ stress distribution of salt formations is generally assumed to be isotropic because salt creep will remove any stress difference after a long geological time, and its ratio of vertical stress over horizontal stress is considered to be 1.0. As for the nonsalt strata, which do not creep significantly during geological period, the lithostatic stress state is generally taken as anisotropic. However, due to the lack of geological history knowledge and site-specific measurements on nonsalt formations, the anisotropic ratio cannot be assessed. In the FLAC<sup>3D</sup> numerical simulations, the vertical stress over horizontal stress ratios for nonsalt strata are estimated and compared by the following equations respectively:

$$k = 1 - \sin \phi \quad \text{Equation 3-11}$$

And:

$$k = \nu / (1 - \nu) \quad \text{Equation 3-12}$$

Where:

$k$  : Vertical-horizontal stress ratio

$\phi$  : Friction angle (°)

$\nu$  : Poisson's ratio

Table 3.5 provides the comparison of nonsalt anisotropic stress ratio value estimated from the two different assessment methods, and shows a reasonably good agreement with each other. As a conservative assumption, the modeled anisotropic stress ratio value in FLAC<sup>3D</sup> will be 0.5 for all the non-salt formations and 1 for all the salt strata.

Table 3.5 Anisotropic Stress Ratio of Geological Units used for Numerical Modeling

Geological Unit	$k = 1 - \sin \phi$	$k = \nu / (1 - \nu)$	Modeled $k$
Upper Caprock	0.364	0.471	0.5
Middle Caprock	0.364	0.471	0.5
Lower Caprock	0.364	0.471	0.5
Watt Mountain	0.245	0.471	0.5
Prairie Evaporite	-	-	1
Keg River	0.364	0.389	0.5
Cold Lake	-	-	1
Ernestina Lake	0.364	0.429	0.5
Lotsberg	-	-	1
Underburden	0.364	0.429	0.5

### 3.5.2 Cavern Waste Disposal Stress Distribution

Salt cavern stability during the cavern creation process is important. To adequately analyze the stress development around the cavern during solution mining and the mechanical response of the disposal salt cavern after abandonment, it is critical to determine an appropriate interpretation and representation of the cavern internal boundary stresses used for numerical simulation in FLAC<sup>3D</sup>.

Three different stages (Figure 3.6) during the cavern sump development were considered for internal boundary stresses interpretation, that is (1) Development stage, before April 2006, the cavern is only filled with brine; (2) Sump operation stage, from April 2006 until the current date, contributing to the solid waste injection and simultaneous solution mining operation, the cavern is filled with unsaturated brine and oilfield disposal sands, the composition of which might be brine, slurry, loose or medium sand or graded-distributed dense sand; (3) Abandonment stage, once the cavern is fully filled with highly consolidated waste sands and a small amount of saturated brine, the cavern will be plugged and sealed for long-term abandonment.

In the cavern development stage, since the cavern is fully filled with brine, the cavern internal pressure (IP) could be easily calculated as the summation of wellhead pressure (WP) and hydraulic pressure (HP), where the equation  $HP = \rho gh$  is used. Wellhead pressure could be read from the provided field data and an averaged value of 4MPa is employed in the calculation. The schematic interpretation of internal stress calculation for the initial stage is shown in Figure 3.7.

The schematic interpretation of internal stress calculation for abandonment stage is shown in Figure 3.8. When considering the abandonment stage, the cavern internal pressure becomes the total of wellhead pressure, hydraulic pressure and sands support

pressure (*SSP*). It is of critical importance to compute a reasonable estimate of the *SSP* for simulation purposes. A thorough literature review was conducted to find previous efforts on computing *SSP* but unfortunately, no related experimental researches were found on *SSP* related to the disposal of sands in an abandonment cavern. Therefore, it has been assumed that the behavior of the waste sands within the cavern will have similar geotechnical properties as tailings and deposits for the tailing dam construction. Rankine's theory for estimating the passive earth pressure is adopted conveniently to approximately calculate the resistance stress offered by the sands in the cavern due to cavern creep after abandonment. The following equation is used:

$$SSP = \gamma_s' \cdot h \cdot k_p + \gamma_w \cdot h \quad \text{Equation 3-13}$$

and

$$k_p = \tan^2(45^\circ + \varphi/2) \quad \text{Equation 3-14}$$

where:

$\gamma_s'$  : Effective unit weight of the disposed sands in salt cavern

$k_p$  : Coefficient of passive earth pressure for waste sands

$\varphi$  : Internal frictional angle of waste sands

Table 3.6 gives the range of total internal pressure if the internal material status in cavern is varied from brine to dense sands. The unit weight and friction angle is estimated roughly from literature on sand tailings for tailings dams. The lowest cavern internal stress, which is due to the cavern filled only with brine is about 19.6MPa, while the highest internal pressure could reach 25.6MPa if the cavern is filled with highly

consolidated disposal sands under which an extra pressure to the cavern is induced by the sand's support against the cavern wall.

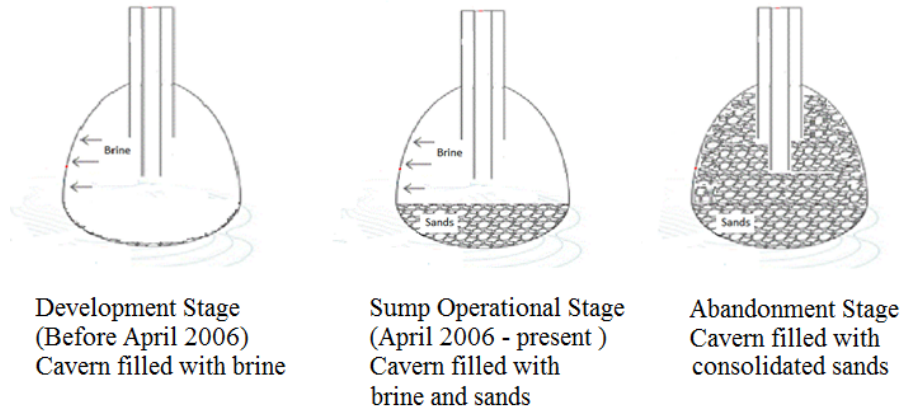


Figure 3.6 Three Different Stages for Interpretation of Cavern Internal Boundary Stresses

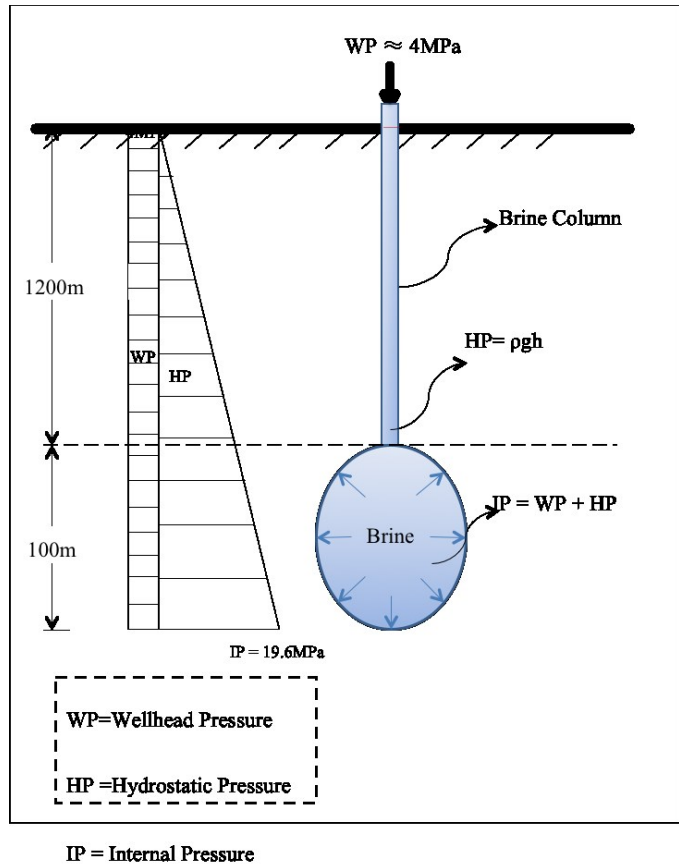
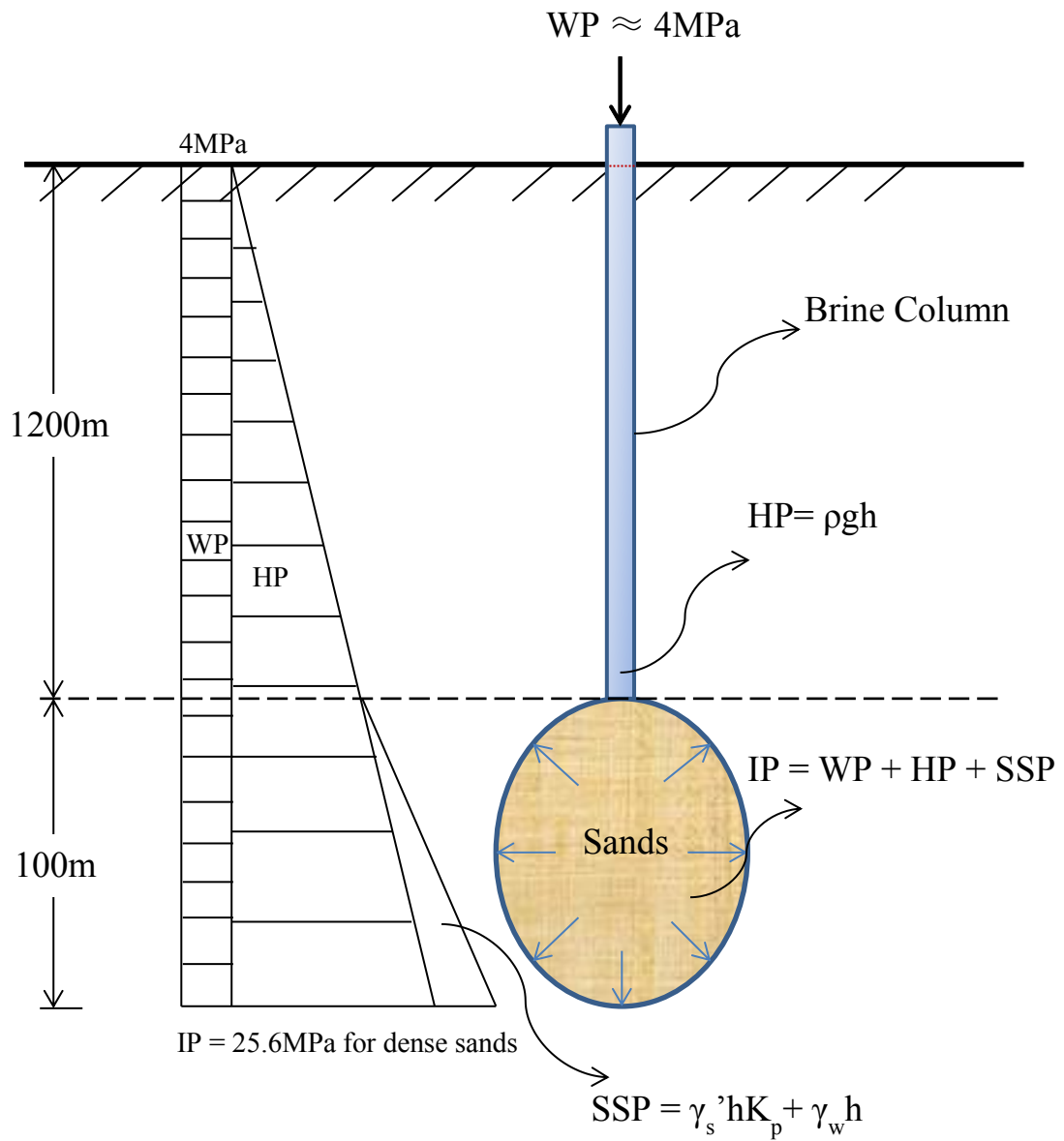


Figure 3.7 Cavern Internal Boundary Stress Analysis for Development Stage



SSP = Sands Support Pressure

Figure 3.8 Cavern Internal Boundary Stress Analysis for Abandonment Stage

Table 3.6 Internal Stress Calculation Ranges with internal material status in cavern

Internal material status	$\gamma$ (KN/m <sup>3</sup> )	Friction Angle (°)	$K_p$	Sand Support Pressure (MPa)	Wellhead Pressure (MPa)	Hydrostatic Pressure (MPa)	Total Internal Pressure (MPa)
Brine	12	0	-	0	4	15.6	19.60
Slurry	13	18	1.89	1.57	4	15.6	21.17
Loose Sand	18	25	2.46	2.97	4	15.6	22.57
Medium Sand	19	30	3.00	3.70	4	15.6	23.30
Dense Sand	21	40	4.60	6.06	4	15.6	25.66

### 3.6 Numerical Modeling Solutions

Engineering mechanics computation is widely utilized as a favorable, convenient and effective solution to adequately analyze the mechanical behavior of underground caverns. The three-dimensional explicit finite-difference program, FLAC<sup>3D</sup> (Itasca Consulting Group, Inc. 2012) was used to assess the geomechanical performance of the waste disposal salt caverns and the mechanical response of the overlying non-salt caprocks.

#### 3.6.1 Finite-Difference Program

FLAC<sup>3D</sup> is a three-dimensional explicit finite-difference program capable of simulating the behavior of three-dimensional structures composed of soil, rock or other materials undergoing plastic flow when their yield limits are reached. Materials can be presented by polyhedral elements within an adjustable three-dimensional grid to fit the shape of the modeling objects. Each element behaves following the prescribed linear or non-linear stress-strain law in response to the applied forces or boundary restraints. The material can yield and flow and the grid can deform in large-strain mode and move with the material represented in the model. The explicit Lagrangian calculation scheme and the mixed-

discretization zoning technique can ensure accurate modeled plastic collapse and flow in FLAC<sup>3D</sup>. FLAC<sup>3D</sup> offers a wide range of capabilities to solve complex three-dimensional problems especially in geomechanics, and embodies special numerical representations for the mechanical response of geological materials. It has fifteen built-in material models, including “null” model to simulate excavations, and plasticity models for brittle rock behavior, and time-dependent volumetric yielding models to interpret the creep material behavior. FLAC<sup>3D</sup> also contains a powerful built-in programming language, FISH, enabling the user to define new variables and functions to analyse specific simulation needs.

The features and capabilities of FLAC<sup>3D</sup> specially for the analysis in this thesis are (1) ability of assigning arbitrary in-situ lithostatic stresses, (2) kinematic and traction boundary conditions, (3) capability to simulate the sequential solution mining process and sump operation process, (4) the built-in one-component power law to characterize the creep behavior of salt units.

### **3.6.2 Three-Dimensional Finite Differential Model**

A three dimensional finite difference model was developed in FLAC<sup>3D</sup> (Version 5.0) to evaluate the structural stability and integrity of the disposal salt caverns, the likelihood of non-salt caprock failure and surface subsidence, interactions between adjacent caverns, both during operation and after abandonment. Additionally, the numerical modeling studies will be used to assess the casing integrity within and above the salt strata.

The performance criterion of the disposal salt caverns is related to the following measurements:

- The stress development around the caverns due to mining and operation of the caverns was assessed to examine the evolution of the deviatoric stresses within the geological units.
- The structural stability and integrity of the salt units surrounding the solution-mined caverns was evaluated with the value of dilation strength over the deviatoric stress ratio  $DSR$  indicating the potential of dilation in salt strata. Extensive salt dilation may lead to the cavern roof and/or wall spalling, and then damage the casing seat. In addition, the microfractures developed within the salt around the caverns may cause the leakage of the caverns, reducing the storage capacity or even bring environmental issues at the site.
- The integrity of the nonsalt overlying strata and the likelihood of failure were assessed examining the factor of safety based on Mohr-Coulomb criterion with respect to the shear failure within the formation. Shear failure of nonsalt caprock may result in the wellbore and/or operational string failure, and reduce the cavern integrity.
- Surface subsidence resulting from the salt cavern closure is studied by evaluating the vertical displacements in the numerical models. Large unexpected amount of surface subsidence at the site may induce damage to the surface structures and facilities and bring about economic loss.
- The volume shrinkage and closure rate of the disposal salt cavern were estimated during operation and after long-term abandonment. High level of cavern shrinkage will directly reduce the storage volume of the waste disposal though the cavern integrity may be raised by increasing internal pressure. More salt caverns may need to be explored and operated for unplaced solid waste resulting in additional project costs.

- The integrity of the cemented casings was evaluated via checking the accumulated casing strains. The casing will be dragged and stretched along the casing axis, resulting from the cavern shrinkage and closure. Excessive strains may lead to the tensile fracturing of the casing.

The axisymmetric FLAC<sup>3D</sup> model developed extends vertically from the ground surface to a depth of 1715 m, with 400 m thickness of underburden considered below the Lotsberg salt formation to ensure the model boundary constraints, and the outer radius of the model is 2000 m. These artificial truncations were selected to isolate the response of the caverns against the boundary effects. The kinematic boundary conditions assigned to the FLAC<sup>3D</sup> models includes no normal displacement along the outer vertical boundaries, and no vertical displacement on the bottom boundary. The upper surface of the model was allowed to deform freely in the vertical and radial directions.

The cavern geometries are obtained based on the field sonar data tracking the cavern development. Assumptions of cavern geometries are made to simplify the simulation problems due to the irregular shape of 1-13 LTBG cavern. The geometry of modeled 1-13 LTBG cavern is assumed to be accumulated cylinders layer by layer and the maximum radius and cavern height were scaled up to 72 m and 99 m respectively, ensuring the full capacity of 750,000 m<sup>3</sup> at abandonment. Considering the fact that the 8-13 LTBG cavern is still in progress and the operation of two PRVP caverns is undetermined, the same geometries will be used for these three caverns in numerical simulations. The two 1-13 cavern and two 8-13 caverns will be located symmetrically beside the centreline of the FLAC<sup>3D</sup> models.

To analyze the structural stability and cavern interaction between adjacent caverns, the geomechanical assessment of disposal salt caverns is based on four types of cavern

combinations, there are (1) sole cavern case, only 1-13 LTBG cavern excavated underground; (2) two horizontal caverns case, considering the existence of both 1-13 LTBG and 8-13 LTBG caverns, (3) two vertical caverns case, the abandonment of 1-13 LTBG cavern will be sequenced with the development of uphole 1-13 PRVP cavern and, (4) four caverns case, full development of two downhole Lotsberg caverns and two uphole Prairie Evaporite caverns. All the case conditions will be simulated based on FLAC<sup>3D</sup> models of same size and gridding method for the purpose of contrasting and comparing the results of the simulations.

Moreover, the geomechanical response of the caverns will be studied based on two diverse injection conditions for every cavern combination case, includes (1) the cavern(s) will be abandoned with saturated brine only, then the internal cavern pressure will be represented by an equivalent pressure applied as tractions normal to the surfaces of the cavern walls, with a vertical pressure gradient of 0.011760 MPa/m and, (2) the cavern(s) will be injected with normally consolidated dense sand waste and then be plugged and abandoned, so the internal cavern pressure will be maintained with a vertical pressure gradient of 0.072366 MPa/m for the Lotsberg and Prairie Evaporite caverns. This gradient is only computed over the height of the cavern, not from the ground surface. These two waste disposal conditions were selected as the lower and upper limit of the cavern internal pressure respectively, and all the other waste injection conditions are expected to lie within this range. Table 3.7 listed all the cases notated by various combinations of cavern numbers and cavern injection conditions that will be studied in FLAC<sup>3D</sup> numerical modeling within this thesis. Among these listed cavern cases, the conditions of caverns injected with brine and dense sands separately will be considered as the worst and most unstable engineering operation problems, resulting from the asymmetrical stress state along the centerline assigned on the model.

Table 3.7 Varied Cases Analyzed in FLAC<sup>3D</sup> Numerical Modeling

	Notation	Case description
Sole Cavern Case	1-13 LTBG brine	1-13 LTBG: brine
	1-13 LTBG dense	1-13 LTBG: dense sands
Two Horizontal Caverns	1-13&8-13 LTBG brine-brine	1-13 LTBG: brine 8-13 LTBG: brine
	1-13&8-13 LTBG dense-brine	1-13 LTBG: dense sands 8-13 LTBG: brine
	1-13&8-13 LTBG dense-dense	1-13 LTBG: dense sands 8-13 LTBG: dense sands
Two Vertical Caverns	1-13 LTBG&PRVP brine-brine	1-13 LTBG: brine 1-13 PRVP: brine
	1-13 LTBG&PRVP dense-brine	1-13 LTBG: dense sands 1-13 PRVP: brine
	1-13 LTBG&PRVP dense-dense	1-13 LTBG: dense sands 1-13 PRVP: dense sands
Four Caverns Case	1-13&8-13 LTBG&PRVP brine-brine-brine-brine	1-13 LTBG: brine 8-13 LTBG: brine 1-13 PRVP: brine 8-13 PRVP: brine
	1-13&8-13 LTBG&PRVP dense-brine-brine-dense	1-13 LTBG: dense sands 8-13 LTBG: brine 1-13 PRVP: brine 8-13 PRVP: dense sands
	1-13&8-13 LTBG&PRVP dense-dense-brine-brine	1-13 LTBG: dense sands 8-13 LTBG: dense sands 1-13 PRVP: brine 8-13 PRVP: brine
	1-13&8-13 LTBG&PRVP dense-dense-dense-dense	1-13 LTBG: dense sands 8-13 LTBG: dense sands 1-13 PRVP: dense sands 8-13 PRVP: dense sands

## **4 SENSITIVITY ANALYSIS OF NUMERICAL MODELING SOLUTIONS IN FLAC<sup>3D</sup>**

### **4.1 Introduction**

To study how well the FLAC<sup>3D</sup> model predicts the cavern operations and abandonment behavior, sensitivity studies are focused on various boundary conditions and potential influencing parameters on the plugged and abandoned salt cavern(s) filled with brine. This is a very critical stage, because it provides a degree of verification that the modeling approach can reasonably represent the field behavior of the caverns. After the reliability analysis the scenario will be repeated so that the operational and creep behavior of the cavern(s) will be simulated under several different combinations of cavern locations.

Initialized with a reference model built for the typical sole cavern case (1-13 LTBG brine), only one boundary value or influencing parameter is varied for each case study. The investigated cases of cavern configurations considered in this chapter can be divided into geometrical parameters, internal algorithm parameters (creep timestep) and mechanical parameters (creep law parameters). After a series of sensitivity studies of cavern cases, the most influencing or questionable parameters encountered during numerical simulations will be examined and described in this chapter.

In Section 4.2, the reference models built for sensitivity studies are depicted in detail from all engineering aspects. Section 4.3, 4.4 and 4.5 represents the results and outcomes for geometrical, algorithm and geomechanical parameters respectively.

## **4.2 Reference Models in Sensitivity Analysis**

The sensitivity studies of FLAC<sup>3D</sup> models detailed in Section 4.3, 4.4 and 4.5 will be based on and compared with the simulation results of the reference models described in this section. The geometrical description and the mechanical parameters settings in the reference models are all conformed to the actual salt cavern site conditions, for the purpose of reasonably illustrating the effects of the varied parameters on the structural stability or integrity of the caverns.

### **4.2.1 Geometrical description of the Reference Model**

The assumed reference model is shaped mimicking the field solution-mined cavern with a maximum radius of 72 m and a height of 99 m, giving the geometrical volume of about 750,000 m<sup>3</sup>. Cavern 1-13 LTBG is located between the depth of 1206 m and 1305 m in the reference model, which starts from the ground and spreads downwards to the depth of 1715 m. The total length of the model is about 4000 m, with caverns symmetrically arranged on both sides of the centerline of entire model.

The reference model is gridded as a Rad-Tunnel model. In FLAC<sup>3D</sup> Rad-Tunnel gridding is a way to grid the entire earth model as a radially graded mesh around parallelepiped-shaped tunnel (Figure B.2 and Figure B.3 in Appendix B). The central parallelepiped tunnel includes all target salt caverns inside. Moreover, to better observe the creep and flow behavior of salt pillar and cavern walls, a gradually densified gridding method is utilized from the earth model edge onto the cavern core area. In addition, the interface of every two formations within the high influenced zone, and the salt pillar edge around the salt cavern is very finely subdivided to detect any possible interface failure during the simulation period. This Rad-tunnel model contains 838,198 grid points and 788,932 zones in total.

#### 4.2.2 Rock Mechanical Material Parameters

The creep behavior in the reference model is described by the material law Power Law with a set of parameters as shown in Table 3.3, Table 3.4 and Table 3.5. Real density of each formation is utilized in the reference model. Initial horizontal stresses, which were attempted to be reconciled with the in-situ conditions, are applied in the reference model.

#### 4.2.3 Internal Algorithm Parameters

The related internal algorithm parameters used in the reference model are listed in Table 4.1. In FLAC<sup>3D</sup> creep calculations; the creep time-step for every algorithm calculation step is set to be 200 s throughout the 50 years creep after abandonment.

Table 4.1 Algorithm Parameters Setting in the Reference Models

Calculation Year	Timestep (second)	Minimum timestep (second)	Maximum timestep (second)	Real running time (minutes)
0-2 year	200	400	4e4	100
2-5year	200	400	1e5	12
5-10year	200	400	2e5	15
10-20year	200	400	2.5e5	18
20-50year	200	400	4e5	32

#### 4.3 Sensitivity Analysis of Geometrical Parameters in FLAC<sup>3D</sup> Models

The geometrical parameters of most concern in the FLAC<sup>3D</sup> numerical modeling of the disposal salt caverns will include the model gridding method and the model outer boundary size. To be specific, the pattern of the model gridding will influence the accuracy of the computation and calculation results, resulting in unrevealed yielding or failure behavior. The model boundary radius is determined artificially thus some degree of unexpected boundary effects may be brought out and varied with the size variation.

The sensitivity analysis of the model gridding generation method and the boundary radius influence will be discussed in Section 4.3.1 and 4.3.2, respectively.

### **4.3.1 Sensitivity Analysis of Gridding Generation Method**

#### **4.3.1.1 Methodology**

Typically, grid generation is the first step when starting to construct and run a model for numerical analysis. It is critical to create a relatively optimal gridding approach that can sufficiently reveal the expected response and behavior, and making the model run efficiently, particularly when up to 90 years of creep time calculations are involved in this thesis.

In this section, the following case with varied gridding method will be presented in comparison with the reference case. It adopts the Rad-Cylindrical gridding method, which grids the earth model in FLAC<sup>3D</sup> as a radially graded mesh around a cylindrical-shaped tunnel. The central cylindrical tunnel is a zone with much more dense gridding (see Appendix B), which will contain all the salt caverns inside. Rad-Cylindrical model includes 1,380,729 grid points and 1,341,600 zones, which are two times of that of reference model (Rad-cylindrical model). Other condition parameters will remain the same as the reference model. Figure 4.1 and Figure 4.2 provides details of the 3D view and the close view of caverns zone area of the Rad-Tunnel and Rad-Cylindrical Model Respectively. As can be seen, in the reference model all the edges and boundaries which are of most research interest become gradually more dense around the cavern(s), while in Rad-Cylindrical model the salt zones are subdivided uniformly and are assigned the same importance. The cavern injection condition considered in this gridding sensitivity study will be the saturated brine case only, which is represented by a vertical pressure gradient of 0.011760 MPa/m.

#### 4.3.1.2 Results and Conclusions

The simulation results comparison is based on both single cavern case (1-13 LTBG brine) and two Lotsberg caverns (1-13&8-13 LTBG dense-brine) case condition. Figure 4.3 illustrates the contour of *DSR* value with respect to the dilation in the salt units surrounding cavern 1-13 LTBG for two different gridding methods following 4 months after the abandonment of disposal caverns. It can be shown that the distributions of the *DSR* value are almost the same for the two gridded models, with an increasing *DSR* value with increasing distance away from the cavern wall. However, the minimum *DSR* value around the salt cavern in the reference is 1.37, which is much less than the value of 1.73 for the Rad-Cylindrical model. Thus the conclusion can be made that the Rad-tunnel gridding has a much better ability of detecting the dilation or tensile failure of the salt strata around the mined caverns than the Rad-Cylindrical gridding.

Table 4.2 summarises the results of sensitivity measurement values during 50 years creep simulation in Rad-Cylindrical and Rad-Tunnel models for the two studied cases in FLAC<sup>3D</sup>. It can be seen that the minimum *SSR* values with respect to the failure potential of the overlying nonsalt strata for two gridding method are equal to each other, which indicates that the gridding methods have little impact on the shear failure of the non-salt units. Moreover, the Rad-Tunnel models could predict slightly more deformation of the geological formations, including surface subsidence and the theoretical casing strains. Additionally, the reference model can save as much as 33% run-time over the calculations under the same case.

In conclusion, Rad-Tunnel Gridding method will be utilized in the following numerical simulation process due to its higher sensitivity to the salt dilation and formation deformation behavior and it is more efficient in calculations.

Table 4.2 Comparison of 50-year Abandonment Behavior Results Simulated in Rad-Cylindrical and Rad-Tunnel Models

Measurements	1-13 LTBG		1-13&8-13 LTBG	
	Rad-Tunnel	Rad-Cylindrical	Rad-Tunnel	Rad-Cylindrical
Surface Subsidence (mm)	9.4	8	16.4	14.8
Maximum Casing Strain	0.000302	0.000262	0.000322	0.000270
Minimum <i>SSR</i>	3.27	3.28	2.47	2.46
Calculation Time	2.6h	4h	3h	4.5h

### 3D View of Rad-Tunnel Model

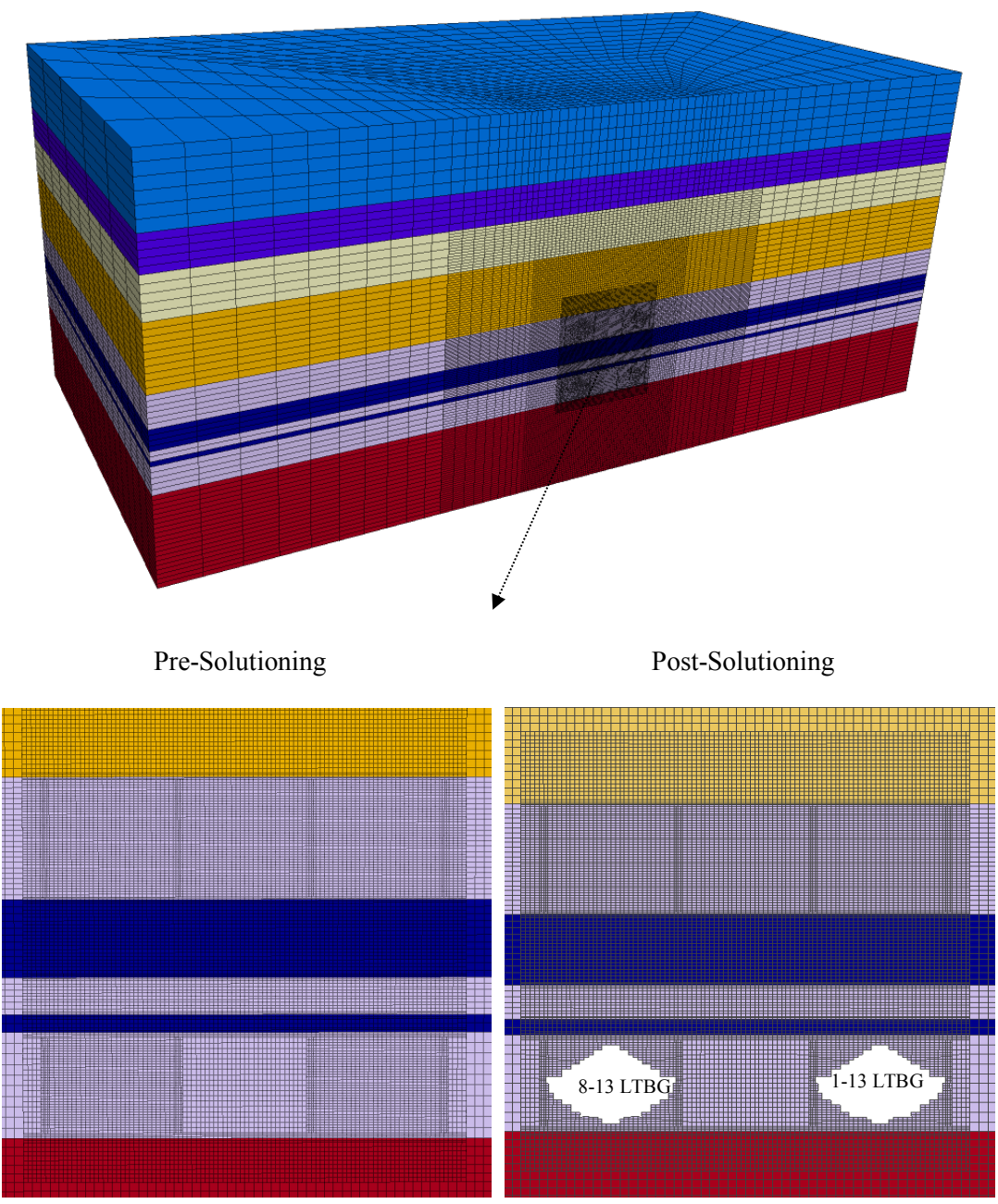


Figure 4.1 Detailed Gridding View of Rad-Tunnel Model (Reference Model)

3D View of Rad-Cylindrical Model

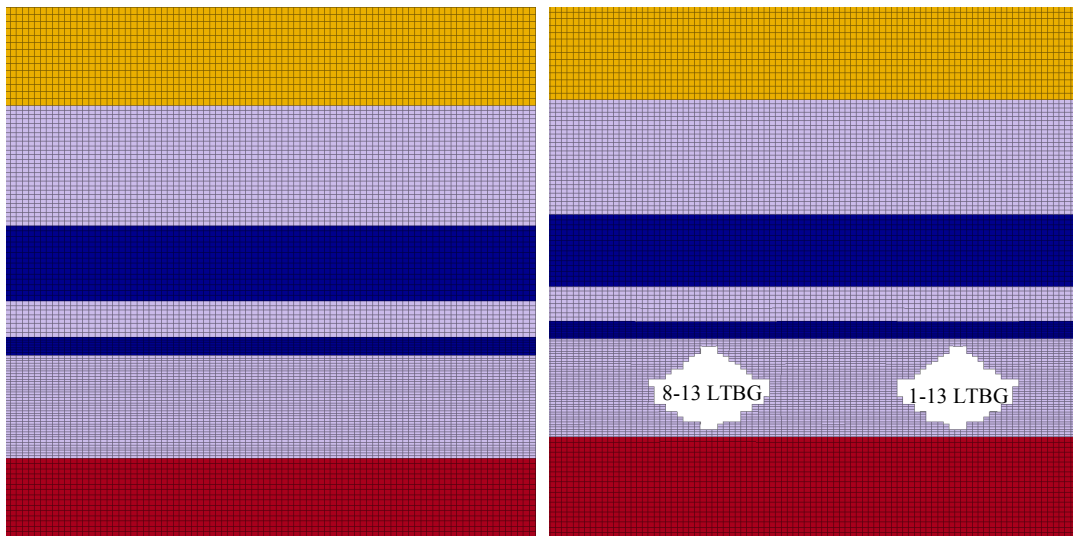
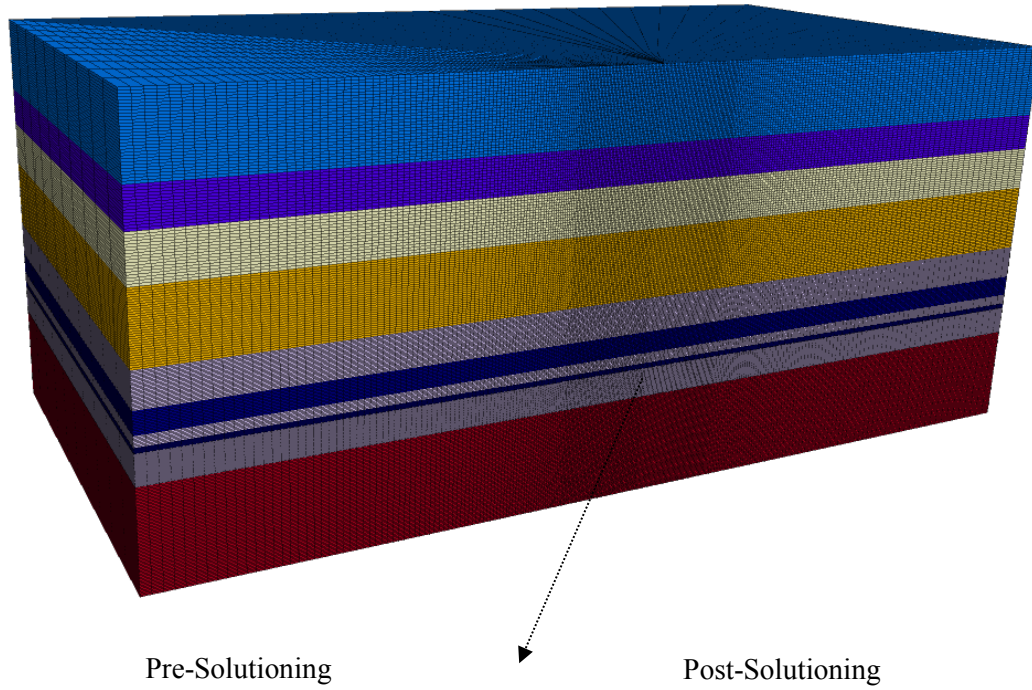


Figure 4.2 Detailed Gridding View of Rad-Cylindrical Model

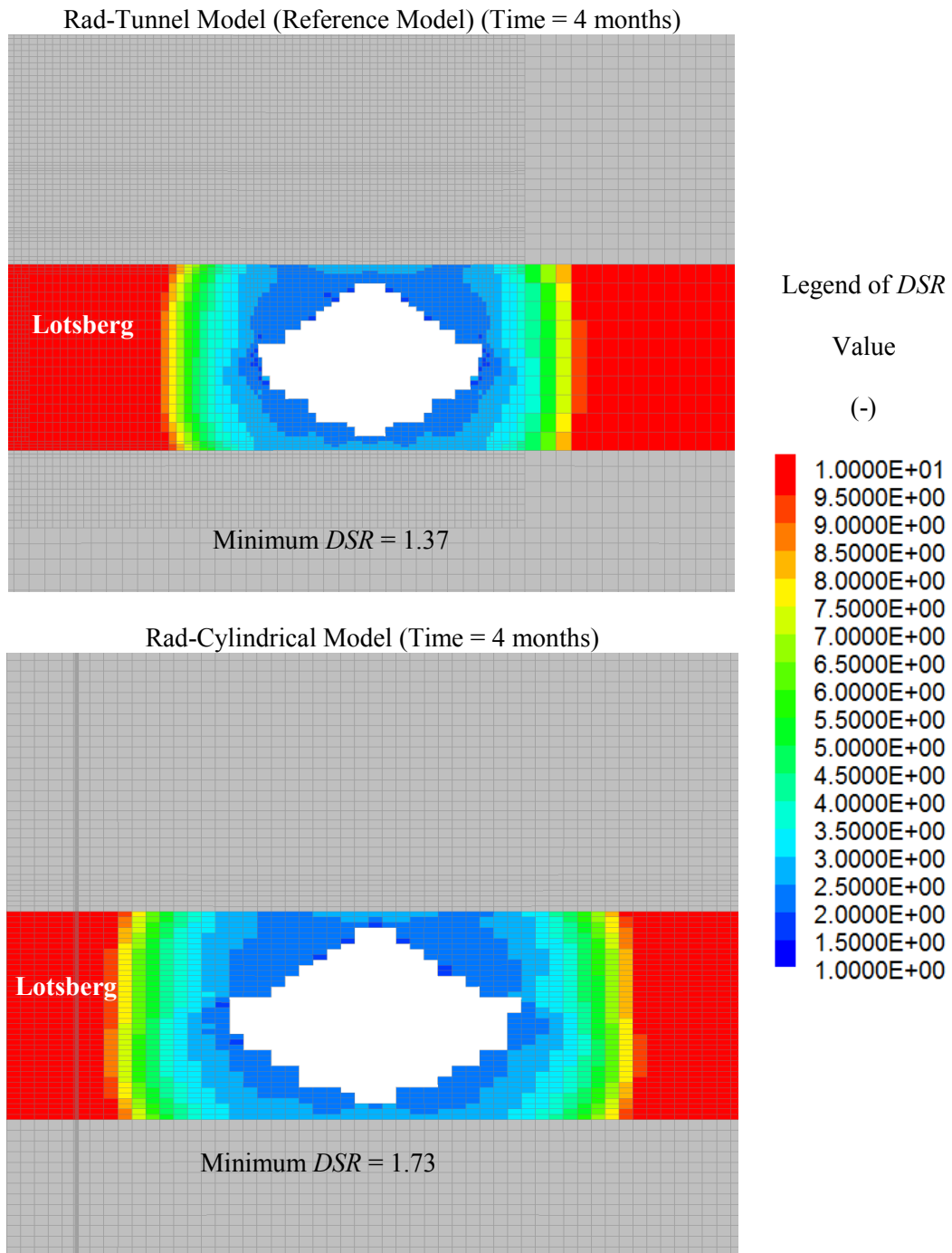


Figure 4.3 Predicted  $DSR$  Value in the Salt Strata Surrounding Cavern 1-13 LTBG

## **4.3.2 Sensitivity Analysis of Boundary Size**

### **4.3.2.1 Methodology**

When modeling infinite bodies or very large bodies, it may not be possible to cover the whole body with zones, due to constraints on memory and computer time. Artificial boundaries are placed sufficiently far away from the area of interest such that the behavior in that area is not affected.

To conduct the boundary effect analysis in FLAC<sup>3D</sup>, several boundary sizes different from the value of 2000 m in the reference model are chosen to run the simulation. It is expected to find a relatively reasonable and optimal boundary value at which the subsidence of the model edge is almost zero and can be ignored so that the boundary effect can be eliminated.

The reference model based on the condition of two Lotsberg caverns (1-13&8-13 LTBG dense-brine) is chosen in the boundary sensitivity analysis and simulated under the injection condition of 1-13 LTBG cavern with dense sands and 8-13 LTBG cavern with saturated brine, since it is less stable as compared to other injection conditions. Boundary sizes tested in the following section include 1000 m, 1200 m, 1500 m, 2500 m and 3000 m respectively, which presents the outer radius of the entire model.

### **4.3.2.2 Results and Conclusions**

Figure 4.4 presents the 50-year abandonment surface subsidence plot for each tested boundary size, and it can be seen that the subsidence at the edge of the model is decreasing as the boundary size increases. When the boundary size is below 1200 m, the boundary effect is so significant that the vertical displacement at the model edge is almost 50% of the maximum surface subsidence. This boundary effect will be largely reduced

when the size value increases to 2000 m, where edge settlement is calculated as only 8% of the maximum displacement. The central subsidence of the model almost remains the same, fluctuating within 2 mm. Table 4.3 provide additional information of the minimum *DSR* values for the Lotsberg salt formation and minimum *SSR* values for the non-salt Ernestina Lake formation and it is clear that even the smallest boundary constraint of 1000 m will not affect the salt dilation and non-salt shear failure behavior. In conclusion, the reference model with 2000 m boundary size value can predict the model behavior with negligible boundary effect.

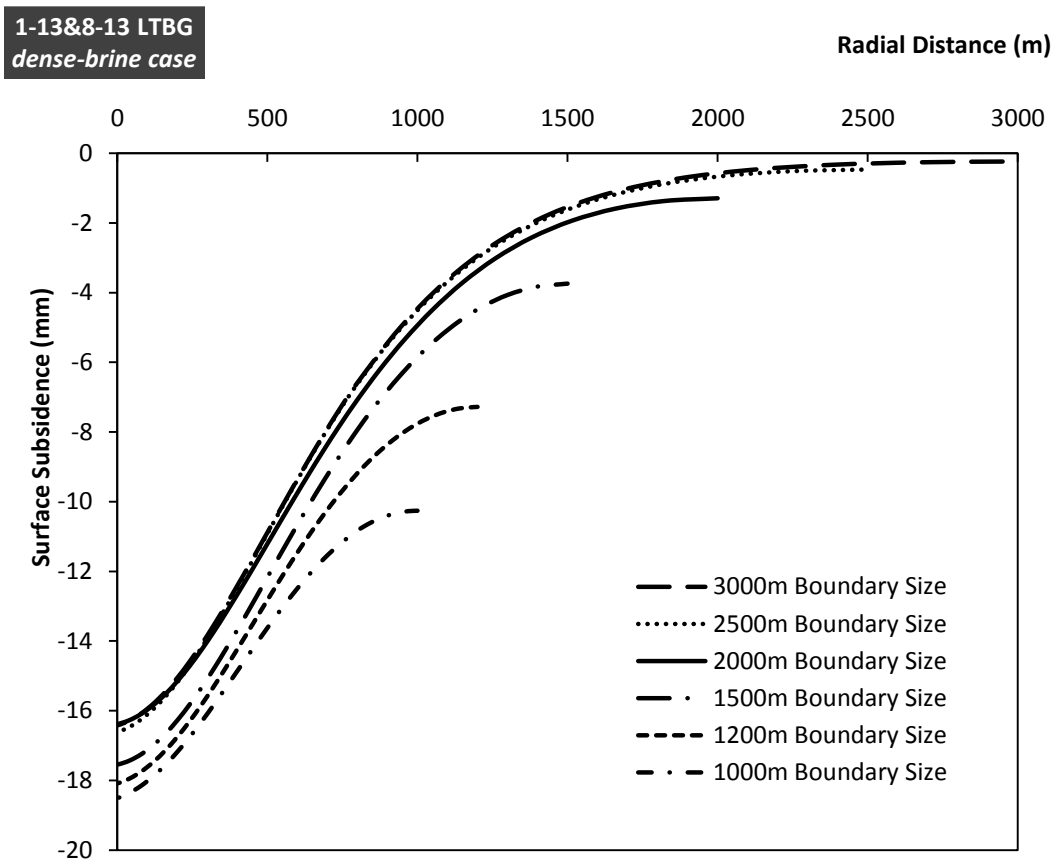


Figure 4.4 Comparison of 50-year Surface Subsidence for Varied Boundary Sizes

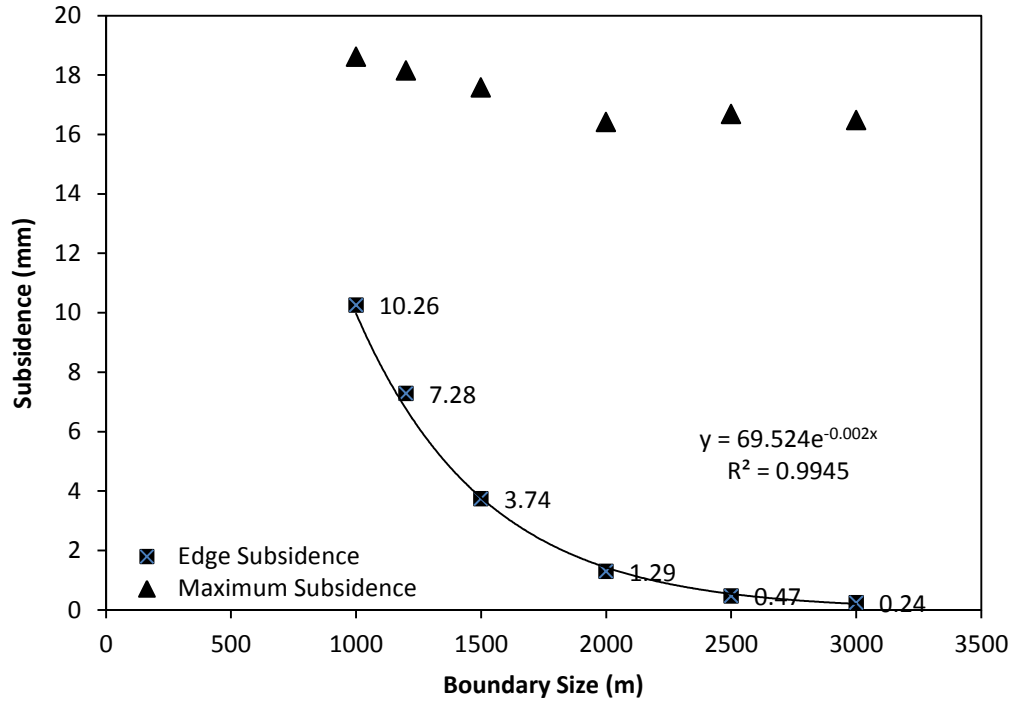


Figure 4.4 Edge Subsidence Varied with Boundary Size

Table 4.3 Summarized 50-year Measurements for Varied Boundary Sizes

Measurements	Boundary Size					
Subsidence (mm)	1000m	1200m	1500m	2000m	2500m	3000m
Centre point	18.61	18.15	17.58	16.42	16.69	16.48
Boundary point	10.26	7.28	3.74	1.29	0.47	0.01
Minimum <i>DSR</i>	2.30	2.30	2.30	2.30	2.30	2.30
Minimum <i>SSR</i>	2.486	2.486	2.485	2.485	2.485	2.484

## 4.4 Sensitivity Analysis of Creep Timestep Parameter

### 4.4.1 Methodology

The first and most critical parameter analyzed for creep computation calculations in numerical modeling is the creep timestep parameter, because the major difference between creep and other constitutive models in FLAC<sup>3D</sup> is the concept of problem time in

the simulation. The creep constitutive law used for the rock type involves timestep in their calculation equations, which may affect the response because the timestep here represents the real time rather than an artificial quantity used only for contributing to step to a steady-state condition.

In a creep simulation, the value of creep timestep needs to be varied in a range to ensure the time-dependent stress changes produced by the creep constitutive law are not larger than the strain-dependent stress changes, preventing large out-of-balance forces. In FLAC<sup>3D</sup> a rough estimation equation for the maximum creep timestep for numerical accuracy is suggested and expressed as the ratio of the material viscosity to the shear modulus,

$$\Delta t_{\max}^{cr} = \eta / G \quad \text{Equation 4-1}$$

For the power law the viscosity can be evaluated as the ratio of the stress magnitude,  $\bar{\sigma}$ , to the creep rate,  $\dot{\epsilon}_{cr}$ . Using equation 4.1 the maximum creep timestep is rewritten as:

$$\Delta t_{\max}^{cr} = \bar{\sigma}^{1-n} / A G \quad \text{Equation 4-2}$$

The stress magnitude,  $\bar{\sigma}$ , also known as the von Mises stress invariant, can be determined from the initial stress state before the creep process begins.

FLAC<sup>3D</sup> also recommends that a creep analysis could begin with an initial creep timestep approximately two to three orders of magnitude smaller than the calculated  $\Delta t_{\max}^{cr}$  using the estimation equation above. Moreover, typically a gradually increased or decreased timestep can be utilized to obtain a good performance efficiently.

In the comparison model for timestep sensitivity studies, the two horizontal caverns (1-13&8-13 LTBG dense-brine) case are researched and analyzed. Table 4.4 shows the

estimated maximum creep timestep values for the Prairie Evaporite salt and Lotsberg salt formation respectively. To make the simulation accurate, the lower maximum creep timestep of  $4.0 \times 10^5$  s is taken as the threshold. The creep simulation will run starting with a trial timestep of  $4.0 \times 10^3$  s, and then this value will be increased to maintain the simulation accuracy within a much shorter simulation interval. A group of testing cases with varied maximum timestep for each abandonment creep behavior simulation period were computed in FLAC<sup>3D</sup> and compared to the reference mode. The names of comparison cases were denoted with T-1, T-2, T-3 and T-4, of which detailed parameters value were indicated in Table 4.5.

Furthermore, to avoid the ‘noise’, which results from a continuous rapid adjustment of the timestep, a latency period of 10 steps is assigned for each timestep change to occur to allow settling of the system. For the creep simulation, soon after the excavation until to 1-year abandonment time, a much smaller maximum timestep is set to accommodate transients behavior from solution excavation, and then as the abandonment simulation proceeds, the maximum timestep was gradually raised by a ratio of 1.05. The threshold of the maximum unbalanced force ratio during the entire simulation is set to be  $5 \times 10^{-7}$ .

Table 4.4 Maximum Creep Timestep Estimation

Parameters	Geological Unit	
	Prairie Evaporite	Lotsberg
n	2.52	5.75
Von Mises Stress (Pa)	$1.96 \times 10^7$	$1.96 \times 10^7$
A	$1.35 \times 10^{-27}$	$2.00 \times 10^{-50}$
G	$2.80 \times 10^9$	$2.78 \times 10^9$
$\Delta t_{\max}^{cr}$	$2.18 \times 10^6$	$4.14 \times 10^5$

Table 4.5 Maximum Timestep for Variation Comparison Cases

Creep Time	Maximum Timestep (s)				
	Reference case	T-1	T-2	T-3	T-4
0 - 1 year	$4.0 \times 10^4$	$4.0 \times 10^3$	$4.0 \times 10^4$	$1.0 \times 10^5$	$3.0 \times 10^5$
1 - 2 year	$4.0 \times 10^4$	$4.0 \times 10^3$	$4.0 \times 10^4$	$2.0 \times 10^5$	$3.0 \times 10^5$
2 - 5 year	$1.0 \times 10^5$	$4.0 \times 10^3$	$4.0 \times 10^4$	$3.0 \times 10^5$	$3.0 \times 10^5$
5 - 10 year	$2.0 \times 10^5$	$4.0 \times 10^3$	$4.0 \times 10^4$	$4.0 \times 10^5$	$3.0 \times 10^5$
10 - 20 year	$2.5 \times 10^5$	$4.0 \times 10^3$	$4.0 \times 10^4$	$4.0 \times 10^5$	$3.0 \times 10^5$
20 - 50 year	$4.0 \times 10^5$	$4.0 \times 10^3$	$4.0 \times 10^4$	$4.0 \times 10^5$	$3.0 \times 10^5$

#### 4.4.2 Results and Conclusions

As shown in Table 4.5, Case T-1 uses the most conservative maximum timestep two orders of magnitude smaller than the estimated maximum timestep, so that it could theoretically generate the most accurate simulation results. It can be seen in Table 4.6 that the reference model and the T-2 model produce almost the same surface subsidence and maximum vertical displacement as the T-1 model and it is also more sensitive to the salt dilation behavior and shear, failure which may occur during the simulations. Among these three tests, the reference model shows the obvious advantage of saving the model simulation time significantly, consuming approximately 88% less runtime than that of the T-1 model. The runtime is a critical factor for this thesis as many different simulations were run to reveal the cavern creep behavior. However, the T-3 and T-4 models reveal zero surface subsidence for the 1-year or 2-year abandonment time, and gives much higher cavern vertical displacement, even the runtime is only 1 to 1.5 hours. In conclusion, the creep timestep parameters set for the reference model could efficiently develop relatively higher calculation accuracy thus they will be repeatedly used in the Chapter 5.

Table 4.6 Results of Creep Timestep Sensitivity Analysis

Creep Year	Reference case	T-1	T-2	T-3	T-4
Surface Subsidence (mm)					
1	4.25	4.25	4.25	0	0
2	5.5	5.5	5.5	2.6	0
5	6.2	6.3	6.6	12	2.8
10	8	8	8	12	10
20	10	10	11	12	10
50	16	16	16	16	18
Maximum Z-displacement (mm)					
1	264	264	264	327	400
2	308	308	308	291	625
5	388	388	388	522	615
10	472	471	471	544	694
20	585	587	590	655	747
50	800	802	806	848	917
Minimum <i>DSR</i>					
4 month	1.37	1.37	1.37	1.27	1.26
Minimum <i>SSR</i>					
4 month	3.22	3.20	2.93	2.50	2.45
Model Total Running Time (hours)					
1 – 50 y	3	25	5	1	1.5

## 4.5 Sensitivity Analysis of Mechanical Parameters

The parameters of the one-component Power law used to simulate the strength and deformation mechanisms of the salt formations require sensitivity analyses to show how the simulation results will be influenced with their changes. The test cases in this section are all based on the single 1-13 Lotsberg cavern case.

### 4.5.1 Elastic Properties

#### 4.5.1.1 Methodology

The elastic properties are important in predicting deformation behavior of the salt caverns. However, the elastic properties determined from both laboratory tests or estimated from wireline logs in field can vary from 6 GPa to 20 GPa for salt strata. Thus some degree of

emphasis needs to be put onto how the elastic properties, particularly the Young's modulus, will influence the simulation results.

The Young's modulus used in the reference model is 7 GPa for the Lotsberg Formation. In the sensitivity studies in this section, only the elastic modulus for the Lotsberg salt will be changed for each test case. Young's modulus was varied as follows: 6 GPa, 10 GPa, 15 GPa and 20 GPa.

#### 4.5.1.2 Results and Conclusions

Table 4.7 demonstrates the sensitivity results of Young's modulus. It shows that increasing Young's modulus will result in some amount of declining surface subsidence, which is primarily the result of a decrease in the closure rate of the caverns. The value of Young's modulus used in the reference case is quite conservative as for the shrinkage responses of the disposal salt caverns. However, the varied Young's modulus has negligible impact on the dilation of the salt and the shear failure of the nonsalt strata.

Table 4.7 Sensitivity Analysis Results of Young's Modulus, Time = 5 years

Young's Modulus (GPa)	Bulk Modulus (GPa)	Shear Modulus (GPa)	Maximum Surface Subsidence (mm)	Minimum DSR
6	4.17	2.38	3.7	1.87
7	4.86	2.78	3.5	1.88
10	6.94	3.97	3.3	1.9
15	10.42	5.95	3.1	1.91
20	13.89	7.94	3	1.93

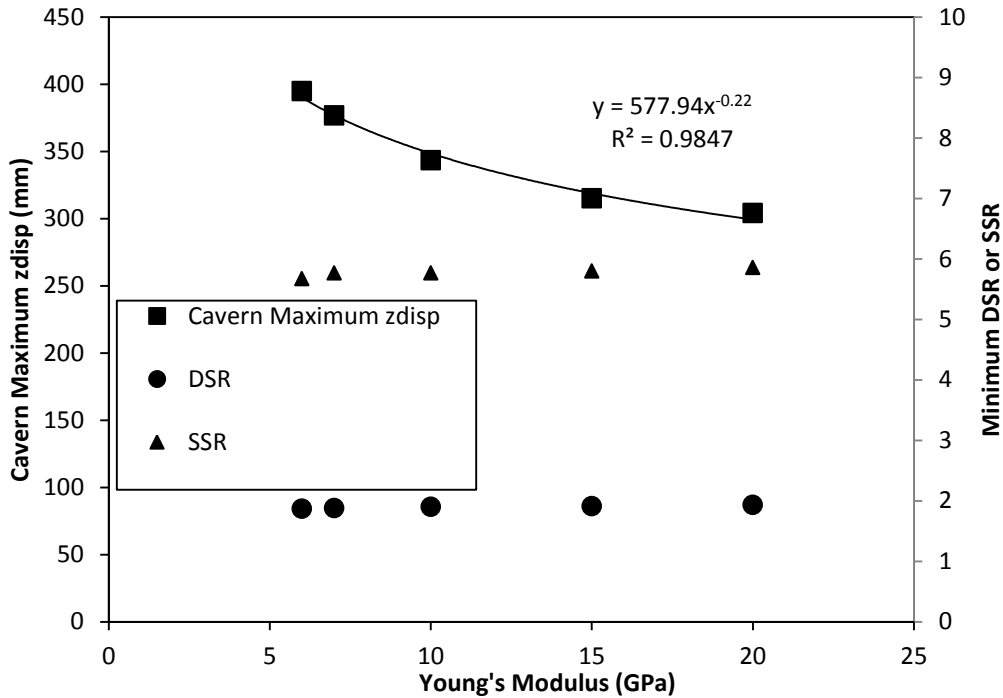


Figure 4.5 Sensitivity Plot of Young's Modulus

## 4.5.2 Power Law Parameters

### 4.5.2.1 Methodology

The parameters, A and n are used to describe one-component Power law for salt strata. Since there is a link between these two parameters, three ways to study the sensitivity of power law parameters are evaluated in this section. Firstly, the n parameter was held constant and only changes in the value of A by order of magnitude were implemented. Secondly, the A parameter was held constant and the n value was varied by 0.25 for every step. Lastly, both A and n were varied simultaneously to obtain the same simulation results as the default models. In the reference models for sensitivity analysis, A is set to be  $2 \times 10^{-50}$ , and n is set to be 5.75, which are derived from laboratory creep tests.

#### 4.5.2.2 Results and Conclusions

Table 4.8 and Table 4.9 contain detailed results of sensitivity analysis of A and n parameter respectively. The deformation behavior of the model is largely influenced by the A and n value respectively because they dominate the flow rule for the salt creep. The degree of marginal effect of A is dramatically enlarged with more positive deviation from A value in the reference model, which is also the case for n parameter. The maximum surface subsidence of the model will even increase to about six times that of the reference results when the A value is increased by two orders of magnitude. Once any parameter (A or n) of the power law increases, the creep rate of the salt will increase and then the salt surrounding the disposal caverns will maintain a stable state at a higher rate, thus the *DSR* value following 5-year creep simulation will also rise as shown in Figure 4.7 and 4.8, indicating more stability of the salt strata. However, the shear failure behavior of the non-salt overlying formations will not be influenced by the change of the power law parameters. Figure 4.9 demonstrates the contour of A and n representing the same deformation results as the reference model. This evidently shows that there is a strong link between the A and n parameter and for this project, every one order of magnitude's increase of A with every 0.15 decreases in n parameter will keep the simulation results the same. In conclusion, the decision of A and n parameters of power law is of critical importance on the study of the dilation response of salt units and the deformation behavior of the model in FLAC<sup>3D</sup> numerical simulations.

Table 4.8 Sensitivity Analysis Results of A parameter for Power Law, Time = 5 years

A	n	Surface subsidence (mm)	Minimum <i>DSR</i>	Minimum <i>SSR</i>
2.00E-52	5.75	1.5	1.14	3.23
2.00E-51	5.75	2	1.45	3.21
2.00E-50	5.75	3.5	1.88	3.17
2.00E-49	5.75	8.2	2.4	3.27
2.00E-48	5.75	18	2.96	3.52

Table 4.9 Sensitivity Analysis Results of n parameter for Power Law, Time = 5 years

A	n	Surface subsidence (mm)	Minimum DSR	Minimum SSR
2.00E-50	5.25	1.2	0.8	1.91
2.00E-50	5.5	1.6	1.2	3.21
2.00E-50	5.75	3.5	1.88	3.17
2.00E-50	6	16	2.78	3.39
2.00E-50	6.25	N/A	N/A	N/A

Notes: N/A indicates calculation overflow in FLAC<sup>3D</sup>.

Table 4.10 Sensitivity Analysis Results of A & n parameter for Power Law, Time = 5 years

A	n	Surface subsidence (mm)	Minimum DSR	Minimum SSR
2.00E-49	5.6	3.42	1.86	3.17
2.00E-50	5.75	3.5	1.88	3.17
2.00E-51	5.9	3.5	1.9	3.17
2.00E-52	6.05	3.6	1.92	3.17

1-13 LTBG  
brine-case

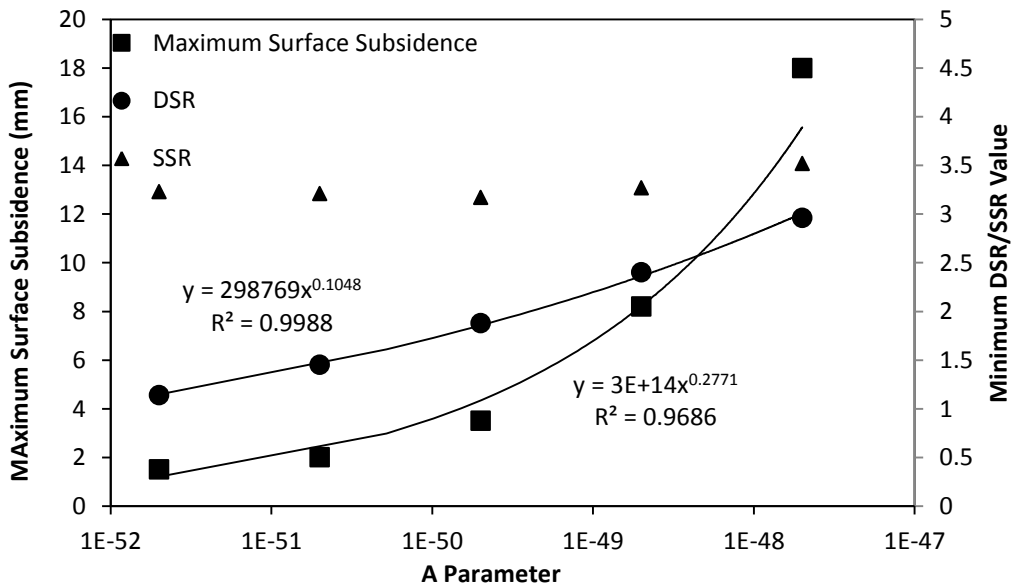


Figure 4.6 Sensitivity Plot of A parameter for Power Law, Time = 5 years

**1-13 LTBG  
brine-case**

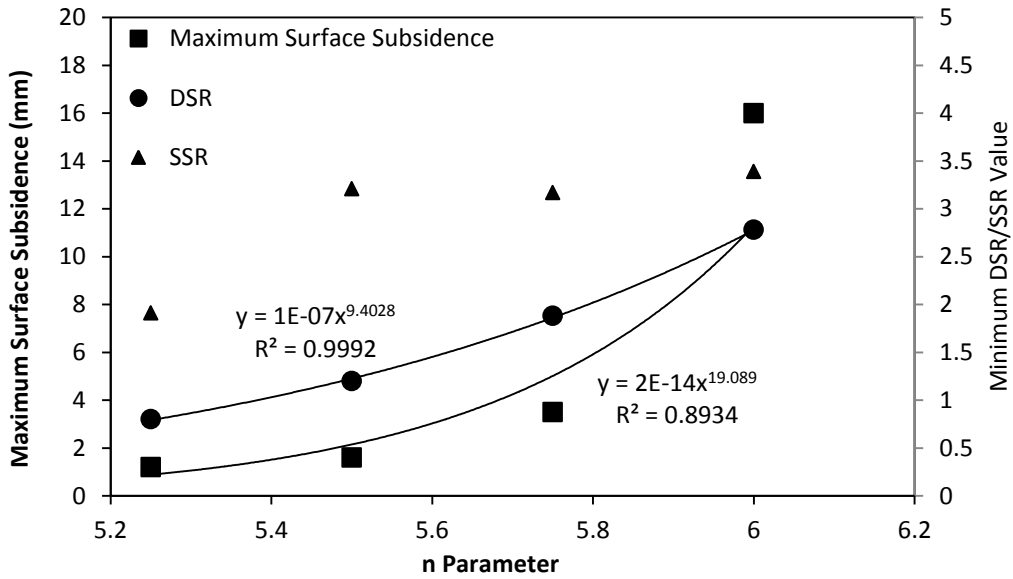


Figure 4.7 Sensitivity Plot of n parameter for Power Law, Time = 5 years

**1-13 LTBG  
brine-case**

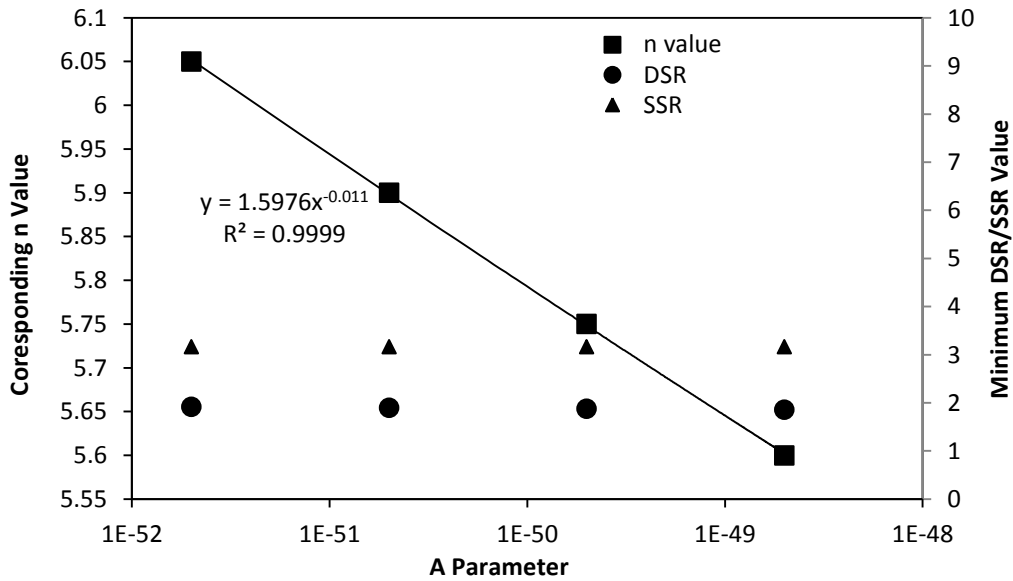


Figure 4.8 Contour of A and n representing same results as Reference Model

## 4.6 Summary and Conclusions

This chapter has described a series of sensitivity analyses of some critical geometrical parameters (gridding method and boundary effects), algorithmic parameters (creep timestep), elastic parameters (Young's modulus) and power law parameters ( $A$  and  $n$ ) in detail for the disposal salt caverns. The reference model for the purpose of comparison was introduced from the point of potential sensitive factors.

The Rad-Tunnel gridding pattern behaves more sensitive to the dilation behavior of the salt strata, more fairly and conservatively presenting the potential of loss of stability of the disposal salt caverns than the Rad-Cylindrical gridding method. Also, it gives slightly more deformation in the modeled geological units and save approximately one third of the computation time in FLAC<sup>3D</sup> simulations.

The size of the outer boundaries can bring a significant influence on the surface subsidence prediction of the model, especially at the edge point. When the outer radius of the model increase to the value of 2000 m, the marginal subsidence of the surface area reduced to almost zero and the maximum subsidence remains in the reasonable range. Fortunately, the boundary size has little effects on the salt dilation and overlying nonsalt shear failure behavior around the disposal caverns.

A good determination of the creep timestep embedded in FLAC<sup>3D</sup> simulation program can benefit the numerical simulation not only in the terms of fairly reasonable results output but also saving massive calculation time. The range of creep timestep predicting adequate deformations and salt dilation or non-salt failure potential will be used in the following FLAC<sup>3D</sup> numerical modeling based on different cavern cases.

The research of elastic parameters shows that the value of Young's modulus has limited influence on the model deformation and as well as the salt dilation and nonsalt shear failure behavior predicted in the FLAC<sup>3D</sup> simulations.

It was shown that the power law parameters could influence the model deformation significantly, along with the dilation behavior of the surrounding salt units of the disposal caverns. Since there existed a high degree of uncertainty in the power law parameters estimation from the laboratory tests, the simulated structural stability and the integrity of the disposal salt caverns in this thesis could be used as a referenced geomechanical assessment.

## 5 LONG-TERM ABANDONMENT BEHAVIOR

### SIMULATION OF WASTE DISPOSAL SALT CAVERNS

#### 5.1 Introduction

The structural stability and creep performance during the solution-mining process and after abandonment of the disposal salt caverns is conservatively evaluated using three-dimensional finite difference model in FLAC<sup>3D</sup>. Various combinations of salt cavern conditions were considered in numerical simulations. The geomechanical assessments are related to (1) salt cavern structural stability and likelihood of failure of salt and their caprocks during the operational and abandonment period, (2) cavern creep closure behavior over time, (3) theoretical casing strains predictions, (4) stress development around the salt caverns, (5) surface subsidence development.

Simulations of the cavern solution mining process are represented as instantaneous excavation of the entire salt cavern(s) and sequential excavations of cavern layers respectively, along with the corresponding modeling results being compared and analyzed. The cavern(s) will be maintained at a constant saturated brine pressure gradient of 0.011760 MPa/m representing the brine injection condition, or at a vertical constant pressure gradient of 0.072366 MPa/m presenting the dense sand disposal condition. Each type of excavation model will be simulated with another 50-year creep period following the full development of all salt caverns.

The long-term abandonment simulation behavior of the sole cavern case, i.e. only 1-13 LTBG cavern, will be discussed in Section 5.2 based on both instantaneous excavations and sequential excavations respectively. The brine injection status is considered for both

solutions. Additionally, 1-13 LTBG cavern excavated sequentially will be simulated with the disposal of the injected dense sands.

The same analysis scenario will be performed on the long-term abandonment creep behavior of two horizontally adjacent Lotsberg caverns in Section 5.3. The simulation comparison of instantaneous and sequential excavations will be evaluated with Cavern 1-13 LTBG containing dense sands at abandonment and Cavern 8-13 LTBG injected with saturated brine. Then the two horizontally adjacent Lotsberg caverns will be modeled under both caverns with brine as well as both caverns with disposal sands in FLAC<sup>3D</sup> numerical modeling studies.

The abandonment performance of the two vertical adjacent caverns (1-13 LTBG&PRVP) was simulated considering only sequential excavation processes. The caverns were assumed to be abandoned at three different injection times, including (1) both caverns with brine, (2) the lower cavern with dense sands while the upper cavern with brine, (3) both of the caverns with dense disposal waste. The detailed descriptions of three-dimensional finite difference models and discussion are presented in Section 5.4.

The full sequential development of four caverns in both Lotsberg and Prairie Evaporite formations were simulated in FLAC<sup>3D</sup> numerical modeling to study the operational and abandonment performance of each cavern and the interactions occur between 1-13 and 8-13 well salt caverns. Various cavern internal pressure conditions, including three symmetrical and one asymmetrical injection scenario are analyzed, compared and discussed in Section 5.5.

## **5.2 Long-term Abandonment Behavior Simulation of Single Cavern**

### **5.2.1 Long-term Abandonment Behavior Considering Instantaneous Excavation**

In the three dimensional finite difference modeling, instantaneous excavation of 1-13 LTBG cavern is considered prior to the abandonment of waste disposal salt cavern. At the start of the abandonment creep behavior simulation, the displacement and velocity of grid points of FLAC<sup>3D</sup> model was reset to be zero. Cavern 1-13 LTBG was held at a saturated brine pressure gradient of 0.011760 MPa/m throughout the 50 years creep simulation. The internal cavern pressure is assumed to be constant over time. The total creep simulation time is 50 years.

### **5.2.2 Long-term Abandonment Behavior Considering Sequential Excavations**

Sequential excavations can reasonably simulate the field operational solution mining processes of the disposal caverns at the site. According to the field sonar data tracking the cavern development progress, the sequential excavations are arranged to start from the beginning of 2006 and will be finished by the end of 2015, assuming a 10-year solution mining schedule. Following the full development of the salt cavern, the 1-13 LTBG cavern was planned to fill with saturated brine or dense sands and abandoned permanently. Table C.1, C.2 and C.3 (Appendix C) detail the 1-13 LTBG cavern solution-mined process and abandonment schedule in FLAC<sup>3D</sup> simulation. In the first 10-year mining period, the cavern simulation will undergo creep for a whole year after each immediate excavation at the beginning of the year, and then in the start of 2016 the abandonment creep simulation proceeds and will model for another 50 years to assess the geomechanical behavior of the salt caverns. Thus the salt caverns will run 60 years in total for creep simulations. Figure 5.1 depicts the three-dimensional finite difference models used for Cavern 1-13 LTBG, and the detailed cavern geometry.

3D View of *Cavern 1-13 LTBG* Model

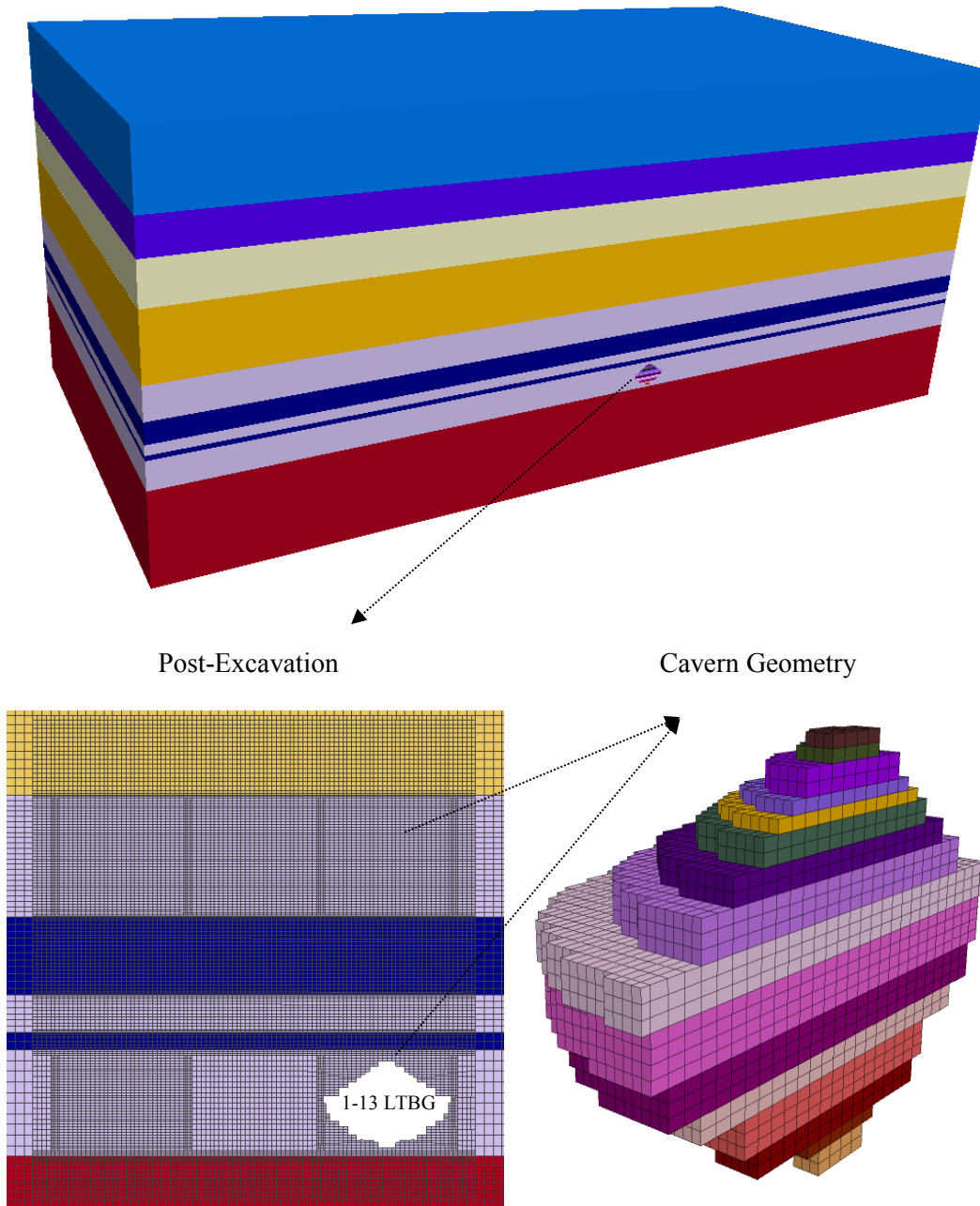


Figure 5.1 Three-Dimensional Finite Difference Model of *Cavern 1-13 LTBG*

### 5.2.3 Results and Conclusions

Table 5.1 summarize the observed deformation simulation results and the *DSR* value with respect to salt dilation potential and the *SSR* value representing the shear failure potential of non-salt overlying strata. It indicates that the sequential excavation modeling predicts slightly more deformation than instantaneous excavations at number of years of abandonment, due to sequential excavations allowing the cavern to creep over a longer period of time and generate more deformation after each excavation procedure. However, instantaneous simulations predict cavern closure ratio at the end of simulation approximately two times of the sequential excavation simulations. Additionally, the predicted *DSR* and *SSR* values as a function of abandonment time are given in Figure 5.2. As shown, during the first few years of abandonment, the *DSR* value under the sequential excavations is apparently higher than the value under instantaneous excavations. This is because that the 10-year solution mining period time considered prior to the abandonment for sequential condition, results in the reduced deviatoric stresses of the salt surrounding the cavern as it creeps and the *DSR* value will grow above the instantaneous case. The value of *DSR* immediately following the final instantaneous excavation is 0.825, which means the salt units around the cavern have dilated and tensile failure may be initialized within the salt. However, the ultimate *DSR* values after 50 years abandonment for both excavation conditions are similar, indicating that the instantaneous excavation methods can predict the final abandonment salt stability adequately as the sequential excavations. The *SSR* values do not vary much during the abandonment modeling and they are identical for both excavation simulations. Thus the excavation simulation method has little impact on the shear failure behavior of the nonsalt units. In conclusion, the instantaneous excavations would result in salt dilation prediction at the end of full excavations but it is not the case in sequential excavations. From a view of long-term

abandonment behavior, both excavations can predict the similar deformation behavior and the structural stability performance. However, the instantaneous excavations simulation will overestimate the cavern volume loss significantly.

More simulations were run for the case of the 1-13 LTBG sequentially solution mined and filled with dense waste sands at abandonment, and compared with the corresponding brine case. The structural stability and integrity of the salt cavern is examined with respect to the potential dilation or tensile failure along the cavern walls and the shear failure of nonsalt caprock formations. When the cavern contents are replaced with saturated brine, the loads that supported the cavern change. The deviatoric stress in the surrounding strata changes and when it exceeds the strength of the formation, salt dilation or nonsalt shear failure will happen. Figure 5.3, 5.4 and 5.5 illustrate the deviatoric stresses distribution, *DSR* value and *SSR* value surrounding the 1-13 LTBG cavern under both brine and dense sands injection respectively. Figure 5.6 plots the *DSR* and *SSR* value change during cavern development and after abandonment. As shown, following the final sequential excavation, the deviatoric stresses of the salt units surrounding the cavern increased immediately and the stress change resulted in the redistribution of the maximum deviatoric stress. As the creep continues with abandonment, salt deviatoric stresses decreases thus the *DSR* value increases, which indicates that the potential of salt dilation diminishes over time. All the *DSR* values during the simulation time for 1-13 LTBG brine and dense sands case are greater than 1.0, so if no salt dilation is expected to occur during the cavern development period, then the integrity of the salt cavern will not be affected by the salt dilation within permanent abandonment. Additionally, the potential of salt dilation is largely diminished by the solid waste sands injection. Since the initial lithostatic anisotropic ratio of 0.5 considered for the overlying nonsalt Ernestina Lake formation in the simulation, the deviatoric stress above the cavern roof in the nonsalt

strata is reduced resulting from cavern internal loads following full excavations. The *SSR* value will remain constant during the abandonment time due to the limited salt cavern creep. The cavern injection conditions have little effect on the shear failure of the overlying nonsalt strata and the *SSR* value remains approximately the same during the simulation for two cavern cases.

Cavern closure is important for assessing the performance of the disposal salt caverns. It depends on the internal pressure of the storage cavern. It assumes that the internal pressure is constant during the 60 years simulation. However, if the caverns were plugged and abandoned, the creep closure will pressurize the caverns and the creep closure rates would be decreased. Figure 5.7 provides the closure rates of the 1-13 LTBG cavern. It can be seen that the cavern shrinks most strongly during the first years of abandonment. Then with the creep time, the cavern closure rate reduces and reaches a nearly constant value, which results in constant internal pressure of the cavern. The final closure predicted after 50-year abandonment under brine is approximately 2.47%, approximately double of the closure of waste injection case. However, the salt cavern volume loss can be expected to be relatively low because of constraints of the overlying and underlying nonsalt strata onto the salt units around the cavern.

As the salt creeps into the disposal cavern, the cemented casing will be dragged along with it and resulting in loading and straining of the casing. The theoretical casing strain is roughly estimated by extracting the vertical displacement along the symmetrical line above the caverns where the casing may be located. Figure 5.8 gives the accumulated theoretical casing strains following the full cavern excavations and at the end of simulation under brine and dense waste. The casing strains are enlarged greatly within the Prairie Evaporite and Cold Lake formation. This is because that the salt strata behaves viscoplastically and tends to flow vertically into the Lotsberg cavern. The predicted

casing strains at the end of abandonment simulation are approximately 0.00025 and 0.00031 for brine and waste injection respectively, which is quite small and no casing failure will be expected to occur.

Due to the constant cavern internal pressure assumption, the real site surface subsidence is expected to be smaller than values predicted in FLAC<sup>3D</sup> modeling. The maximum surface subsidence will occur at the point along the symmetrical line of salt cavern. Figure 5.9 and Figure 5.10 illustrate the surface subsidence plots under the brine and dense waste sands for Cavern 1-13 LTBG respectively. Figure 5.11 depicts the surface subsidence plot versus creep time of the 1-13 LTBG cavern bearing different internal pressure. The maximum surface subsidence at the end of simulation will reach 10.52 mm and 6.47 mm for brine and waste sands respectively. The surface subsidence rate can be estimated from the slope of plots that from about 20 years after abandonment it will remain constant to be approximately 0.12115mm/year and 0.06069 mm/year.

Table 5.1 Comparison of Simulation Results for Instantaneous Excavations and Sequential Excavations (*1-13 LTBG brine*)

	Instantaneous Excavations		Sequential Excavations	
	1yr abandonment	50yr abandonment	1yr abandonment	50yr abandonment
Maximum Surface Subsidence (mm)	2.4	9.4	4.03	10.52
Maximum Casing Strains	0.000166	0.000302	0.000208	0.00031
Minimum <i>DSR</i>	1.572	2.37	1.98	2.41
Minimum <i>SSR</i>	3.19	3.27	3.2	3.28
Cavern Closure (%)	1.400	4.563	0.122	2.472

**1-13 LTBG  
brine-case**

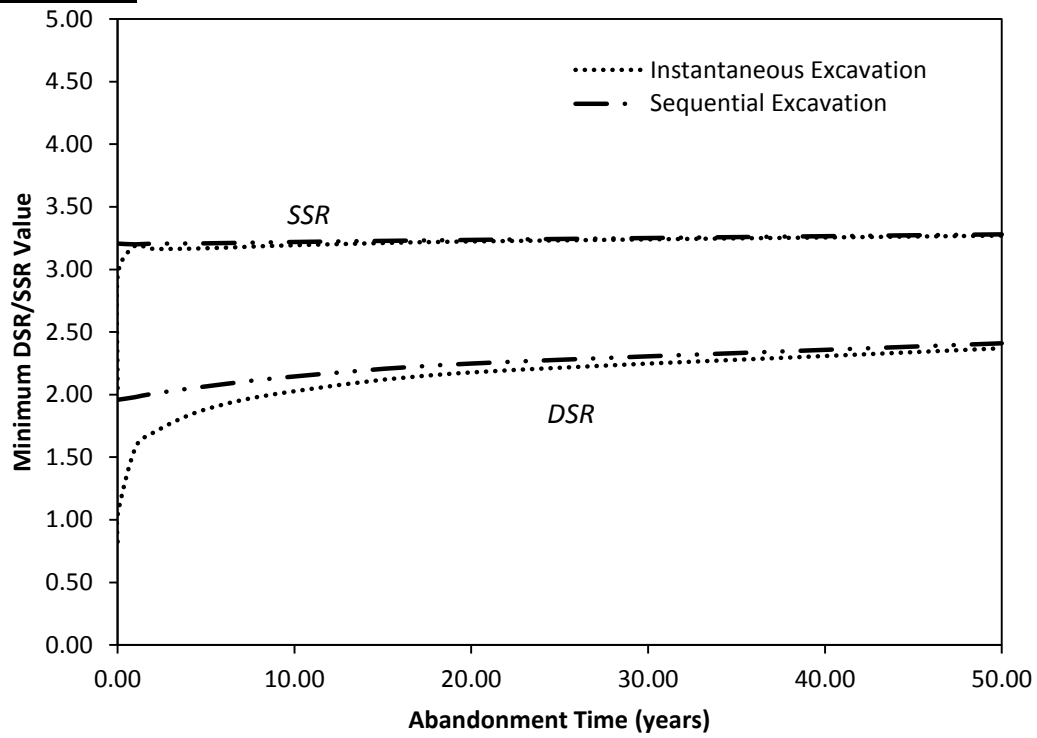
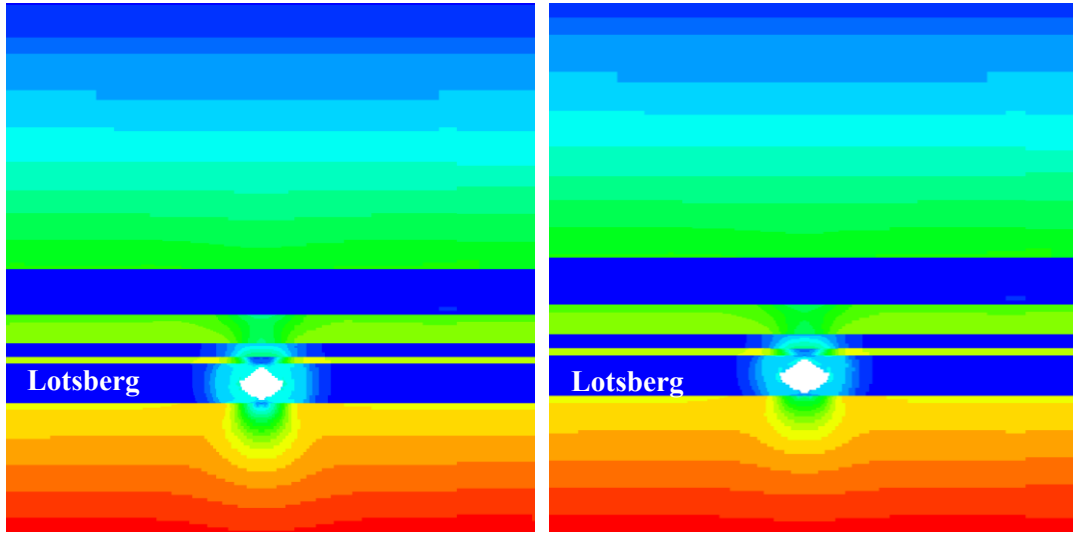
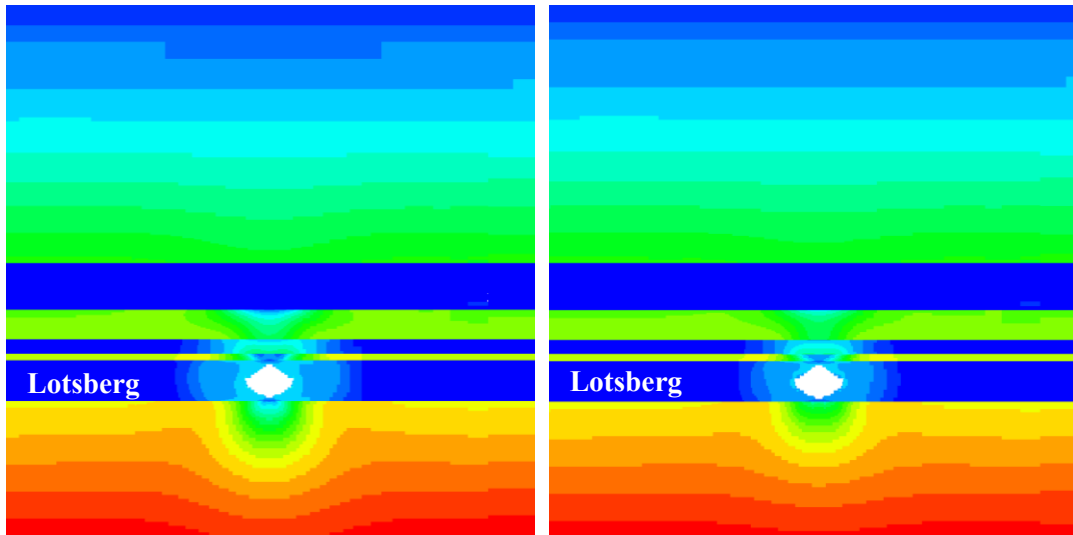


Figure 5.2 Predicted *DSR* and *SSR* Value Evolution over Abandonment Time (*1-13 LTBG brine*)

Following final sequential development (Time = 10 years)



End of Simulation (Time = 60 years)



1-13 LTBG brine

1-13 LTBG dense

Legend of Deviatoric Stresses  
(Pa)

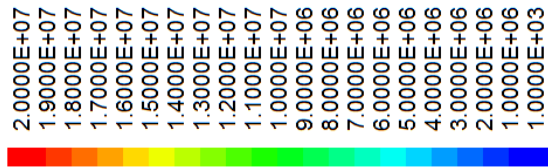
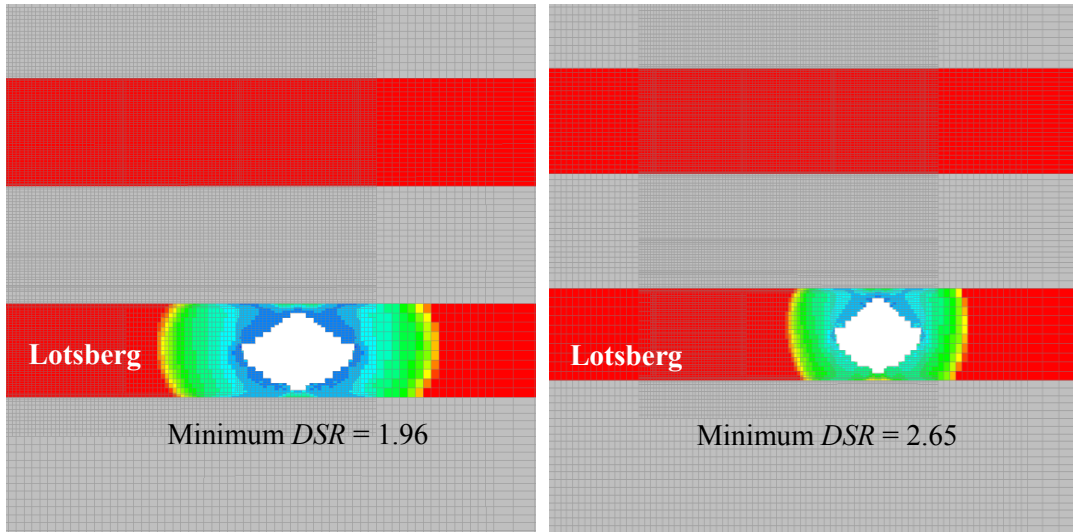
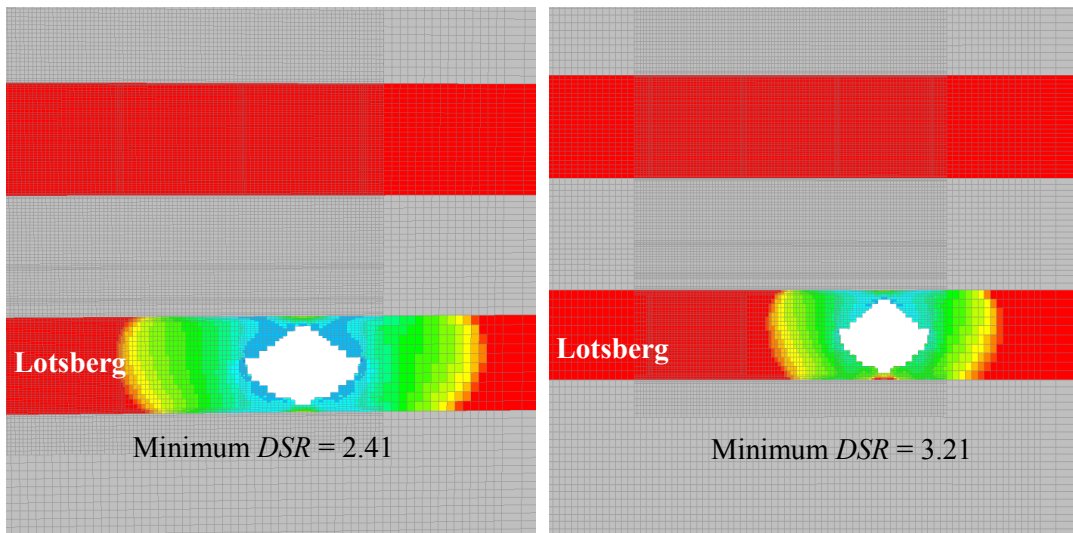


Figure 5.3 Contour of Deviatoric Stresses Surrounding *Cavern 1-13 LTBG*

Following final sequential development (Time = 10 years)



End of Simulation (Time = 60 years)



1-13 LTBG brine

1-13 LTBG dense

Legend of *DSR* Value  
(-)

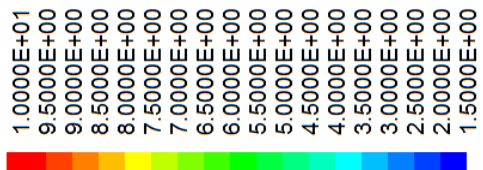
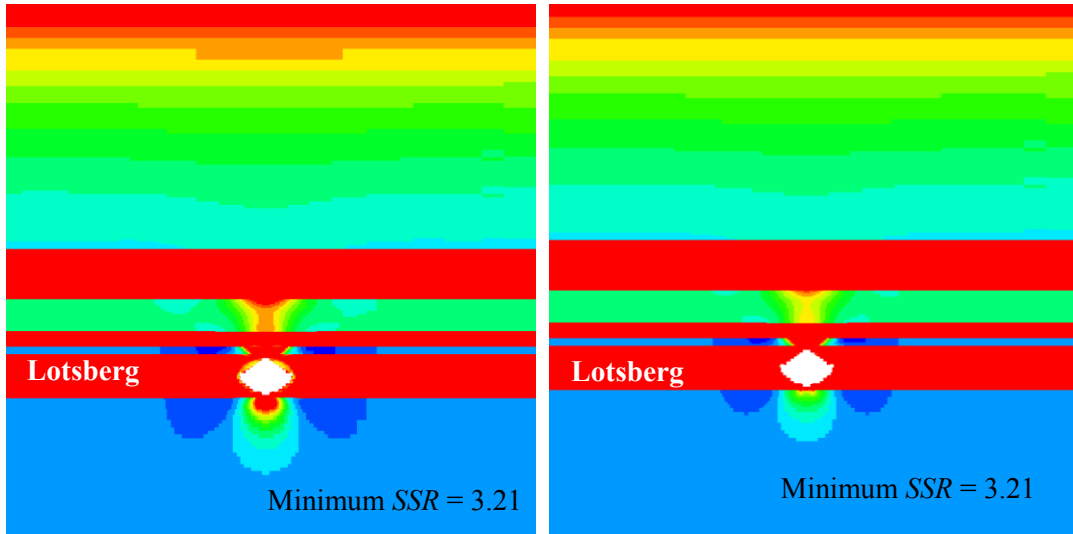
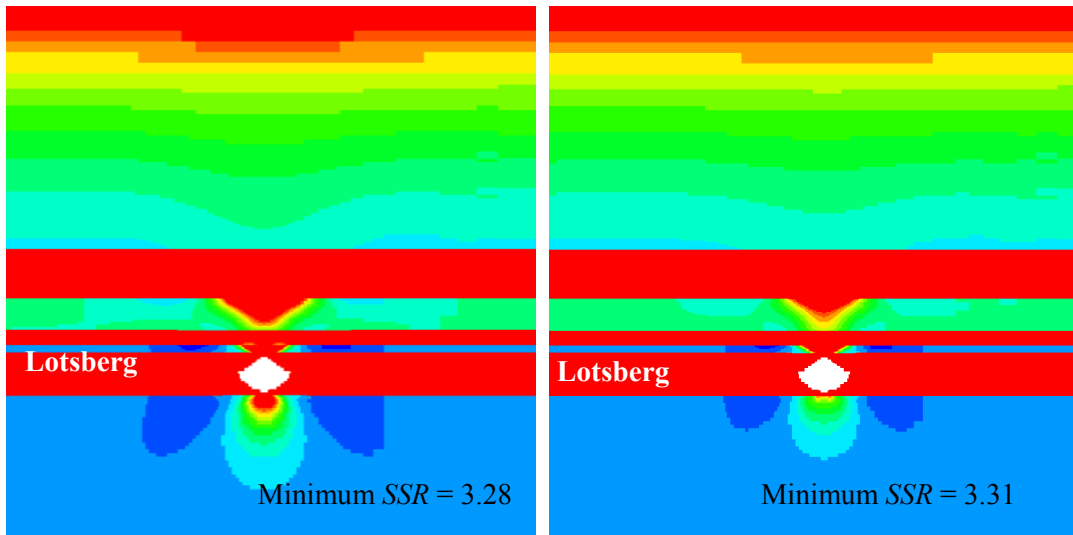


Figure 5.4 *DSR* Value Distributions Surrounding *Cavern 1-13 LTBG*

Following final sequential development (Time = 10 years)



End of Simulation (Time = 60 years)



1-13 LTBG brine

1-13 LTBG dense

Legend of SSR Value  
(-)

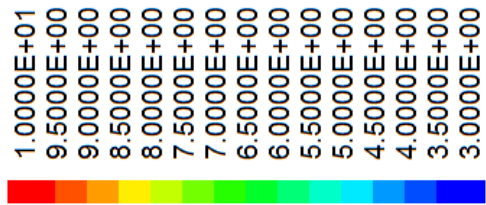


Figure 5.5 SSR Value Distributions Surrounding *Cavern 1-13 LTBG*

**1-13 LTBG  
Cases VS.**

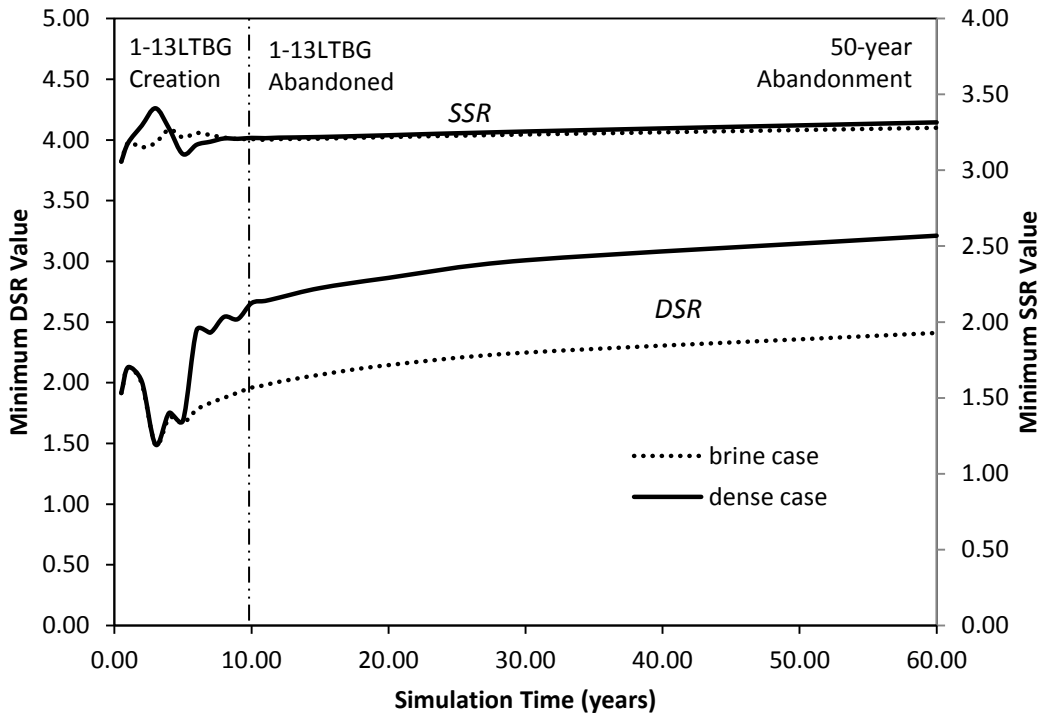


Figure 5.6 DSR and SSR Value Change with Simulation Time for *Cavern 1-13 LTBG*

**1-13 LTBG  
Cases VS.**

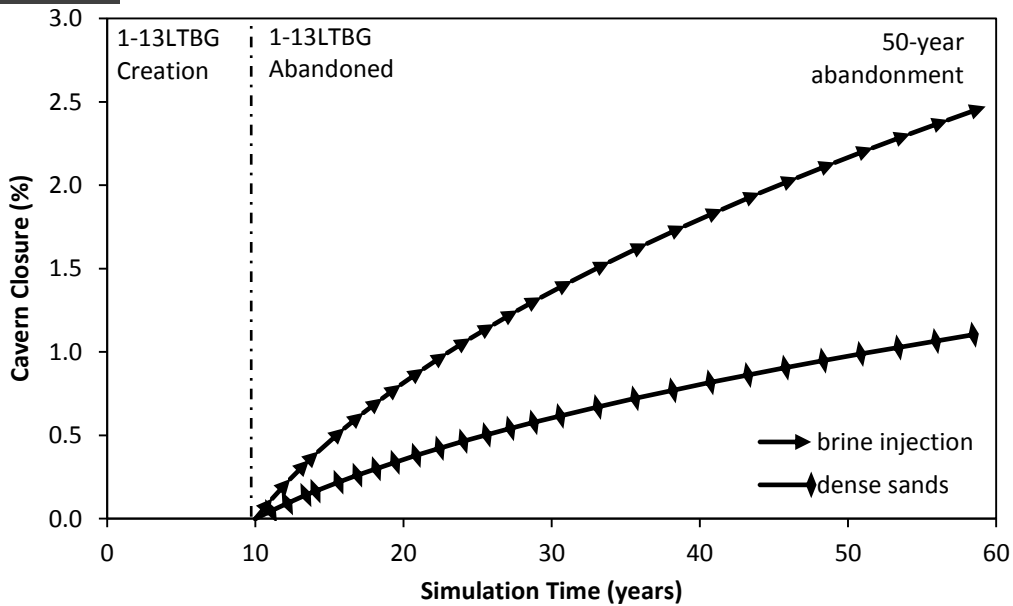


Figure 5.7 Predicted Cavern Closure as a Function of Time for *Cavern 1-13 LTBG*

**1-13 LTBG  
Cases VS.**

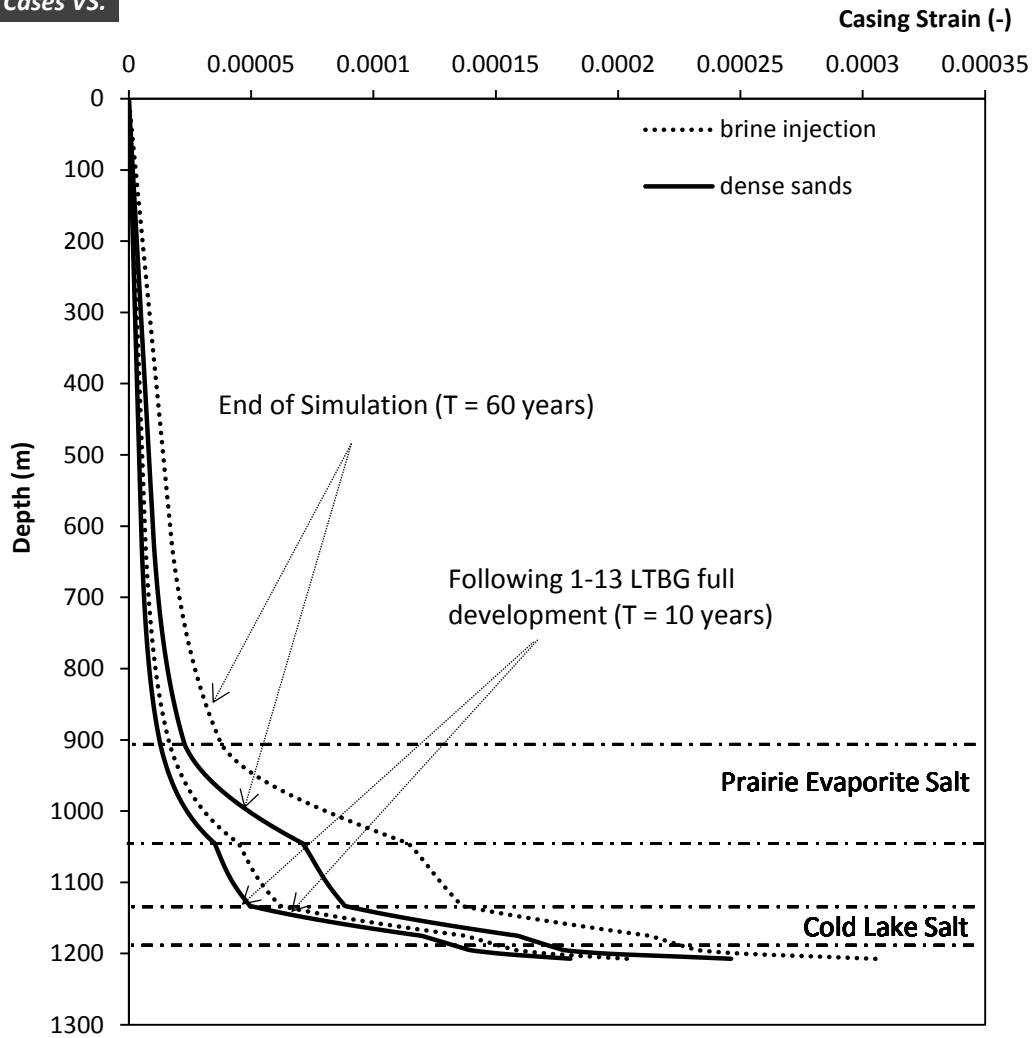


Figure 5.8 Accumulated Vertical Strains along the Axis of Symmetry during Abandonment Simulation of *Cavern 1-13 LTBG*

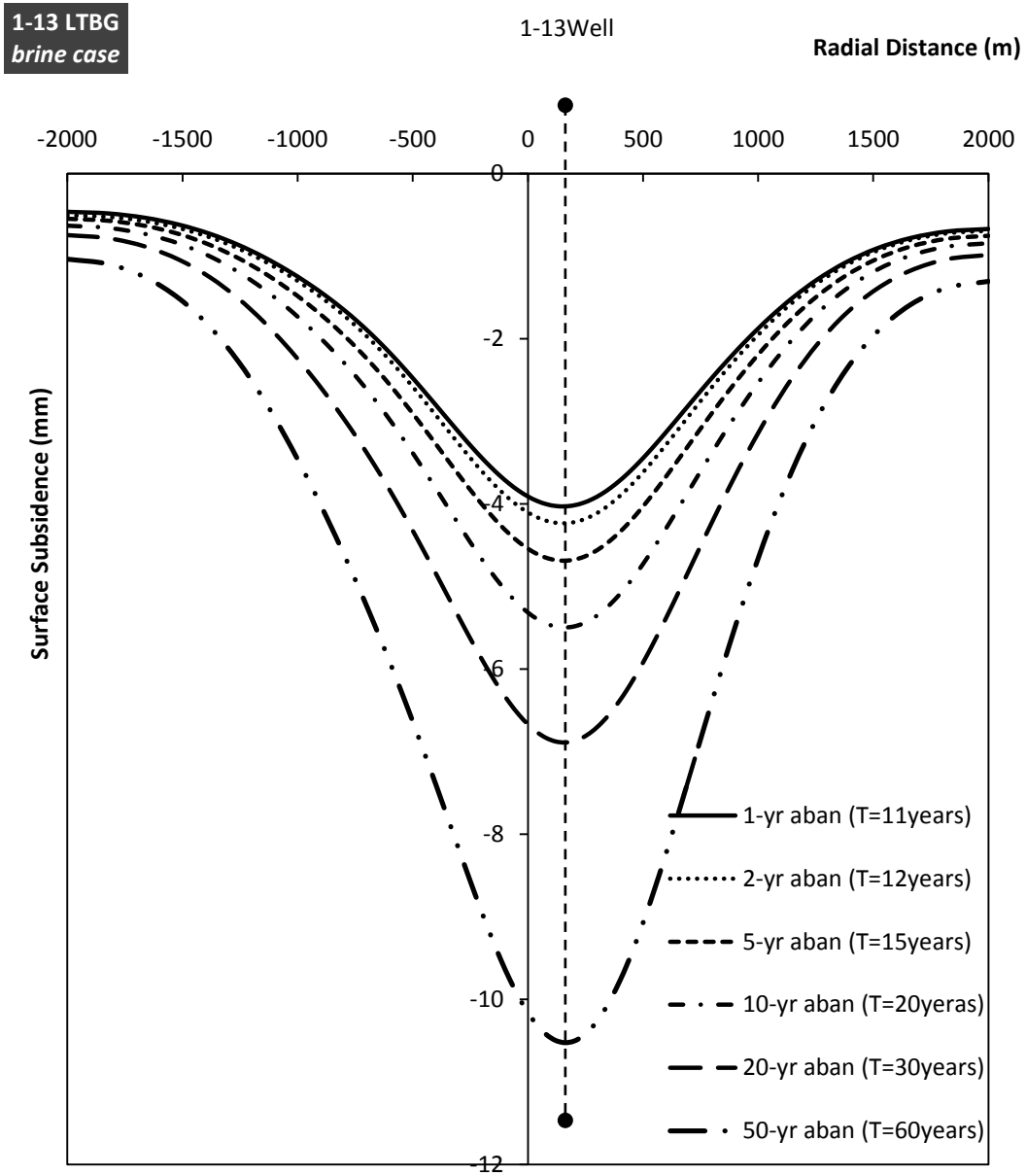


Figure 5.9 Surface Subsidence Plot under *1-13 LTBG brine case*

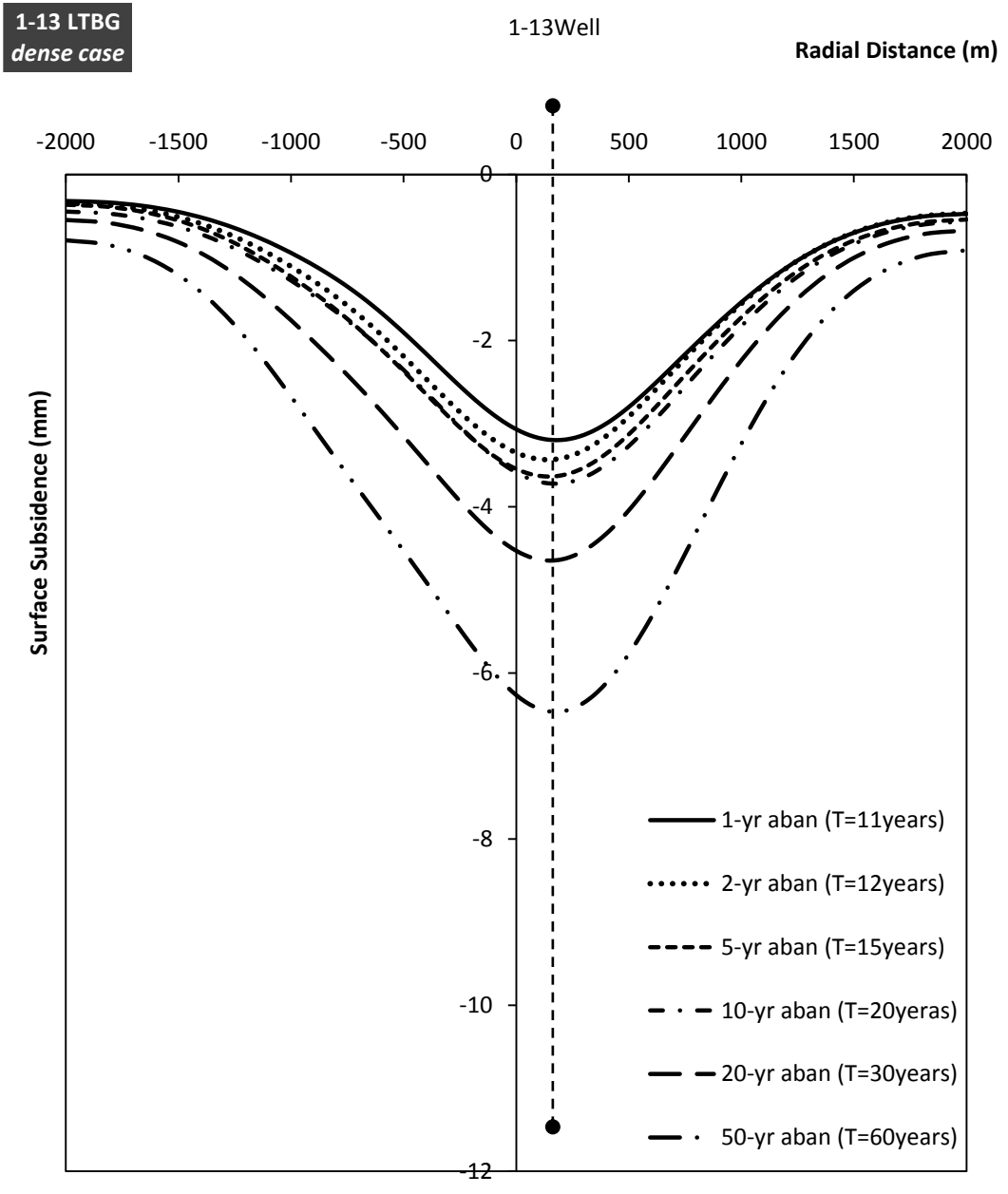


Figure 5.10 Surface Subsidence Plot under *1-13 LTBG dense* case

**1-13 LTBG  
Cases VS.**

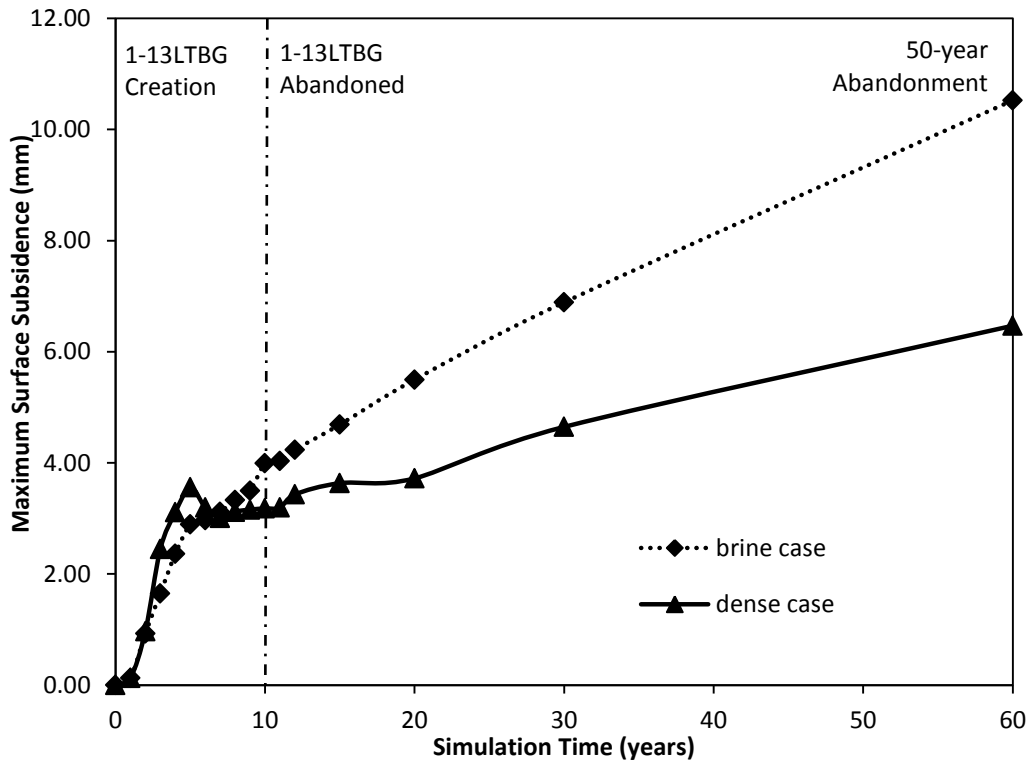


Figure 5.11 Predicted Maximum Surface Subsidence over Time (*1-13 LTBG*)

Table 5.2 Summarized Simulation Results for *Cavern 1-13 LTBG*

	1-13 LTBG brine		1-13 LTBG dense	
	T = 10 years	T = 60 years	T = 10 years	T = 60 years
Maximum Surface Subsidence (mm)	3.99	10.52	3.18	6.47
Maximum Casing Strains	0.000204	0.000305	0.000180	0.000246
Cavern Closure (%)	0	2.47	0	1.10
Minimum <i>DSR</i>	1.96	2.41	2.66	3.21
Minimum <i>SSR</i>	3.21	3.28	3.21	3.32

## **5.3 Long-term Abandonment Behavior Simulation of Lotsberg Caverns**

The analysis initiated in Section 5.2 will be used for the complete scenario of the full development of two horizontal Lotsberg caverns in FLAC<sup>3D</sup> numerical modeling in this section. Firstly, the contrast of instantaneous and sequential excavations will be performed based on the specific injection conditions. Then using the sequential excavation studies, the long-term abandonment creep behavior of the two Lotsberg caverns will be simulated and analyzed for three different cavern internal pressure cases.

### **5.3.1 Long-term Abandonment Behavior Considering Instantaneous Excavation**

Instantaneous excavations of both Cavern 1-13 LTBG and Cavern 8-13 LTBG were performed simultaneously in the three-dimensional finite difference program. To simulate the field operation, the existing 1-13 LTBG cavern will be filled with dense sand disposal and sealed represented by a vertical pressure gradient of 0.072366 MPa/m, and the 8-13 Lotsberg cavern will be held at a constant brine pressure gradient of 0.011760 MPa/m. The total creep simulation time for the two Lotsberg caverns is 50 years.

### **5.3.2 Long-term Abandonment Behavior Considering Sequential Excavations**

The sequential excavations process and schedule of two Lotsberg caverns are described in Table C.4, C.5 and C.6 (Appendix C). As shown, Cavern 1-13 LTBG will be solution mined from 2006 to 2015, and then plugged and abandoned, followed by the 10-year solution mining of Cavern 8-13 LTBG at the horizontal depth. The excavated depth of the cavern filled with saturated brine in the previous year will be injected with waste disposal and be held at a dense sands pressure in the following year. Similarly, one-year of creep will be simulated after each excavation operation. Then the 1-13 LTBG cavern will be

sealed and the two Lotsberg caverns will run another 50 years creep to analyze the long-term geomechanical behavior and structural stabilities. The simulation time in FLAC<sup>3D</sup> will be 70 years in total. The three-dimensional finite difference models for 1-13 & 8-13 LTBG are shown in Figure 5.12. Both Lotsberg caverns have the same geometry.

3D View of Cavern 1-13 & 8-13 LTBG Model

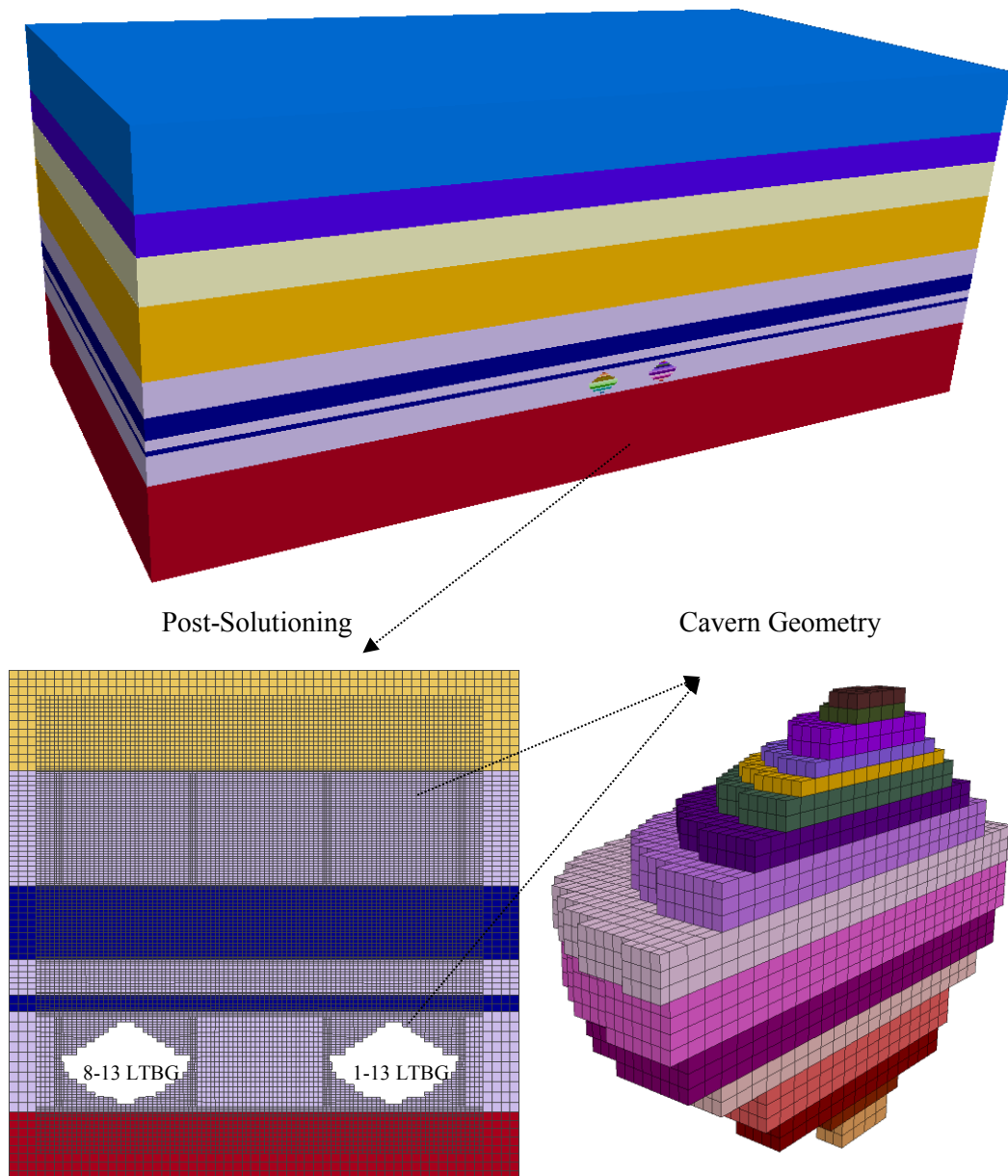


Figure 5.12 Three-Dimensional Finite Difference Model of *Cavern 1-13&8-13 LTBG*

### 5.3.3 Results and Conclusions

Figure 5.13 illustrates the predicted *DSR* and *SSR* value plots over abandonment time and Table 5.3 summaries the deformation simulation results for the instantaneous and sequential excavations simulations. Similar conclusions can be made that, the instantaneous excavation solution is able to predict approximately identical salt dilation behavior surrounding the salt cavern and overlying nonsalt shear failure behavior as the sequential excavation solutions at long-term abandonment. However, as for the short-term structural stability and integrity of the disposal salt caverns followed by the full cavern development, instantaneous solutions may predict dilation failure of the salt units around the caverns, which is not observed in sequential mining simulations. Moreover, instantaneous excavations will underestimate the surface subsidence compared with sequential simulations, with a reduced level of underestimation over creep time. Additionally, instantaneous solutions will predict approximately double the cavern volume loss for each disposal cavern of sequential excavations.

The simulation results of sequential solution under more cavern injection conditions are given in Figure 5.14 to Figure 5.22. The deviatoric stresses development around the two horizontal Lotsberg caverns due to caverns mining and operation was illustrated in Figure 5.14. In this Figure, Cavern 1-13 LTBG was filled with dense waste disposal and Cavern 8-13 LTBG was held at a brine pressure. The *DSR* and *SSR* values distributions are provided in Figure 5.15 and Figure 5.16 respectively. As shown, the higher deviatoric stresses of the salt units tend to flow around the lower-pressurized Cavern 8-13 LTBG following the full development of the two Lotsberg caverns. Still no salt dilation ( $DSR > 1$ ) or non-salt shear failure ( $SSR > 1$ ) was observed during the creation of both Lotsberg caverns and after 50 years abandonment simulations, as the given *DSR* and *SSR* values plots varied with simulation time in Figure 5.17. The *DSR* and *SSR* values

fluctuated during the cavern solution mining process due to the irregular excavations at certain stages. Figure 5.17 also indicates that as long as either cavern is held at brine pressure at abandonment, the minimum *DSR* value remains the same as the condition of both caverns with brine inside. This is because the greatest potential for salt dilation is usually located around the edge of the lower pressure-supported cavern. The potential of salt dilation will be largely reduced once both caverns are plugged and abandoned with dense waste disposal. However, the non-salt shear failure potential is not as sensitive as the salt dilation with respect to the cavern internal pressures. The values of *SSR* do not vary much with increased cavern pressure, and they stay constant at the end of simulation for dense-brine and dense-dense case. The case of both caverns with brine show a slight gradual decay on the *SSR* value but it may be expected the value will stay above one in the foreseeable future. Additionally, the nonsalt shear failure behavior is noticeably influenced by the excavations of horizontal adjacent caverns, independent of the injection conditions.

The cavern closure behavior is presented in Figure 5.18 for Cavern 1-13&8-13 LTBG under various cases. Conclusions can be drawn that its internal carrying pressure dominates the cavern closure behavior, and it is not influenced much by the injection conditions of the horizontal adjacent salt caverns. The volume loss of Cavern 8-13 LTBG with brine is only reduced approximately 0.1% at 50-year creep if the adjacent Cavern 1-13 LTBG is held at an increased pressure from brine to dense sands. However, when Cavern 8-13 LTBG is filled with disposal sands at abandonment, half of the cavern volume loss will diminish and the shrinkage rate will reduce to 1.25% at the end of simulations.

The accumulated casing strains for both Lotsberg caverns under dense-brine case are shown in Figure 5.19. The casing strains of Cavern 1-13 LTBG increases from 0.00021

following the full development of both caverns to around 0.00029 at the end of simulation. The corresponding casing strains for Cavern 8-13 LTBG is 0.00021 and 0.00033 respectively. Thus the casing strains of either cavern only increase slightly during the 50-year abandonment time. This is because that the salt creep above the cavern roof is relatively nonexistent following the whole period of cavern development and operation, then the strains will remain nearly constant throughout the abandonment simulation. The casing strains reacting with different cavern internal pressures of Cavern 1-13 LTBG and 8-13 LTBG were represented in Figure 5.20 and Figure 5.21 separately. The figures suggested that the influence of the cavern injection conditions on the casing strain is similar onto the cavern closure behavior. Cavern accumulated casing strains are primarily determined by its internal cavity loads.

The surface subsidence plots for two horizontal Lotsberg caverns case were given in Appendix C, Figures C.1 to C.3. The change of maximum surface subsidence for the two caverns during simulation was illustrated in Figure 5.22. The maximum surface subsidence when both caverns held brine pressure is around 25.54 mm, and this number will reduce to nearly half when both caverns were abandoned with dense waste disposal. The surface subsidence rate estimated from the plots for the brine-brine case is approximately 0.2895 mm/year and for the dense-dense case is around 0.1261 mm/year.

**1-13&8-13 LTBG  
dense-brine case**

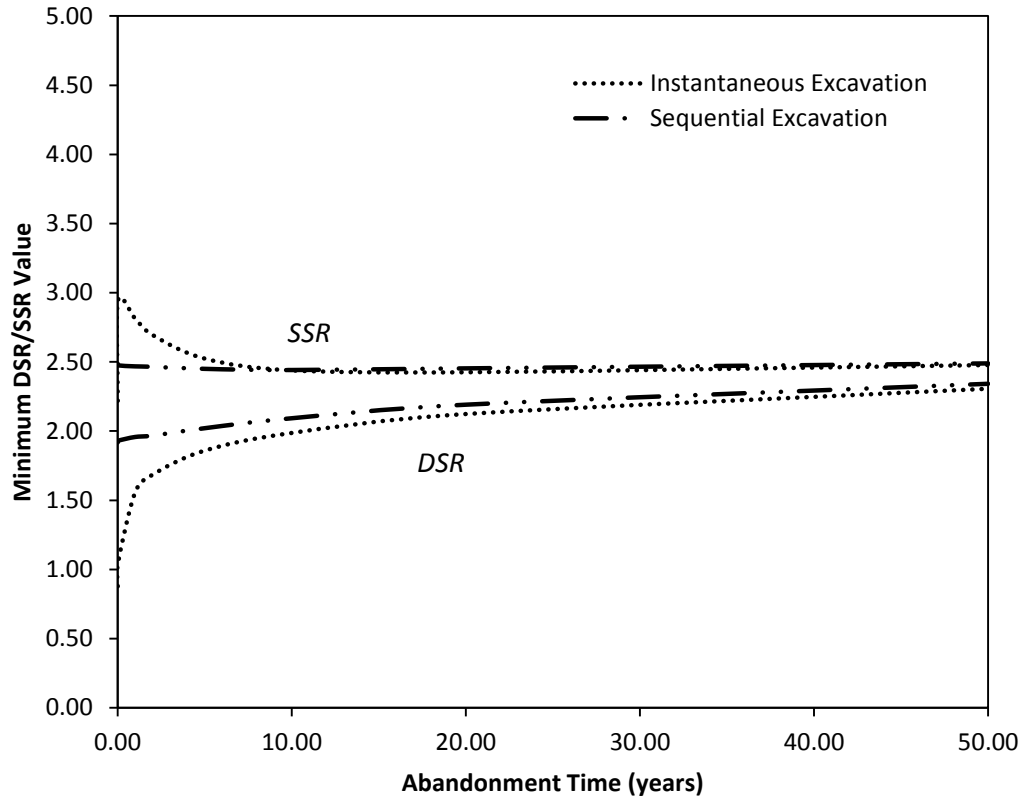
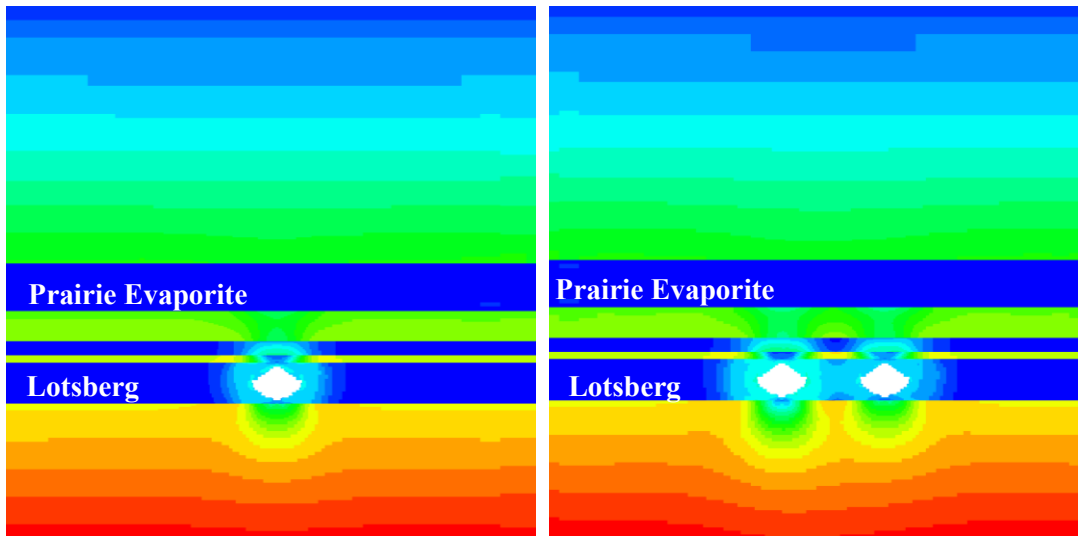


Figure 5.13 Predicted *DSR* and *SSR* Value Evolution over Abandonment Time (*1-13&8-13 LTBG dense-brine*)

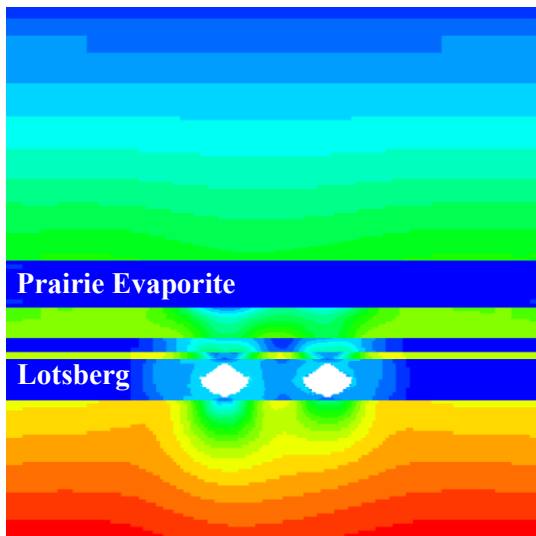
Table 5.3 Comparison of Simulation Results for Instantaneous Excavations and Sequential Excavations (*1-13&8-13 LTBG dense-brine*)

	Instantaneous Excavations		Sequential Excavations	
	1y abandonment	50y abandonment	1y abandonment	50y abandonment
Maximum Surface Subsidence (mm)	4.3	16.4	8.6	19.2
Maximum Casing Strains	0.000232	0.000315	0.000202	0.00032
Cavern 1-13 LTBG Closure (%)	0.80	2.53	0.43	1.52
Cavern 8-13 LTBG Closure (%)	1.42	4.76	0.13	2.66



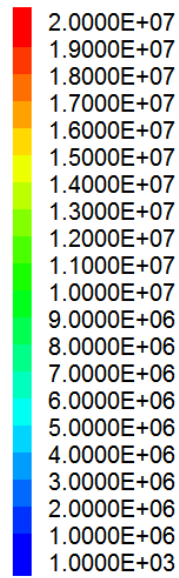
Following Cavern 1-13 LTBG development (Time = 10 years)

Following Cavern 8-13 LTBG development (Time = 20 years)



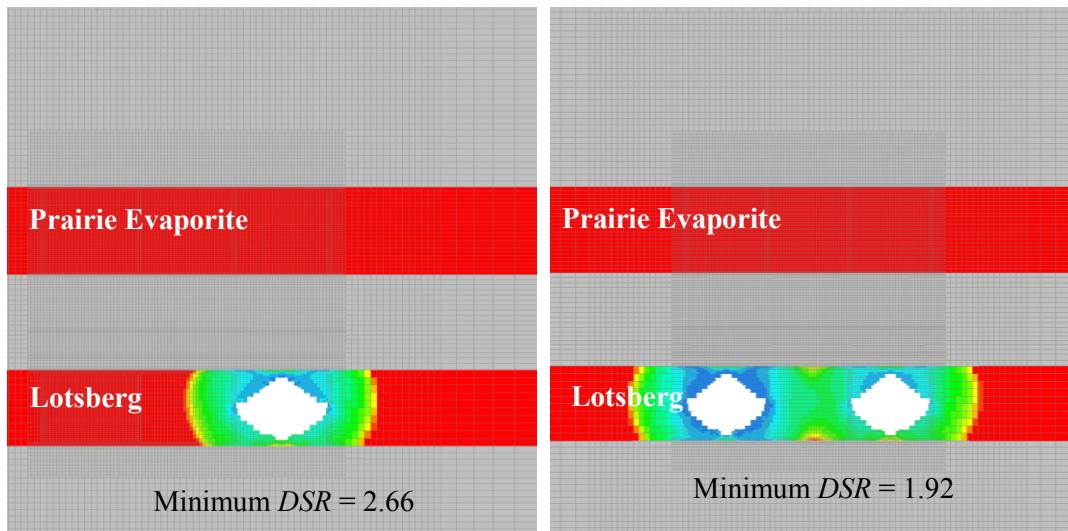
End of Simulation (Time = 70 years)

Legend of Deviatoric Stress (Pa)



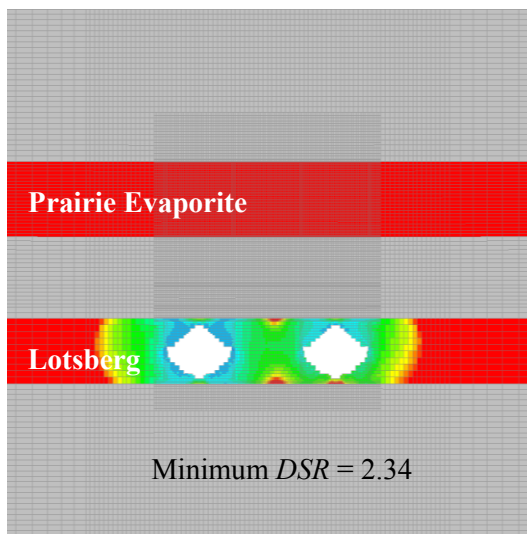
1-13&8-13 LTBG dense-brine

Figure 5.14 Contour of Deviatoric Stresses Surrounding *Cavern 1-13&8-13 LTBG*



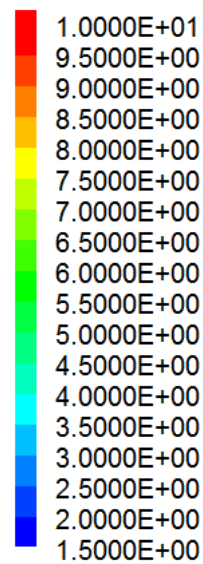
Following Cavern 1-13 LTBG development (Time = 10 years)

Following Cavern 8-13 LTBG development (Time = 20 years)



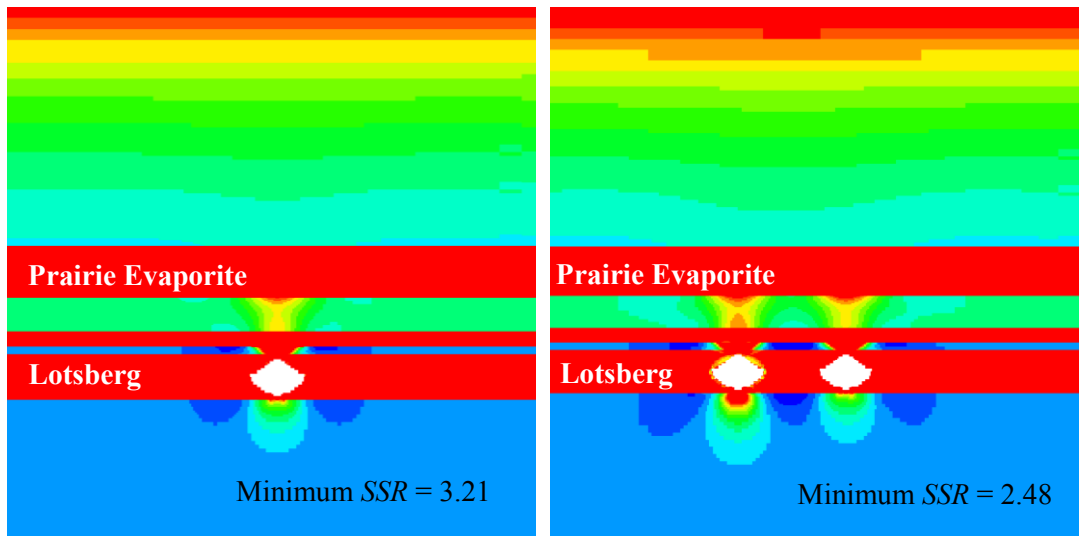
End of Simulation (Time = 70 years)

Legend of *DSR* Value



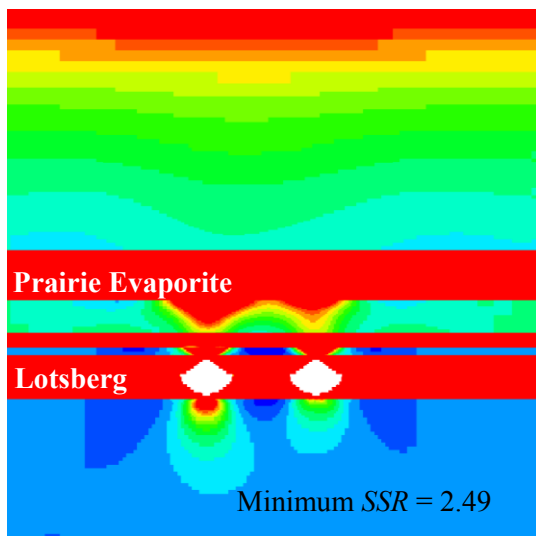
1-13&8-13 LTBG dense-brine

Figure 5.15 *DSR* Value Distributions Surrounding *Cavern 1-13&8-13 LTBG*

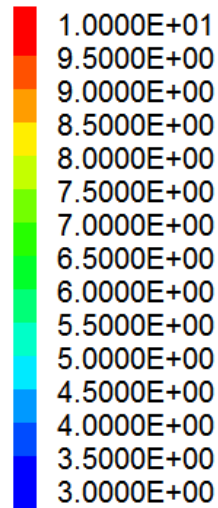


Following Cavern 1-13 LTBG development (Time = 10 years)

Following Cavern 8-13 LTBG development (Time = 20 years)



Legend of SSR Value



End of Simulation (Time = 70 years)

1-13&8-13 LTBG dense-brine

Figure 5.16 SSR Value Distributions Surrounding *Cavern 1-13&8-13 LTBG*

**1-13&8-13 LTBG**  
**Cases VS.**

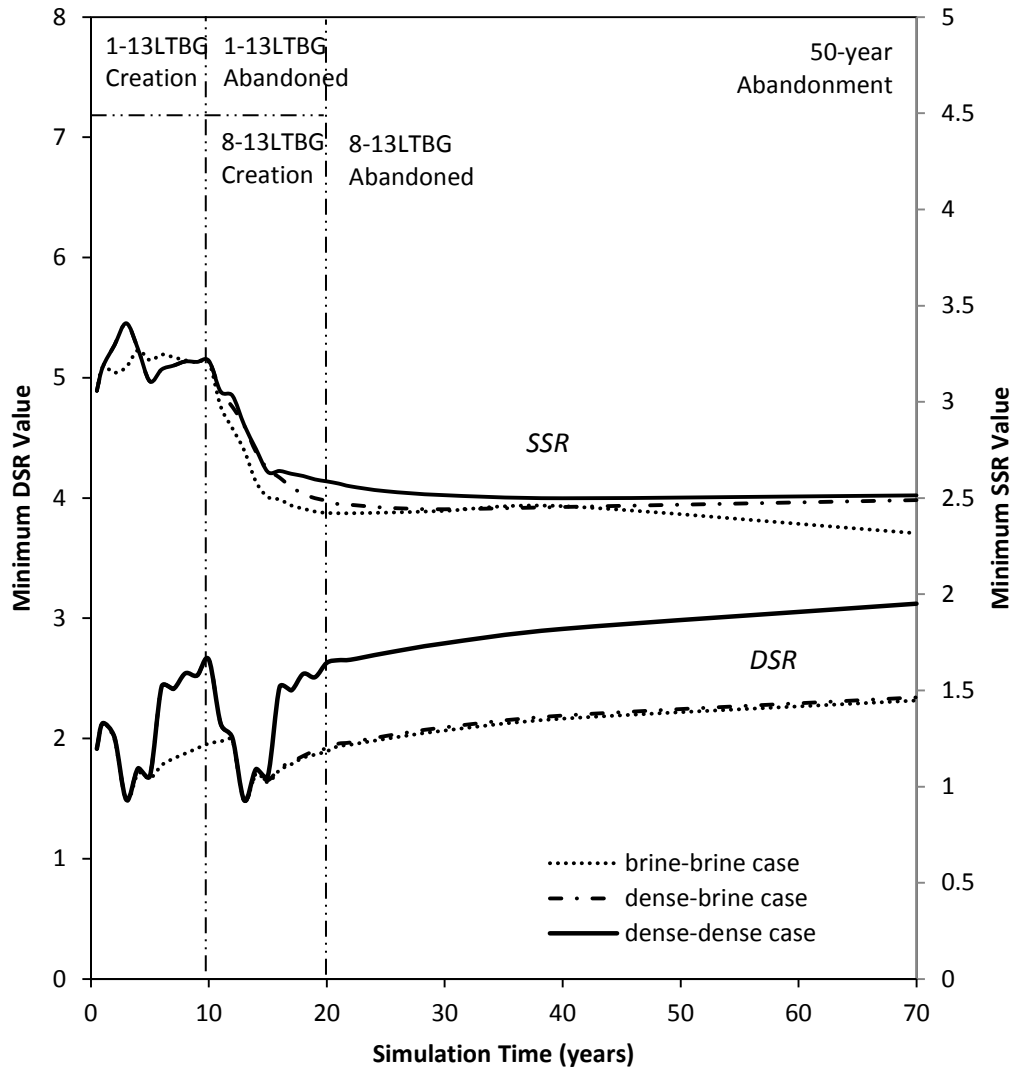


Figure 5.17 *DSR and SSR Value Varied with Simulation Time for Cavern 1-13&8-13 LTBG*

**1-13&8-13LTBG**  
**Case VS.**

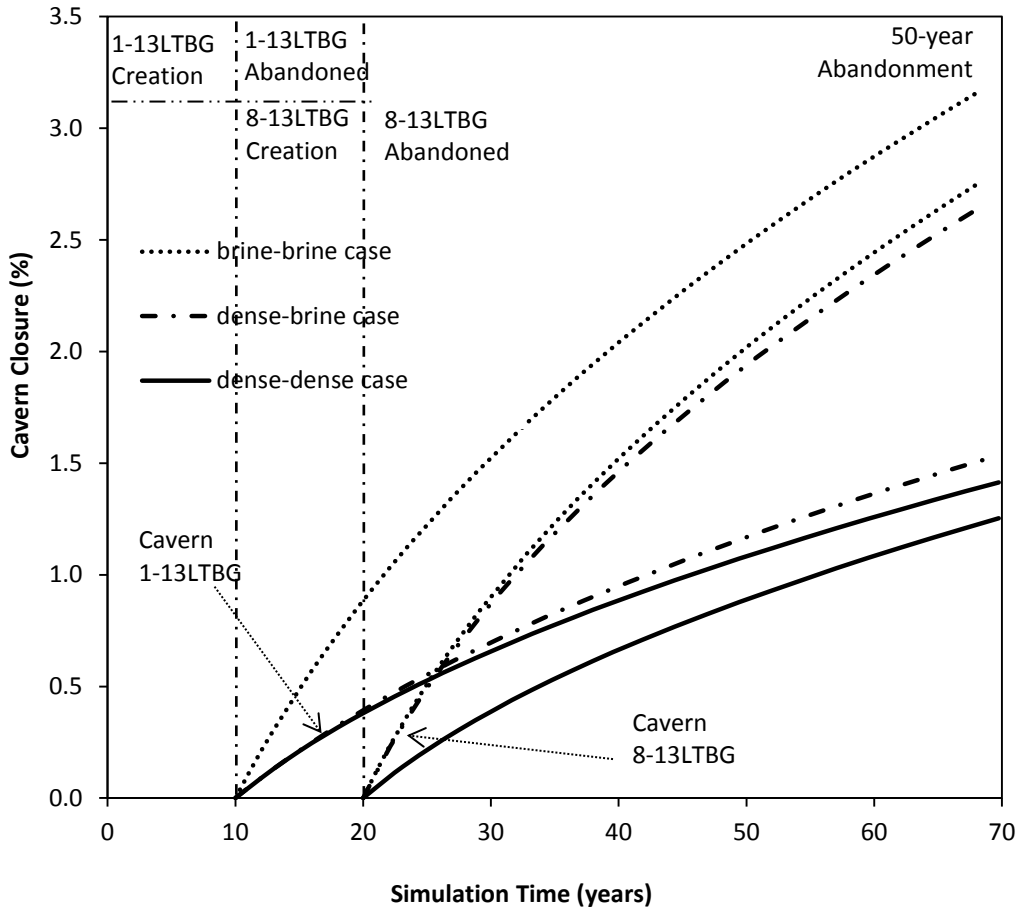


Figure 5.18 Predicted Caverns Closure as a Function of Time for *Cavern 1-13&8-13 LTBG*

**1-13&8-13 LTBG  
dense-brine case**

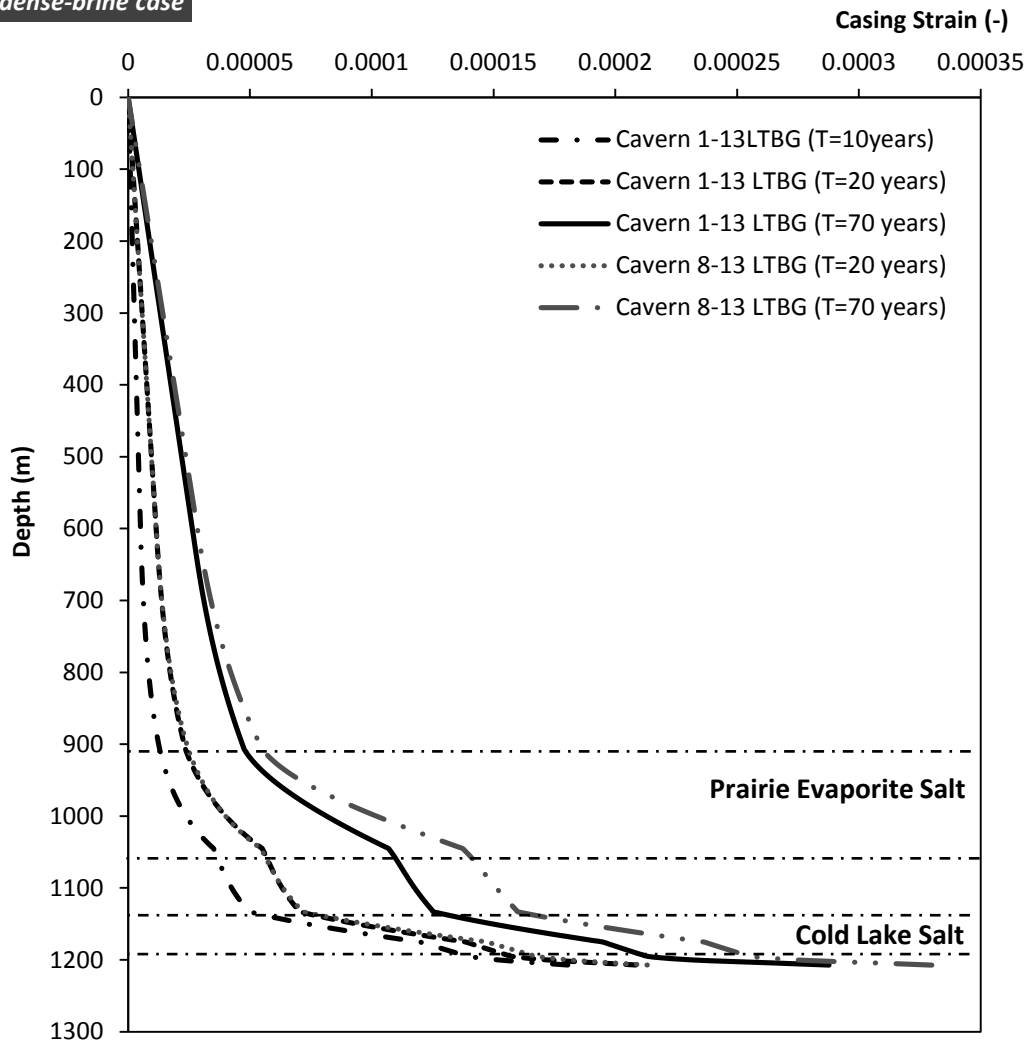


Figure 5.19 Accumulated Vertical Strains along the Axis of Symmetry during Abandonment Simulation (*1-13&8-13 LTBG dense-brine*)

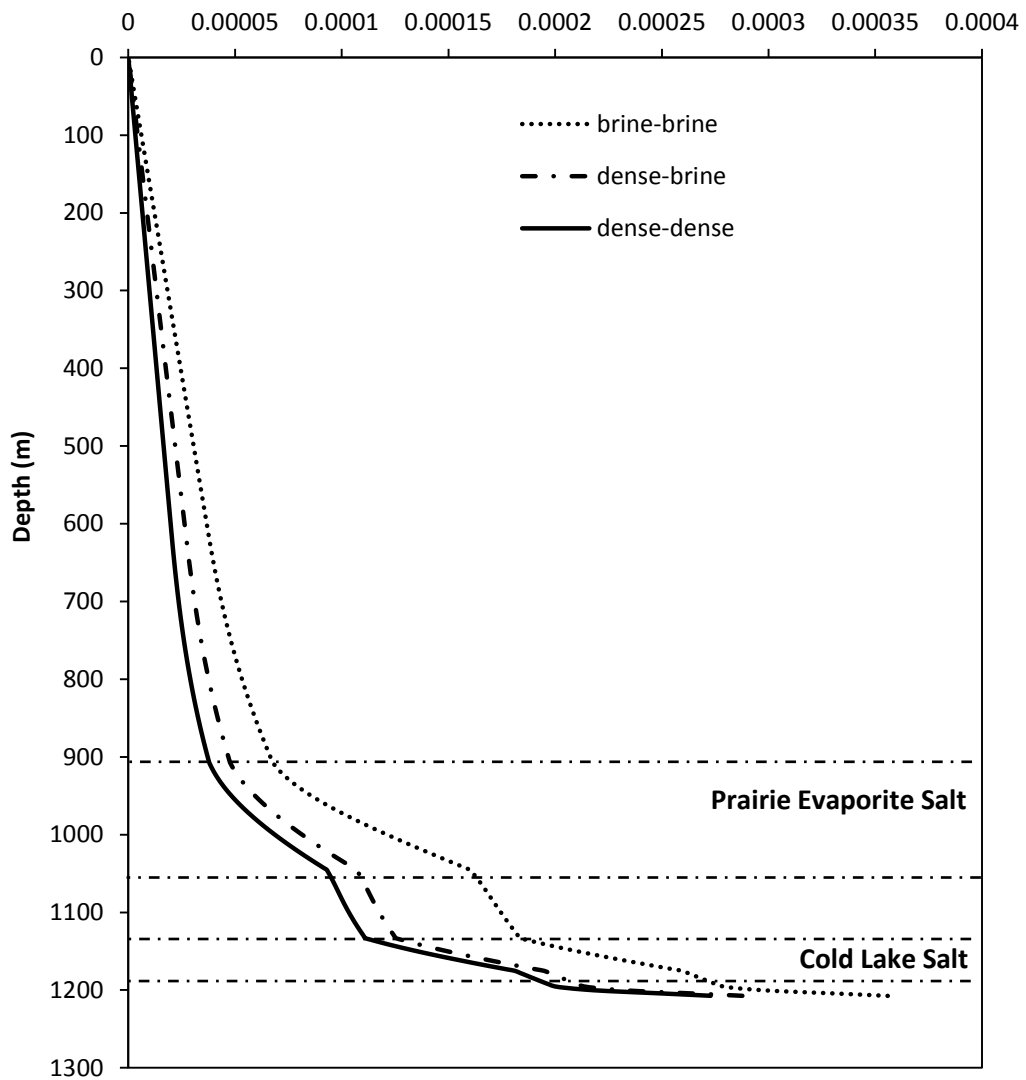


Figure 5.20 Accumulated Casing Strains at the End of Simulation for Cavern 1-13  
LTBG (1-13&8-13 LTBG)

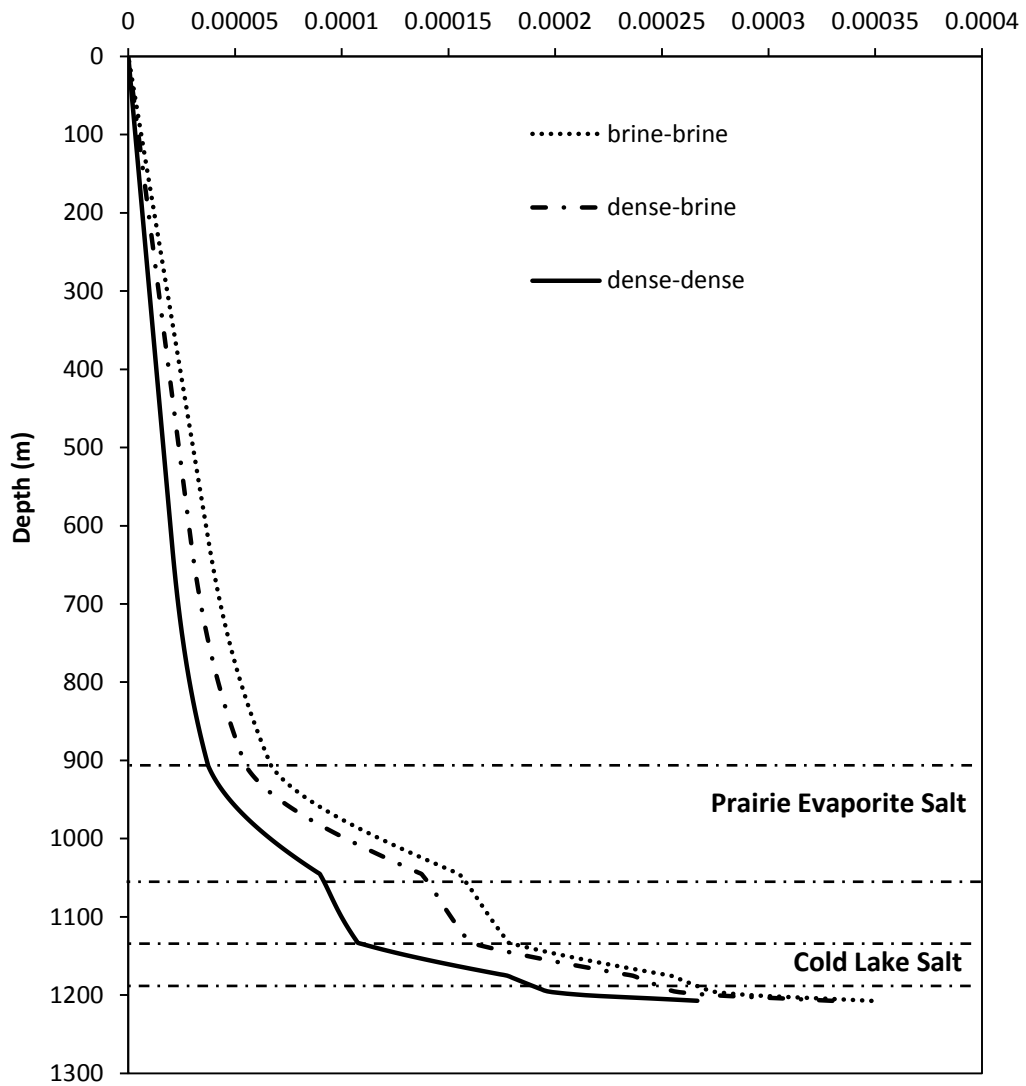


Figure 5.21 Accumulated Casing Strains at the End of Simulation for Cavern 8-13  
LTBG (1-13&8-13 LTBG)

**1-13&8-13 LTBG  
Cases VS.**

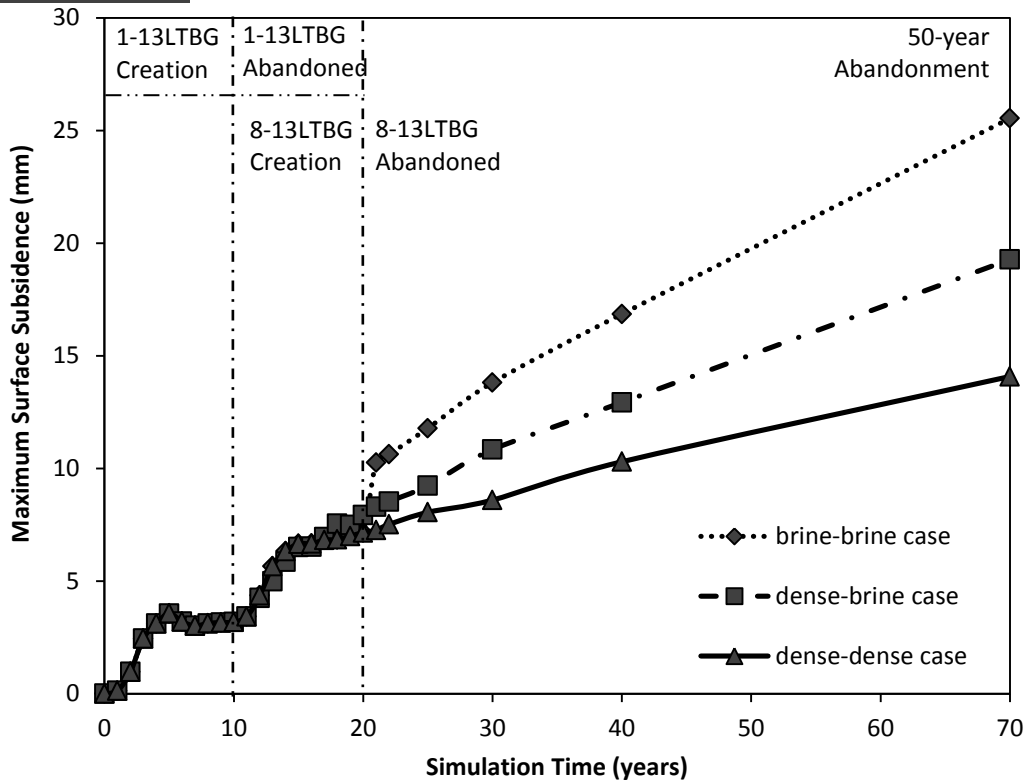


Figure 5.22 Predicted Maximum Surface Subsidence over Time (*1-13&8-13 LTBG*)

## **5.4 Long-term Abandonment Behavior Simulation of Vertical Adjacent Caverns**

### **5.4.1 Long-term Abandonment Behavior Considering Sequential Excavations**

Two vertical adjacent caverns within one well are expected to have more issues with structural stability and integrity of the salt and non-salt strata. The same sequential excavation scenario will be applied onto the three-dimensional finite difference program of two adjacent vertical 1-13 caverns located at Lotsberg and Prairie Evaporite formation separately in this section. The solution-mining schedules of 1-13 LTBG & PRVP caverns under three injection conditions are given in Figures C.7, C.9, and C.10 in Appendix C. Cavern 1-13 LTBG was still excavated from the year 2006 and expected to be fully developed and abandoned at the end of 2015. The solution mining creation of the uphole Prairie Evaporite 1-13 cavern proceeds at the beginning of 2016 and it is assumed to be plugged and sealed 10 years later in 2026 for permanent abandonment. Numerical simulations of abandonment will last for 50 years and thus the total creep simulation time will be 70 years in total. Figure 5.23 provides the three-dimensional finite difference model of Cavern 1-13 LTBG & PRVP as well as the identical cavern geometry assigned to both caverns.

3D View of Cavern 1-13 LTBG & PRVP Model

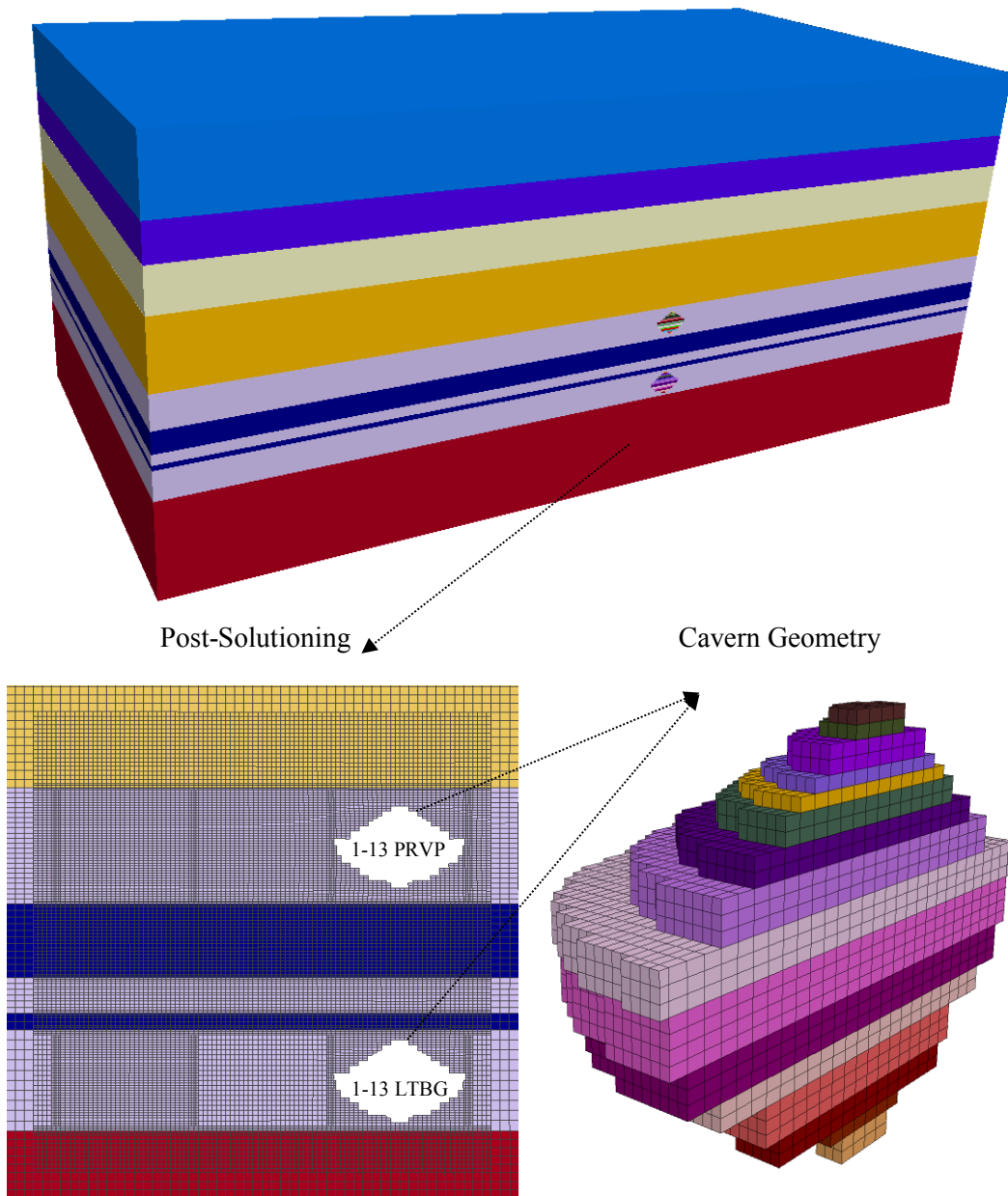


Figure 5.23 Three-Dimensional Finite Difference Model of *Cavern 1-13 LTBG & PRVP*

#### 5.4.2 Results and Conclusions

The development of deviatoric stresses, distributions of *DSR* values and *SSR* values at the site during the creation, operation, and abandonment of the two vertical 1-13 well caverns under dense-brine case of most interest and are provided in Figure 5.24, Figure 5.25 and Figure 5.26 respectively. Due to the fact that the cavern 1-13 LTBG fluid pressure relieve the compressive stresses caused by the geological loads acting on the strata, the highest potential for nonsalt shear failure will initialize within the Ernestina Lake Formation some distance away from the cavern maximum edge. With the development of uphole Prairie Evaporite cavern, the deviatoric stresses of the underlying strata decreased thus its shear potential was reduced. Moreover, the excavation and fluid injection of the Cavern 1-13 PRVP results in the horizontal extension of the shear potential zone within the Ernestina Lake units surrounding the downhole cavern where the deviatoric stresses increases. However, the maximum deviatoric stresses decrease so that the minimum *SSR* value grows from 3.21 to 3.57 during the development of the uphole cavern. Within the same operational period, the salt dilation of lower cavern edge decayed with time due to decreasing deviatoric stresses and the most dilation potential area moved to the outer edge of the uphole cavern with *DSR* value equal to 1.79. The dilation potential of all salt units slightly diminishes during the permanent abandonment of both caverns as it creeps. In addition, the shear failure potential of non-salt overlying and underlying strata decreases.

The change in values of *DSR* and *SSR* with simulation time for the two vertical caverns under all considered cases is presented in Figure 5.27. It is expected that the potential of salt dilation under dense-dense case is the least among three different cases. The figure indicates that the minimum *DSR* value of the dense-brine case remains similar for the value of both caverns filled with saturated brine. This is because the maximum salt

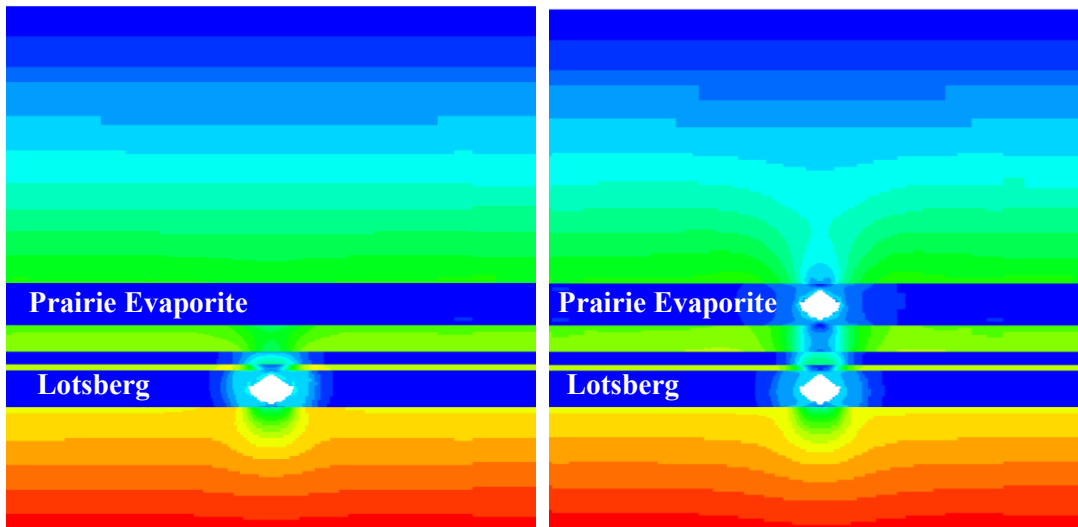
dilation potential always happens surrounding the salt cavern held at brine pressure. Additionally, the *SSR* plots over simulation time show an interesting trend in the case of asymmetrical injection situation (Cavern 1-13 LTBG with dense disposal and Cavern 1-13 PRVP with brine) tend to have the least shear failure potential within the Ernestina Lake than any of the other symmetrical injection cases. This is due to the unique anisotropic initial in-situ stress distributions assigned onto the site, and the brine pressure of the uphole cavern reduced the deviatoric stresses within the most potential shear layers. All the predicted values in Figure 5.27 remain above 1 during simulations, indicating no salt dilation or non-salt shear failure is expected for the two vertical adjacent caverns. Additionally, the greatest shear failure potential always stays symmetrically of the caverns within the Ernestina Lake Formation, and the solution mining of uphole cavern has little influence on this potential shear zone.

The predicted cavern closures as a function of time was drawn in Figure 5.28. The given curves verify that the cavern internal pressure itself only influences the cavern closure. The closure ratio of uphole cavern held at brine pressure is predicted to reach approximately 15.6% at the end of simulation, and this number will drop dramatically to about 7.5% when the internal pressure is raised to dense sands support pressure. The closure rate of the uphole cavern is significantly larger than the downhole cavern closure, because the steady state creep rate for the Prairie Evaporite salt is higher than the Lotsberg salt.

The simulated theoretical accumulated casing strains in *FLAC*<sup>3D</sup> numerical modeling for both caverns at dense-brine state are illustrated in Figure 5.29. It can be seen that the casing strains of the uphole cavern bottom increased noticeably from 0.00185 to 0.00548 during the 50-year creep simulation. This is because the Cold Lake salt tends to flow into the uphole cavern, where larger salt deviatoric stresses and cavern closure exist, and then

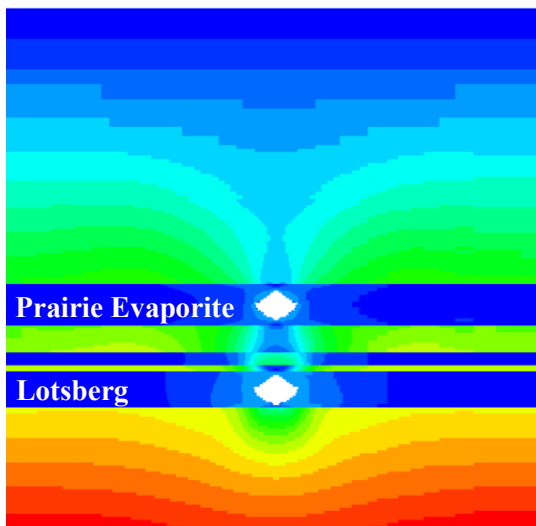
drag the upper part of the Cavern 1-13 LTBG casing significantly. Due to the upward flow of the overlying rock, the strains of downhole casing shoes decreased mildly during the permanent abandonment. As suggested that if J-55 grade steel casing is used for all the disposal salt caverns, the casing will begin to yield at a strain of 0.0018 with ultimate failure occurring at 0.0025 strain, the casing of Cavern 1-13 LTBG is predicted to yield following the uphole cavern development and failure of the casing is expected to occur within the 50-year abandonment. Figure 5.30 represents the case comparison in terms of predicted casing strains for Cavern 1-13 LTBG&PRVP. The casing conditions turn out to be reasonably for both waste-filled uphole and downhole caverns. As long as the disposal cavern in Prairie Evaporite salt is held at brine pressure, casing failure is predicted to occur for the downhole salt caverns.

The predicted maximum surface subsidence plots for cavern injection cases comparison were shown in Figure 5.31. When the uphole cavern is brine-filled, the simulated maximum surface vertical subsidence exceeds 0.08 m around the center of the cavern field, which is only half the suggested subsidence value of 0.15 m by Van Sambeek (2000). Also the surface subsidence will be significantly reduced to 0.046 m by injecting the dense waste disposal into the uphole Prairie Evaporite cavern.



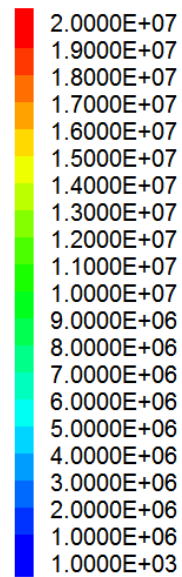
Following Cavern 1-13 LTBG development (Time = 10 years)

Following Cavern 1-13 PRVP development (Time = 20 years)



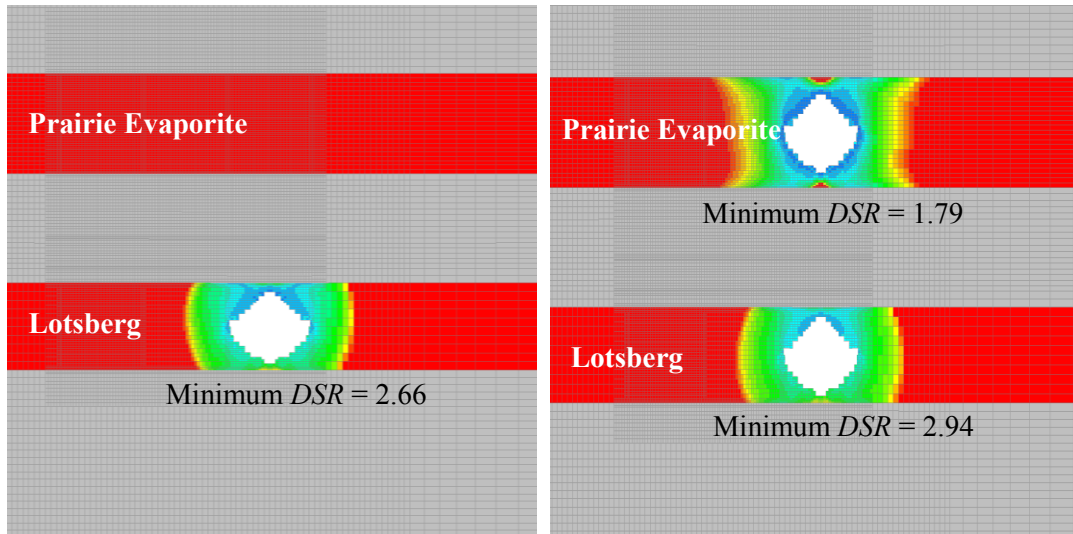
End of Simulation (Time = 70 years)

Legend of Deviatoric Stress (Pa)



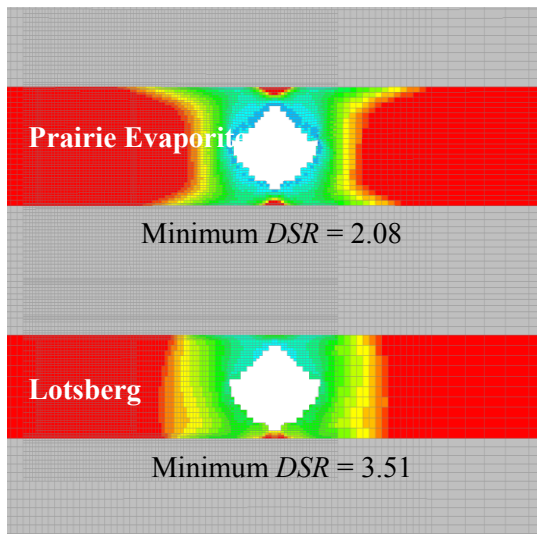
1-13 LTBG & PRVP dense-brine

Figure 5.24 Contour of Deviatoric Stresses Surrounding *Cavern 1-13 LTBG & PRVP*



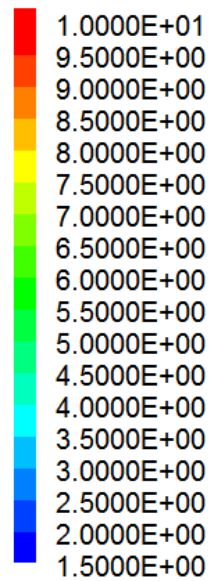
Following Cavern 1-13 LTBG development (Time = 10 years)

Following Cavern 1-13 PRVP development (Time = 20 years)



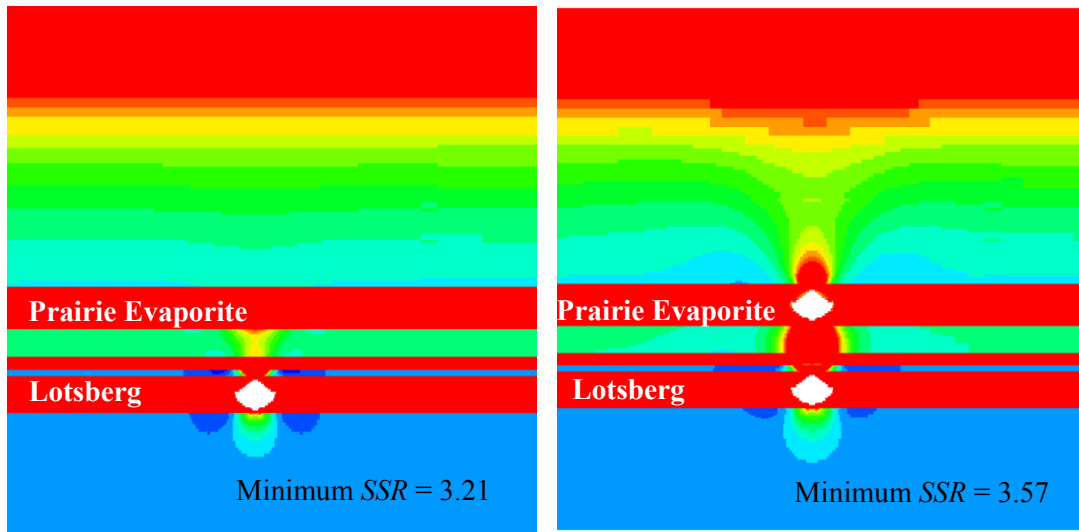
End of Simulation (Time = 70 years)

Legend of  $DSR$  Value



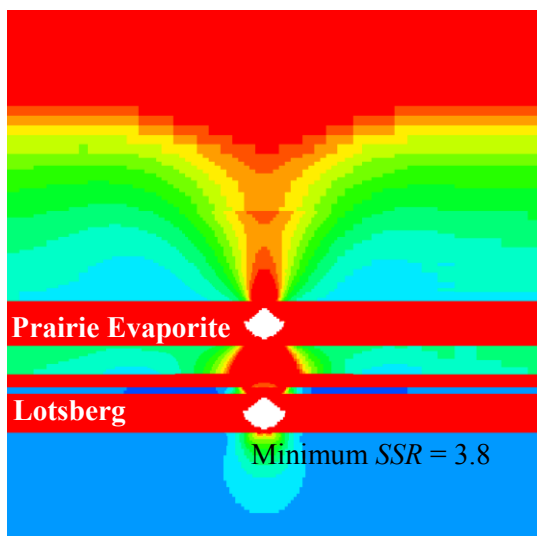
1-13 LTBG & PRVP dense-brine

Figure 5.25  $DSR$  Value Distributions Surrounding *Cavern 1-13 LTBG & PRVP*



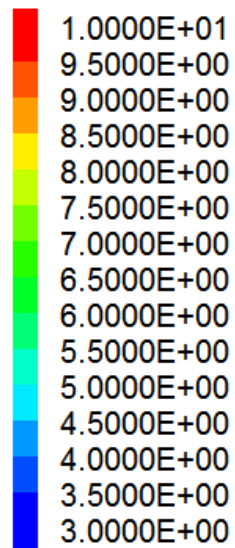
Following Cavern 1-13 LTBG development (Time = 10 years)

Following Cavern 1-13 PRVP development (Time = 20 years)



End of Simulation (Time = 70 years)

Legend of SSR Value



1-13 LTBG & PRVP dense-brine

Figure 5.26 SSR Value Distributions Surrounding *Cavern 1-13 LTBG & PRVP*

**1-13 LTBG&PRVP  
Cases VS.**

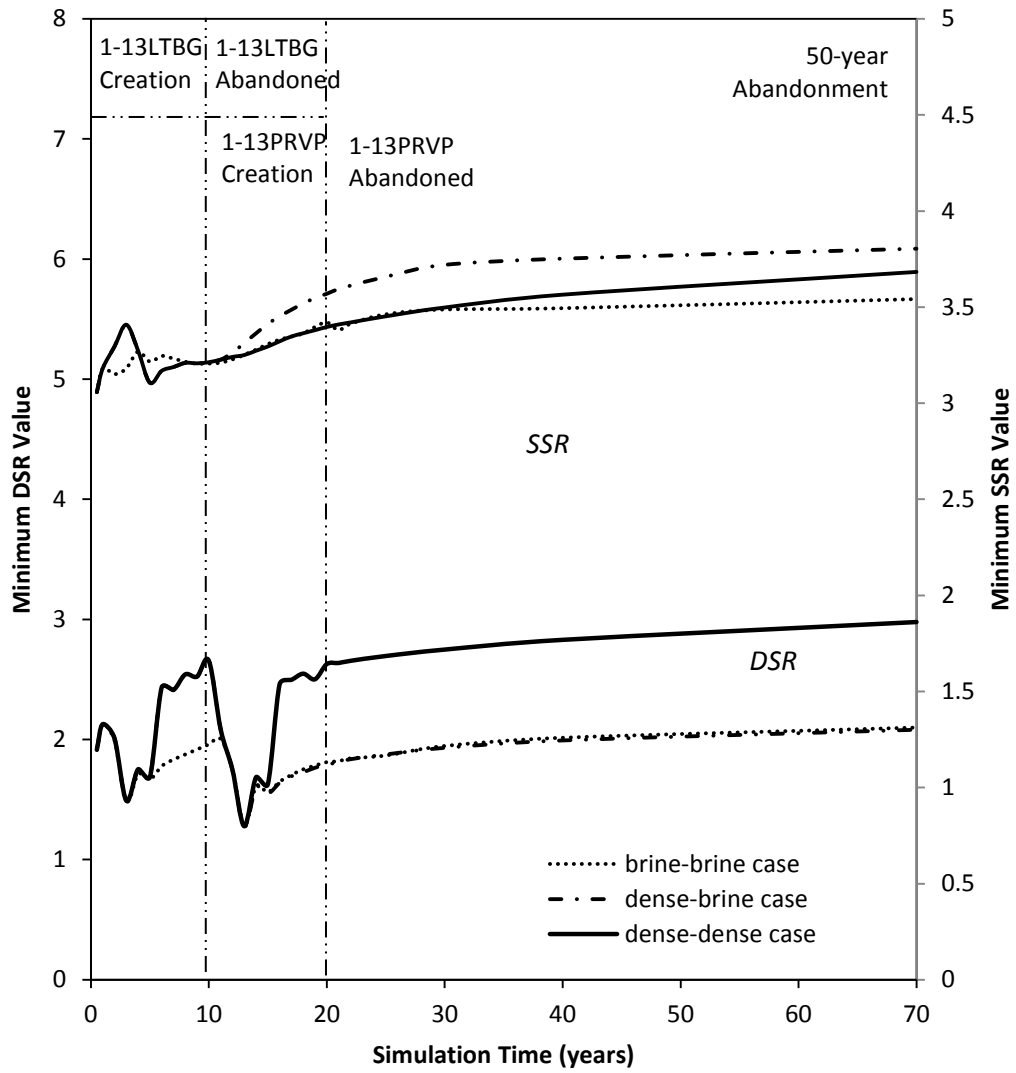


Figure 5.27 DSR and SSR Value Varied with Simulation Time (*Cavern 1-13 LTBG & PRVP*)

**1-13 LTBG&PRVP  
Cases VS.**

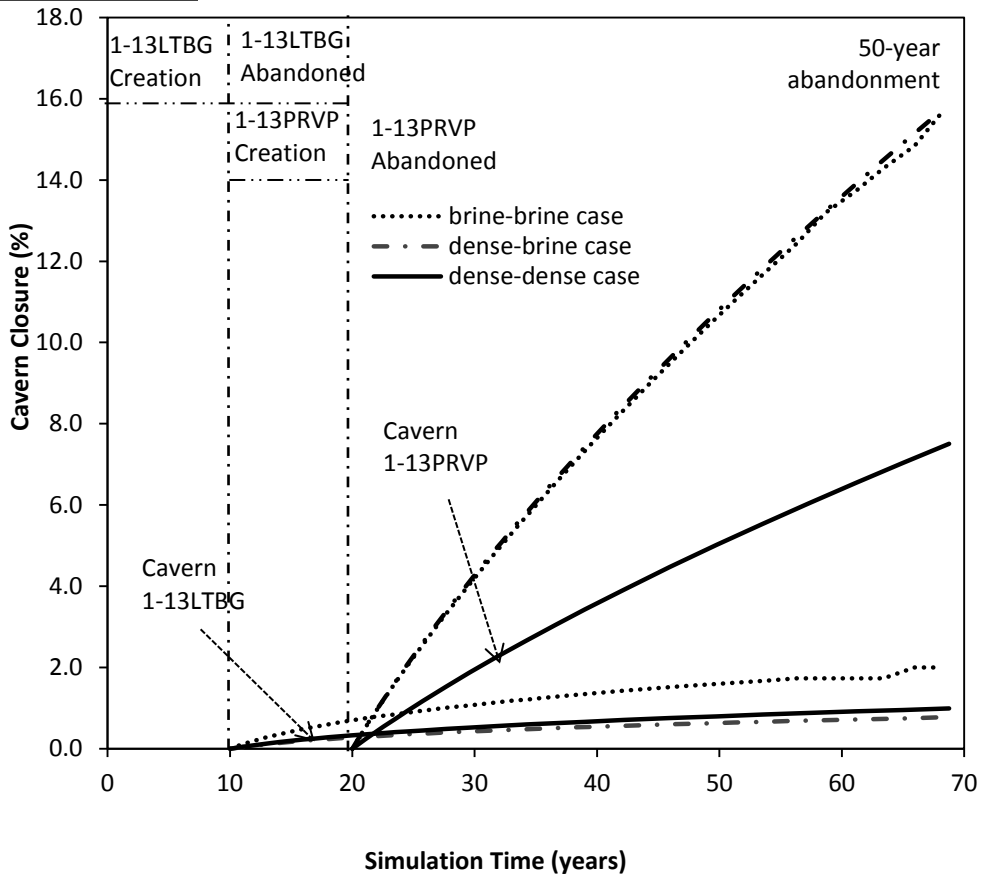


Figure 5.28 Predicted Caverns Closure as a Function of Time (1-13 LTBG & PRVP)

**1-13 LTBG&PRVP  
dense-brine case**

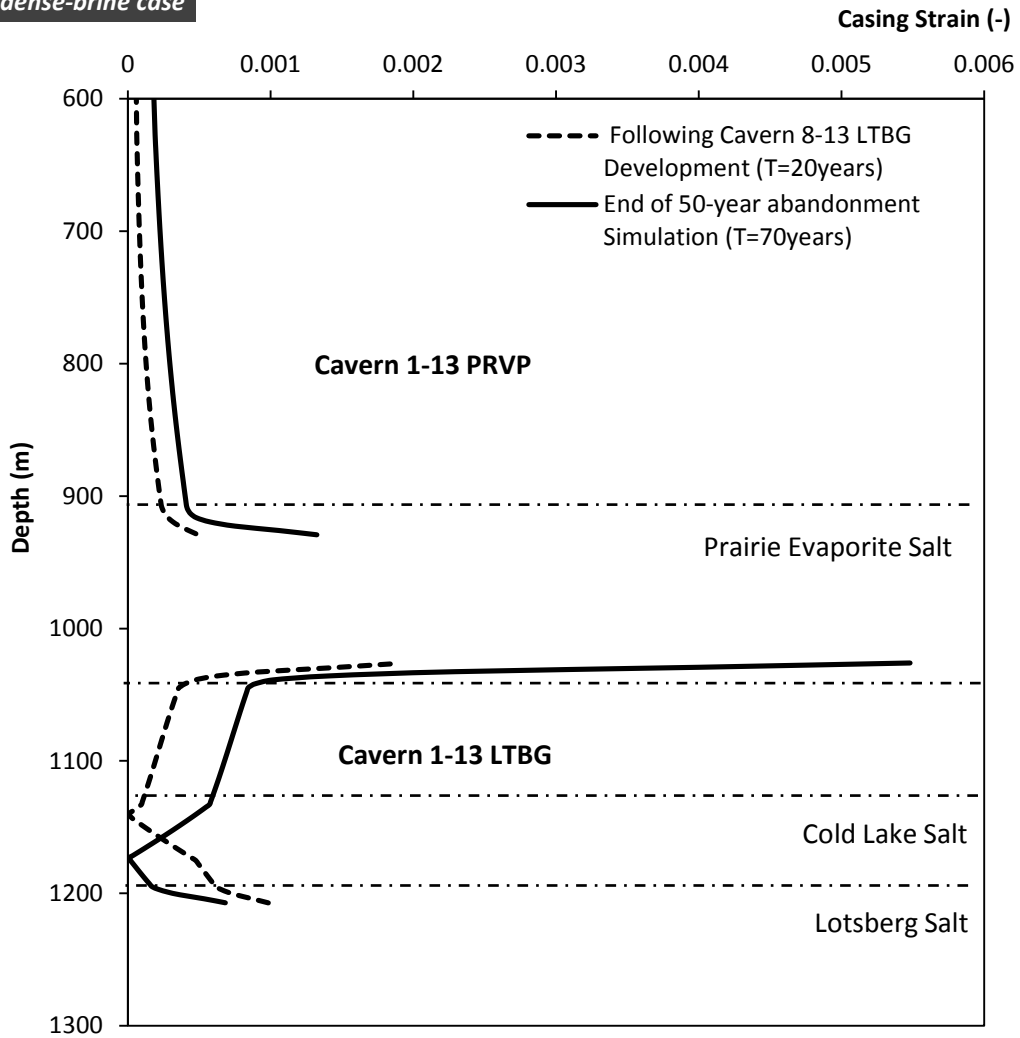


Figure 5.29 Accumulated Casing Strains during Simulation for Cavern 1-13 LTBG and Cavern 1-13 PRVP (*1-13 LTBG & PRVP dense-brine*)

**1-13 LTBG&PRVP  
Cases VS.**

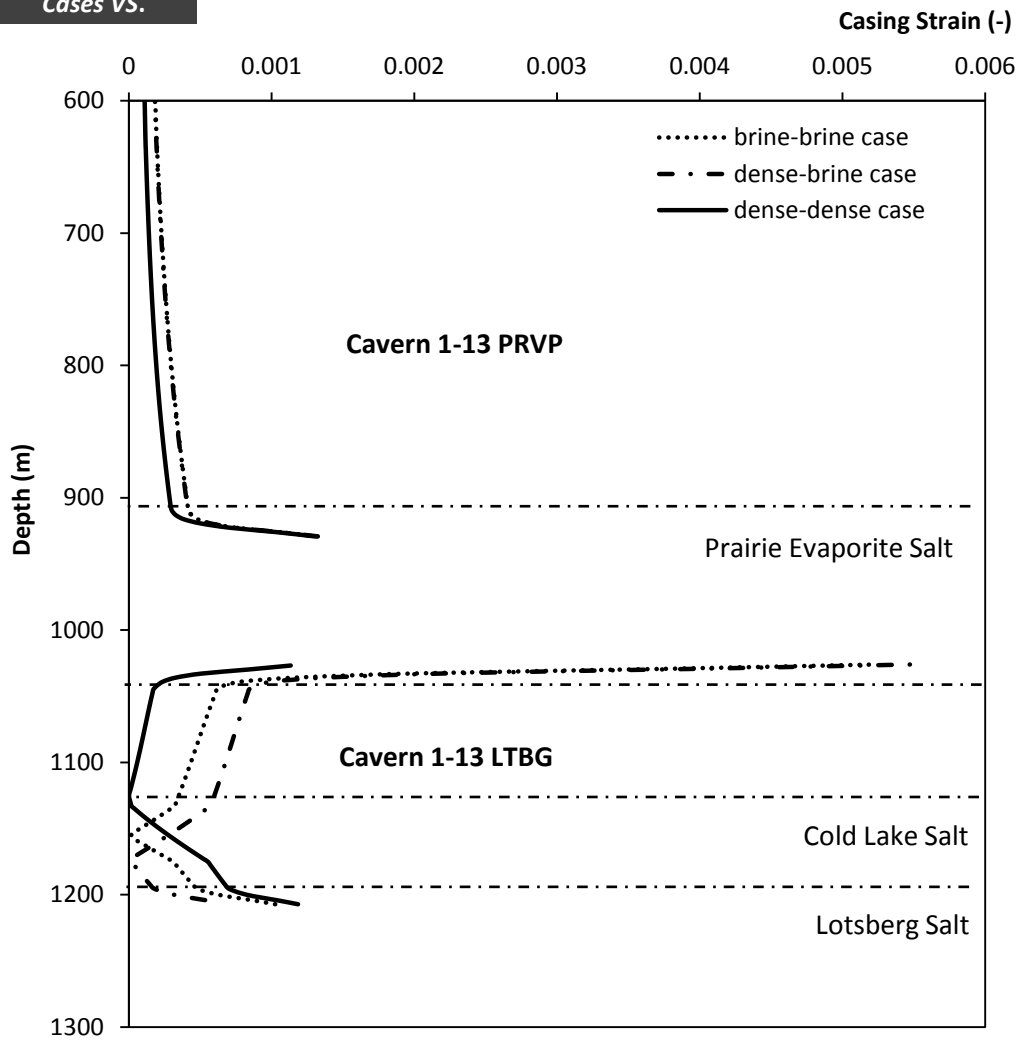


Figure 5.30 Accumulated Casing Strains during Simulation for Cavern 1-13 LTBG and Cavern 1-13 PRVP (*1-13 LTBG & PRVP*)

**1-13 LTBG&PRVP  
Cases VS.**

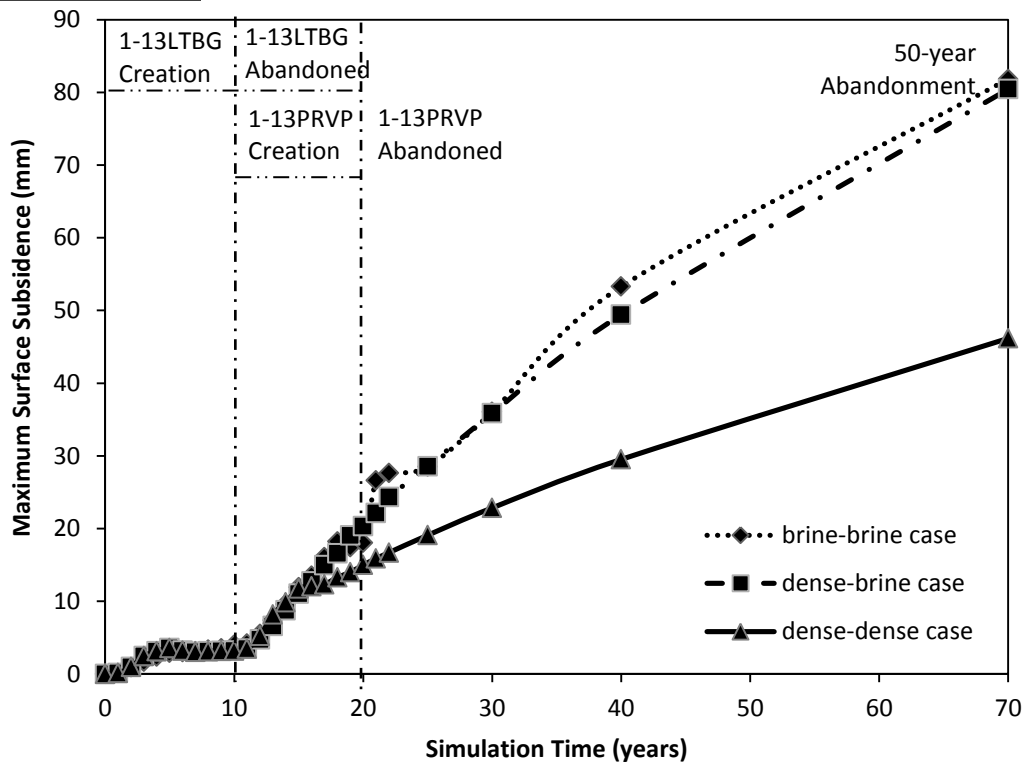


Figure 5.31 Predicted Maximum Surface Subsidence over Time (*1-13 LTBG & PRVP*)

## **5.5 Long-term Abandonment Behavior Simulation of Full Development of Lotsberg and Prairie Evaporite Caverns**

### **5.5.1 Long-term Abandonment Behavior Considering Sequential Excavations**

It was initially planned to solution mine two downhole Lotsberg salt caverns and then two vertical uphole disposal caverns in the Prairie Evaporite. This combination of four caverns is seldom designed and practiced in georeservoir engineering, thus no former experience can be consulted and studied. In this section, the sequential excavations and 50-year permanent abandonment simulation scenario of two horizontal Lotsberg caverns and two vertical 1-13 well caverns case will be repeated for the three-dimensional difference finite program for the complete development of Lotsberg and Prairie Evaporite salt caverns. Four difference combinations of cavern injection conditions as listed in Table 3.7 were simulated and compared, including three symmetrical injection conditions and one asymmetrical injection condition. The asymmetrical case consists of caverns along one diagonal line filled with saturated brine while the caverns aligned on the other diagonal line injected with dense waste disposal, which is notated as *1-13 & 8-13 LTBG & PRVP dense-brine-brine-dense* case. The full development of all the four target caverns will be planned to finish at the end of year 2045 according to sequential excavations and then a 50-year abandonment simulation will be conducted in the FLAC<sup>3D</sup> numerical modelling. The total creep simulation time will be 90 years in FLAC<sup>3D</sup>. The schedules of all the four analyzed cases were provided in Figures C.10 to Figure C.12 in Appendix C. Figure 5.32 illustrates the three-dimensional finite difference models of four caverns along with the cavern geometry.

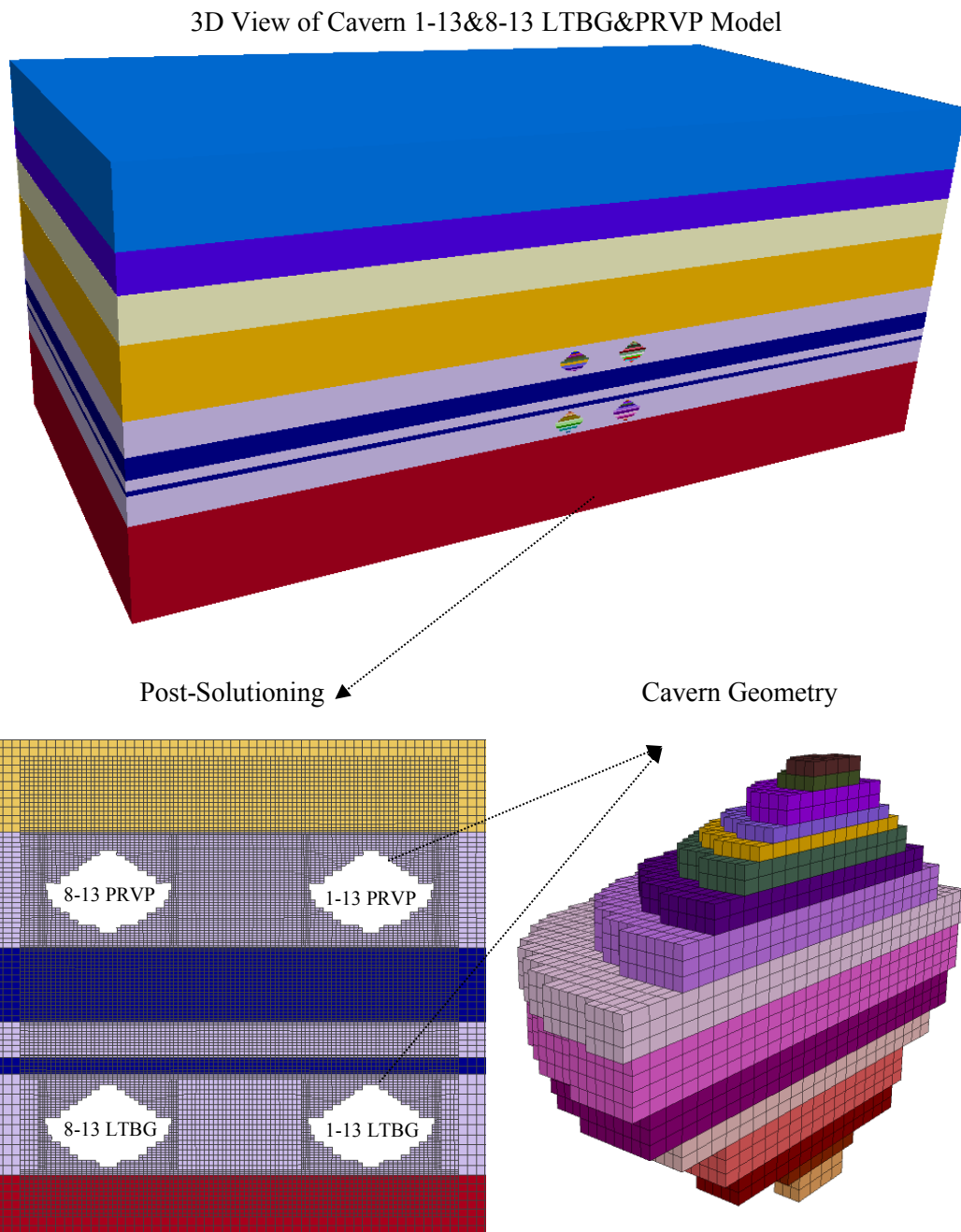


Figure 5.32 Three-Dimensional Finite Difference Model of *Cavern 1-13&8-13 LTBG&PRVP*

## 5.5.2 Results and Conclusions

The caverns of asymmetrical injection conditions are of most research interest because of their unpredictable long-term geomechanical behavior, as compared with other symmetrical cases. Figure 5.33, Figure 5.34 and Figure 5.35 demonstrates the deviatoric stresses, *DSR* values and *SSR* values contours evolution during the cavern development, operation, and abandonment of the asymmetrical case respectively. As shown, the deviatoric stresses generated on the upper-dense cavern side are higher than the upper-brine cavern side at the end of simulation at this project site assigned specific in-situ stresses. Thus, the most potential of non-salt shear failure is initially expected to occur on the centre of the four caverns within the Ernestina Lake Formation prior to the introduction of 8-13 PRVP cavern. Following the full development of all caverns the most potential shear failure will align symmetrically along the lower brine-filled 8-13 LTBG cavern within the Ernestina Lake units, as well as the underlying formation which needs to be paid attention due to the large area of low *SSR* value along the diagonal line. However, this potential of failure diminishes with time due to the salt flow induced decreasing deviatoric stress of the nonsalt strata. The greatest potential for salt dilation is always predicted on the outer edge of the newly abandoned brine-filled caverns. The last excavated 8-13 PRVP cavern shows very low potential of salt dilation, and the high dilation zone within the Prairie Evaporite Formation diminishes during permanent abandonment. On the contrary, the potential salt dilation of the Lotsberg salt on the left of the lower brine-filled 8-13 LTBG Cavern shows a trend of expansion resulting from the decreasing deviatoric stresses. Figure 5.36 depicts the minimum *DSR* and *SSR* values observed of all geological units during simulations varied with time for cases comparison. No salt dilation or non-salt shear failure is predicated during the simulation time. The potential of nonsalt shear failure increases dramatically due to the solution mining of

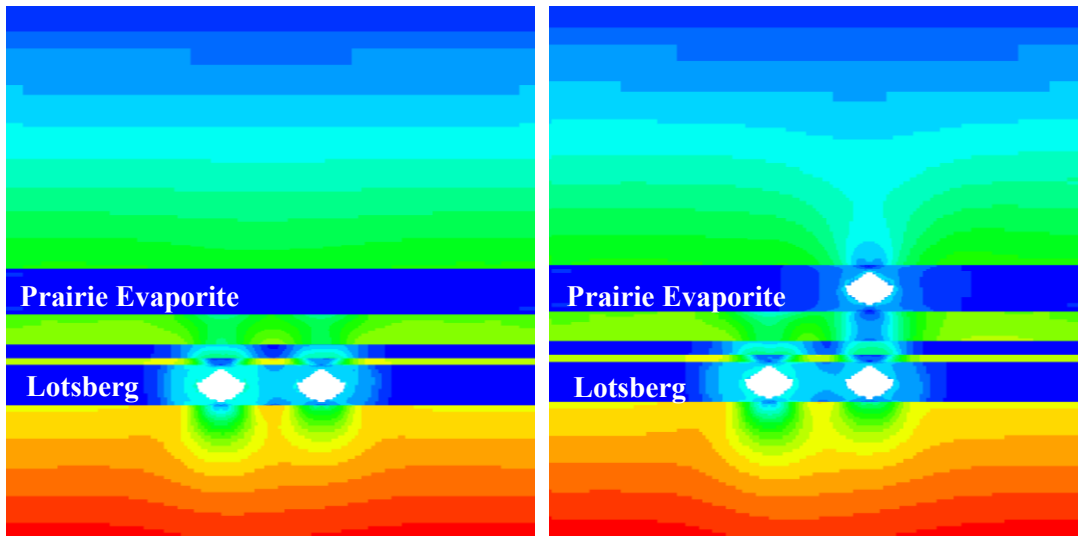
brine-filled horizontal Lotsberg cavern along with the decreasing *SSR* value, and then reduces slightly during the development of uphole Prairie Evaporite caverns. The separate *DSR* value of each cavern during the 90-year creep simulation is shown in Figure 5.37, and it indicates that the salt dilation potential along the cavern edge of each cavern during the cavern creation is mainly determined by its internal pressures and will be influenced at a certain level by the excavations of horizontal adjacent caverns. However, the ultimate potential of salt dilation is largely and significantly dominated by the injection conditions of the cavern itself, no matter the cavern internal pressure situations of the pre-existing surrounding salt caverns.

Figure 5.38 gives the predicted cavern closure for each cavern as a function of simulation time under all injection situations. The uphole Prairie Evaporite caverns shrinks remarkably more than the lower Lotsberg caverns due to higher steady state creep rate. The suggested conclusion that the cavern closure is totally determined by the cavern internal pressure itself is verified again. The final closure of the uphole brine caverns at the end of 90-year simulation exceeds 18% and it will drop approximately to half of the value when the internal pressure increases to the dense sands support pressure. The shrinkage rate of downhole Lotsberg caverns is within 2% even under brine-filled conditions due to small steady state creep rate.

The predicted accumulated casing strains of each cavern under asymmetrical injection conditions are depicted in Figure 5.39 and Figure 5.40. On the side of upper-dense and lower-brine caverns, all the maximum casing strains are at the similar level and within the casing yield limit of value of 0.0018. However, on the other side of upper-brine and lower-dense side, the maximum of the Cavern 1-13 LTBG casing strains will exceed the casing failure limit of 0.0025 value. This is due to the much higher creep rate and cavern closure rate of the Prairie Evaporite units. If the PRVP cavern is injected with dense solid

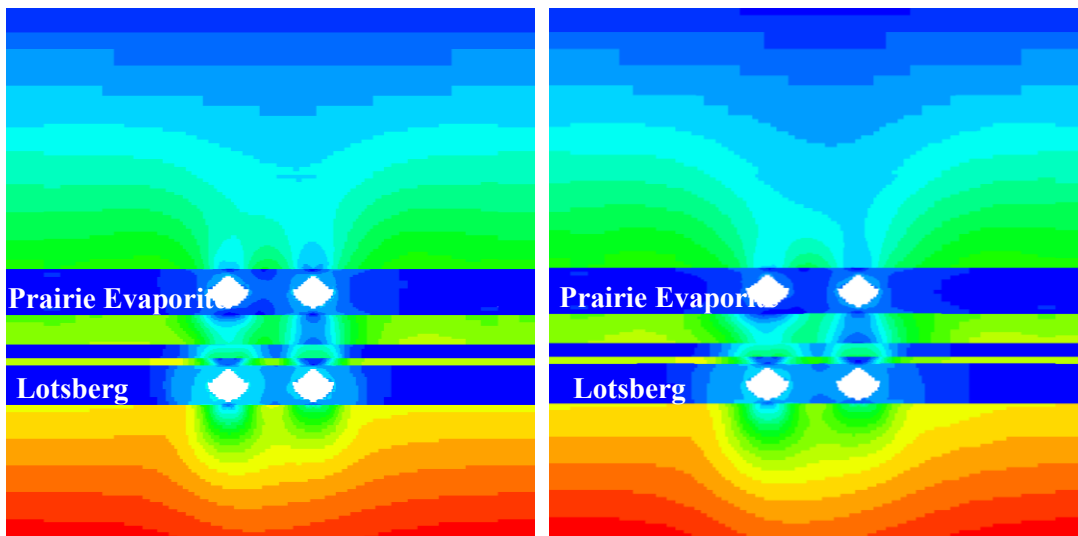
waste, the cavern shrinkage will slow down due to high cavern support pressure and then the casing dragging will be reduced as compared to the brine-filled case. Figure 5.41 and Figure 5.42 illustrates the casing strains for cases comparison. Only the case of caverns all filled with dense sands will ensure the casing strains remains within the yield limit and no casing tensile failure is predicted during the simulations.

The maximum surface subsidence plots for case comparison were provided in Figure 5.43. The cases of two uphole caverns filled with saturated brine will generate more than 0.15 m elevation change of the ground surface at site, resulting in effects on the area drainage as suggested by Van Sambeek (2000). The surface subsidence rate estimated for the asymmetrical case will be approximately 1.5224 mm/year, thus it is expected to exceed 0.15 m about 9 years later. Even the all dense-filled cavern case has a surface subsidence growth rate of 0.9851 mm/year and will reach the threshold after another 55 years creep.



Following Cavern 8-13 LTBG development (Time = 20 years)

Following Cavern 1-13 PRVP development (Time = 30 years)



Following Cavern 8-13 PRVP development (Time = 40 years)

End of Simulation (Time = 90 years)

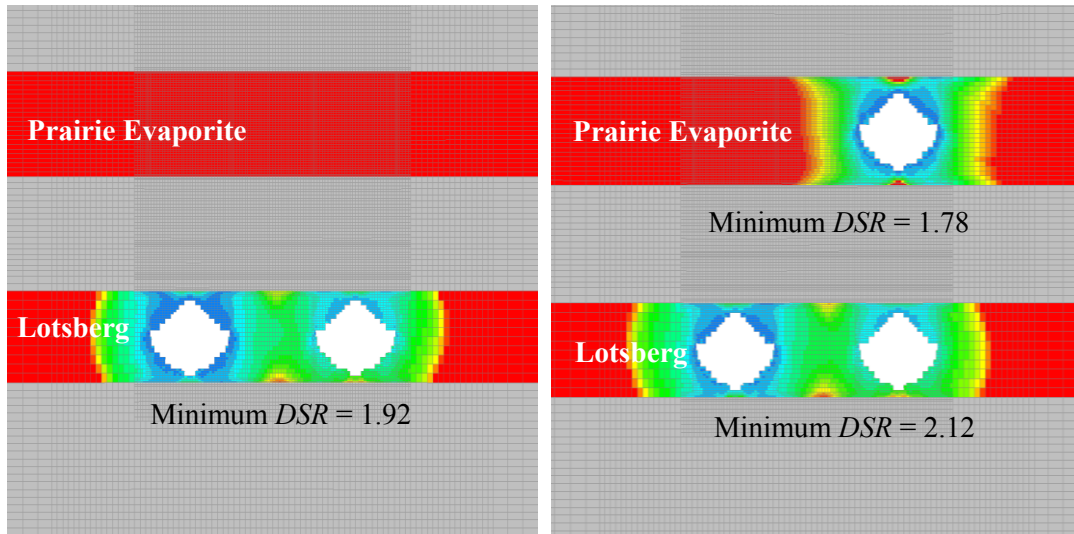
1-13&8-13 LTBG&PRVP  
dense-brine-brine-dense

Legend of  
Deviatoric  
Stress  
(Pa)



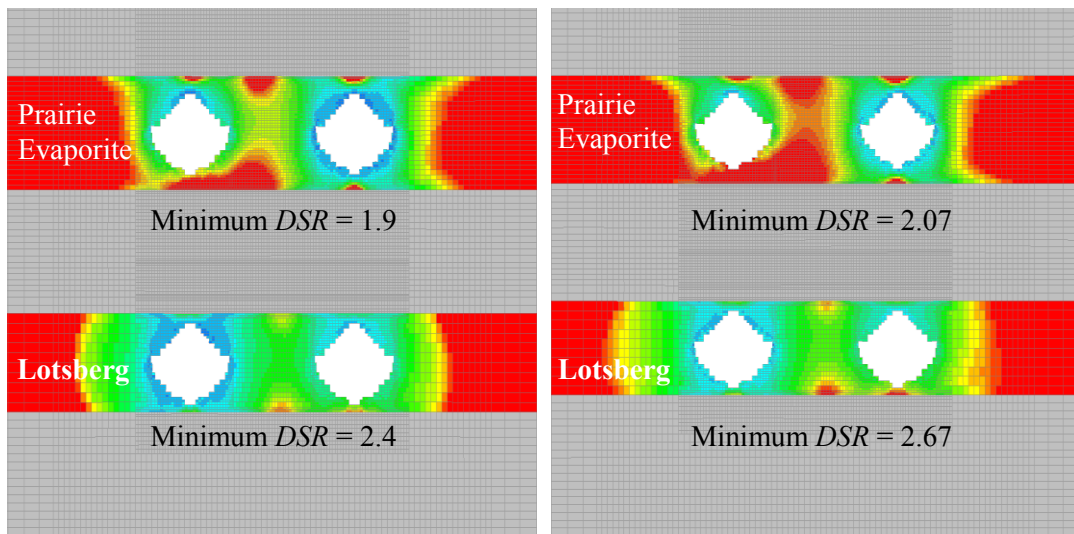
Figure 5.33 Contour of Deviatoric Stresses Surrounding *Cavern 1-13&8-13*

***LTBG&PRVP***



Following Cavern 8-13 LTBG development (Time = 20 years)

Following Cavern 1-13 PRVP development (Time = 30 years)



Following Cavern 8-13 PRVP development (Time = 40 years)

End of Simulation (Time = 90 years)

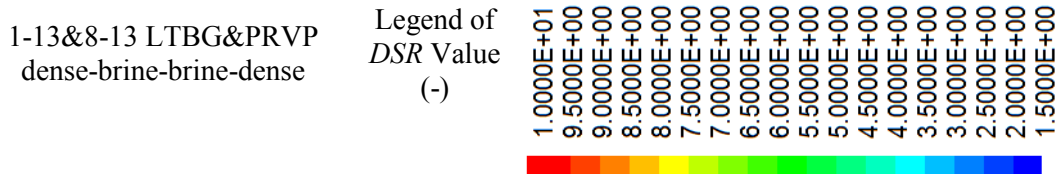


Figure 5.34 DSR Value Distributions Surrounding *Cavern 1-13&8-13 LTBG&PRVP*

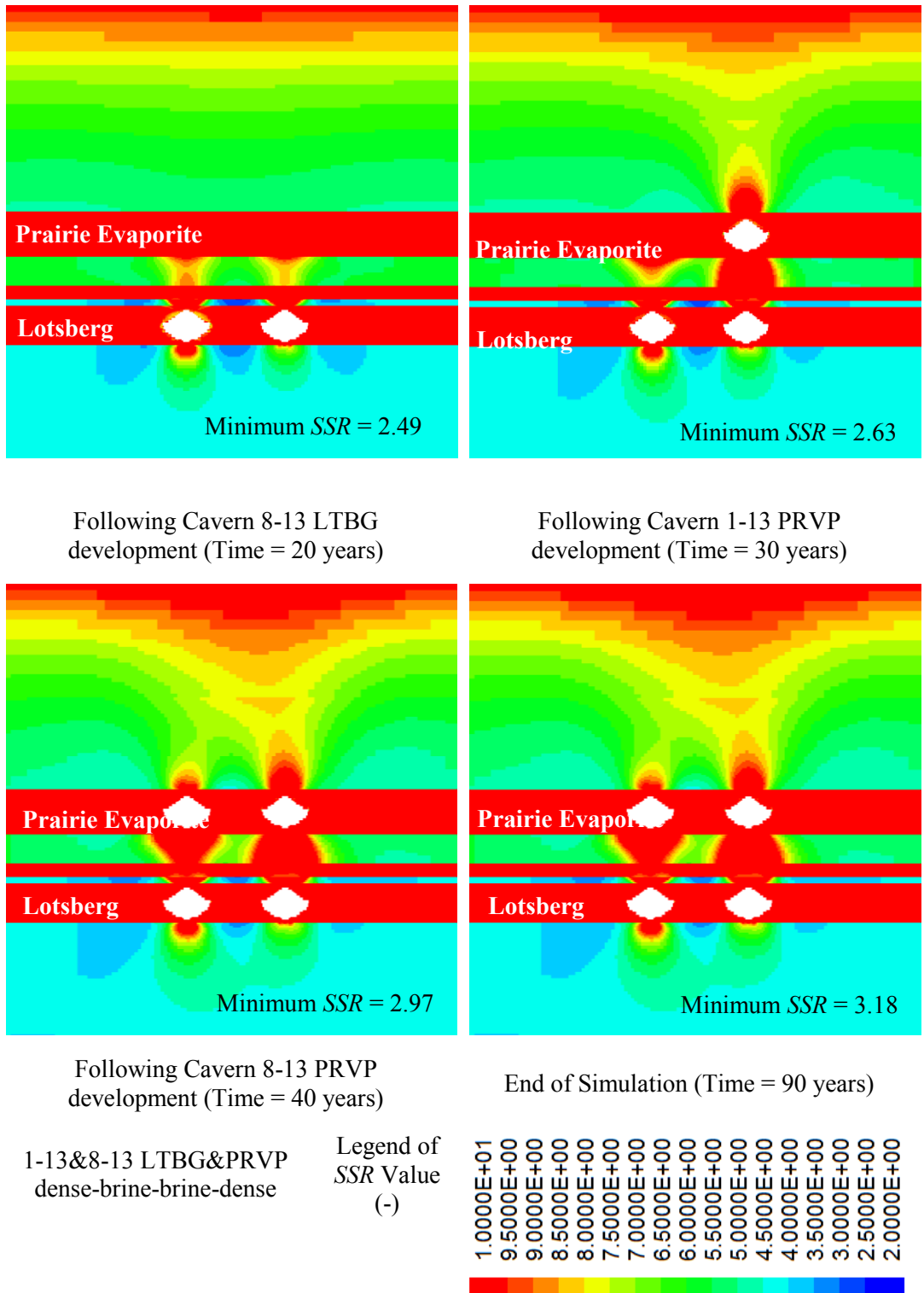


Figure 5.35 SSR Value Distributions Surrounding *Cavern 1-13&8-13 LTBG&PRVP*

**1-13&8-13 LTBG&PRVP  
Cases VS.**

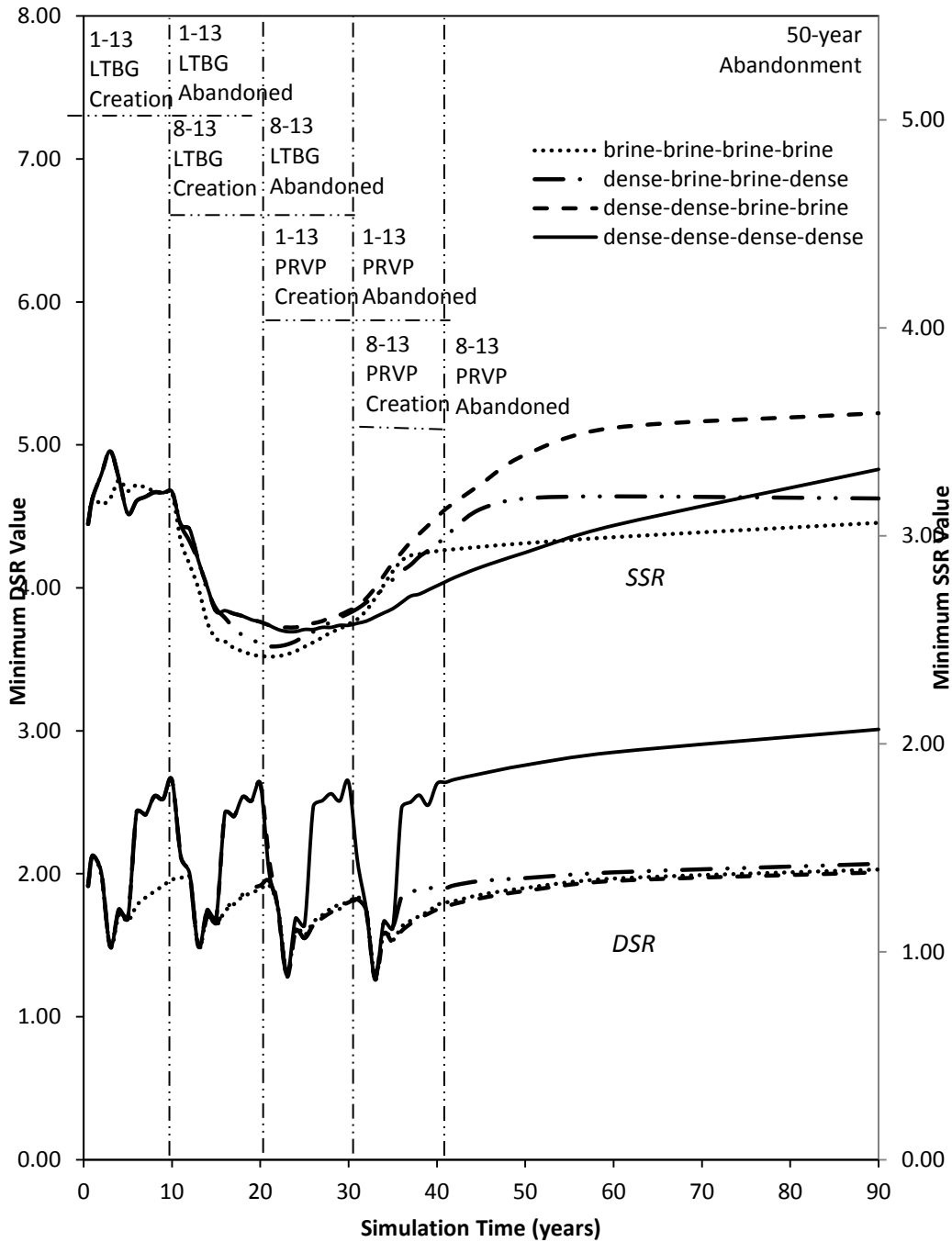


Figure 5.36 Minimum *DSR* and *SSR* Value Varied with Simulation Time (*Cavern 1-13&8-13 LTBG&PRVP*)

**1-13&8-13 LTBG&PRVP  
Cases VS.**

Green -> brine-brine-brine-brine  
 Blue -> dense-brine-brine-dense  
 Red -> dense-dense-brine-brine  
 Black -> dense-dense-dense-dense

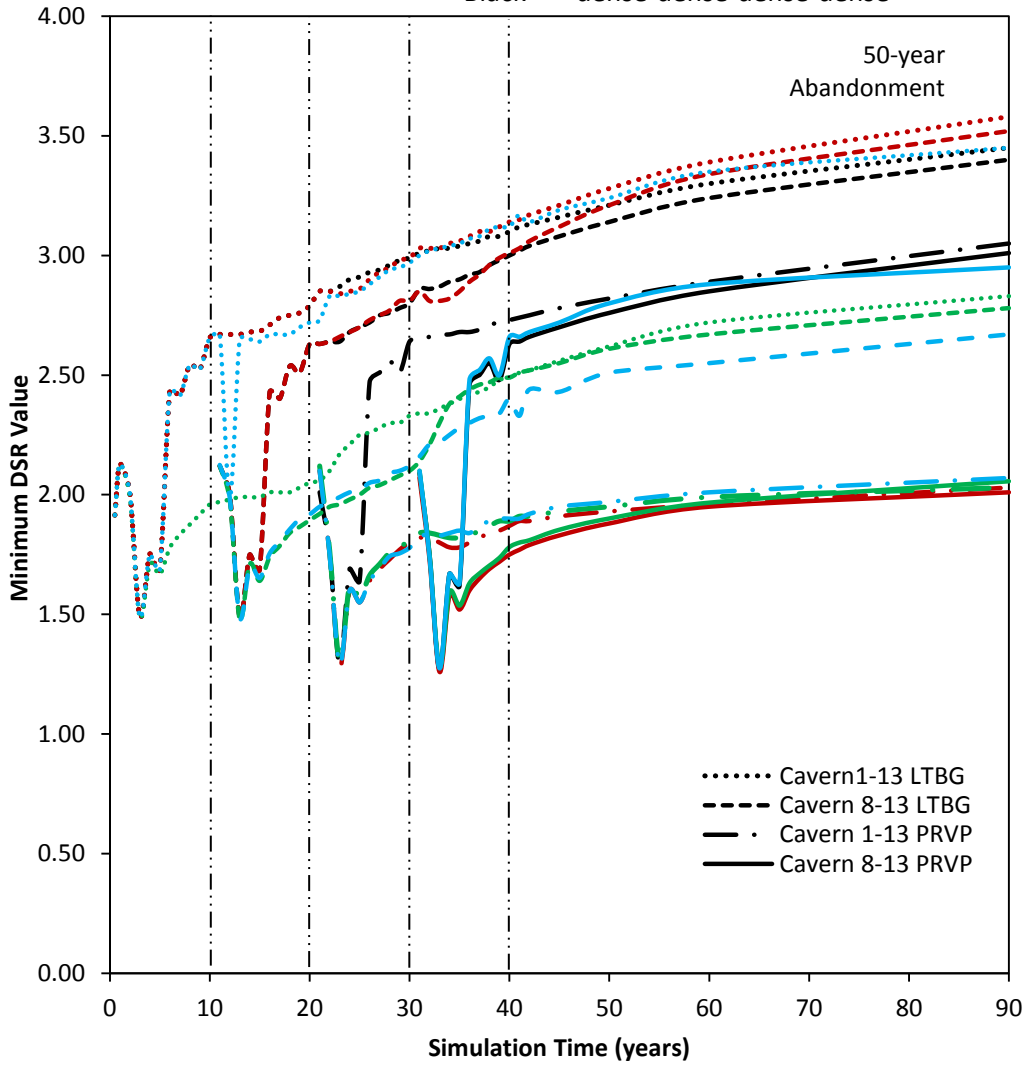


Figure 5.37 DSR Value Evolution of Each Cavern during Simulation (*1-13&8-13 LTBG&PRVP*)

**1-13&8-13LTBG&PRVP  
Cases VS.**

Green -> brine-brine-brine-brine  
 Blue -> dense-brine-brine-dense  
 Red -> dense-dense-brine-brine  
 Black -> dense-dense-dense-dense

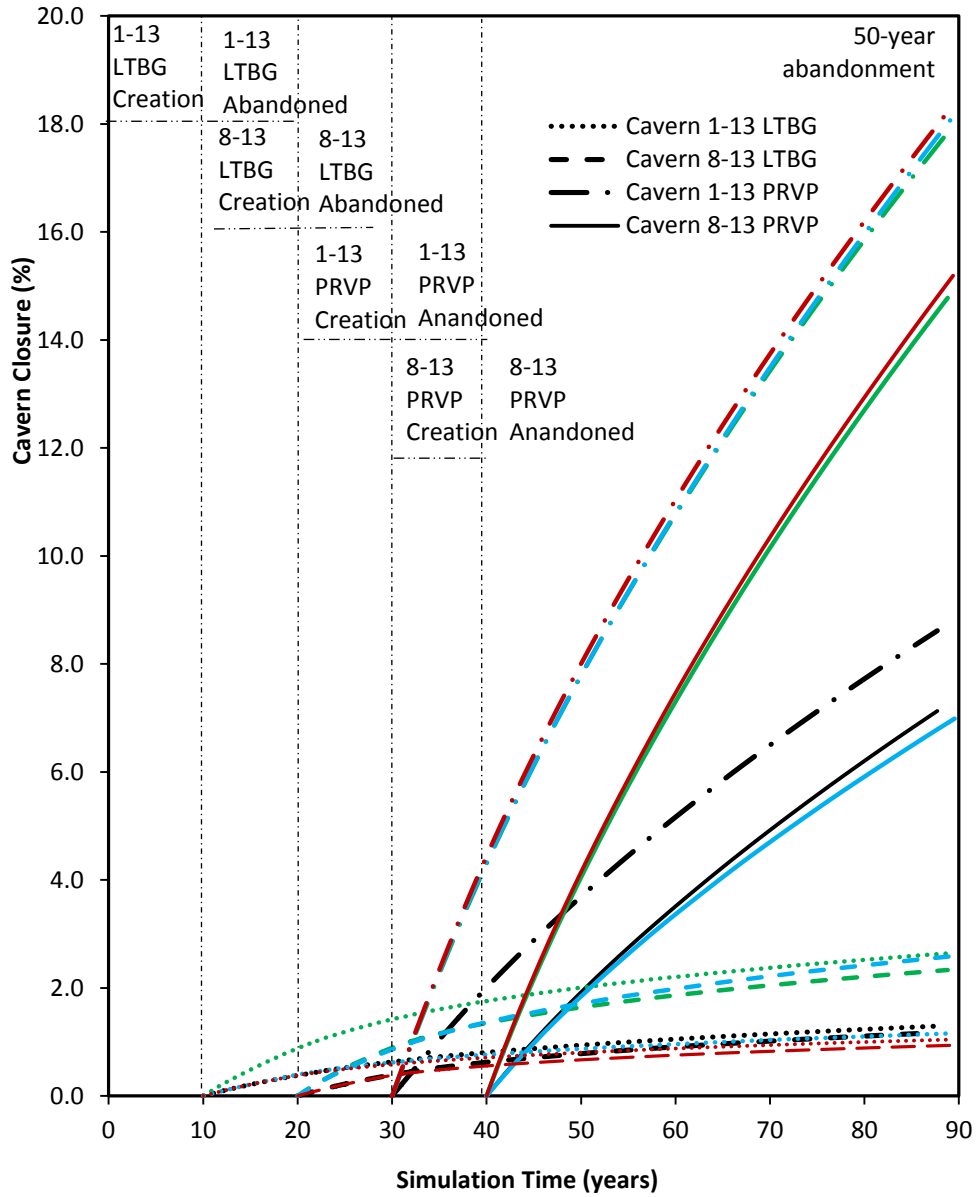


Figure 5.38 Predicted Caverns Closure as a Function of Time (*1-13&8-13  
LTBG&PRVP*)

**1-13&8-13 LTBG&PRVP**  
*dense-brine-brine-dense*

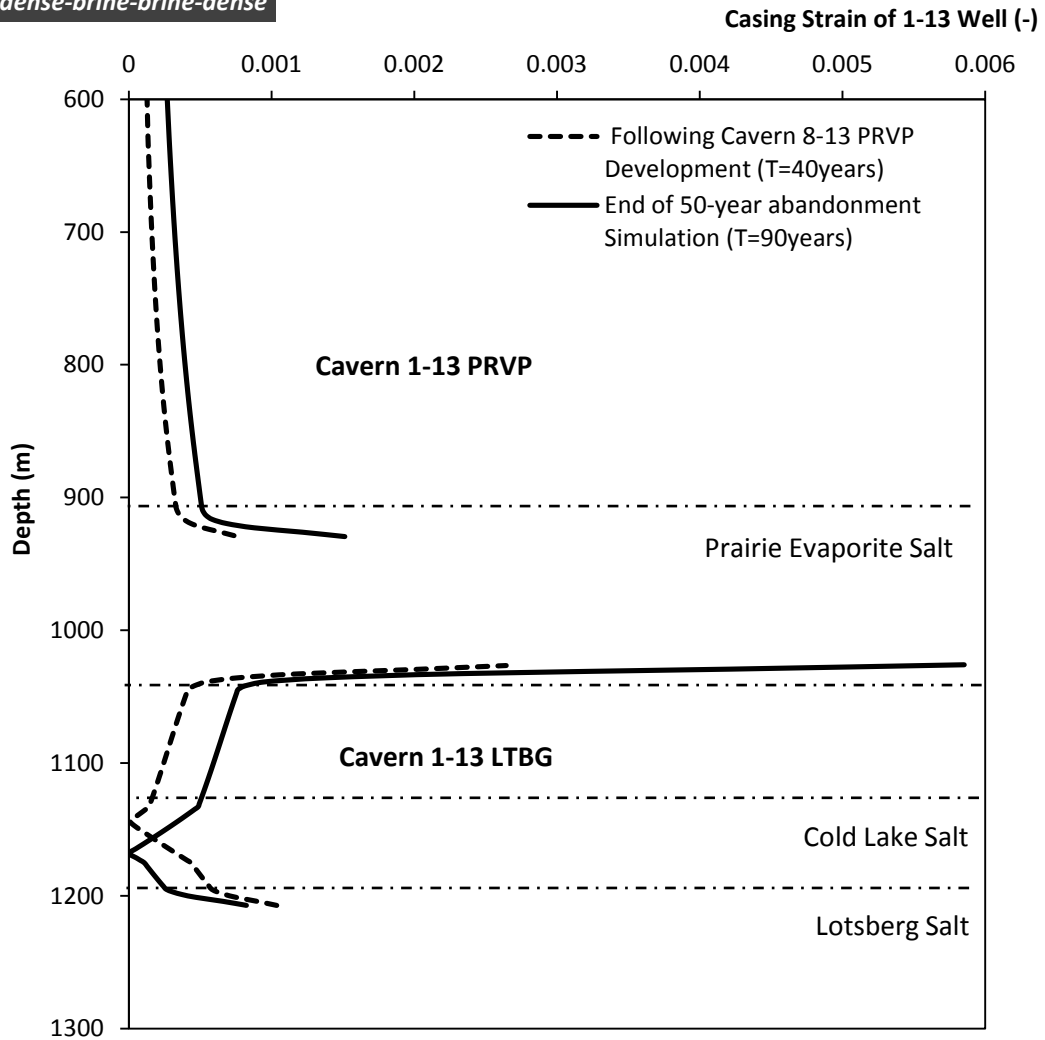


Figure 5.39 Accumulated Casing Strains during Simulation for Cavern 1-13 LTBG and Cavern 1-13 PRVP (*1-13 LTBG&PRVP dense-brine-brine-dense*)

**1-13&8-13 LTBG&PRVP**  
*dense-brine-brine-dense*

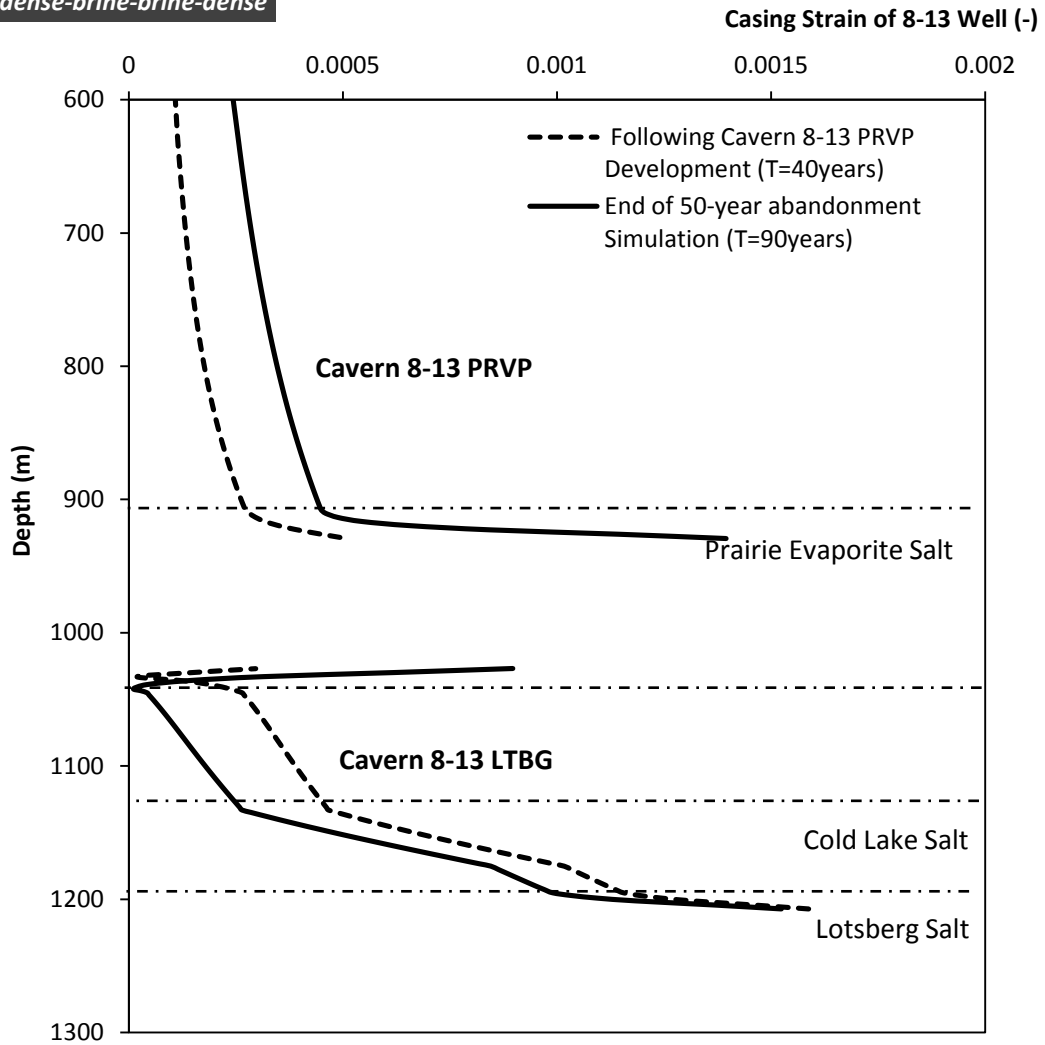


Figure 5.40 Accumulated Casing Strains during Simulation for Cavern 8-13 LTBG and Cavern 8-13 PRVP (*1-13 LTBG&PRVP dense- brine-brine-dense*)

**1-13&8-13 LTBG&PRVP  
Cases VS.**

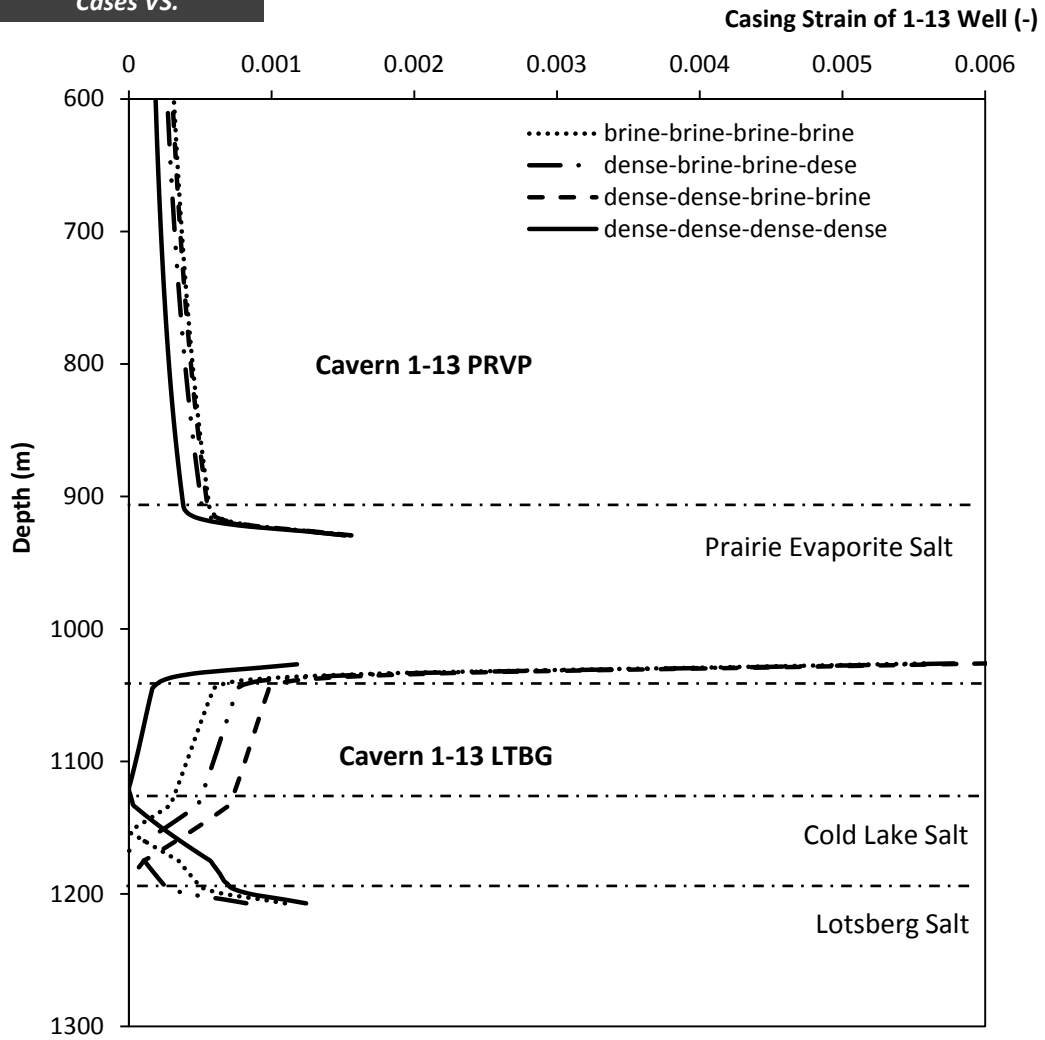


Figure 5.41 Accumulated Casing Strains during Simulation for 1-13 Well Caverns (*1-13&8-13 LTBG&PRVP*)

**1-13&8-13 LTBG&PRVP  
Cases VS.**

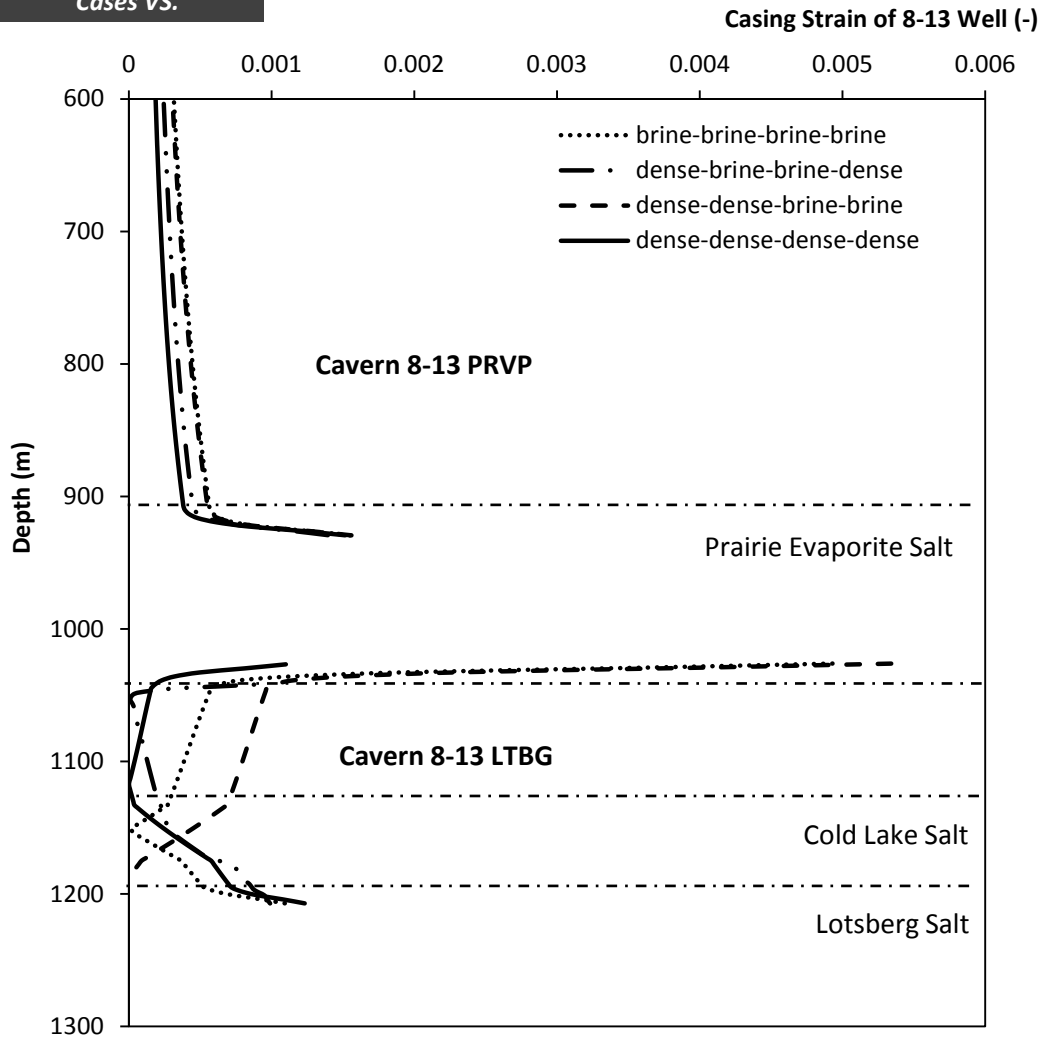


Figure 5.42 Accumulated Casing Strains during Simulation for 8-13 Well Caverns (*1-13&8-13 LTBG&PRVP*)

**1-13&8-13 LTBG&PRVP  
Cases VS.**

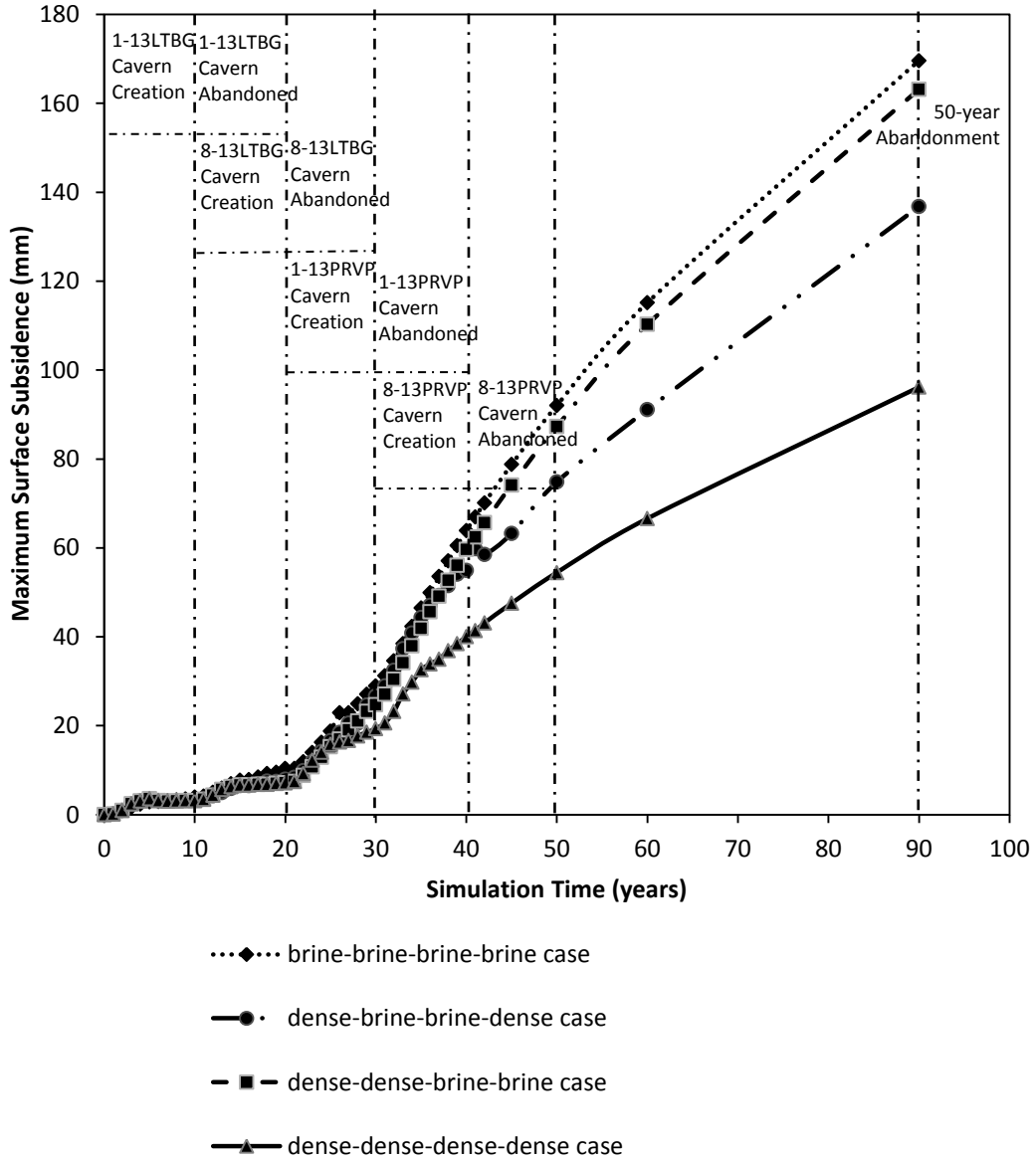


Figure 5.43 Predicted Maximum Surface Subsidence over Time (*1-13&8-13 LTBG&PRVP*)

## 5.6 Summary and Conclusions

A series of three-dimensional finite difference simulations were conducted in the FLAC<sup>3D</sup> numerical modeling studies to evaluate the geomechanical performance of solution-mined disposal salt caverns during development, operation and abandonment. The geomechanical assessment includes the structural stability and integrity analysis of the disposal caverns throughout the simulation, the cavern volumetric closure behavior over long-term abandonment, and the theoretical accumulated casing strains along the axis of the symmetry of the caverns, as well as the induced surface subsidence at the site. The numerical analysis were based on four cavern combinations, that is (1) single Lotsberg cavern, (2) two horizontal adjacent Lotsberg caverns, (3) two vertical uphole and downhole caverns, (4) two horizontal adjacent Lotsberg caverns and two uphole Prairie Evaporite caverns. For each cavern combination, various cavern injection conditions were considered and compared to study the influence of cavern internal pressure onto the long-term geomechanical behavior of the disposal salt caverns. Additionally, two different simulation methods for the cavern creation, including instantaneous excavations and sequential excavations, were simulated and compared to analyze its influence in predicted results.

Main conclusions derived from the various numerical simulations are listed as follows:

- The instantaneous excavation solutions used to simulate the cavern solution-mining development process can predict similar long-term abandonment salt dilation behavior surrounding the target caverns as well as the nonsalt overlying shear failure behavior as sequential excavation solutions. However, the instantaneous simulations tend to predict dilation failure of the salt units surrounding caverns following the full cavern development in terms of short-term

structural stability and integrity, which can be considered to be more conservative than sequential solutions. Additionally, the instantaneous excavations will overestimate the cavern volumetric shrinkage at almost double the sequential excavations, but the predicted surface subsidence is less than the value of sequential solutions.

- As long as no salt dilation is observed during the development of salt caverns, then the cavern stability and integrity will not be affected by the salt dilation within permanent cavern abandonment, because the salt dilation potential will slightly diminished during the permanent abandonment as the salt creeps. The most salt dilation potential is always predicted at the outer edge of newly mined and abandoned brine-filled caverns. In addition, the edge salt dilation behavior for each cavern during cavern creations is mainly dependent on its internal pressures, and will affected at a certain level by the excavations of horizontal adjacent caverns. However, the ultimate salt dilation potential is totally dominated by the injection conditions of the cavern itself, no matter the cavern internal pressures of pre-existing adjacent caverns. The development of uphole Prairie Evaporite caverns shows little influence on the salt dilation behavior of lower Lotsberg disposal caverns. Moreover, for any cavern combination, the potential of salt dilation will be significantly diminished with the disposal of waste sands into the salt caverns as compared with the brine-filled caverns. One thing needs to mention is that for the four cavern case under asymmetrical injection conditions, the salt dilation potential area surrounding the lower brine-filled cavern shows a trend of expansion, which is usually supposed to decay for other studied cases.
- The cavern internal pressures have little impact on the nonsalt shear failure potential of the overlying strata based on the specific in-situ stresses conditions

assigned on the geological strata. However, the shear failure behavior of the nonsalt overlying units is remarkably influenced by the solution-mining of adjacent horizontal caverns, independent of its injection conditions. The greatest shear failure potential for all cavern combinations is always located symmetrically of the caverns within the overlying Ernestina Lake Formation, and the solution mining of uphole cavern has little influence onto this potential shear zone. If no shear failure occurs during the cavern creation, then no more shear expected during the long-term abandonment. However, this conclusion is only based on the specific lithostatic stresses distribution and may not applicable for other geological conditions.

- Cavern closure behavior is depended on the cavern internal pressures and the steady state creep rate of the salt strata. For both brine and waste injection, the cavern internal pressure is assumed to be constant during the long-term simulation. However, the cavern shrinkage will pressurize the caverns and the internal pressure will increase, which will in turn lead to the decrease of the cavern closure rate. It can be concluded that its internal carrying pressure dominates the cavern volumetric closure, and the horizontally adjacent salt caverns and their injection conditions will not be affect it. For the salt cavern site in this thesis, where the Prairie Evaporite Formation has a higher steady state creep rate than the Lotsberg Formation, the volume loss of the uphole caverns during abandonment is significantly larger than the downhole salt caverns. Thus the development and operation of Prairie Evaporite caverns should be paid greater attention to its potential storage volume loss and the corresponding economic costs. However, if the uphole caverns can be filled with dense waste disposal at abandonment, its cavern closure will be significantly reduced to less

than half of the brine-filled conditions and accepted volume shrinkage will be expected during permanent abandonment.

- The casing strains are predicted to be increased greatly within the salt formations due to its creep flow vertically. The cavern internal support pressure itself primarily determines the accumulated casing strains of each cavern. If caverns only exist within the Lotsberg Formation, no yielding or tensile failure during permanent abandonment is predicted. However, if uphole and downhole caverns are excavated vertically aligned within the same well, the casings of the lower Lotsberg caverns is predicted to yield or failed during 50-year abandonment as long as the upper Prairie Evaporite caverns abandoned with saturated brine, if J-55 grade steel casing used for this project. The condition of all caverns filled with solid waste will relieve this casing stretching performance significantly and the casing strains will be within the yield limit during 50-years abandonment simulation.
- The predicted surface is quite small for sole cavern case and two horizontal Lotsberg caverns case. According to Van Sambeek's suggestion, the elevation change of less than about 0.15 m will not affect the area drainage significantly. When vertical uphole caverns involved, the surface subsidence is largely determined by the pressure conditions of Prairie Evaporite caverns. As long as the uphole cavern is filled with brine, the surface subsidence will increase dramatically even the downhole Lotsberg caverns are filled with dense waste. For the four cavern case, the largely induced surface subsidence will be of the most concern and potential damages onto the surface facilities and area drainage may be brought onto the site, because that even all the caverns injected with dense waste, the maximum surface subsidence will reach 0.09 m at the end of

simulation and will grow at a rate of approximately 0.9851 mm/year, expected to exceed the 0.15 m threshold in another 55 years.

## **6 CONCLUSIONS AND RECOMMENDATIONS**

### **6.1 General**

The overall growth in world population, the resulting increase in industrial activity and the recognition of environment and health impacts from indiscriminate disposal of waste products has led to the need for an alternative to traditional methods of land filling and costly high temperature combustion for the management of wastes.

The disposal of oil field wastes into the purposely-built salt caverns becomes feasible and legal since the Argonne National Laboratory had performed a preliminary technical and legal evaluation of the subjects in 1996 as the requirement by the U.S. Department of Energy. In the past decades, there has been an increased worldwide in the number of salt caverns that are specifically solution-mined as storage facilities for hydrocarbon and oilfield waste, rather than for only brine production or other chemical feedstock. Solution mined caverns in salt formations are becoming a preferred method due to their favourable and appreciable geomechanical properties including low permeability and high ductility. Because the history of the salt cavern used for solid waste disposal is very limited, as well as the information of the post-closure behavior of the disposal caverns monitored in the field, more predictions and simulations of the geomechanical performance and response of the waste-filled salt caverns during operation and permanent abandonment are required to get a better knowledge of the potential long term risks associated with disposal waste caverns.

The objective of this thesis has been to analyze the numerical observations of the structural stability and integrity of the salt caverns plugged and abandoned with waste disposal during its development, operation, and permanent abandonment, as well as the

failure potential of the overlying nonsalt caprocks and the associated cavern casings. Multiple-cavern configurations were also considered and simulated under various cavern injection conditions and the interactions between adjacent caverns were evaluated in the three-dimensional finite difference models. It has been shown that for all the cavern configurations simulated, the structural stability and integrity intensity of the salt caverns will be highly increase once all the salt caverns are injected with oil filed waste disposal, and the induced deformation and cavern volume loss will be significantly mitigated as well. It is suggested to convert the hydrocarbon gas or liquid storage caverns to waste disposal caverns at the end of their lives to prevent potential cavern collapse or relieve the accompanying risks or environmental hazards. The following section provides specific conclusions regarding each component of the research in this thesis.

## **6.2 Conclusions**

To provide a degree of verification of how well the modeling approach and scenario can reasonably represent the geomechanical performances of the salt caverns, sensitivity analyses focused on parametric properties of the three-dimensional finite difference programs were conducted over a wide-range. The following conclusions were summarized:

- The Ran-Tunnel gridding approach shows more sensitivity to the dilation behavior of the salt strata, presents more conservative potential of stability loss of the waste disposal salt caverns, and predicts more deformation of the geological units than the Rad-Cylindrical gridding with higher efficiency.
- The boundary effects onto the deformation behavior of the salt caverns can be eliminated significantly by increasing the outer radius of the three-dimensional model to more than 2000 m. However, the boundary size shows little effect on

the salt dilation surrounding the caverns and shear behavior of the non-salt overlying units.

- The creep timestep settings embedded in FLAC<sup>3D</sup> program will influence the analytical outcomes significantly and need to be fairly determined for the sake of reasonable results as well as efficiency.
- The elastic parameters used to characterize the salt mechanical behavior have limited influences on the model deformation as well as the structural stability and integrity of the salt caverns predicted in FLAC<sup>3D</sup> simulations.
- The Power law parameters for describe the salt deformation mechanism can influence the deformation behavior and structural stability behavior significantly, thus they need to accurately determined in the laboratory testing studies to adequately present the geomechanical response of the disposal salt caverns.

Various three-dimensional finite simulations have been performed in FLAC<sup>3D</sup> numerical studies to evaluate the geomechanical performance of solution-mined disposal salt caverns during its development, operation and abandonment. Different cavern combinations have been considered including up to four-multiple-cavern cases. For each salt cavern, two injection situations were analyzed and compared to study the influence of cavern pressures onto the long-term geomechanical behavior of the disposal salt caverns. The conclusions were listed below:

- The instantaneous-excavation solution used to simulate the cavern solution-mining process predicts similar long-term structural stability and integrity behavior of the salt caverns as the sequential-excavation approach. As for short-term performance, the instantaneous-solution predicts salt dilation following the full cavern development, which is not the case for sequential-

approach. Additionally, sequential-solution can give more reasonable deformation and volumetric closure behavior than instantaneous-approach.

- As long as no salt dilation is observed during the development of salt caverns, then the cavern stability and integrity will not be affected by the salt dilation within permanent cavern abandonment. The most salt dilation potential is always predicted onto the outer edge of newly mined and abandoned brine-filled caverns. The ultimate salt dilation potential is totally dominated by the injection conditions of the cavern itself, not be influenced much by pre-existing adjacent caverns. The development of uphole Prairie Evaporite caverns shows little influence on the salt dilation behavior of lower Lotsberg disposal caverns. However, the case of lower cavern is filled and brine while the upper cavern is waste filled is not suggested from an engineering point because the potential of salt dilation surrounding the lower brine-filled caverns is ascending with abandonment time. The potential of salt dilation will be significantly diminished with the disposal of waste sands into the salt caverns compared with the brine-filled caverns, no matter the number of existing caverns at that time.
- For the specific-site conditions, the shear failure behavior of the nonsalt overlying caprock is remarkably influenced by the solution-mined horizontal adjacent caverns, rather than its internal cavern support pressure. The solution mining of an uphole cavern has much less influence on the greatest shear potential zone.
- The volumetric closure behavior of the caverns is highly independent on its cavern internal pressure and the steady-state creep rate of the ambient salt strata and it will not be affected by the horizontal and vertical adjacent salt caverns and their injection conditions. In this thesis, the volume loss of the

uphole Prairie Evaporite caverns during abandonment is significantly larger than the downhole Lotsberg caverns under same injection conditions. However, if the uphole caverns can be filled with dense waste disposal at abandonment, its cavern closure will be significantly reduced to less than half of the brine-filled conditions and accepted volume shrinkage will be expected during permanent abandonment.

- The accumulated casing strains of each cavern are primarily determined by the cavern internal support pressure itself. The appearance of the uphole Prairie Evaporite caverns filled with brine will lead to the potential tensile failure of casings of the lower Lotsberg caverns, even if they were waste-filled. This situation can be mitigated by injecting dense sands waste into the upper caverns and the lower casing will stay safe at least within 50-year abandonment after the development of all the caverns. This estimation is a conservative failure estimate because it assumes that casing failure will not be influenced by probable slippage or casing string resistance and other causes.
- At this specific site for disposal salt caverns, surface subsidence for only Lotsberg caverns is quite small and within the tolerance. However, if the Prairie Evaporite salt caverns are developed, the induced surface subsidence will exceed the suggested affecting threshold during permanent abandonment and cause damage to the ground facilities and structures as well as the area drainage, even if the all the existing caverns were injected with dense waste.

### **6.3 Recommendations for Future Research**

The following recommendations may be useful for future studies of geomechanical assessment for waste disposal salt caverns:

- Utilize a more suitable constitutive model for the behavior of the rocksalt, e.g. WIPP model which is specially designed for the waste disposal salt caverns. The Norton power law used in this thesis does not take into account of the temperature effects onto the rocksalt creep rate. Although in-situ temperatures are not significantly elevated, it is expected that the creep rates will increase and accompanying with the growing cavern deformation and volumetric closure.
- The knowledge of the initial stress state at the salt cavern site and the material properties is of fundamental importance both for understanding the formation behavior and the numerical modeling studies of waste disposal salt caverns. It can be suggested to conduct a three-dimensional geomechanical history match analysis of the field geotechnical instrumentation results.
- The interpretation of the cavern internal caverns pressure representing the waste disposal is a key factor for long-term cavern geomechanical behavior. It is highly recommended that laboratory testing studies need to be conducted onto the waste disposal to assess their geomechanical properties both pre- and post- injection operation.

## REFERENCES

- Boulianne M., 2004. A Numerical Investigation of the Creep (Viscoplastic) Behavior of Circular Opening and Pillar in Rocksalt. The 57<sup>th</sup> Canadian Geotechnical Conference, Session 5G, 25-32 p.
- Buchholz S. A., and Nielnd J. D., 2012. Geomechanical Analysis of Solid Disposal Caverns for Canadian Natural Resources Limited Kirby In Situ Oil Sands Project Alberta Canada. Prepared for Canadian Natural Resources Limited, Topical Report RSI-2314, RESPEC, Rapid City, South Dakota, December.
- Davidson, B. C., 1997. Salt Solution Caverns for Petroleum Industry Wastes. Society of Petroleum Engineers, Dallas, Texas, 51- 61 p.
- Duyvestyn, G. M., and Davidson B. C., 1998. Salt Solution Caverns for Petroleum Industry Toxic Granular Solid Waste Disposal. Society of Petroleum Engineers, Trondheim, Norway, 8-10 July, 239 – 246 p.
- Gardner, G.H.F.; Gardner L.W., Gregory A.R., 1974. Formation Velocity and Density - The Diagnostic Basics for Stratigraphic Traps. *Geophysics* 39, 770–780 p.
- Goodman, R. E., 1980. Introduction to Rock Mechanics, John Wiley and Sons, New York, NY.
- Greenberg, M.L., Castagna, J.P., 1992. Shear-wave velocity estimation in porous rocks: Theoretical formulation, preliminary verification and applications. *Geophysical Prospecting* 40, 195–209.
- Grobe, M., 2000. Distribution and Thickness of Salt within the Devonian Elk Point Group, Western Canada Sedimentary Basin. Alberta Energy and Utilities Board, Alberta Geological Survey.
- Hamilton W.N., 1971. Salt in East-Central Alberta. Research Council of Alberta.
- Heerden W.L., 1987. Comparison of Static and Dynamic Elastic Moduli of Rock Material. Pretoria, South Africa: Council for Scientific and Industrial Research, National Mechanical Engineering Research Institute. CSIR Research Report 646, 95 pages.
- Herrmann, W., Wawersik, W.R., Lauson, H.S., 1980a. Analysis of Steady State Creep of Southeastern New Mexico Bedded Salt. Sandia National Laboratories, SAND80-0558.
- Herrmann, W., Wawersik, W.R., Lauson, H.S., 1980b. Creep Curves and Fitting Parameters for Southeastern New Mexico Bedded Salt. Sandia National Laboratories, SAND80-0558.

- Itasca Consulting Group, Inc., 2011. FLAC<sup>3D</sup> Fast Lagrangian Analysis of Continua in 3 Dimensions, 5<sup>th</sup> Ed. (FLAC<sup>3D</sup> Version 5.0), Minneapolis, MN.
- Martínez-Martínez J., Benavente D., García-del-Cura, M.A., 2012. Comparison of the Static and Dynamic Modulus in Carbonate Rocks. Bull Eng Geol Environ 71, 263-268.
- Pierre B., Benoit B., and Mehdi K. J., 2005. Deep Salt Caverns Abandonment. Post-Ming 2005,
- Retigan J. L., 1995. Numerical Modeling of Week Island Subsidence and Laboratory Testing of Weeks Island Salt. Solution Mining Research Institute Spring Meeting, New Orleans, Louisiana, April 30 – May 3, 0-21 p.
- Rankine, W.J.R., 1857. On the stability of Loose Earth. Philosophical Transactions of the Royal Society of London 147, 9–27.
- RG2, 2013. Geomechanical Study for Salt Caverns: Laboratory Testing Results LIND 8B-WD-13-57-5W4. Project report prepared by Reservoir Geomechanics Research Group (RG2) for *Company*, 99 p.
- Savich, A.I., 1984. Generalized Relations between Static and Dynamic Indices of Rock Deformability. Hydrotechnical Construction 18(8), 394-400.
- Tomasko D., Elcock D., Veil J., and Caudle D., 1999. Risk Analysis for Disposing Nonhazardous Oil Field Wastes in Salt Caverns. Performed under Argonne Nation Lab Contract No. W-31-109-ENG-38, Argonne National Laboratory, Argonne, Illinois, January.
- Van Sambeek, L. L., 2000. An Introduction to Subsidence Over Salt and Potash Mining Facilities. Solution Mining Research Institute Fall Meeting, San Antonio, TX, October 15-18, 0-10 p.
- Veil, J. A., Smith, K. P., and Tomasko D., 1998. Disposal of NORM-Contaminated Oil Field Wastes in Salt Caverns. Prepared for U.S. Department of Energy, Office of Fossil Energy under Contract W-31-109-ENG-38, Argonne National Laboratory, Argonne, Illinois, August.
- Veil, J., Elcock D., Raivel M., Caudle D., Ayers R.C., Grunewald B., 1996. Preliminary Technical and Legal Evaluation of Disposing of Nonhazardous Oil Field Waste into Salt Caverns. Prepared for the U.S. Department of Energy, Office of Fossil Energy under Contract W-31-109-ENG-38, Argonne National Laboratory, Argonne, Illinois, June.

# APPENDIX A Geological Review

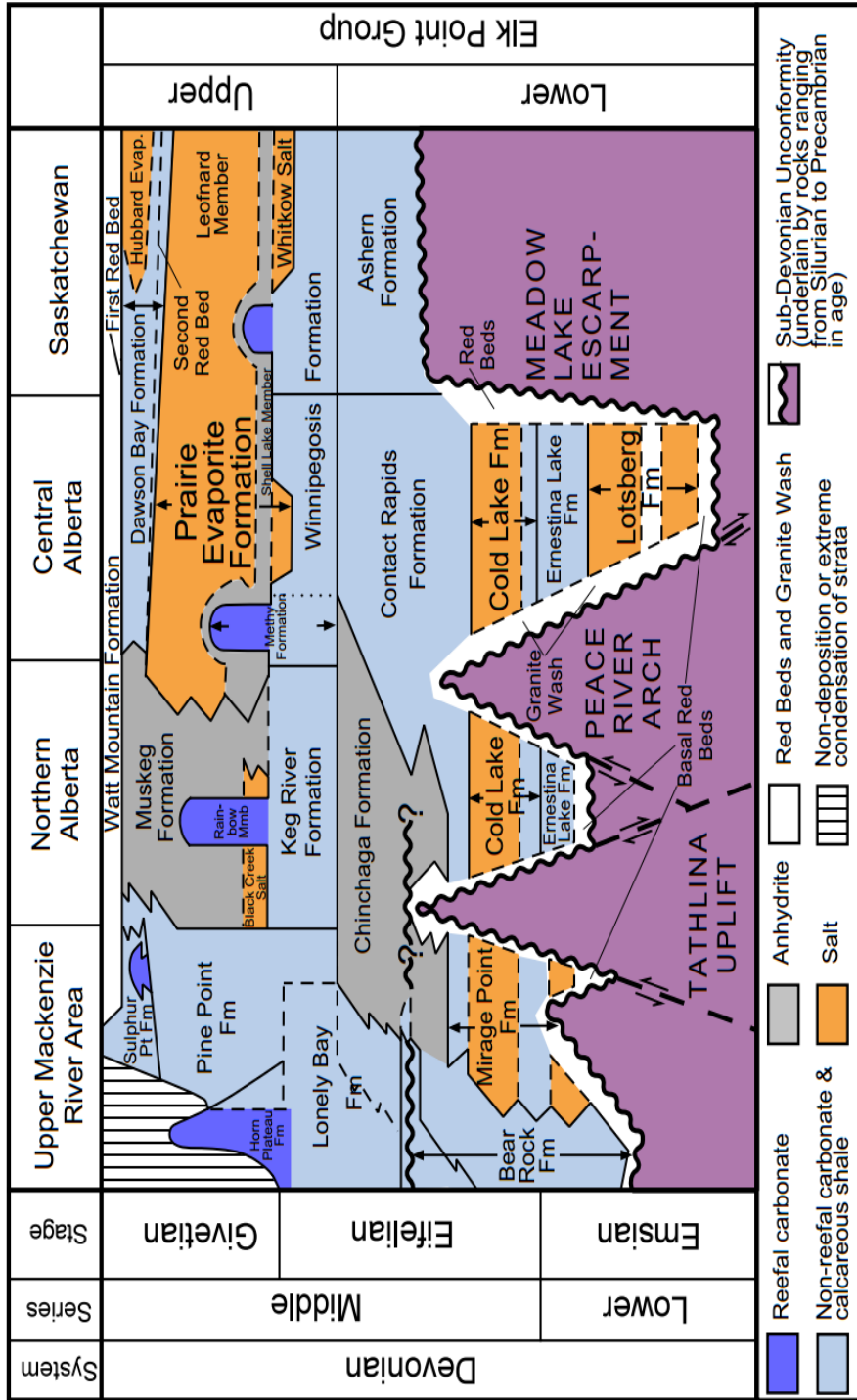


Figure A. 1 Schematic Formations of the Elk Point Group (Meijer Drees, 1986)

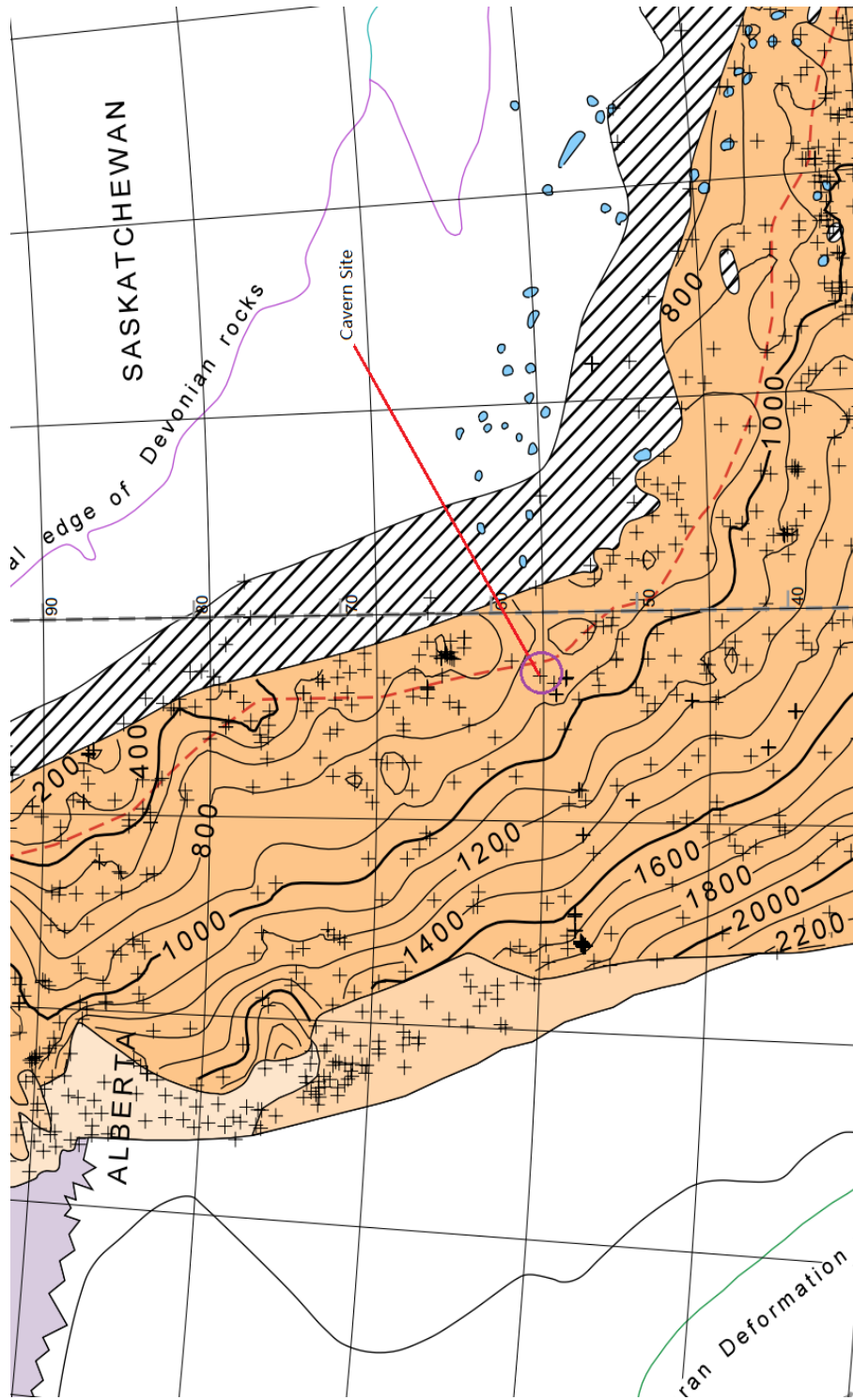


Figure A. 2 Contour of Depth to Prairie Evaporite Formation

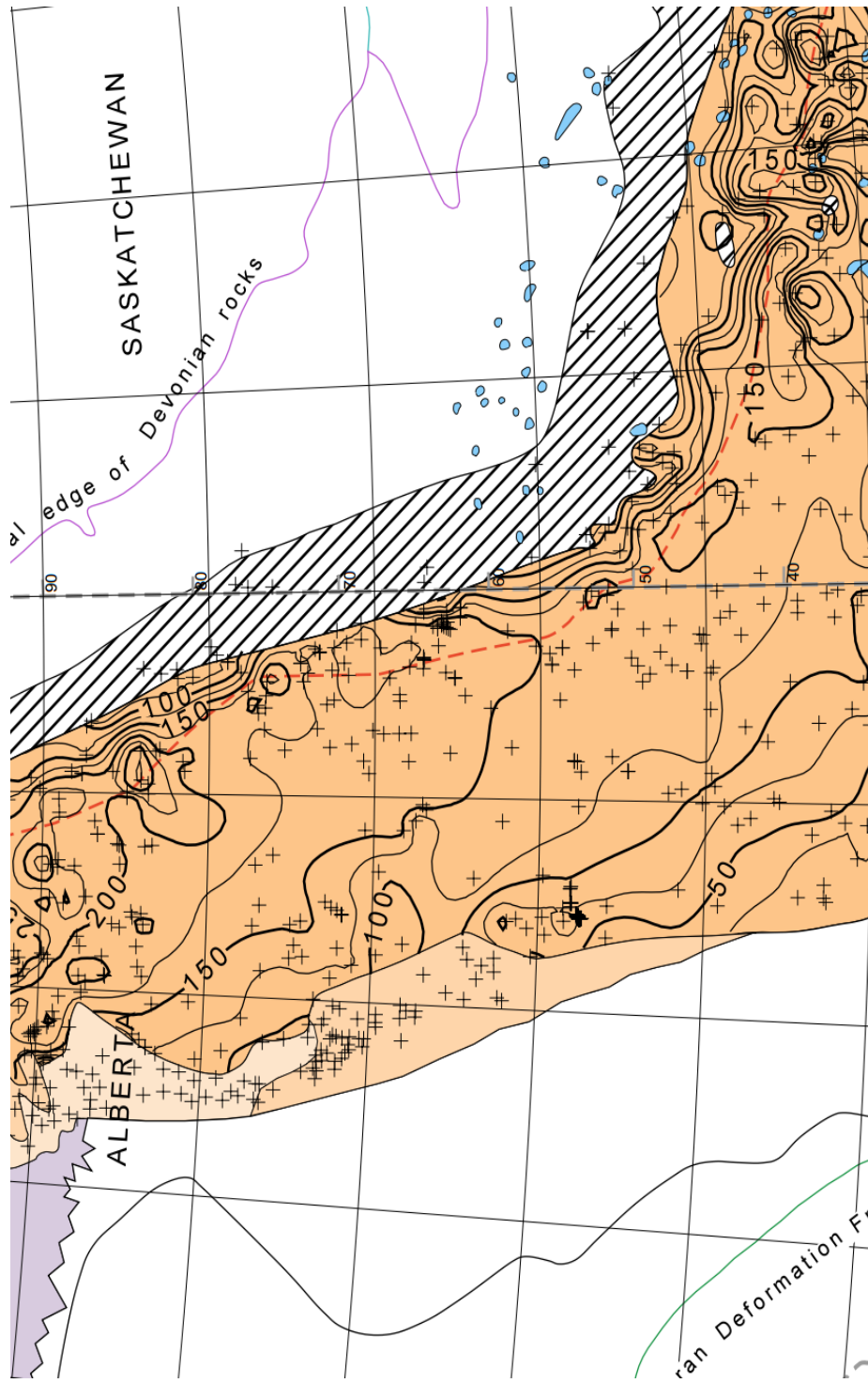


Figure A. 3 Isopach Contour of Prairie Evaporite Formation

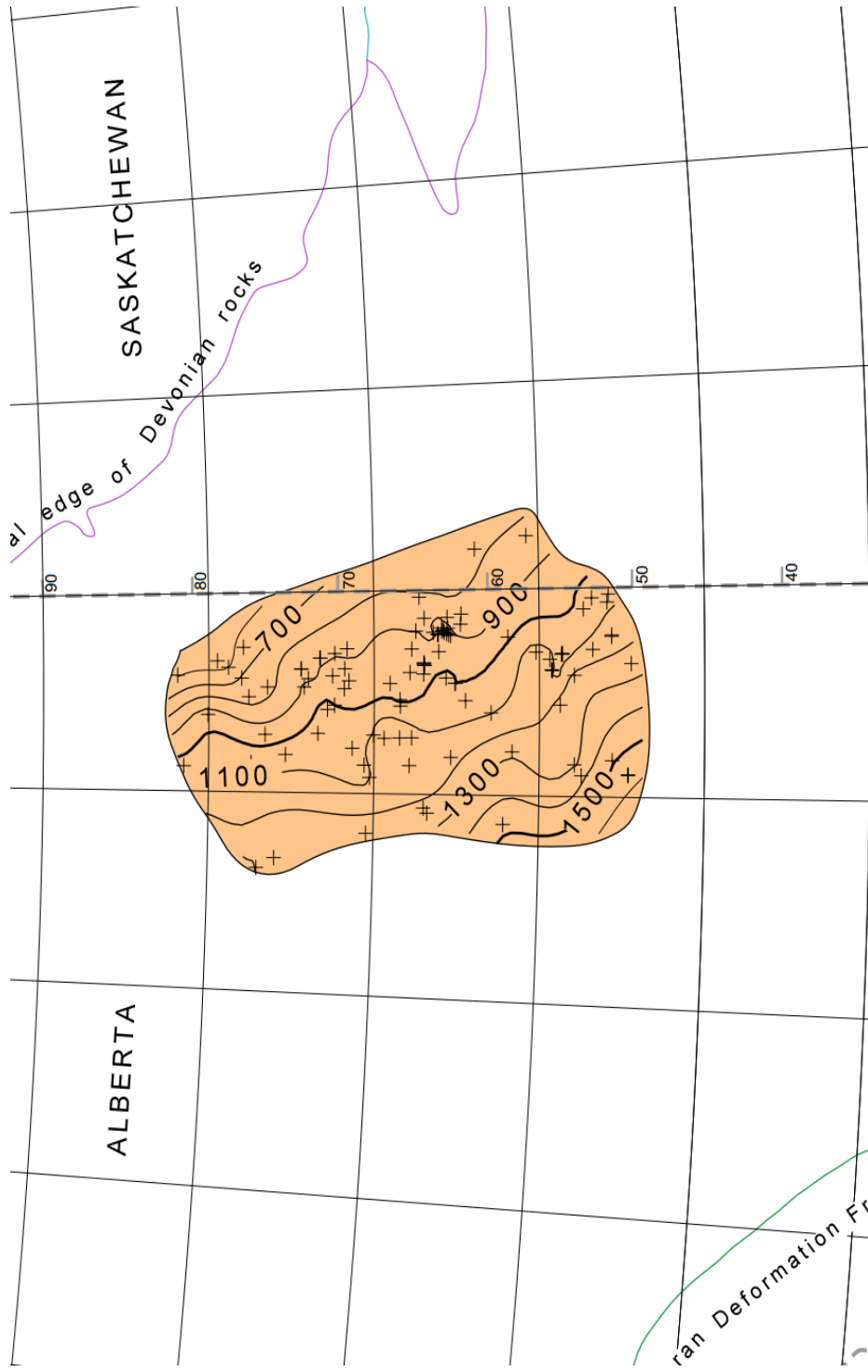


Figure A. 4 Contour of Depth to Cold Lake Formation

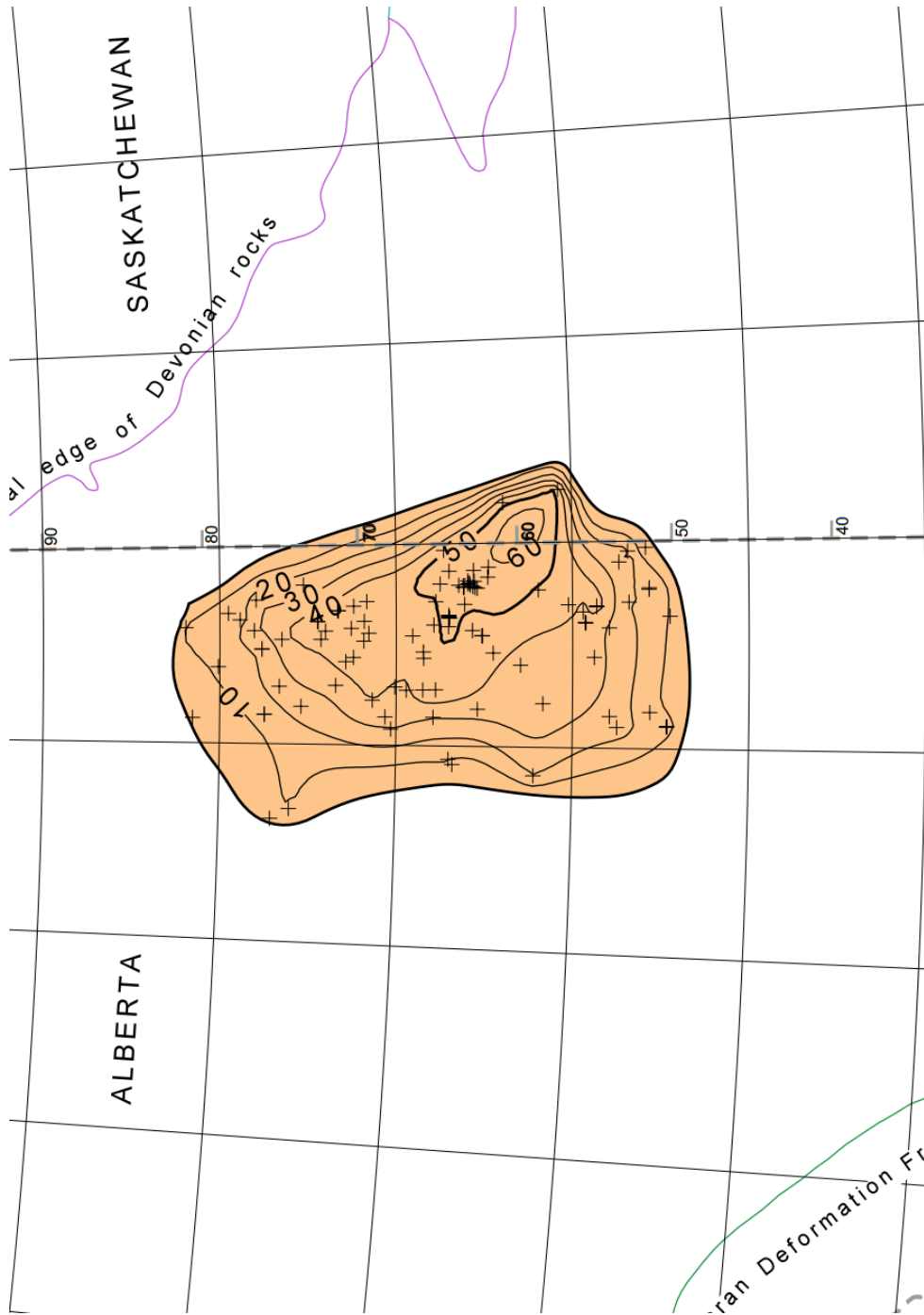


Figure A. 5 Isopach Contour of Cold Lake Formation

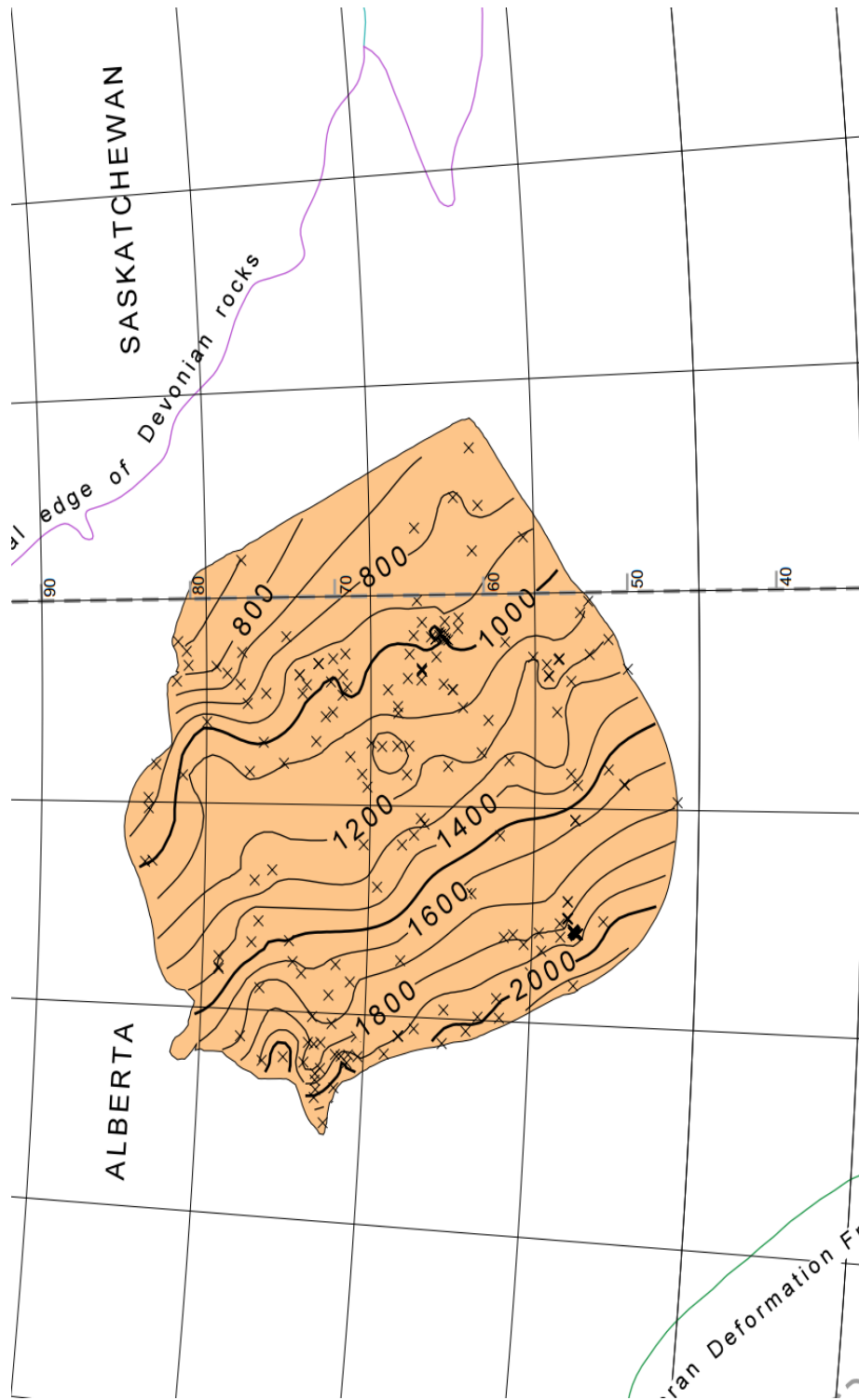


Figure A. 6 Contour of Depth to Lotsberg Formation

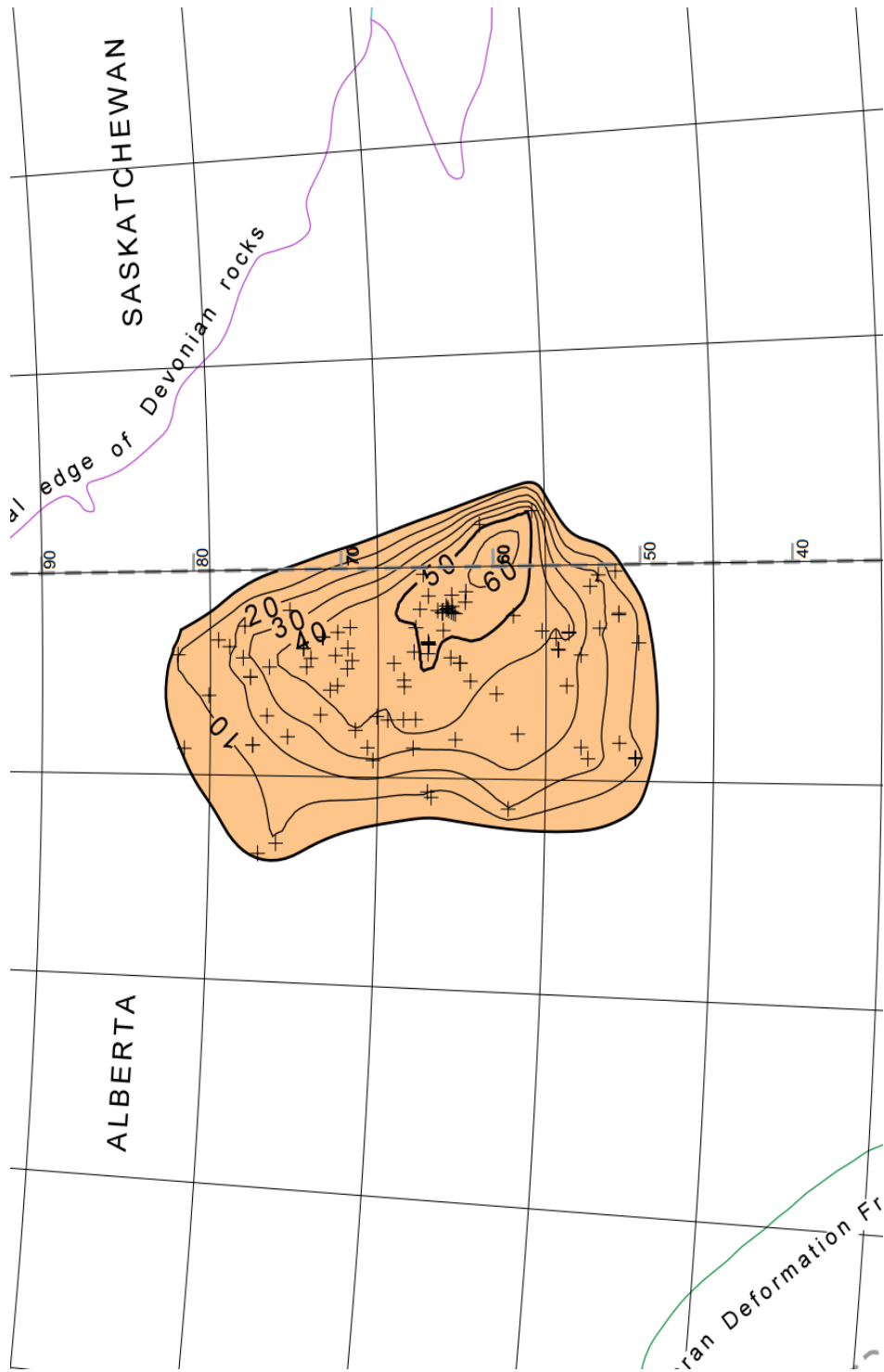


Figure A. 7 Isopach Contour of Lotsberg Formation

## APPENDIX B Numerical Analytical Methodology

Table B. 1 Static and Dynamic Young's Modulus Comparison for salt and Nonsalt

Units

Geological Unit	Dynamic Young's Modulus (GPa)	Static Young's Modulus (GPa)			Predicted Static Value (Savich, 1984)
	RokDoc	UCS Test	STC Test	CMC Test	$E_s = 0.161(E_d)^{1.227}$
Upper Caprock	30	-	-	-	10.45
Middle Caprock	6	-	-	-	1.45
Lower Caprock	10	-	-	-	2.72
Watt Mountain	40	22	3	-	14.88
Prairie Evaporite	37	2	N/A	7	13.52
Keg River	50	14	15	-	19.56
Cold Lake	37	-	-	-	13.52
Ernestina Lake	40	10	4	-	14.88
Lotsberg	37	3	-	7	13.52
Underburden	30	22	-		10.45

Notes: - indicates no available tests performed on the formation specimens in laboratory.

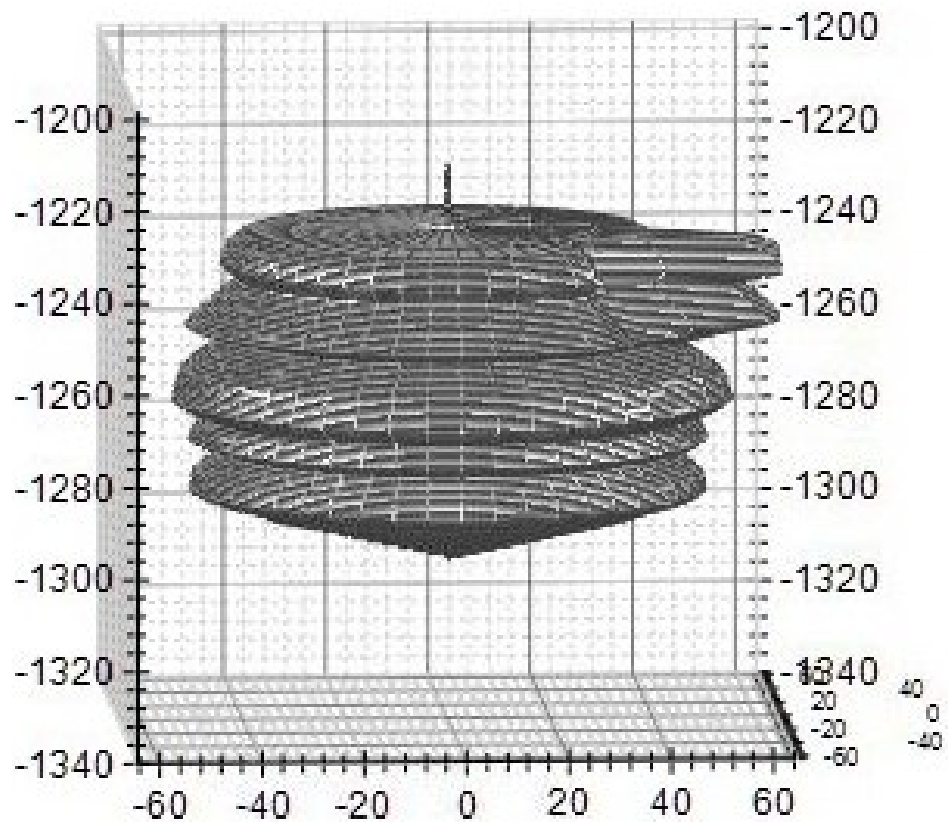


Figure B. 1 Cavern 1-13 LTBG 3D Configuration in WinUBro





## APPENDIX C Numerical Modeling Results

Table C. 1 Details of Cavern Sequential Excavations Steps

Excavation Step	Lotsberg Cavern		Prairie Evaporite Cavern	
	Depth from (m)	Depth to (m)	Depth from (m)	Depth to (m)
1	1305	1301	1026	1022
2	1301	1296	1022	1017
3	1296	1290	1017	1011
4	1290	1283	1011	1004
5	1283	1275	1004	996
6	1275	1267	996	988
7	1267	1255	988	976
8	1255	1245	976	966
9	1245	1238	966	959
10	1238	1232	959	953
11	1232	1226	953	947
12	1226	1222	947	943
13	1222	1218	943	939
14	1218	1214	939	935
15	1214	1210	935	931

Table C. 2 Cavern *1-13 LTBG brine* Case Solution Mining and Abandonment Schedule

Year	Excavation State	Injection State	Simulation Time (Year)	Stage
2006	Step 1~3	Step 1~3 with brine	1	Operation
2007	Step 4~5	Step 4~5 with brine	2	Operation
2008	Step 6	Step 6 with brine	3	Operation
2009	Step 7	Step 7 with brine	4	Operation
2010	Step 8	Step 8 with brine	5	Operation
2011	Step 9	Step 9 with brine	6	Operation
2012	Step 10~11	Step 10~11 with brine	7	Operation
2013	Step 12~13	Step 12~13 with brine	8	Operation
2014	Step 14~16	Step 14~16 with brine	9	Operation
2015			10	Operation
2016			11	Abandonment
2017			12	Abandonment
2020			15	Abandonment
2025			20	Abandonment
2035			30	Abandonment
2065			60	Abandonment

Table C. 3 Cavern *1-13 LTBG dense* Case Solution Mining and Abandonment Schedule

Year	Excavation State	Injection State		Simulation Time (Year)	Stage
2006	Step 1~3	Step 1~3 with brine		1	Operation
2007	Step 4~5	Step 4~5 with brine	Step 1~3 with sands	2	Operation
2008	Step 6	Step 6 with brine	Step 4~5 with sands	3	Operation
2009	Step 7	Step 7 with brine	Step 6 with sands	4	Operation
2010	Step 8	Step 8 with brine	Step 7 with sands	5	Operation
2011	Step 9	Step 9 with brine	Step 8 with sands	6	Operation
2012	Step 10~11	Step 10~11 with brine	Step 9 with sands	7	Operation
2013	Step 12~13	Step 12~13 with brine	Step 10~11 with sands	8	Operation
2014	Step 14~16	Step 14~16 with brine	Step 12~13 with sands	9	Operation
2015			Step 14~16 with sands	10	Operation
2016				11	Abandonment
2017				12	Abandonment
2020				15	Abandonment
2025				20	Abandonment
2035				30	Abandonment
2065				60	Abandonment

Table C. 4 Cavern *1-13&8-13 LTBG brine-brine* Case Solution Mining and

Abandonment Schedule

Year	Excavation State	Injection State	Simulation Time (Year)	Stage
1-13 LTBG Cavern				
2006	Step 1~3	Step 1~3 with brine	1	Operation
2007	Step 4~5	Step 4~5 with brine	2	Operation
2008	Step 6	Step 6 with brine	3	Operation
2009	Step 7	Step 7 with brine	4	Operation
2010	Step 8	Step 8 with brine	5	Operation
2011	Step 9	Step 9 with brine	6	Operation
2012	Step 10~11	Step 10~11 with brine	7	Operation
2013	Step 12~13	Step 12~13 with brine	8	Operation
2014	Step 14~16	Step 14~16 with brine	9	Operation
2015			10	Operation
8-13 LTBG Cavern				
2016	Step 1~3	Step 1~3 with brine	11	Operation
2017	Step 4~5	Step 4~5 with brine	12	Operation
2018	Step 6	Step 6 with brine	13	Operation
2019	Step 7	Step 7 with brine	14	Operation
2020	Step 8	Step 8 with brine	15	Operation
2021	Step 9	Step 9 with brine	16	Operation
2022	Step 10~11	Step 10~11 with brine	17	Operation
2023	Step 12~13	Step 12~13 with brine	18	Operation
2024	Step 14~16	Step 14~16 with brine	19	Operation
2025			20	Operation
2026			21	Abandonment
2027			22	Abandonment
2030			25	Abandonment
2035			30	Abandonment
2045			40	Abandonment
2075			70	Abandonment

Table C. 5 Cavern *1-13&8-13 LTBG dense-brine* Case Solution Mining and Abandonment Schedule

Year	Excavation State	Injection State		Simulation Time (Year)	Stage
1-13 LTBG Cavern					
2006	Step 1~3	Step 1~3 with brine		1	Operation
2007	Step 4~5	Step 4~5 with brine	Step 1~3 with sands	2	Operation
2008	Step 6	Step 6 with brine	Step 4~5 with sands	3	Operation
2009	Step 7	Step 7 with brine	Step 6 with sands	4	Operation
2010	Step 8	Step 8 with brine	Step 7 with sands	5	Operation
2011	Step 9	Step 9 with brine	Step 8 with sands	6	Operation
2012	Step 10~11	Step 10~11 with brine	Step 9 with sands	7	Operation
2013	Step 12~13	Step 12~13 with brine	Step 10~11 with sands	8	Operation
2014	Step 14~16	Step 14~16 with brine	Step 12~13 with sands	9	Operation
2015			Step 14~16 with sands	10	Operation
8-13 LTBG Cavern					
2016	Step 1~3	Step 1~3 with brine		11	Operation
2017	Step 4~5	Step 4~5 with brine		12	Operation
2018	Step 6	Step 6 with brine		13	Operation
2019	Step 7	Step 7 with brine		14	Operation
2020	Step 8	Step 8 with brine		15	Operation
2021	Step 9	Step 9 with brine		16	Operation
2022	Step 10~11	Step 10~11 with brine		17	Operation
2023	Step 12~13	Step 12~13 with brine		18	Operation

2024	Step 14~16	Step 14~16 with brine		19	Operation
2025				20	Operation
2026				21	Abandonment
2027				22	Abandonment
2030				25	Abandonment
2035				30	Abandonment
2045				40	Abandonment
2075				70	Abandonment

Table C. 6 Cavern *1-13&8-13 LTBG Dense-Dense-Case* Solution Mining and Abandonment Schedule

Year	Excavation State	Injection State		Simulation Time (Year)	Stage
1-13 LTBG Cavern					
2006	Step 1~3	Step 1~3 with brine		1	Operation
2007	Step 4~5	Step 4~5 with brine	Step 1~3 with sands	2	Operation
2008	Step 6	Step 6 with brine	Step 4~5 with sands	3	Operation
2009	Step 7	Step 7 with brine	Step 6 with sands	4	Operation
2010	Step 8	Step 8 with brine	Step 7 with sands	5	Operation
2011	Step 9	Step 9 with brine	Step 8 with sands	6	Operation
2012	Step 10~11	Step 10~11 with brine	Step 9 with sands	7	Operation
2013	Step 12~13	Step 12~13 with brine	Step 10~11 with sands	8	Operation
2014	Step 14~16	Step 14~16 with brine	Step 12~13 with sands	9	Operation
2015			Step 14~16 with sands	10	Operation
8-13 LTBG Cavern					
2016	Step 1~3	Step 1~3 with brine		11	Operation
2017	Step 4~5	Step 4~5 with brine	Step 1~3 with sands	12	Operation
2018	Step 6	Step 6 with brine	Step 4~5 with sands	13	Operation
2019	Step 7	Step 7 with brine	Step 6 with sands	14	Operation
2020	Step 8	Step 8 with brine	Step 7 with sands	15	Operation
2021	Step 9	Step 9 with brine	Step 8 with sands	16	Operation
2022	Step 10~11	Step 10~11 with brine	Step 9 with sands	17	Operation
2023	Step 12~13	Step 12~13 with brine	Step 10~11 with sands	18	Operation

2024	Step 14~16	Step 14~16 with brine	Step 12~13 with sands	19	Operation
2025			Step 14~16 with sands	20	Operation
2026				21	Abandonment
2027				22	Abandonment
2030				25	Abandonment
2035				30	Abandonment
2045				40	Abandonment
2075				70	Abandonment

Table C. 7 Cavern *1-13 LTBG&PRVP brine-brine* Case Solution Mining and Abandonment Schedule

Year	Excavation State	Injection State	Simulation Time (Year)	Stage
1-13 LTBG Cavern				
2006	Step 1~3	Step 1~3 with brine	1	Operation
2007	Step 4~5	Step 4~5 with brine	2	Operation
2008	Step 6	Step 6 with brine	3	Operation
2009	Step 7	Step 7 with brine	4	Operation
2010	Step 8	Step 8 with brine	5	Operation
2011	Step 9	Step 9 with brine	6	Operation
2012	Step 10~11	Step 10~11 with brine	7	Operation
2013	Step 12~13	Step 12~13 with brine	8	Operation
2014	Step 14~16	Step 14~16 with brine	9	Operation
2015			10	Operation
1-13 PRVP Cavern				
2016	Step 1~3	Step 1~3 with brine	11	Operation
2017	Step 4~5	Step 4~5 with brine	12	Operation
2018	Step 6	Step 6 with brine	13	Operation
2019	Step 7	Step 7 with brine	14	Operation
2020	Step 8	Step 8 with brine	15	Operation
2021	Step 9	Step 9 with brine	16	Operation
2022	Step 10~11	Step 10~11 with brine	17	Operation
2023	Step 12~13	Step 12~13 with brine	18	Operation
2024	Step 14~16	Step 14~16 with brine	19	Operation
2025			20	Operation
2026			21	Abandonment
2027			22	Abandonment
2030			25	Abandonment
2035			30	Abandonment
2045			40	Abandonment
2075			70	Abandonment

Table C. 8 Cavern *1-13 LTBG&PRVP dense-brine* Case Solution Mining and Abandonment Schedule

Year	Excavation State	Injection State		Simulation Time (Year)	Stage
1-13 LTBG Cavern					
2006	Step 1~3	Step 1~3 with brine		1	Operation
2007	Step 4~5	Step 4~5 with brine	Step 1~3 with sands	2	Operation
2008	Step 6	Step 6 with brine	Step 4~5 with sands	3	Operation
2009	Step 7	Step 7 with brine	Step 6 with sands	4	Operation
2010	Step 8	Step 8 with brine	Step 7 with sands	5	Operation
2011	Step 9	Step 9 with brine	Step 8 with sands	6	Operation
2012	Step 10~11	Step 10~11 with brine	Step 9 with sands	7	Operation
2013	Step 12~13	Step 12~13 with brine	Step 10~11 with sands	8	Operation
2014	Step 14~16	Step 14~16 with brine	Step 12~13 with sands	9	Operation
2015			Step 14~16 with sands	10	Operation
1-13 PRVP Cavern					
2016	Step 1~3	Step 1~3 with brine		11	Operation
2017	Step 4~5	Step 4~5 with brine		12	Operation
2018	Step 6	Step 6 with brine		13	Operation
2019	Step 7	Step 7 with brine		14	Operation
2020	Step 8	Step 8 with brine		15	Operation
2021	Step 9	Step 9 with brine		16	Operation
2022	Step 10~11	Step 10~11 with brine		17	Operation
2023	Step 12~13	Step 12~13 with brine		18	Operation

2024	Step 14~16	Step 14~16 with brine		19	Operation
2025				20	Operation
2026				21	Abandonment
2027				22	Abandonment
2030				25	Abandonment
2035				30	Abandonment
2045				40	Abandonment
2075				70	Abandonment

Table C. 9 Cavern *1-13 LTBG&PRVP dense-dense* Case Solution Mining and Abandonment Schedule

Year	Excavation State	Injection State		Simulation Time (Year)	Stage
1-13 LTBG Cavern					
2006	Step 1~3	Step 1~3 with brine		1	Operation
2007	Step 4~5	Step 4~5 with brine	Step 1~3 with sands	2	Operation
2008	Step 6	Step 6 with brine	Step 4~5 with sands	3	Operation
2009	Step 7	Step 7 with brine	Step 6 with sands	4	Operation
2010	Step 8	Step 8 with brine	Step 7 with sands	5	Operation
2011	Step 9	Step 9 with brine	Step 8 with sands	6	Operation
2012	Step 10~11	Step 10~11 with brine	Step 9 with sands	7	Operation
2013	Step 12~13	Step 12~13 with brine	Step 10~11 with sands	8	Operation
2014	Step 14~16	Step 14~16 with brine	Step 12~13 with sands	9	Operation
2015			Step 14~16 with sands	10	Operation
1-13 PRVP Cavern					
2016	Step 1~3	Step 1~3 with brine		11	Operation
2017	Step 4~5	Step 4~5 with brine	Step 1~3 with sands	12	Operation
2018	Step 6	Step 6 with brine	Step 4~5 with sands	13	Operation
2019	Step 7	Step 7 with brine	Step 6 with sands	14	Operation
2020	Step 8	Step 8 with brine	Step 7 with sands	15	Operation
2021	Step 9	Step 9 with brine	Step 8 with sands	16	Operation
2022	Step 10~11	Step 10~11 with brine	Step 9 with sands	17	Operation
2023	Step 12~13	Step 12~13 with brine	Step 10~11 with sands	18	Operation

2024	Step 14~16	Step 14~16 with brine	Step 12~13 with sands	19	Operation
2025			Step 14~16 with sands	20	Operation
2026				21	Abandonment
2027				22	Abandonment
2030				25	Abandonment
2035				30	Abandonment
2045				40	Abandonment
2075				70	Abandonment

Table C. 10 Cavern *1-13&8-13 LTBG&PRVP Brine-Brine-Brine-Brine-Case*

Solution Mining and Abandonment Schedule

Year	Excavation State	Injection State	Simulation Time (Year)	Stage
1-13 LTBG Cavern				
2006	Step 1~3	Step 1~3 with brine	1	Operation
2007	Step 4~5	Step 4~5 with brine	2	Operation
2008	Step 6	Step 6 with brine	3	Operation
2009	Step 7	Step 7 with brine	4	Operation
2010	Step 8	Step 8 with brine	5	Operation
2011	Step 9	Step 9 with brine	6	Operation
2012	Step 10~11	Step 10~11 with brine	7	Operation
2013	Step 12~13	Step 12~13 with brine	8	Operation
2014	Step 14~16	Step 14~16 with brine	9	Operation
2015			10	Operation
8-13 LTBG Cavern				
2016	Step 1~3	Step 1~3 with brine	11	Operation
2017	Step 4~5	Step 4~5 with brine	12	Operation
2018	Step 6	Step 6 with brine	13	Operation
2019	Step 7	Step 7 with brine	14	Operation
2020	Step 8	Step 8 with brine	15	Operation
2021	Step 9	Step 9 with brine	16	Operation
2022	Step 10~11	Step 10~11 with brine	17	Operation
2023	Step 12~13	Step 12~13 with brine	18	Operation
2024	Step 14~16	Step 14~16 with brine	19	Operation
1-13 PRVP Cavern				
2026	Step 1~3	Step 1~3 with brine	21	Operation
2027	Step 4~5	Step 4~5 with brine	22	Operation
2028	Step 6	Step 6 with brine	23	Operation
2029	Step 7	Step 7 with brine	24	Operation
2030	Step 8	Step 8 with brine	25	Operation
2031	Step 9	Step 9 with brine	26	Operation
2032	Step 10~11	Step 10~11 with brine	27	Operation
2033	Step 12~13	Step 12~13 with brine	28	Operation
2034	Step 14~16	Step 14~16 with brine	29	Operation
2035			30	Operation
8-13 PRVP				
2036	Step 1~3	Step 1~3 with brine	31	Operation
2037	Step 4~5	Step 4~5 with brine	32	Operation
2038	Step 6	Step 6 with brine	33	Operation

2039	Step 7	Step 7 with brine	34	Operation
2040	Step 8	Step 8 with brine	35	Operation
2041	Step 9	Step 9 with brine	36	Operation
2042	Step 10~11	Step 10~11 with brine	37	Operation
2043	Step 12~13	Step 12~13 with brine	38	Operation
2044	Step 14~16	Step 14~16 with brine	39	Operation
2045			40	Operation
2046			41	Abandonment
2095			90	Abandonment

Table C. 11 Cavern *1-13&8-13 LTBG&PRVP Dense-Brine-Brine-Dense-Case* Solution Mining and Abandonment Schedule

Year	Excavation State	Injection State		Simulation Time (Year)	Stage
1-13 LTBG Cavern					
2006	Step 1~3	Step 1~3 with brine		1	Operation
2007	Step 4~5	Step 4~5 with brine	Step 1~3 with sands	2	Operation
2008	Step 6	Step 6 with brine	Step 4~5 with sands	3	Operation
2009	Step 7	Step 7 with brine	Step 6 with sands	4	Operation
2010	Step 8	Step 8 with brine	Step 7 with sands	5	Operation
2011	Step 9	Step 9 with brine	Step 8 with sands	6	Operation
2012	Step 10~11	Step 10~11 with brine	Step 9 with sands	7	Operation
2013	Step 12~13	Step 12~13 with brine	Step 10~11 with sands	8	Operation
2014	Step 14~16	Step 14~16 with brine	Step 12~13 with sands	9	Operation
2015			Step 14~16 with sands	10	Operation
8-13 LTBG Cavern					
2016	Step 1~3	Step 1~3 with brine		11	Operation
2017	Step 4~5	Step 4~5 with brine		12	Operation
2018	Step 6	Step 6 with brine		13	Operation
2019	Step 7	Step 7 with brine		14	Operation
2020	Step 8	Step 8 with brine		15	Operation
2021	Step 9	Step 9 with brine		16	Operation
2022	Step 10~11	Step 10~11 with brine		17	Operation
2023	Step 12~13	Step 12~13 with brine		18	Operation
2024	Step 14~16	Step 14~16 with brine		19	Operation

2025					
1-13 PRVP Cavern					
2026	Step 1~3	Step 1~3 with brine		21	Operation
2027	Step 4~5	Step 4~5 with brine		22	Operation
2028	Step 6	Step 6 with brine		23	Operation
2029	Step 7	Step 7 with brine		24	Operation
2030	Step 8	Step 8 with brine		25	Operation
2031	Step 9	Step 9 with brine		26	Operation
2032	Step 10~11	Step 10~11 with brine		27	Operation
2033	Step 12~13	Step 12~13 with brine		28	Operation
2034	Step 14~16	Step 14~16 with brine		29	Operation
2035				30	Operation
8-13 PRVP					
2036	Step 1~3	Step 1~3 with brine		31	Operation
2037	Step 4~5	Step 4~5 with brine	Step 1~3 with sands	32	Operation
2038	Step 6	Step 6 with brine	Step 4~5 with sands	33	Operation
2039	Step 7	Step 7 with brine	Step 6 with sands	34	Operation
2040	Step 8	Step 8 with brine	Step 7 with sands	35	Operation
2041	Step 9	Step 9 with brine	Step 8 with sands	36	Operation
2042	Step 10~11	Step 10~11 with brine	Step 9 with sands	37	Operation
2043	Step 12~13	Step 12~13 with brine	Step 10~11 with sands	38	Operation
2044	Step 14~16	Step 14~16 with brine	Step 12~13 with sands	39	Operation
2045			Step 14~16 with sands	40	Operation
2046				41	Abandonment
2095				90	Abandonment

Table C. 12 Cavern *1-13&8-13 LTBG&PRVP Dense-Dense-Brine-Brine-Case* Solution Mining and Abandonment Schedule

Year	Excavation State	Injection State		Simulation Time (Year)	Stage
1-13 LTBG Cavern					
2006	Step 1~3	Step 1~3 with brine		1	Operation
2007	Step 4~5	Step 4~5 with brine	Step 1~3 with sands	2	Operation
2008	Step 6	Step 6 with brine	Step 4~5 with sands	3	Operation
2009	Step 7	Step 7 with brine	Step 6 with sands	4	Operation
2010	Step 8	Step 8 with brine	Step 7 with sands	5	Operation
2011	Step 9	Step 9 with brine	Step 8 with sands	6	Operation
2012	Step 10~11	Step 10~11 with brine	Step 9 with sands	7	Operation
2013	Step 12~13	Step 12~13 with brine	Step 10~11 with sands	8	Operation
2014	Step 14~16	Step 14~16 with brine	Step 12~13 with sands	9	Operation
2015			Step 14~16 with sands	10	Operation
8-13 LTBG Cavern					
2016	Step 1~3	Step 1~3 with brine		11	Operation
2017	Step 4~5	Step 4~5 with brine	Step 1~3 with sands	12	Operation
2018	Step 6	Step 6 with brine	Step 4~5 with sands	13	Operation
2019	Step 7	Step 7 with brine	Step 6 with sands	14	Operation
2020	Step 8	Step 8 with brine	Step 7 with sands	15	Operation
2021	Step 9	Step 9 with brine	Step 8 with sands	16	Operation
2022	Step 10~11	Step 10~11 with brine	Step 9 with sands	17	Operation
2023	Step 12~13	Step 12~13 with brine	Step 10~11 with sands	18	Operation
2024	Step 14~16	Step 14~16 with brine	Step 12~13 with sands	19	Operation
2025			Step 14~16 with sands		

1-13 PRVP Cavern					
2026	Step 1~3	Step 1~3 with brine		21	Operation
2027	Step 4~5	Step 4~5 with brine		22	Operation
2028	Step 6	Step 6 with brine		23	Operation
2029	Step 7	Step 7 with brine		24	Operation
2030	Step 8	Step 8 with brine		25	Operation
2031	Step 9	Step 9 with brine		26	Operation
2032	Step 10~11	Step 10~11 with brine		27	Operation
2033	Step 12~13	Step 12~13 with brine		28	Operation
2034	Step 14~16	Step 14~16 with brine		29	Operation
2035				30	Operation
8-13 PRVP					
2036	Step 1~3	Step 1~3 with brine		31	Operation
2037	Step 4~5	Step 4~5 with brine		32	Operation
2038	Step 6	Step 6 with brine		33	Operation
2039	Step 7	Step 7 with brine		34	Operation
2040	Step 8	Step 8 with brine		35	Operation
2041	Step 9	Step 9 with brine		36	Operation
2042	Step 10~11	Step 10~11 with brine		37	Operation
2043	Step 12~13	Step 12~13 with brine		38	Operation
2044	Step 14~16	Step 14~16 with brine		39	Operation
2045				40	Operation
2046				41	Abandonment
2095				90	Abandonment

Table C. 13 Cavern *1-13&8-13 LTBG&PRVP Dense-Dense-Dense-Dense-Case*

Solution Mining and Abandonment Schedule

Year	Excavation State	Injection State		Simulation Time (Year)	Stage
1-13 LTBG Cavern					
2006	Step 1~3	Step 1~3 with brine		1	Operation
2007	Step 4~5	Step 4~5 with brine	Step 1~3 with sands	2	Operation
2008	Step 6	Step 6 with brine	Step 4~5 with sands	3	Operation
2009	Step 7	Step 7 with brine	Step 6 with sands	4	Operation
2010	Step 8	Step 8 with brine	Step 7 with sands	5	Operation
2011	Step 9	Step 9 with brine	Step 8 with sands	6	Operation
2012	Step 10~11	Step 10~11 with brine	Step 9 with sands	7	Operation
2013	Step 12~13	Step 12~13 with brine	Step 10~11 with sands	8	Operation
2014	Step 14~16	Step 14~16 with brine	Step 12~13 with sands	9	Operation
2015			Step 14~16 with sands	10	Operation
8-13 LTBG Cavern					
2016	Step 1~3	Step 1~3 with brine		11	Operation
2017	Step 4~5	Step 4~5 with brine	Step 1~3 with sands	12	Operation
2018	Step 6	Step 6 with brine	Step 4~5 with sands	13	Operation
2019	Step 7	Step 7 with brine	Step 6 with sands	14	Operation
2020	Step 8	Step 8 with brine	Step 7 with sands	15	Operation
2021	Step 9	Step 9 with brine	Step 8 with sands	16	Operation
2022	Step 10~11	Step 10~11 with brine	Step 9 with sands	17	Operation
2023	Step 12~13	Step 12~13 with brine	Step 10~11 with sands	18	Operation
2024	Step 14~16	Step 14~16 with brine	Step 12~13 with sands	19	Operation
2025			Step 14~16 with sands		

1-13 PRVP Cavern					
2026	Step 1~3	Step 1~3 with brine		21	Operation
2027	Step 4~5	Step 4~5 with brine	Step 1~3 with sands	22	Operation
2028	Step 6	Step 6 with brine	Step 4~5 with sands	23	Operation
2029	Step 7	Step 7 with brine	Step 6 with sands	24	Operation
2030	Step 8	Step 8 with brine	Step 7 with sands	25	Operation
2031	Step 9	Step 9 with brine	Step 8 with sands	26	Operation
2032	Step 10~11	Step 10~11 with brine	Step 9 with sands	27	Operation
2033	Step 12~13	Step 12~13 with brine	Step 10~11 with sands	28	Operation
2034	Step 14~16	Step 14~16 with brine	Step 12~13 with sands	29	Operation
2035			Step 14~16 with sands	30	Operation
8-13 PRVP					
2036	Step 1~3	Step 1~3 with brine		31	Operation
2037	Step 4~5	Step 4~5 with brine	Step 1~3 with sands	32	Operation
2038	Step 6	Step 6 with brine	Step 4~5 with sands	33	Operation
2039	Step 7	Step 7 with brine	Step 6 with sands	34	Operation
2040	Step 8	Step 8 with brine	Step 7 with sands	35	Operation
2041	Step 9	Step 9 with brine	Step 8 with sands	36	Operation
2042	Step 10~11	Step 10~11 with brine	Step 9 with sands	37	Operation
2043	Step 12~13	Step 12~13 with brine	Step 10~11 with sands	38	Operation
2044	Step 14~16	Step 14~16 with brine	Step 12~13 with sands	39	Operation
2045			Step 14~16 with sands	40	Operation
2046				41	Abandonment
2095				90	Abandonment

**1-13&8-13LTBG**  
*brine-brine case*

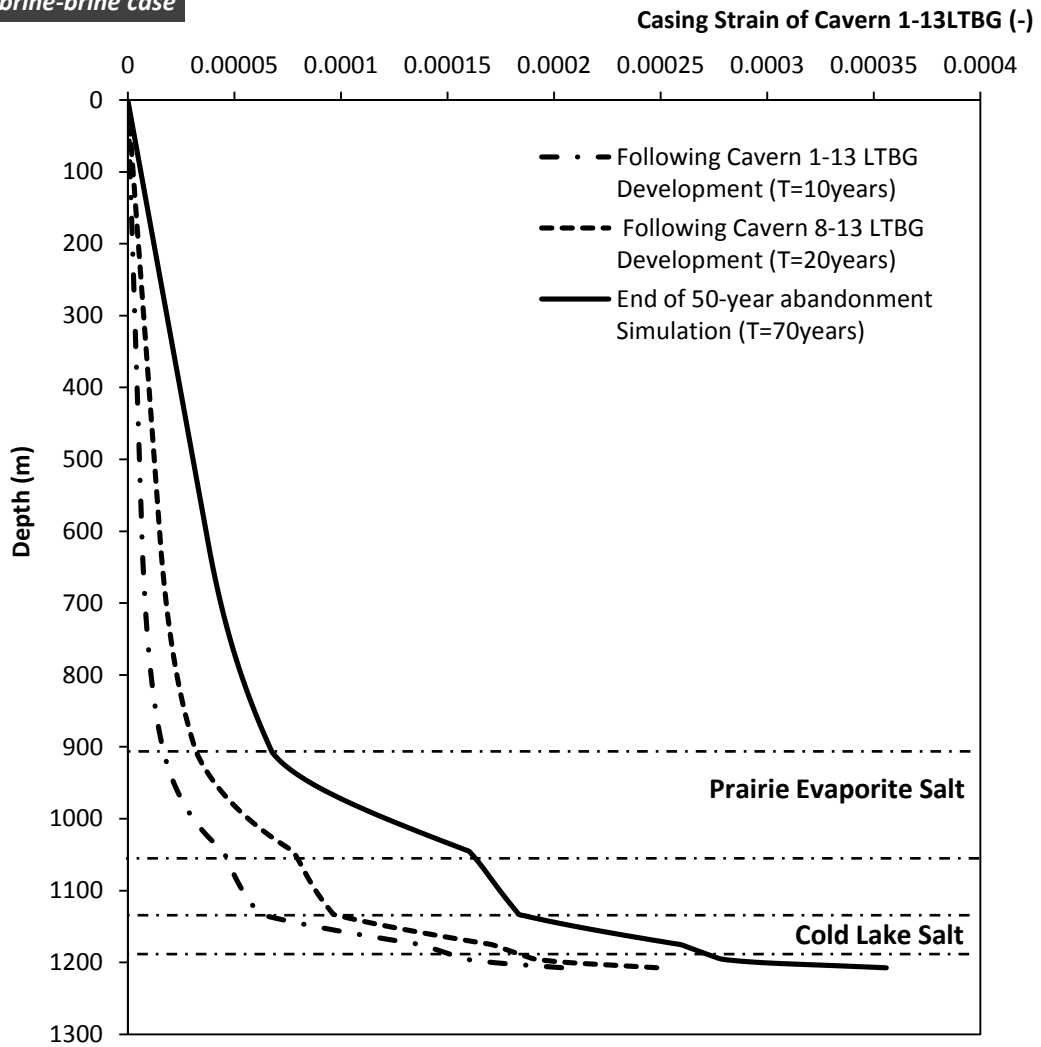


Figure C. 1 Accumulated Vertical Strains along the Axis of Symmetry of Cavern 1-13 LTBG during Abandonment Simulation (*1-13&8-13 LTBG brine-brine*)

**1-13&8-13 LTBG  
brine-brine case**

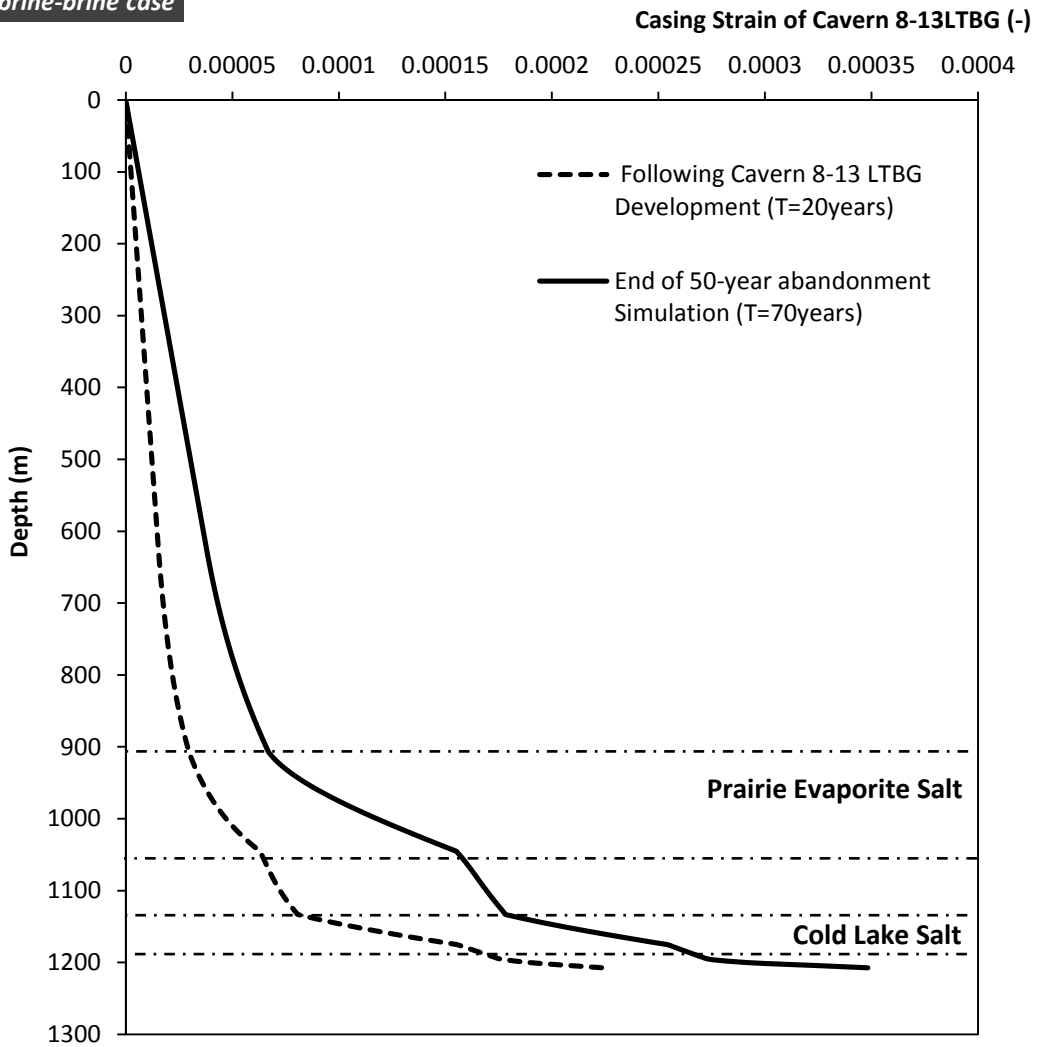


Figure C. 2 Accumulated Vertical Strains along the Axis of Symmetry of Cavern 8-13 LTBG during Abandonment Simulation (*1-13&8-13 LTBG brine-brine*)

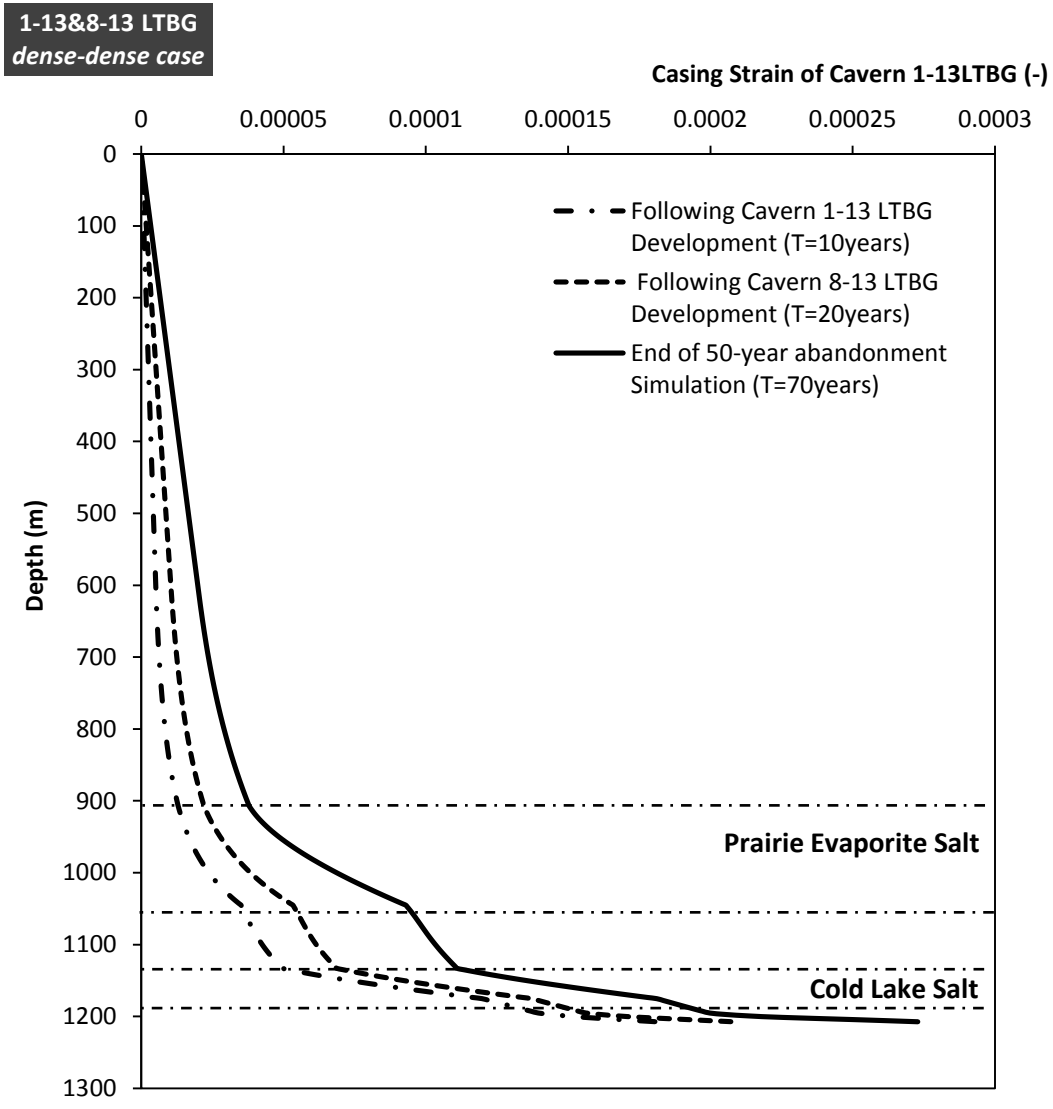


Figure C. 3 Accumulated Vertical Strains along the Axis of Symmetry of Cavern 1-13 LTBG during Abandonment Simulation (*1-13&8-13 LTBG dense-dense*)

**1-13&8-13 LTBG**  
*dense-dense case*

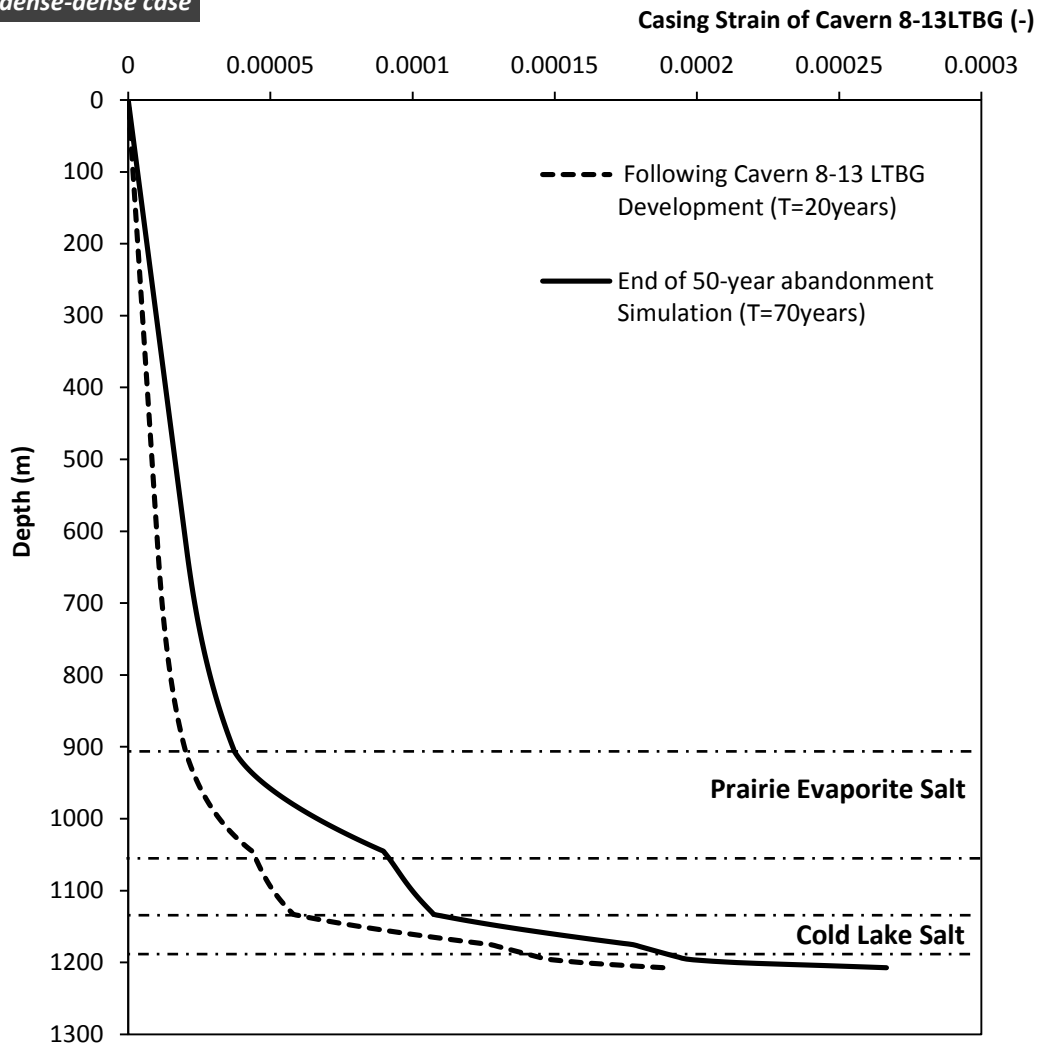


Figure C. 4 Accumulated Vertical Strains along the Axis of Symmetry of Cavern 8-13 LTBG during Abandonment Simulation (*1-13&8-13 LTBG dense-dense*)

**1-13&8-13 LTBG  
brine-brine case**

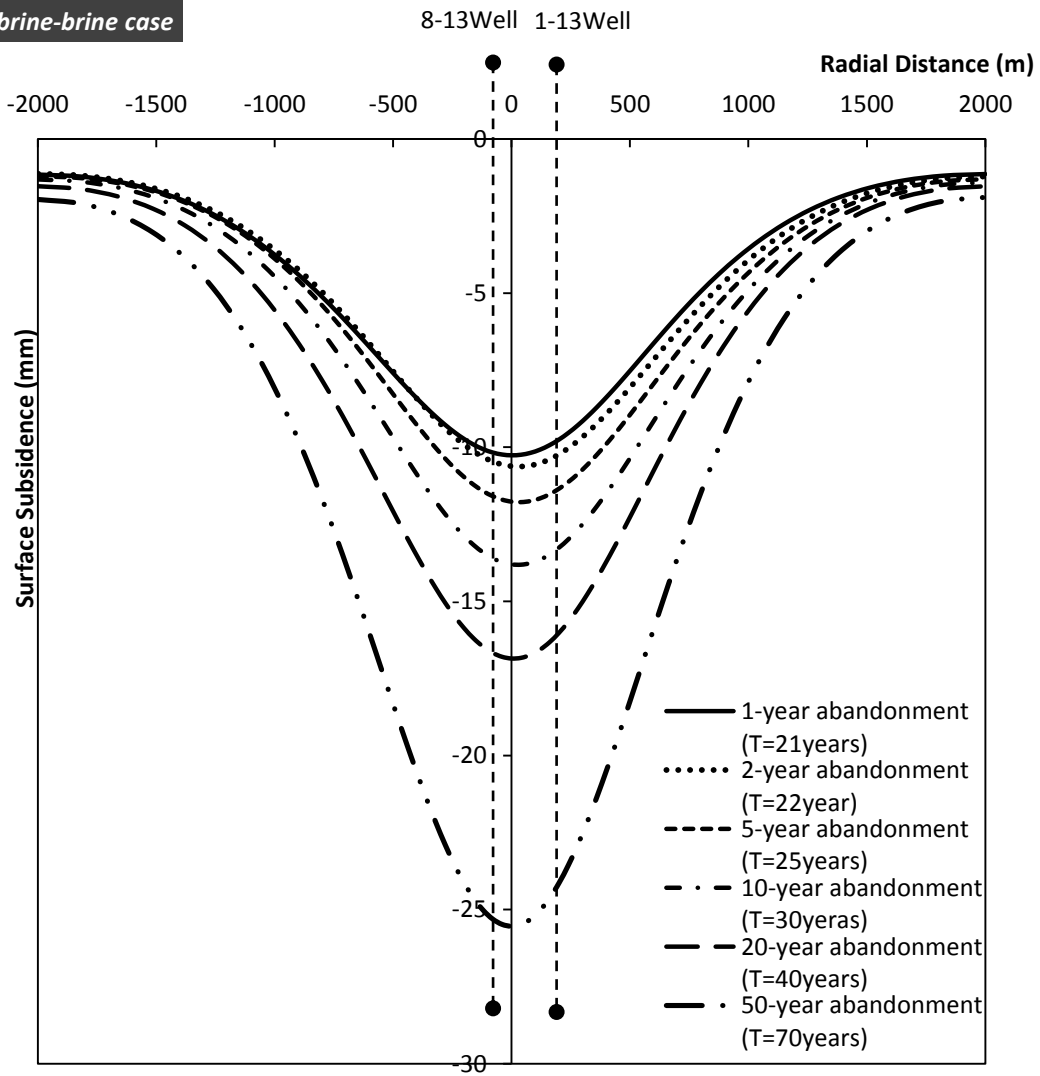


Figure C. 5 Surface Subsidence Plot (1-13&8-13 LTBG brine-brine)

**1-13&8-13 LTBG  
dense-brine case**

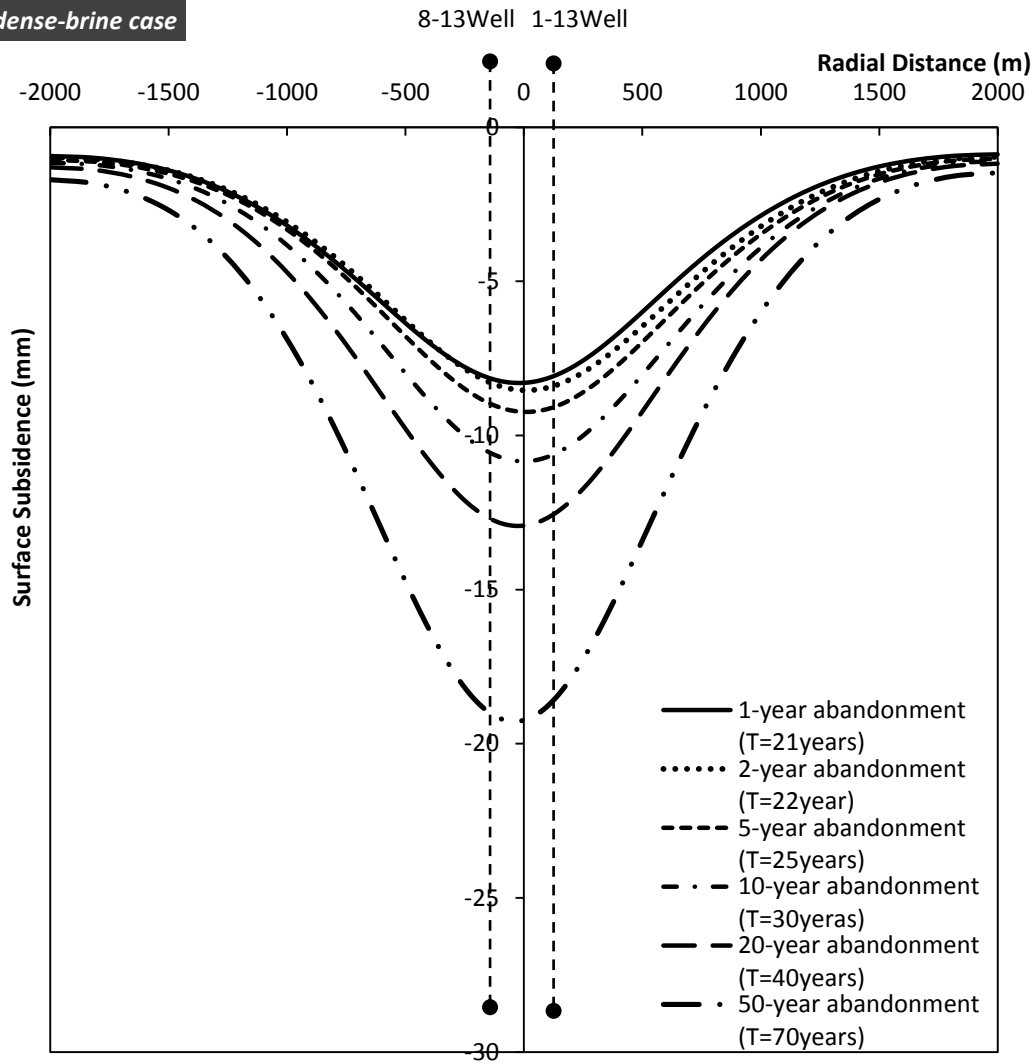


Figure C. 6 Surface Subsidence Plot (1-13&8-13 LTBG dense-brine)

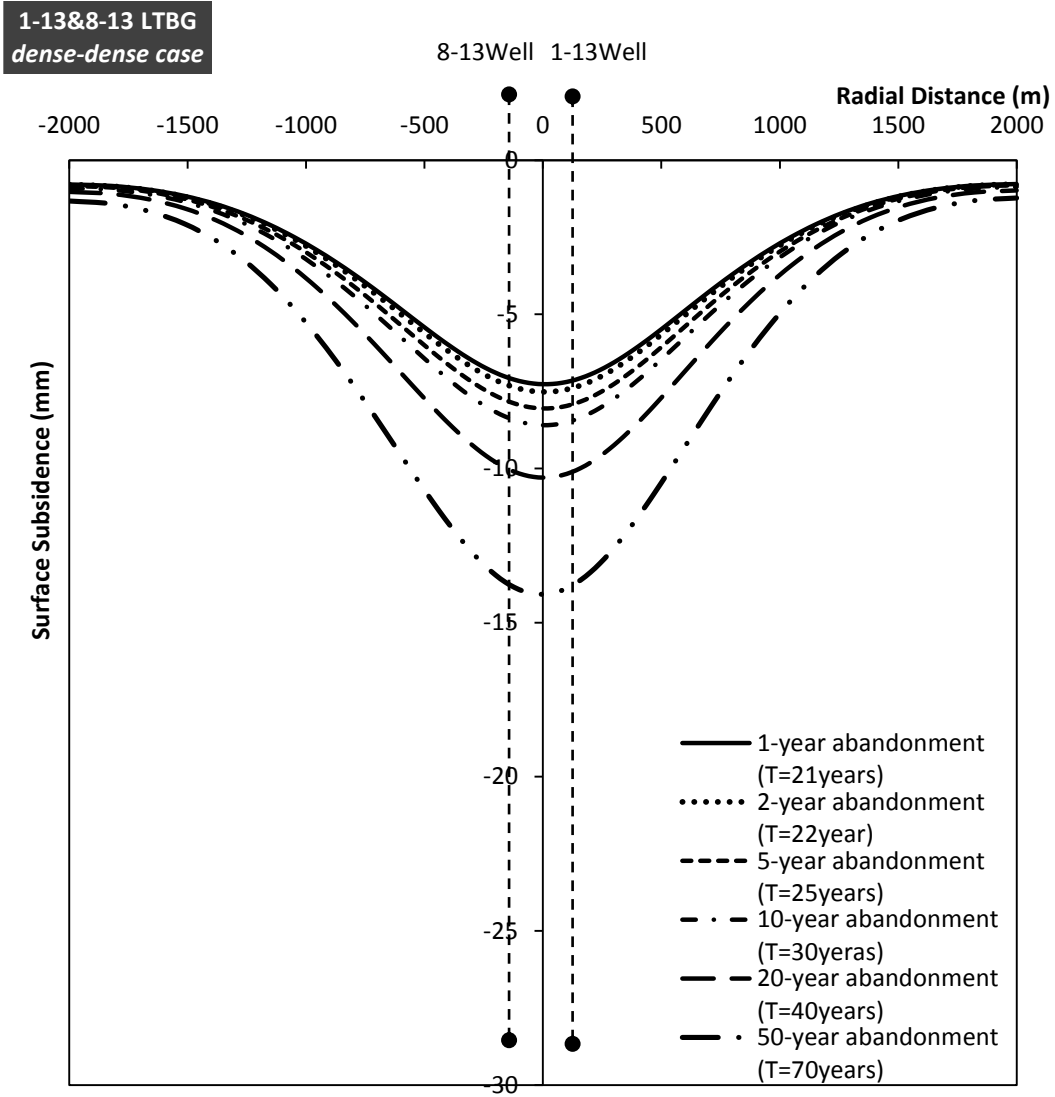


Figure C. 7 Surface Subsidence Plot (1-13&8-13 LTBG dense-dense)

**1-13 LTBG&PRVP  
brine-brine case**

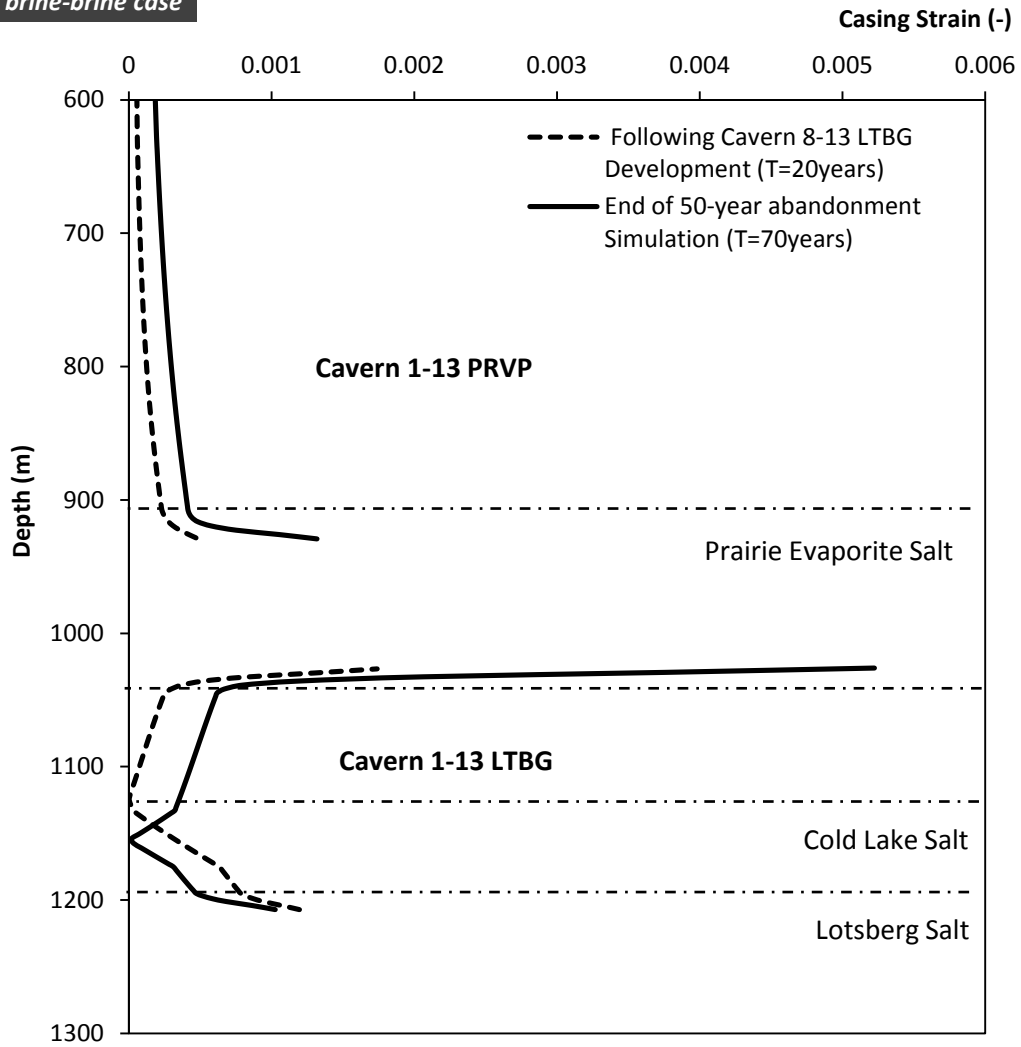


Figure C. 8 Accumulated Casing Strains during Simulation for Cavern 1-13 LTBG and Cavern 1-13 PRVP (*1-13 LTBG&PRVP brine-brine*)

**1-13 LTBG&PRVP  
dense-dense case**

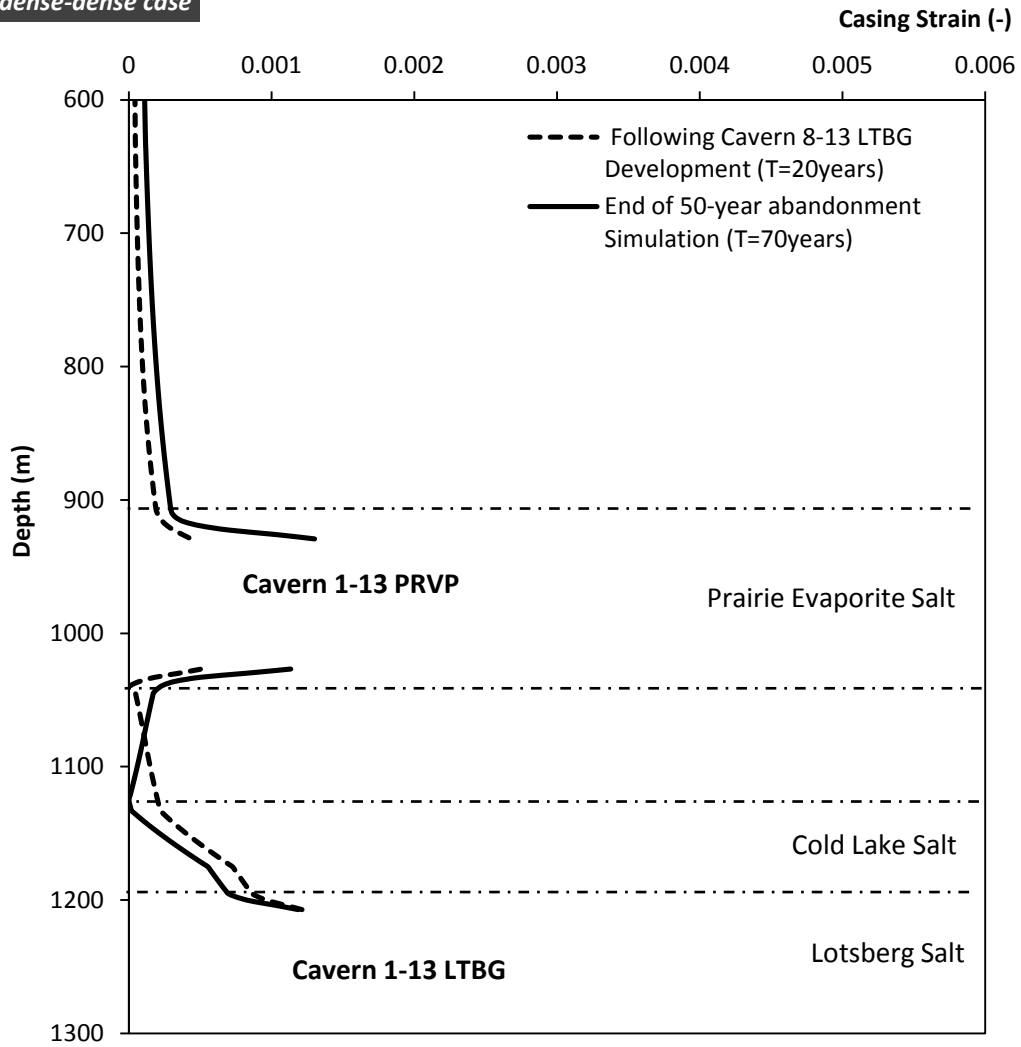


Figure C. 9 Accumulated Casing Strains during Simulation for Cavern 1-13 LTBG and Cavern 1-13 PRVP (*1-13 LTBG&PRVP dense-dense*)

**1-13 PRVP&LTBG  
brine-brine case**

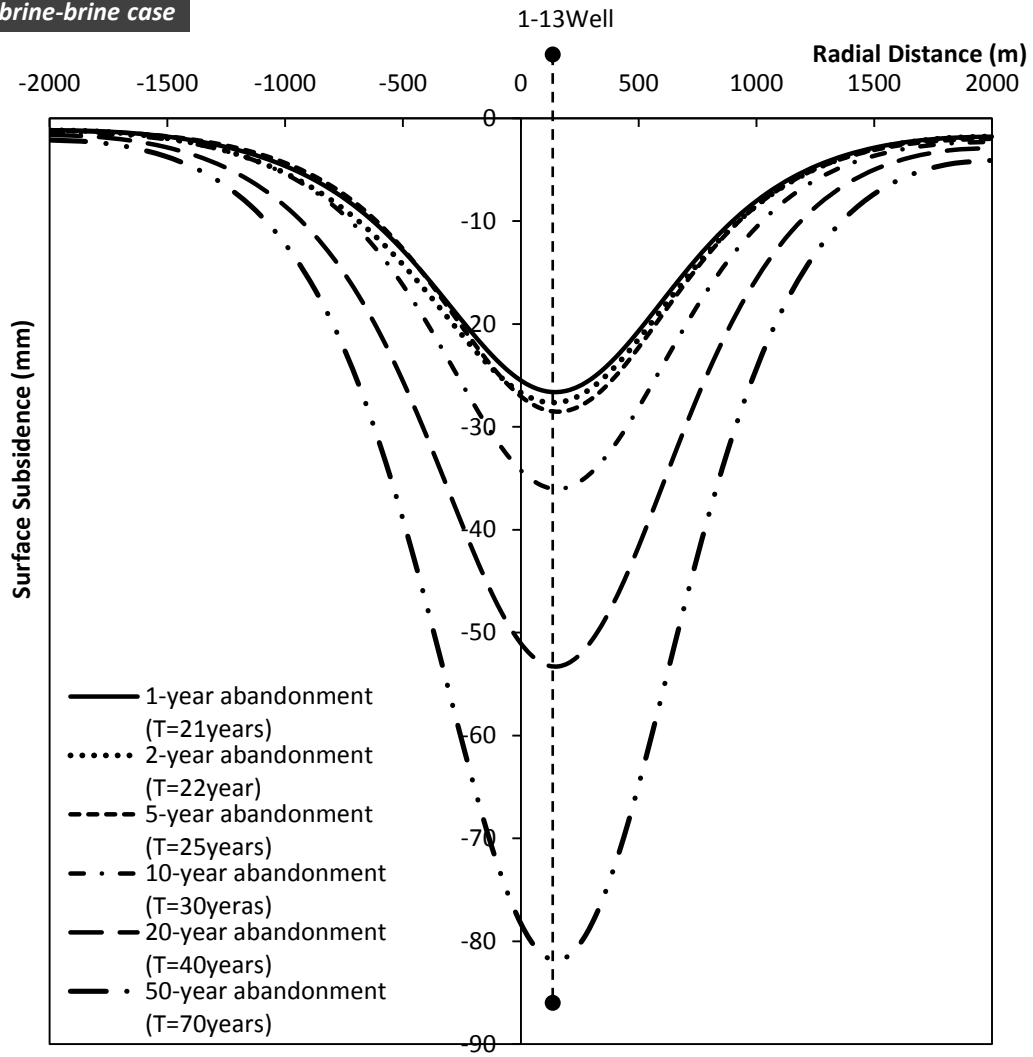


Figure C. 10 Surface Subsidence Plot (1-13LTBG&PRVP brine-brine)

1-13 LTBG&PRVP  
dense-brine case

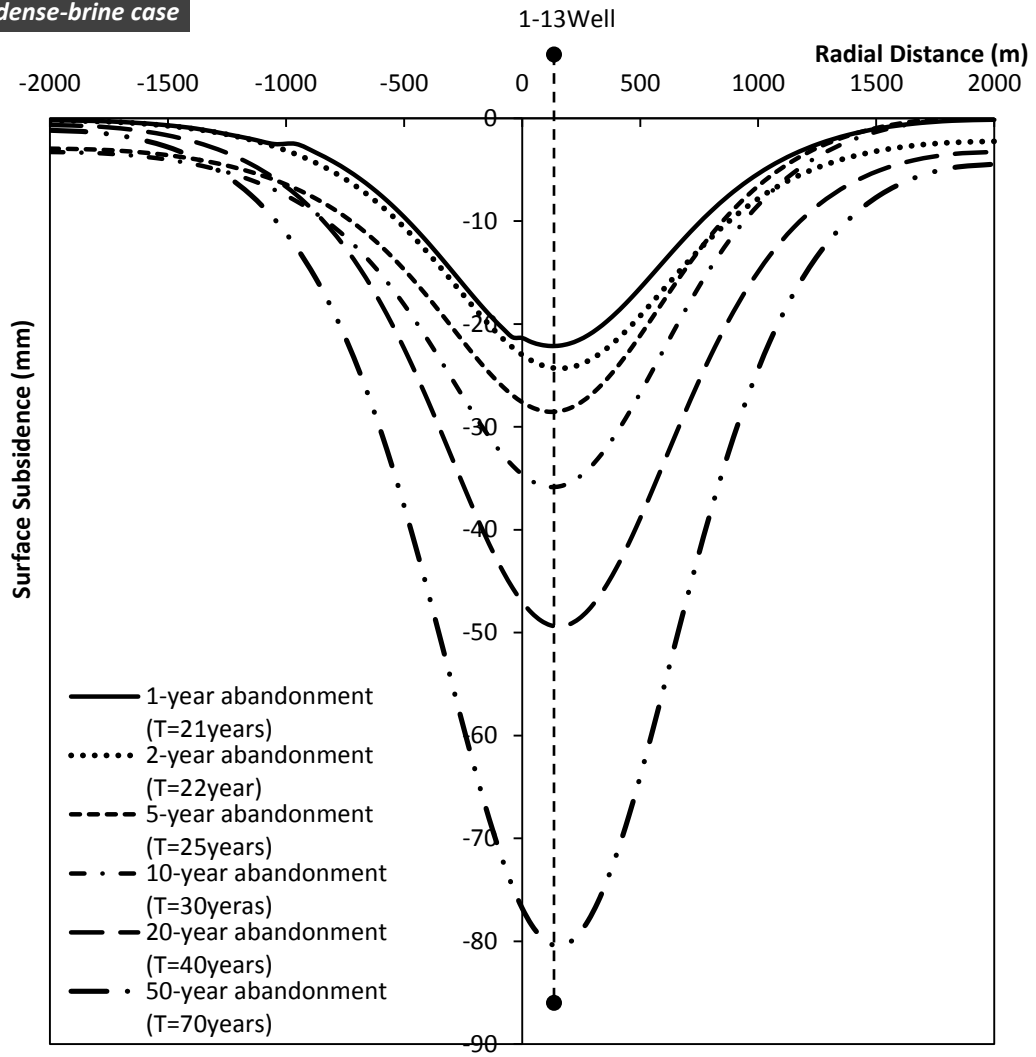


Figure C. 11 Surface Subsidence Plot (*1-13LTBG&PRVP dense-brine*)

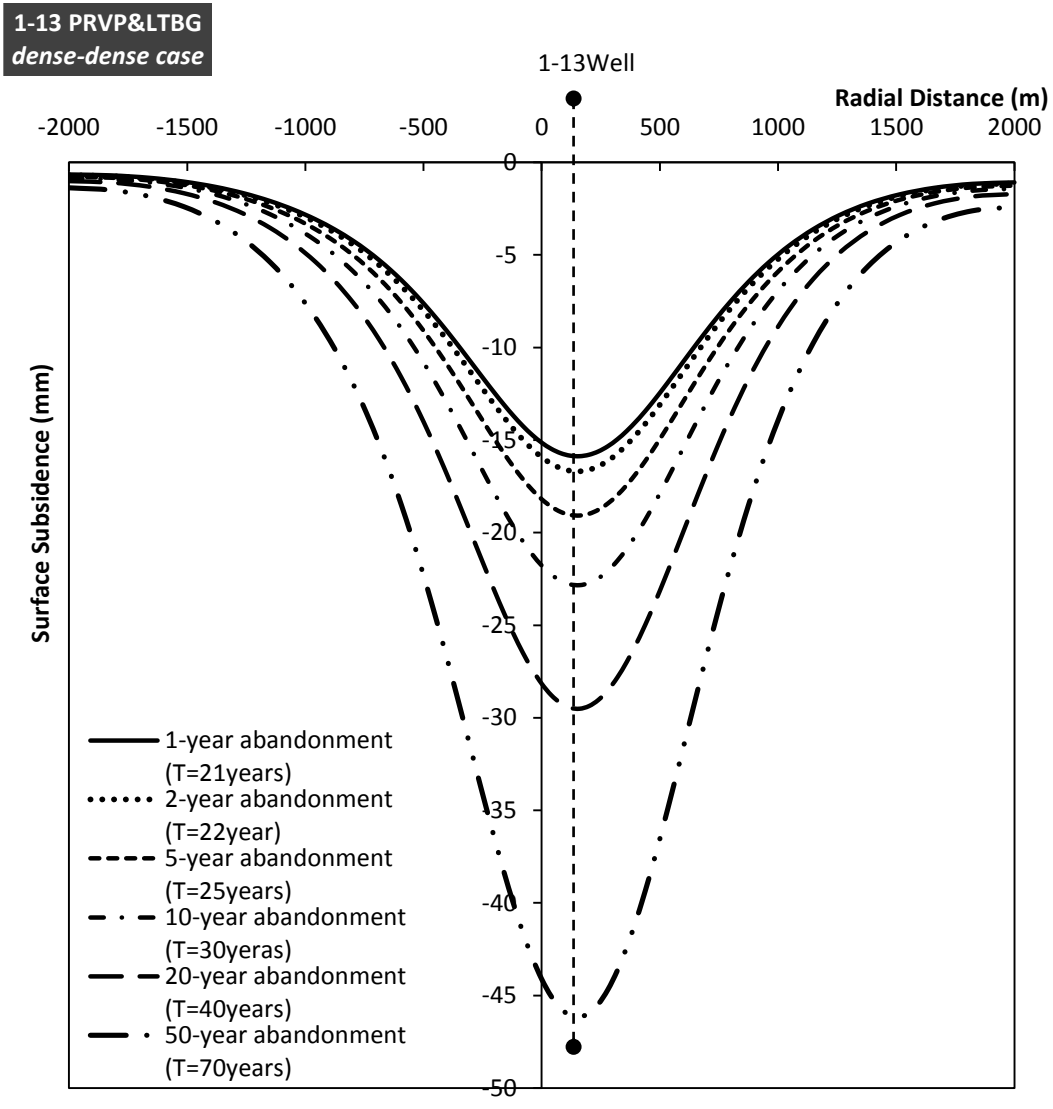


Figure C. 12 Surface Subsidence Plot (*1-13LTBG&PRVP dense-dense*)

**1-13&8-13 LTBG&PRVP  
brine-brine-brine-brine case**

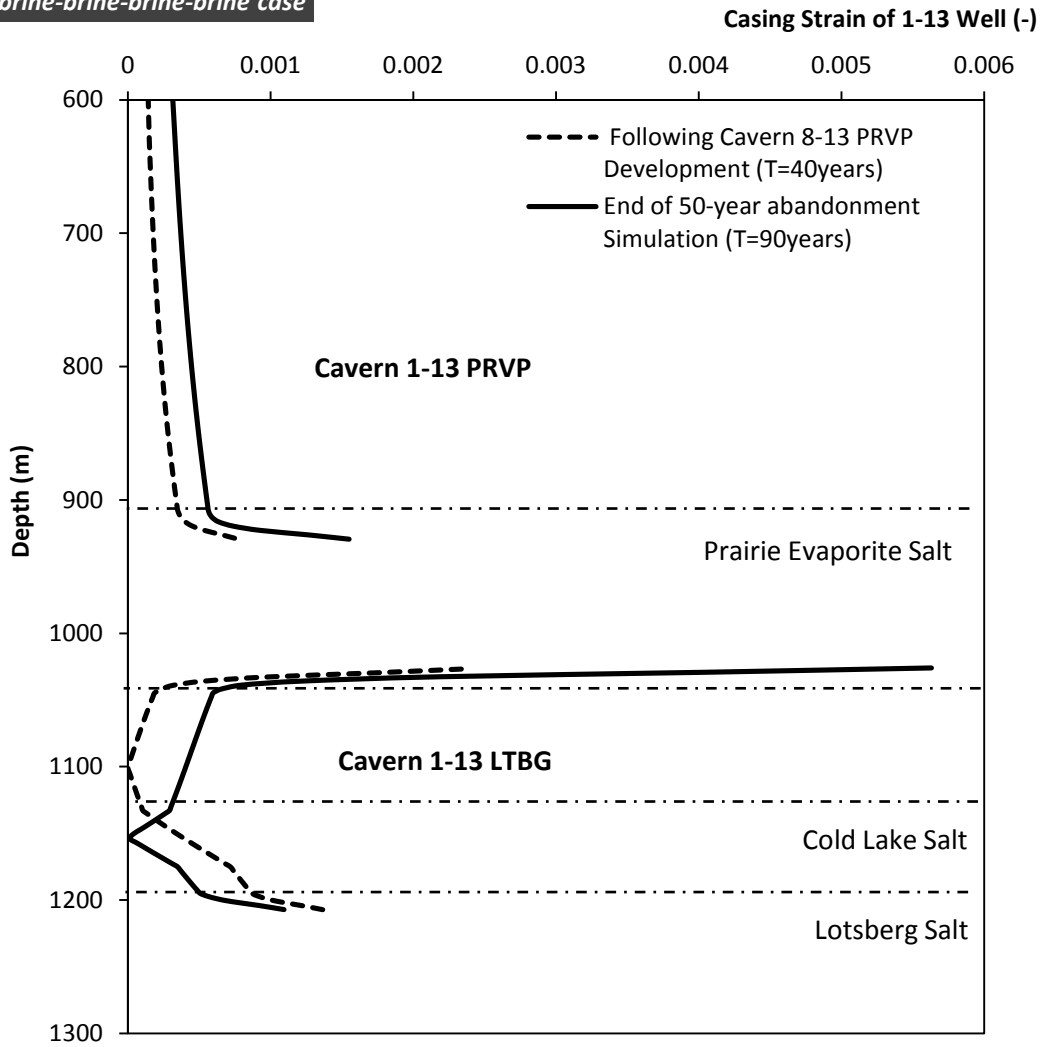


Figure C. 13 Accumulated Casing Strains during Simulation for Cavern 1-13 LTBG and Cavern 1-13 PRVP (*1-13 LTBG&PRVP brine-brine-brine-brine*)

**1-13&8-13 LTBG&PRVP  
brine-brine-brine-brine case**

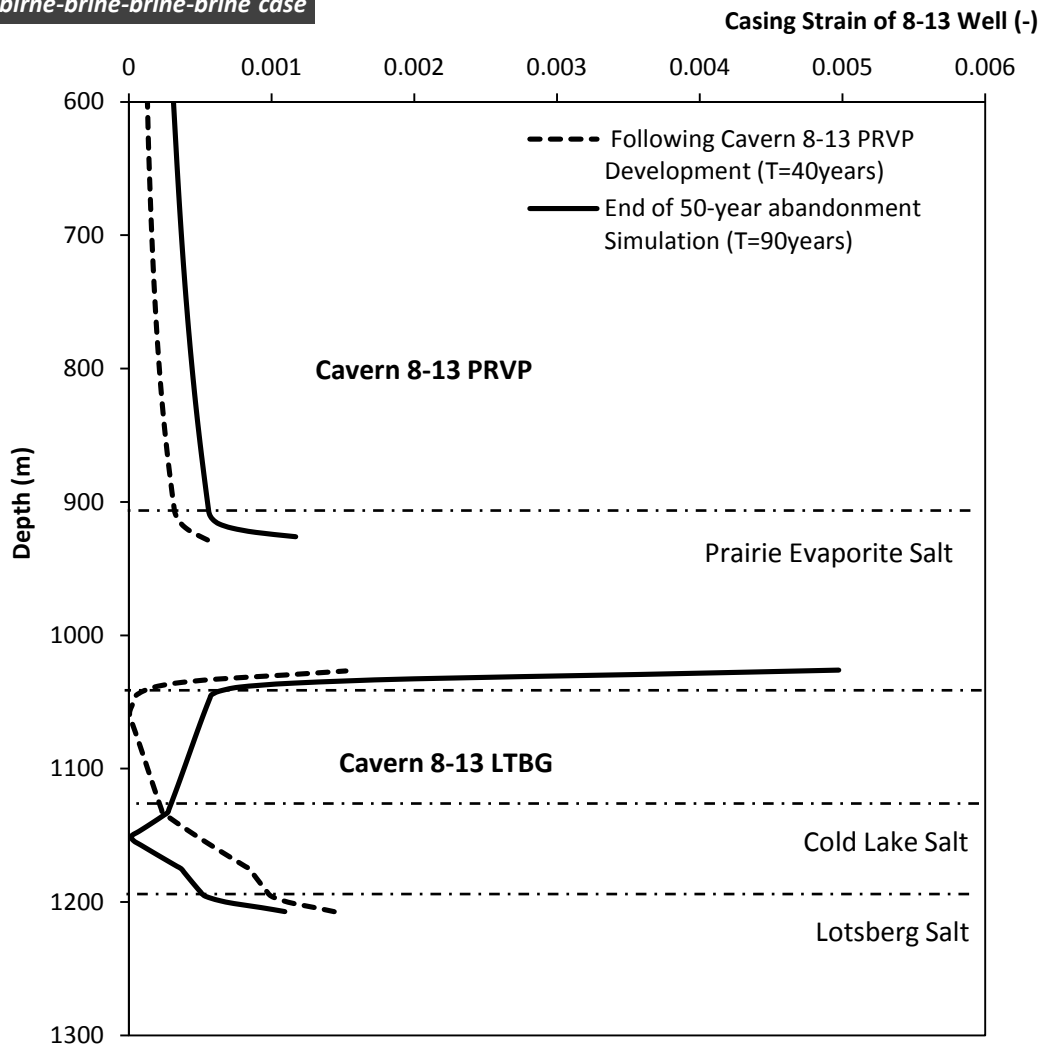


Figure C. 14 Accumulated Casing Strains during Simulation for Cavern 8-13 LTBG and Cavern 8-13 PRVP (*1-13 LTBG&PRVP brine-brine-brine-brine*)

**1-13&8-13 LTBG&PRVP  
dense-dense-brine-brine case**

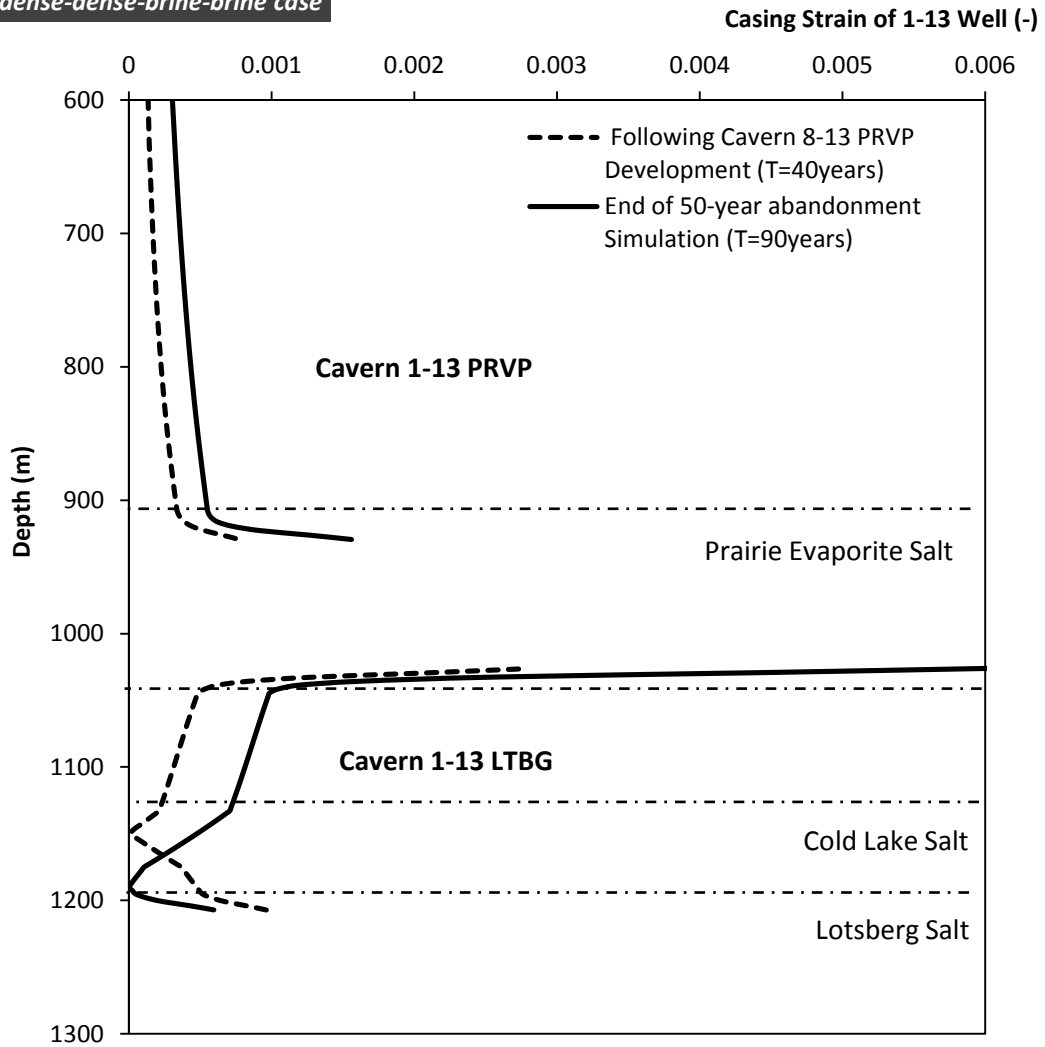


Figure C. 15 Accumulated Casing Strains during Simulation for Cavern 1-13 LTBG and Cavern 1-13 PRVP (*1-13 LTBG&PRVP dense-dense-brine-brine*)

**1-13&8-13 LTBG&PRVP  
dense-dense-brine-brine case**

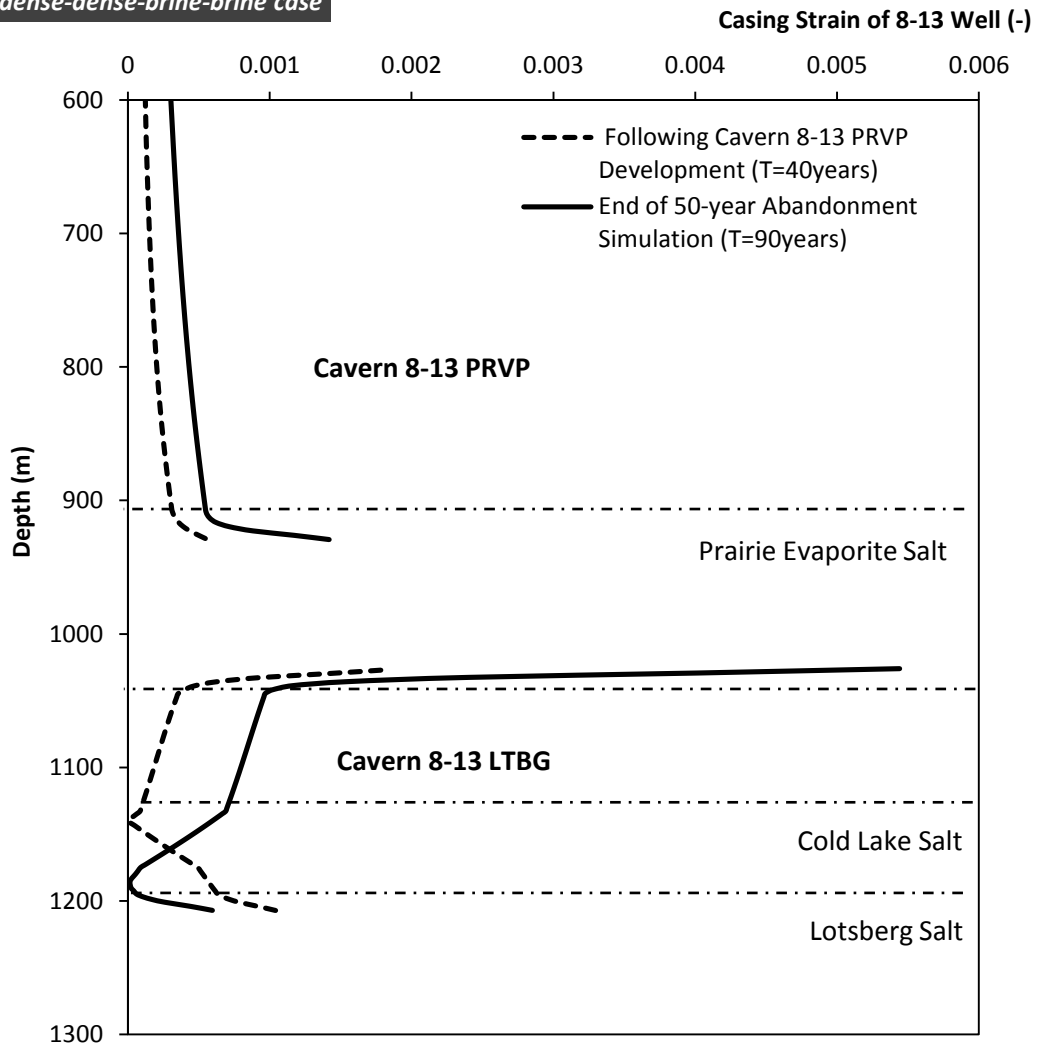


Figure C. 16 Accumulated Casing Strains during Simulation for Cavern 8-13 LTBG and Cavern 8-13 PRVP (*1-13 LTBG&PRVP dense-dense-brine-brine*)

**1-13&8-13 LTBG&PRVP**  
*dense-dense-dense-dense case*

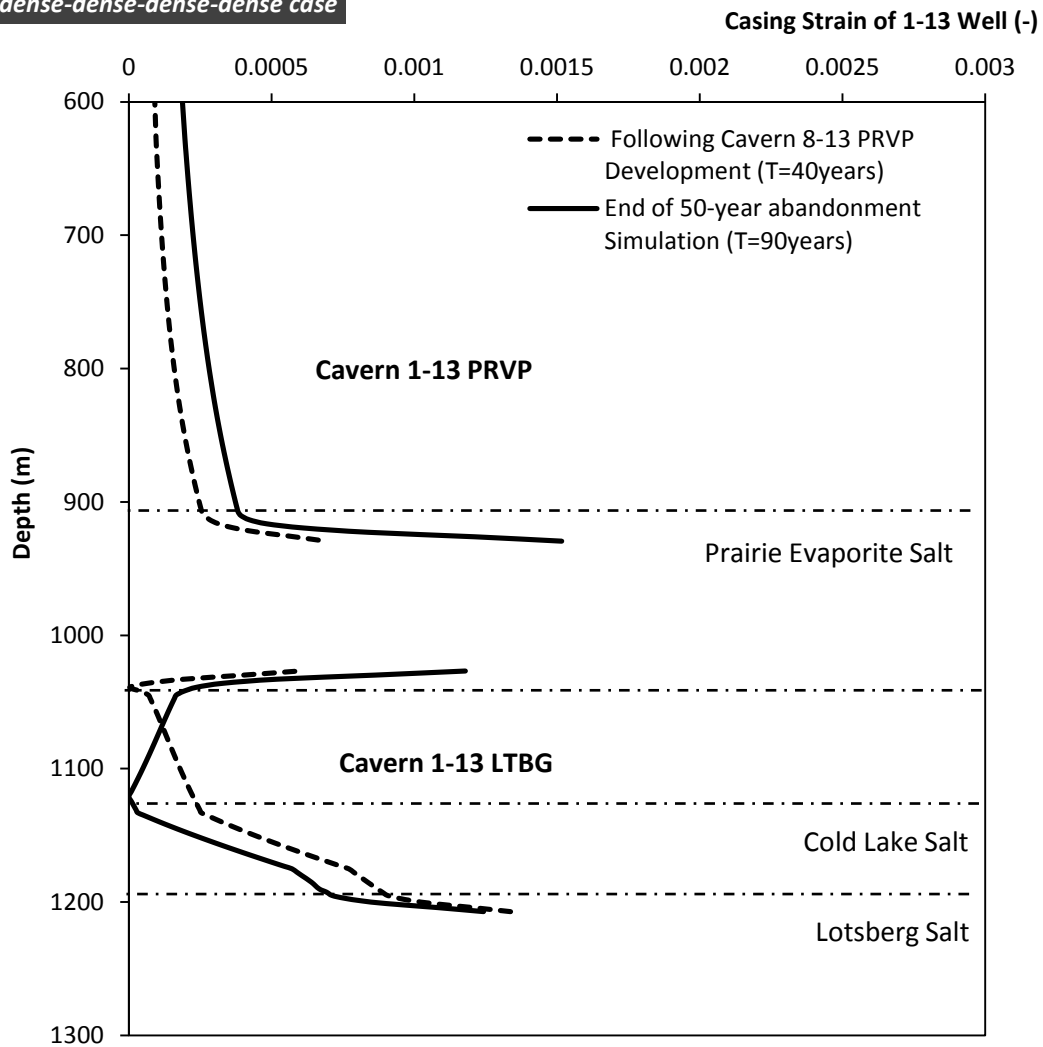


Figure C. 17 Accumulated Casing Strains during Simulation for Cavern 1-13 LTBG and Cavern 1-13 PRVP (*1-13 LTBG&PRVP dense-dense-dense-dense*)

**1-13&8-13 LTBG&PRVP**  
*dense-dense-dense-dense case*

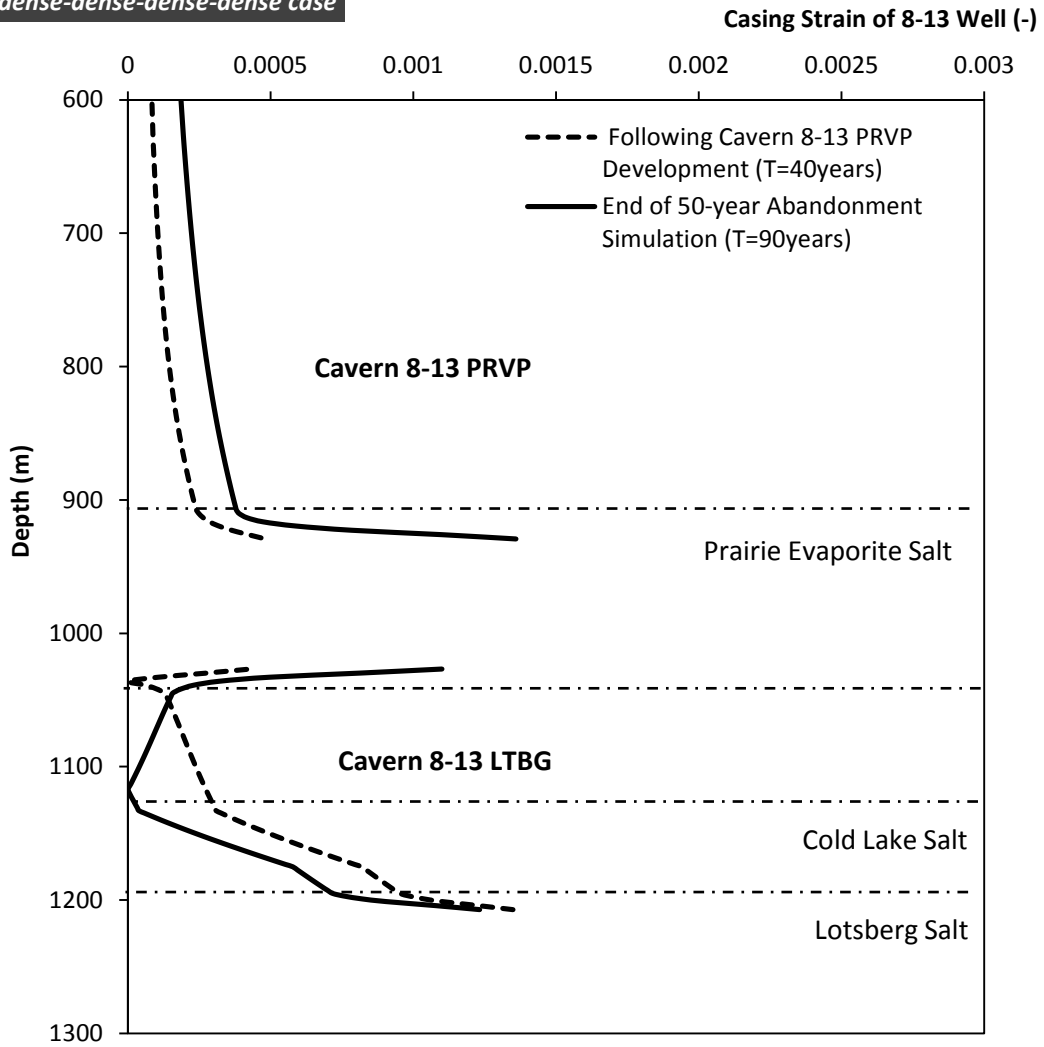


Figure C. 18 Accumulated Casing Strains during Simulation for Cavern 8-13 LTBG and Cavern 8-13 PRVP (*1-13 LTBG&PRVP dense-dense-dense-dense*)

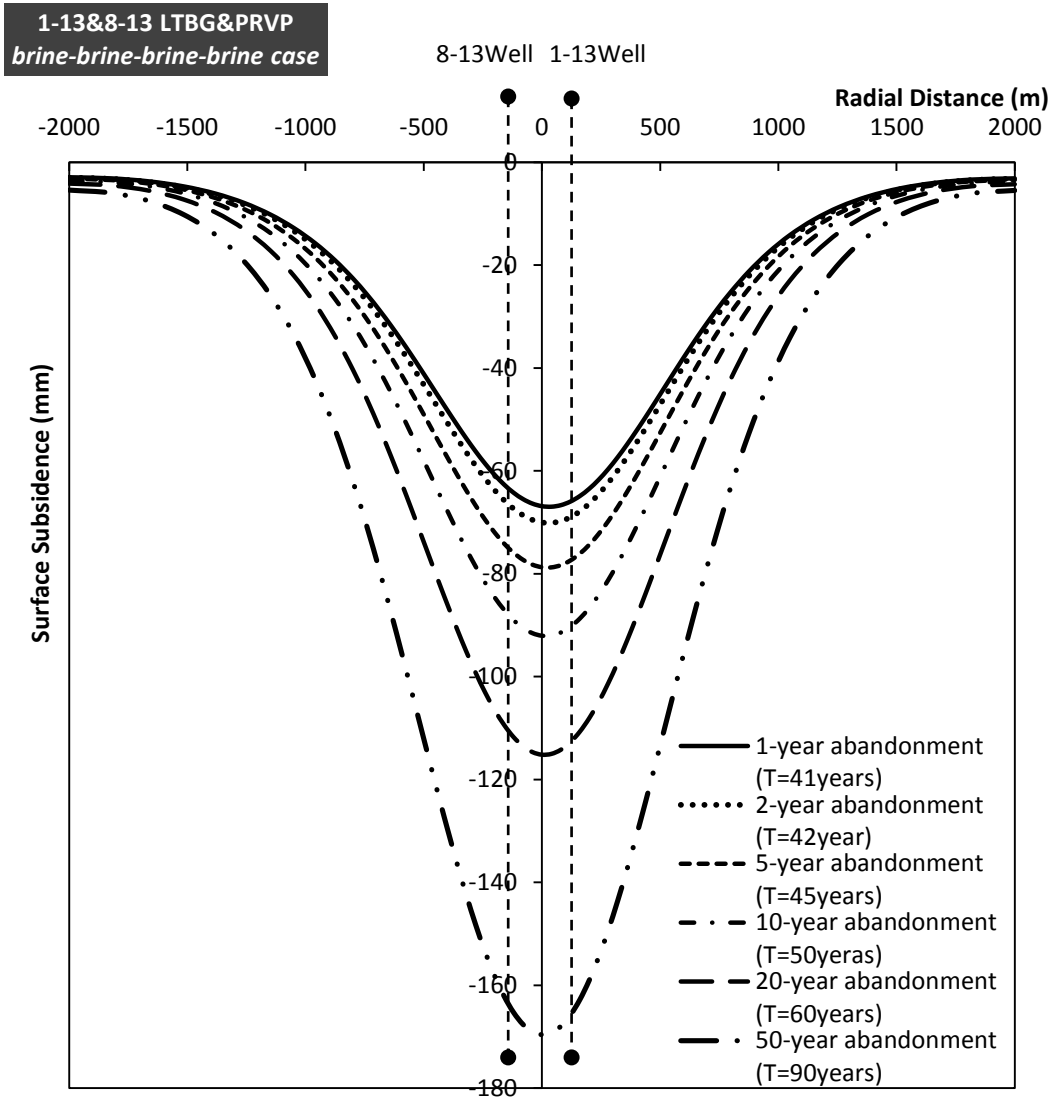


Figure C. 19 Surface Subsidence Plot (*1-13&8-13 LTBG&PRVP brine-brine-brine-brine*)

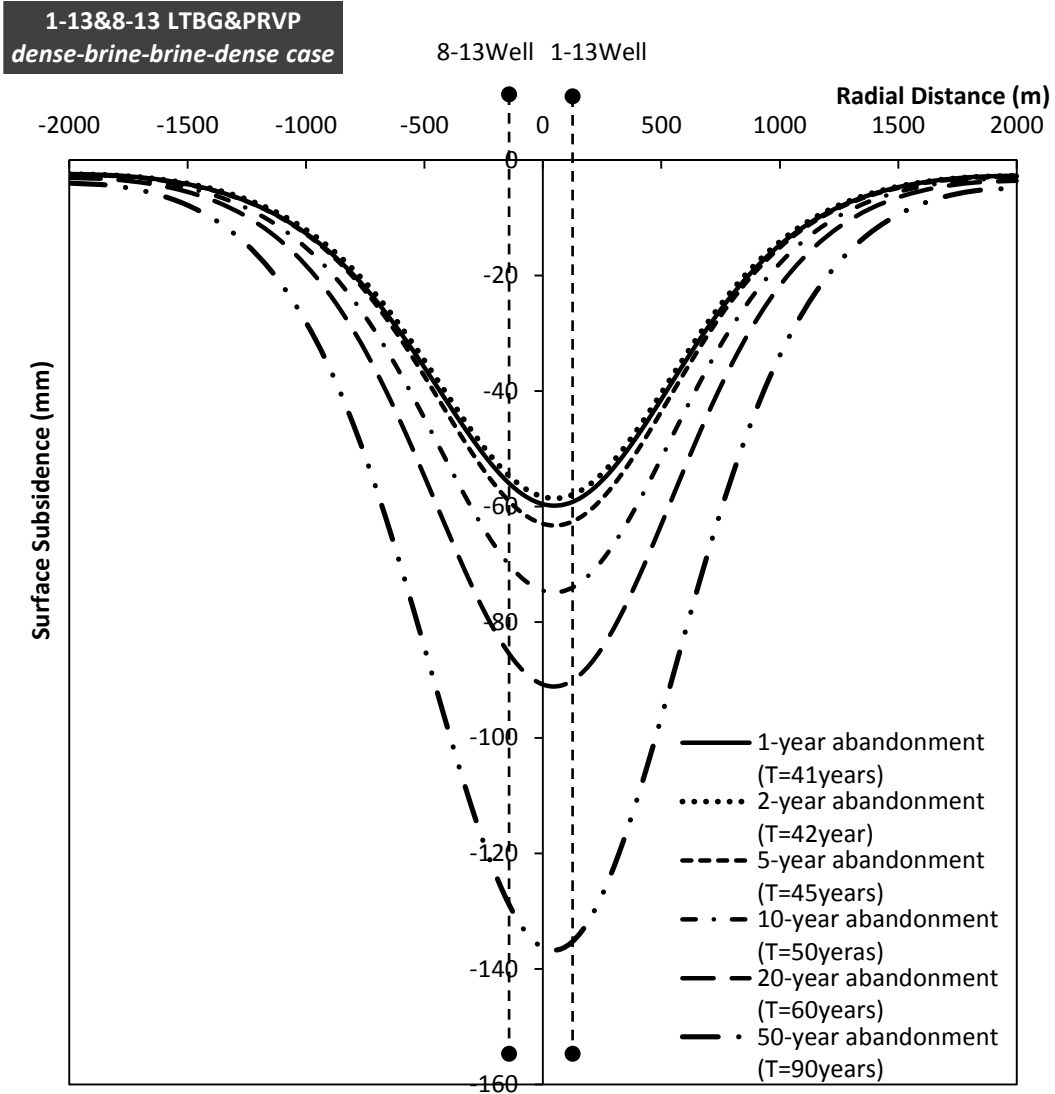


Figure C. 20 Surface Subsidence Plot (*1-13&8-13 LTBG&PRVP dense-brine-brine-dense*)

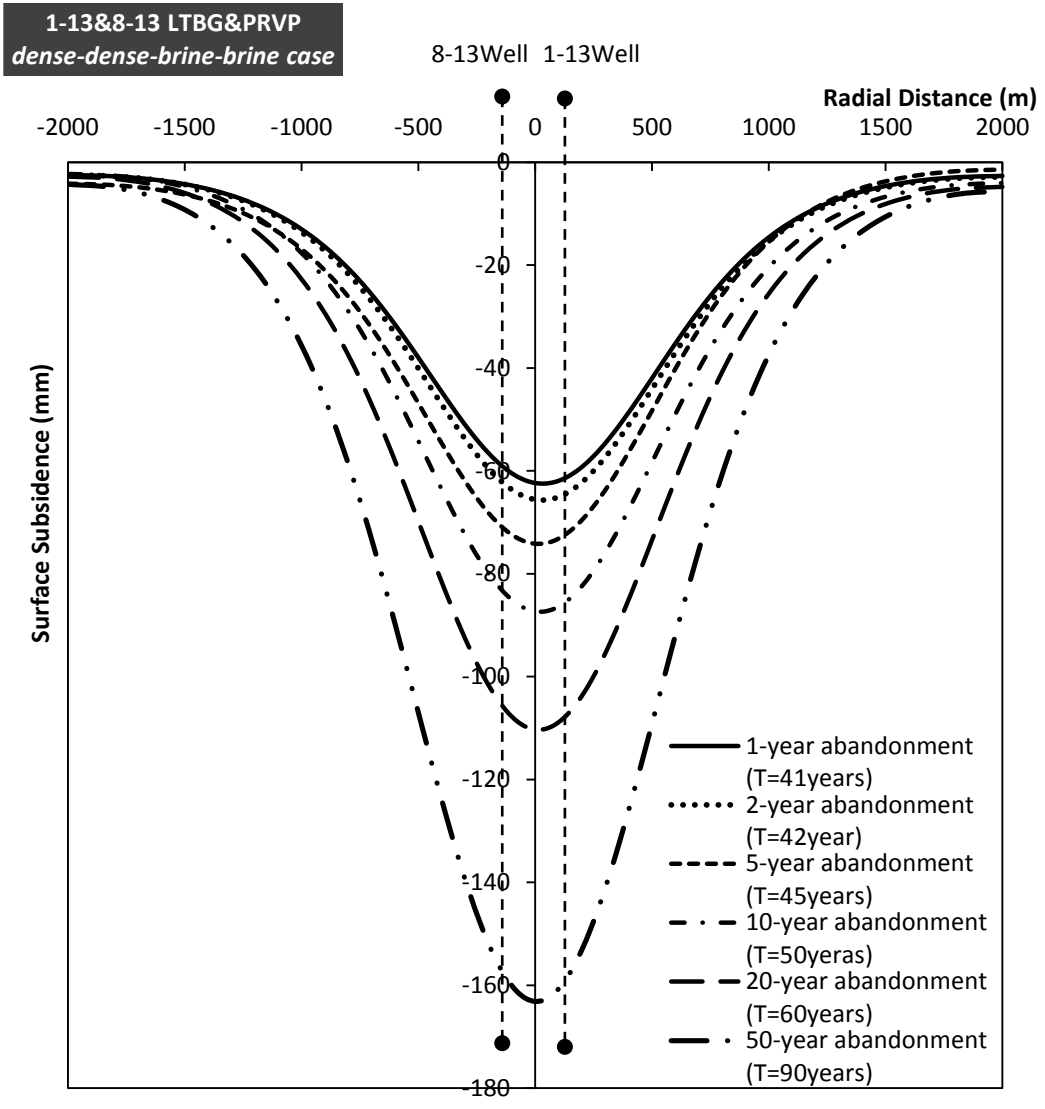


Figure C. 21 Surface Subsidence Plot (*1-13&8-13 LTBG&PRVP dense-dense-brine-brine*)

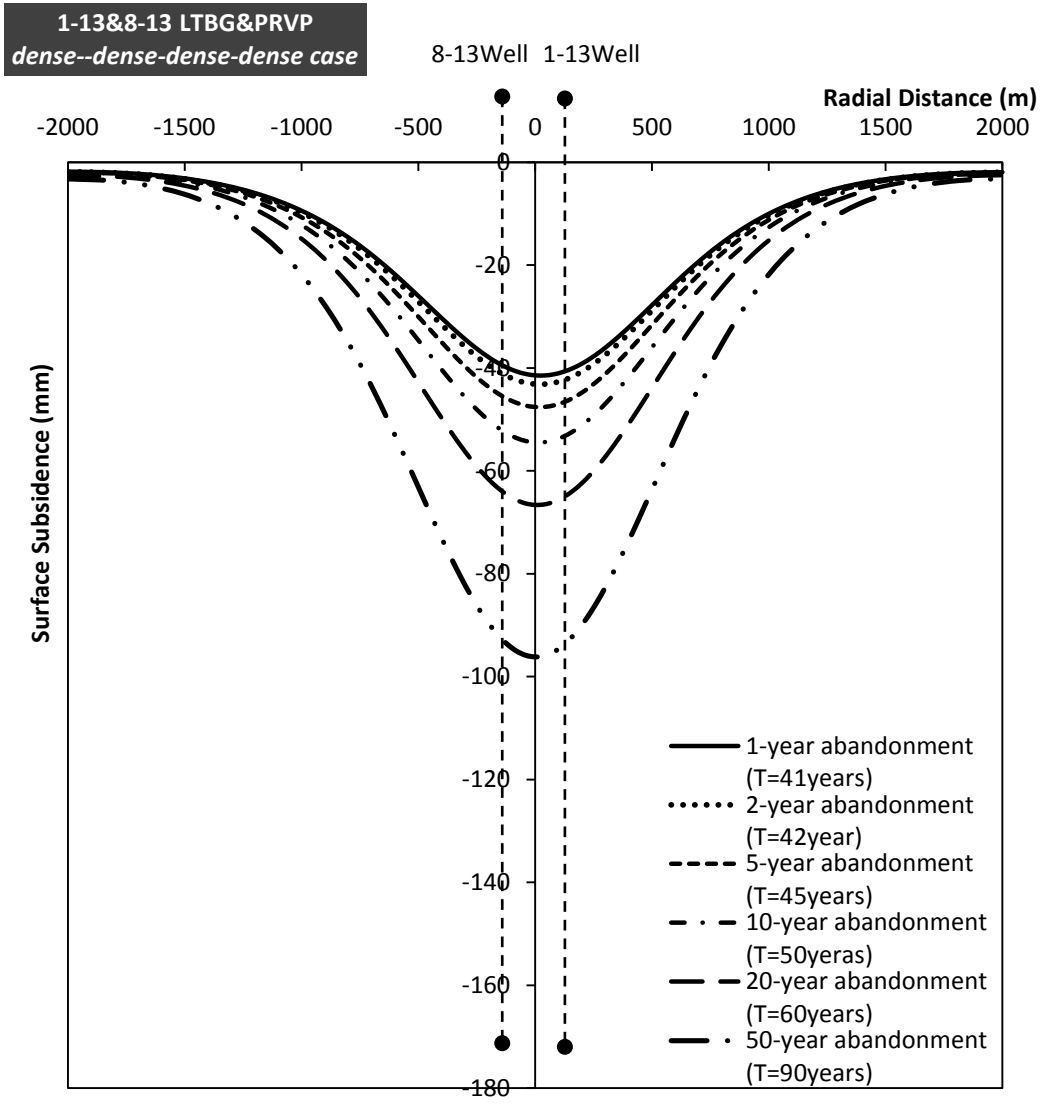


Figure C. 22 Surface Subsidence Plot (*1-13&8-13 LTBG&PRVP dense-dense-dense-dense*)